MAY 11, 2022
VOLUME 122
NUMBER 9

pubs.acs.org/CR

CHEMICAL REVIEWS

ACS Publications
Most Trusted. Most Cited. Most Read.

www.acs.org

CHEMICAL REVIEWS

pubs.acs.org/CR

Review

Nanocellulose for Sustainable Water Purification

Rasel Das, Tom Lindström,* Priyanka R. Sharma, Kai Chi, and Benjamin S. Hsiao*

Cite This: *Chem. Rev.* 2022, 122, 8936–9031

Read Online

ACCESS | Metrics & More | Article Recommendations | Supporting Information

ABSTRACT: Nanocelluloses (NC) are nature-based sustainable biomaterials, which not only possess cellulosic properties but also have the important hallmarks of nanomaterials, such as large surface area, versatile reactive sites or functionalities, and scaffolding stability to host inorganic nanoparticles. This class of nanomaterials offers new opportunities for a broad spectrum of applications for clean water production that were once thought impractical. This Review covers substantial discussions based on evaluative judgments of the recent literature and technical advancements in the fields of coagulation/flocculation, adsorption, photocatalysis, and membrane filtration for water decontamination through proper understanding of fundamental knowledge of NC, such as purity, crystallinity, surface chemistry and charge, suspension rheology, morphology, mechanical properties, and film stability. To supplement these, discussions on low-cost and scalable NC extraction, new characterizations including solution small-angle X-ray scattering evaluation, and structure–property relationships of NC are also reviewed. Identifying knowledge gaps and drawing perspectives could generate guidance to overcome uncertainties associated with the adaptation of NC-enabled water purification technologies. Furthermore, the topics of simultaneous removal of multipollutants disposal and proper handling of post/spent NC are discussed. We believe NC-enabled remediation nanomaterials can be integrated into a broad range of water treatments, greatly improving the cost-effectiveness and sustainability of water purification.

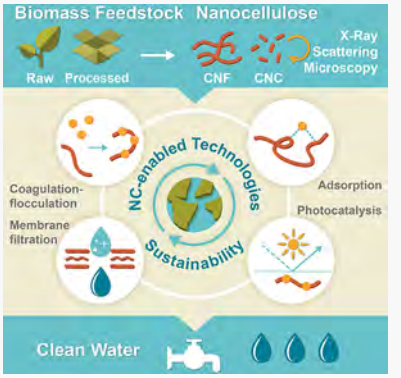

CONTENTS

Received: August 2, 2021
Published: March 25, 2022

1. INTRODUCTION

Today, about 1.8 billion people are facing absolute water shortage and 4 billion people are experiencing water scarcity at least one month per year.[1] In the U.S., it has also been reported that more than 63 million Americans (almost one-fifth of the population) are exposed to water contamination that is higher than any situation during recent decades.[2] These challenges are due to the shrinking freshwater supply, which is frequently polluted by a range of diverse pollutants at concentrations that are incompatible for human use. In augmenting clean water production, many water remediation materials, such as activated carbon, carbon nanotube (CNT), graphene and their derivatives, zeolites, and metallic nanoparticles, have been utilized in varying water purification technologies.[3] However, the high costs of these materials, as well as their adverse toxicity effects on the environment and ecosystems, have prompted the community to search for alternative low-cost and safe nanostructured alternatives[3,4] without losing essential physicochemical properties.[5]

In the utilization of sustainable nanomaterials, abundant and low-/no-valued plant biomass feedstocks, containing cellulosic polymer, are an important source for extracting nanocellulose (NC), especially by using environmentally friendly methods with low consumptions of energy, chemical and water.[6] NC includes all nanostructured cellulosic materials, comprising of cellulose nanofibrils (CNF), cellulose nanocrystals (CNC), bacterial nanocellulose (BNC), as well as tunicate cellulose nanocrystals (t-CNC) and algae cellulose particles. Basic background on these various cellulosic nanomaterials can be found in some excellent recent reviews dealing with characterization methods,[7] processing, mechanical properties of films and composites,[8] as well as some focused topics of NC (e.g., CNC materials).[9−12] Conversion of cellulose microfibers to NCs can increase the surface area by many folds (e.g., NC's specific surface area is nearly 500 m^2/g),[13] and enable multifaceted functionalities through chemical and enzymatic treatments, enhancing the reactivity and changing the physicochemical properties.

NC is a biodegradable nanoscale polymeric fibrous particle, having an aspect ratio of 200−5000,[14] modulus of 70−130 GPa, and degree of crystallinity between 60 and 80%,[15] depending on the extraction process and conditions, as well as biomass sources. The chains in CNF and CNC are aggregated together in a highly specific and ordered manner, exhibiting unique characteristics that open up a multitude of opportunities for the development of sustainable, efficient and affordable water remediation nanomaterials.[7] For example, NC has been demonstrated as an effective coagulant/flocculant, adsorbent, catalyst support, and membrane material, suitable for removing a wide range of organic, inorganic and biological water pollutants in multiple scales, where their removal capacities are sometimes equal or better than the best performing water remediation materials reported in the literature.[16−18] In addition, NC has exhibited tremendous application potentials in electronics, cosmetics, food coatings, drug delivery, adhesives, and tissue engineering, just to name a few.[7]

Basic information on the use of NC and its composites for water purification can be found in several earlier reviews published by Ahankari et al.,[19] Carpenter et al.,[5] Voisin et al.,[17] Tapia-Orozco et al.,[20] Mahfoudhi and Boufi,[15,21] Abouzeid et al.,[22] Köse et al.,[23] Mautner,[24] Tan et al.,[25] Yuan et al.,[26] Ibrahim et al.,[27] Wang,[28] Pandey et al.,[29] Thomas et al.,[30] Ibrahim et al.,[31]

https://doi.org/10.1021/acs.chemrev.1c00683
Chem. Rev. 2022, 122, 8936−9031

and Santos et al.[32] Interested readers can further explore the following books and book chapters, covering compelling and useful details about NC for water purification, by Kumar,[33] Mathew et al.,[34] Muhamad et al.,[35] Wilson et al.,[36] Gopakumar et al.,[37] and Yusuf.[38] However, the chemistry of NC in water remediation is generally absent in these reviews, where the recent reviews of wastewater treatment chemistry did not include the emerging potential of NC.[39,40] Furthermore, most of the above reviews focused mainly on the NC applications for a specific field of water purification without paying attention to the holistic approaches of NC extraction and characterization. Considering the rapid knowledge development in the areas of NC chemistry, structure−property relationships, mechanistic behavior, and sustainable extraction technology development in the past decades, this Review represents a comprehensive review of the current-state-of-the art usage of NC for water purification, as well as our perspective of its future.

1.1. Why the Choice of NC—Is It Thermostable, Biocompatible, and Biodegradable?

Studying the stability of NC at high temperatures is an important criterion for many industrial and consumer applications. This because polymers usually lose conformations, break inter- and intramolecular bonds, degrade its backbone (molecular weight), and decrease viscoelastic properties at high temperatures. The mechanism of thermal degradation in NC has been discussed by Lichtenstein and Lavoine.[41] Generally, NC is comparable with synthetic polymers with good thermal stability as its degradation occurs at relatively high temperatures (between 200 and 300 °C), depending on the preparation routes. For example, Chen et al. reported the onset thermal degradation temperature (T_{onset}) of typical CNC to be ∼275 °C.[42] The T_{onset} is defined as the temperature where the weight loss is ≥1% (i.e., $dW/dT \geq -1$) with an increase in temperature of 1 °C. However, this temperature was found to decrease to ∼220 °C for CNC with sulfuric acid hydrolysis and increase to 322 °C for CNC with oxalic acid hydrolysis.[42] Isogai and colleagues reported the thermal decomposition temperatures (T_d) of 275, 222, and 264 °C for the pristine cellulose, 2,2,6,6-tetramethylpiperidine 1-oxyl (TEMPO)-oxidized CNF (TOCNF with sodium carboxylate groups) and TOCNF (with free carboxyl groups), respectively.[43] The T_d was defined as the temperature where 5.0% weight loss occurred in the thermogravimetric curves. In another study, it was reported that the T_{onset} of CNF (280 °C) was higher than CNC (∼230 °C), and the maximum weight loss that took place for CNF was 331 °C and for CNC was 248 °C.[44]

As NCs offer high temperature stability,[45] good colloidal behavior,[46] consistent viscoelastic property, and versatile interfacial interaction ability with varying polymeric materials; they are often used as nanofillers in nanocomposites made by the wet-state process to improve the thermal stability of the composite in the dry state. However, there are further research opportunities for development of NC-based composite materials with good thermal stability in the wet state and under different environments. This is because most of the studies dealing with NC thermostability were carried out in the dry state,[42−44] and under the nitrogen environment.[42,43] However, in some application, such as water purification and gel applications, the process can involve the heating of NC or its composites in the presence of oxygen and water. Thus, in-depth investigations of the thermal stability in the wet state or under oxygen environment are warranted. Recently, it has been reported that dispersed NC in water could start to degrade at 110 °C under air atmosphere, but NC appeared to possess comparable thermal stability at high temperature and high pressure conditions when compared with other polymers, such as xanthan and guar gum.[47] However, it has also been shown that the thermal stability of NC varied depending on their source, functional state, methods of production, and drying process, etc.[42,43,46] Therefore, different degradation temperatures for NC are expected, and one has to consider all of these parameters for the determination of appropriate NC thermal stability.

Unlike synthetic polymers, NC lacks toxicity, and is biocompatible and biodegradable. A material is biocompatible when it neither triggers immunological responses nor is toxic to living tissues after exposure to blood or other bodily fluids. Negligible inflammatory and foreign body responses of cellulose-based materials are claimed in the literature and thence considered as biocompatible.[48] Some in vivo biocompatibility tests have shown that a range of modified celluloses and regenerated celluloses including hydroxyethyl cellulose, cellulosic polyion complexes, methyl cellulose, aminoethyl cellulose, and ethyl cellulose have minimal foreign body reaction.[49] Helenius and colleagues performed in vivo biocompatibility tests for nanostructured cellulose isolated from *Acetobacter xylinum*. There were no macroscopic inflammatory signs around the implanted rats. The BNC was well integrated with rats tissue and no chronic body responses were observed during the study.[48] Another report has been published on peptide-modified bacterial cellulose (BC) membranes, and minimal effects of irritating tissues were observed.[50] Similar observations are found true for BC-based biocomposites.[51] Contrary to BC, few minimal studies on CNF and CNC have been found in the literature. Chen et al. claimed that citrate-based fluorophore-modified CNC can be considered as safe biomaterial as they observed good cell viability, attributing quite low cytotoxicity.[52] Non/low-cytotoxicity has also been found viable for chitosan/CNC, poly(vinyl alcohol)/CNC and polyethylenimine/CNF composites.[53−55] After testing the cytocompatibility of microfibrillated cellulose (MFC) films, it is concluded that the trimethylammonium-modified MFC is more cytocompatible as compared with carboxymethylated and pristine MFC.[56] Selecting carboxylated NC is found judicial as it makes enhanced biocompatibility as reported in some publications.[53]

To consider NC as a biodegradable material, it has to be degradable by bacteria, fungi, or other kinds of organisms. In a review by Lindström and Österberg, the consideration of NC being a biodegradable polymer has been well received.[57] This is because the crystalline and amorphous regions of NC can be enzymatically degraded by many microorganisms available in soil. Moreover, nanoscale dimension of cellulose would increase the exposure of its milieu.[58] A study showed that the BC film in soil could be completely degraded in 4 weeks.[59] Several other studies also reported the biodegradable properties of NC.[60,61] For example, the addition of CNC into a starch and glycerol film could increase the biodegradability of the film, whereas CNC immobilized bacteriocin could cause a moderate decrease of biodegradability due to antibacterial activity of bacteriocin.[62] In another study, it has been shown that the addition of NC considerably increased the biodegradability of poly(vinyl alcohol)/NC composite.[63] In the case of CNF, it has been shown that the addition of pristine and modified CNF (acetylated) could decrease the fungal degradation ability of thermoplastic starch film. It was thought that the denser architecture and higher crystallinity of CNF might restrict the enzyme activity, which would slow down the hydrolysis rate.[64]

https://doi.org/10.1021/acs.chemrev.1c00683
Chem. Rev. 2022, 122, 8936−9031

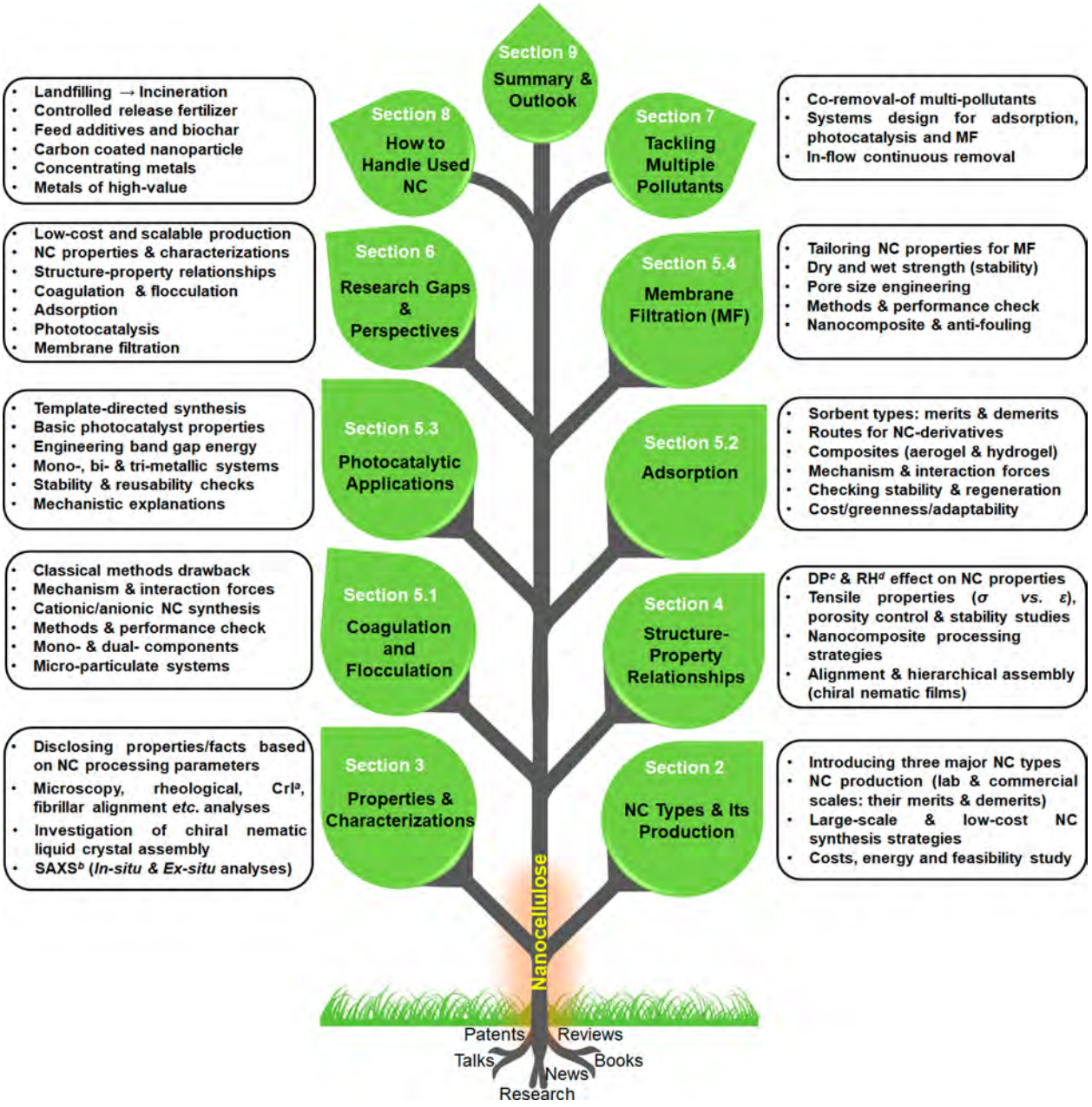

Figure 1. Schematic illustration of a guide tree depicting the summaries of major sections in this Review. It shows 11 leaves (light green color), representing broad titles and subtitles of the Review. The important topics that are discussed in these sections are highlighted in rectangular boxes at the right and left sides of the leaves ([a]crystallinity index, [b]small-angle X-ray scattering, [c]degree of polymerization, and [d]relative humidity). The roots of the tree depict the sources from where information is extracted for writing the sections.

Some other studies showed that the crystallinity regions favored the formation of a dense water layer, which would thwart the cellulose-degrading enzyme accessibility.[65] Similar to this, it has been shown that adding BC with starch could cause a slight decrease of biodegradation behavior after incubation in soil. The authors hypothesized that since BC has a higher crystallinity region, it might resist the microorganisms attack in the soil.[66]

On the basis of this studied literature, we think that NC has good compatibility with living tissues. However, the extent of biodegradability varies depending on its type, pretreatment methods, functionalities, etc. However, as humans lack cellulolytic enzymes in our body, we cannot digest it properly. Many derivatives of NC are reported, yet their investigations based on the effects of sample preparation and methodologies on NC biodegradability are sparsely studied. For example, NC has been studied as a scaffold for metals/metal oxides nucleation, but the biocompatibility and biodegradability of the NC-nanoparticles composites were not given due attention. Moreover, different NC types would have varied topography, sizes, crystallinity, surface chemistry, and surface charge. NCs have shown positive effects on the adhesion and proliferation of human cells.[67] However, contradictory statements can also be found in the literature, such as some periodate oxidized and carboxymethylated NC have been reported to cause inflammation and may be responsible for chronic complications.[68,69]

1.2. How to Use This Review

This Review aims to thoroughly discuss the preparation, properties, characterizations and relevant applications of NC

https://doi.org/10.1021/acs.chemrev.1c00683
Chem. Rev. 2022, 122, 8936−9031

Table 1. Comparison of Some Morphological Parameters and Physical Properties of CNF, CNC, and BNC[a]

NC type	length	cross-section	degree of polymerization	crystallinity/crystal structure
CNF	0.1−2 μm	5−60 nm	>500	primarily Iβ, lowest degree of crystallinity
CNC	100−250 nm	5−70 nm	500−1500	primarily Iβ, medium degree of crystallinity
BNC	different kinds of nanofiber in network	20−100 nm	4000−10 000	Iα (shell) and 1β (core), highest degree of crystallinity

[a]The results are adapted with permission from ref 71.

Table 2. Comparison of Some Structural Parameters of Wood-Based CNF, BNC, and *Cladophora* Algae[a]

material	crystallinity index (%)	size of crystalline region (nm)	length (nm)	diameter (nm)	surface area by H_2O (m^2/g)
CNF from wood	≈ 50−80	≈100	100−2000	5−70	0.5−1
BNC	≈ 84−89	≈300	900	10−100	
Cladophora algae	>95	≈600	4000	15−30	95

[a]Values are taken from refs 71 and 72.

(mainly CNF and CNC) through proper understanding of fundamental knowledge in purity and crystallinity, surface chemistry and surface charge, particle rheology, and morphology and mechanical properties and stability for clean water production. To achieve this aim, we have considered foregoing limitations of existing reviews and also critically evaluated the relevant literature (i.e., 840 including Supporting Information) that has been published during the last 20 years, while giving priorities to highlight those of very recent important articles (last five years). The synopsis of each major section of this review follows the guideline tree as shown in Figure 1. Section 2 provides a substantial discussion on general classification of NC materials and low-cost NC production methods. Section 3 outlines the characterization results of NC properties with an emphasis on synchrotron X-ray scattering (in situ and ex situ) and high-resolution microscopy. Mechanistic interpretations and corresponding structure−property relationships of NC are discussed in section 4. In section 5, we draw a clear picture of NC (both modified and unmodified) and their composite materials contribution to offer a multitude of improvements, especially in the fields of coagulation and flocculation, adsorption, photocatalysis, and membrane filtration for water purification. We give our perspectives on the challenges and knowledge gaps that have been buried in ever-expanding literature and highlight new scopes for future NC-based research development in section 6. We discuss avant-garde and research breakthroughs for tackling multiple wastewater pollutants in section 7. In section 8, the opportunities to upcycle/recycle post- or spent materials after reuse are corroborated. Section 9 covers the summary and outlook of this review. This Review is of general interest to the wide scientific community especially in the fields of chemistry, material, and polymer sciences. The discussed topics will not only help established researchers but also early career investigators who are in the field or are looking for new research opportunities to explore.

2. GENERAL CLASSIFICATION OF NC MATERIALS AND NC PRODUCTION TECHNOLOGY

Before describing different production routes of NC, it is appropriate to first introduce the morphological parameters and some physical properties of three different subcategories of NC as shown in Table 1. On the basis of their sources, there are some important differences between CNF (extracted from wood), BNC, and NC in algae (e.g., *Cladophora*), where the comparisons are illustrated in Table 2. Readers interested to know the details of these nanoscale celluloses are referred to an earlier review.[70]

2.1. Cellulose Nanofibers (CNF)

The major processes to extract CNF materials are mainly from woody biomass sources; however, there is a growing interest in using nonwoody biomass feedstocks, such as agricultural residues. There are several excellent reviews detailing the varying production routes to extract CNF from different feedstocks.[73−75] In these production routes, the raw feedstocks must first be pretreated to remove the lignin component by adopting one of the many different pulping processes. There have also been a myriad of different organosolv-pulping procedures reported, mostly developed during the 1980s−1990s in Germany. Only a few procedures have been adopted in full scale in Germany, while most of them failed to be commercialized for varying reasons. There is another promising solvent process involving the use of sulfur dioxide-ethanol−water (40−65%) mixtures,[76,77] which has been under the consideration of American Process Inc. (API). This process has several advantages: (a) the recovery of the solvents is simple as sulfur dioxide and ethanol can be recycled, which decreases the operational costs and (b) the rapid impregnation of the feedstocks by ethanol can lead to rapid pulping and easy handling of wood chips of large diversity.[78−82] The historical evolution of producing MFC, nowadays called CNF, started in the late 1970s.[83,84] The original investigators simply used a high-pressure homogenizer to delaminate the bleached kraft pulp and were successful to obtain an NC hydrogel. To delaminate the fibers, which are typically assembled by the cohesion forces, it is reasonable to use low energy consumption methods like chemical or enzymatic pretreatments. The pretreatments can be accomplished by two pathways: (a) electrostatically induced swelling of the fibers through the incorporation of charged groups by chemical oxidation or grafting and (b) mild acid or enzymatic treatments. Typically, the pristine cell wall of higher plants can contain a small amount of surface charge. However, during pulping and bleaching processes, the ester groups in residual hemicellulose can be hydrolyzed leading to a lower charge density. This can explain the observation that unbleached pulps are easier to defibrillate as compared to bleached pulps because unbleached pulps have a higher level of swelling and therefore a less degree of cell wall cohesion.[85] One widely accepted theory to explain the above observation is that the existence of lignin (<20 wt %) can contribute to the delamination of cellulose fibers because of the radical scavenging capability of residual lignin, preventing the cohesion between cellulose radicals during mechanical defibrillation.[86] Another factor relevant to chemical treatments is that dried fibers have higher cohesion because of the well-known "hornification"

https://doi.org/10.1021/acs.chemrev.1c00683
Chem. Rev. 2022, 122, 8936−9031

phenomenon of fibers during drying.[87] Therefore, never dried fibers are preferred for pretreatment procedures. Likewise, drying of NC materials is also subjected to hornification, which can result in considerable difficulty in NC manufacturing. High charge content will alleviate the hornification phenomenon. Interestingly, it has also been reported that the addition of lignin can assist the dispersion of NC and prevent hornification.[88]

The delamination methods commonly used to defibrillate the cellulose fibers can be divided into two classes: (a) conventional methods, such as homogenization,[83,84] refining,[89,90] and microfluidization,[91] and (b) modern methods, such as extrusion,[92] steam explosion,[93] ball milling,[94] ultrasonification,[95,96] aqueous counter collision,[97] cryo-crushing,[98,99] and high speed blenders.[100] All these delamination methods have advantages and disadvantages. The most common methods are homogenization and microfluidization, which are effective in fiber defibrillation, but also suffer the impediment of chamber clogging and high energy consumption (*it was not until the adoption of pretreatment step when these methods became a standard process to manufacture NC*). To deal with the clogging issue, one approach is by incorporating hydrophilic polymers or cellulose derivatives, such as carboxymethyl cellulose (CMC), methyl cellulose, hydroxymethyl cellulose, hydroxypropyl cellulose, poly(acrylic acid), carrageenan, and guar gum, in the cellulose fiber suspension, which can alleviate the clogging problem to some extent.[101]

The chemical process can be very effective to defibrillate the cellulose fibers (pulps) into NC. One example is the incorporation of charged groups on the cellulose chains by oxidation process, for example, TEMPO-mediated oxidation.[102] The cell walls in cellulose fibers after pulping possess instinctively occurring charged groups (e.g., carboxyl groups, formed by ester cleavage of hemicellulose moieties during pulping). Additional surface charge through different chemical modifications, including carboxylation via periodate-chlorite oxidation,[103,104] sulfonation,[105] carboxymethylation,[106] TEMPO-oxidation,[102] cationization,[107] nitro-oxidation,[108−110] and phosphorylation[111] would result in easy defibrillation of cellulose fibers using low-energy mechanical treatments. It has been reported that the initial charge content in wood pulp fibers is typically between 30−250 μeg/g, where it can be increased to 300−2000 μeg/g after subsequent chemical treatments.[112] The presence of a high charge in cellulose fibers can significantly decrease the energy consumption to defibrillate cellulose fibers into NC.

2.2. Cellulose Nanocrystals (CNC)

CNC was first reported by Nickerson and Habrle in 1947[113] and was then deconstructed by the seminal work of Rånby who used sulfuric acid.[114] The concentration of sulfuric acid is vital in the CNC production. It has now been widely accepted that the most common sulfuric acid concentration in hydrolysis is around 64 wt %.[115] At around the same time, Battista[116,117] demonstrated the hydrochloric acid hydrolysis route, which has become commercialized, to produce so-called microcrystalline cellulose (MCC) products. It is interesting to note that CNC demonstrated by Rånby is much thinner and shorter than MCC. This is because the hydrolysis with hydrochloric acid creates fewer charged groups on MCC than those on CNC using sulfuric acid to induce hydrolysis (the process creates charged sulfate half-ester). The higher charge density can repel CNC particles, prevent aggregation and stabilize the dispersion, whereas MCC particles often aggregate into clusters in the dispersion phase. Marchessault and co-workers first observed that liquid crystal phases could be obtained from fibrillar polysaccharides,[118] where Dong and co-workers reported that the CNC suspensions could form a stable chiral nematic liquid phase.[119,120] The history and the various preparation routes to tailor the physical behavior and performance of CNC have recently been reviewed.[121] It was found that the critical nematic liquid phase starts at a critical CNC concentration, which strongly depends on the extent of ultrasonication (see Figure 2). When the volume fraction of the liquid phase exceeds the value of 1.0, the chiral nematic phase disappears and a birefringent nematic phase can be developed.

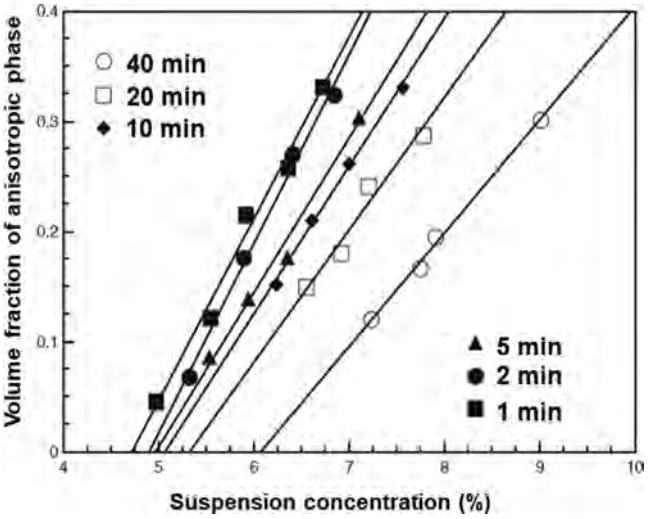

Figure 2. Relationship between the concentration of total suspension and the anisotropic phase's volume fraction for the suspensions prepared by ultrasonication for different times. The straight lines represent the fitted results of the experimental data. The figure is reproduced from with permission from ref 122. Copyright 1998 Springer Nature.

Early investigations to fabricate CNC using sulfuric acid indicated that there is only a narrow processing window, that is, the sulfuric acid concentration is 60−64 wt % and the hydrolysis temperature is 45−65 °C, which permits the efficient yield of CNC.[9,123] For the bleached kraft pulp, the best CNC yield has been obtained at a sulfuric acid concentration of 58−62 wt % and temperature of 50−60 °C.[124,125] Recently, several studies reported that CNC with the cellulose II crystalline structure (CNC-II) could also be formed during concentrated sulfuric acid hydrolysis. For example, Sebe et al. discovered that CNC-II formed at narrow reaction conditions (regarding the amount and the added time of sulfuric acid) during hydrolysis of MCC, and the resulting CNC-II was ribbon-like, substantially smaller than typical needle-shaped CNC with cellulose I structure.[126] Later, Xing et al. reported the creation of CNC-II when using 56−64 wt % sulfuric acid hydrolysis to treat Tetra pak and eucalyptus wood at a short hydrolysis time (<20 min) at 45 °C.[127] Apart from the sulfuric or hydrochloric acid, there has been some interest in using other mineral acids (such as phosphoric acid[128] or hydrobromic acid[129]), acid blends (citric/hydrochloric acid),[130,131] organic acids (e.g., oxalic acid),[132] oxidizing agents (TEMPO-oxidation),[102] and ionic liquids (tetrabutylammonium acetate)[133] to prepare CNC. A comprehensive review of the varying production routes of CNC could be found in a recent article by Vanderfleet and Cranston.[121] Overall, the production of CNC has been mainly focused on

https://doi.org/10.1021/acs.chemrev.1c00683
Chem. Rev. 2022, 122, 8936−9031

sulfuric acid hydrolysis, which has been found to be a reliable approach to create chiral nematic liquid crystals.

2.3. Bacterial Nanocellulose (BNC)

BNC has many different forms and is widespread in nature. There are several reviews on these materials.[134−136] Two major approaches to produce BNC involve the fermentation of (a) sugars and (b) plant carbohydrates via microorganisms (e.g., representative cellulose-producing bacteria include *Gluconacetobacter hansenii*, *Rhizobium*, and *Rhodobacter*). For example, one can use static cultures to fabricate a never dried thick BNC pellicle at the air−liquid interface (*BNC is biosynthesized in a continuous mode*) or the agitated culture medium to form irregular pellets (*BNC is biosynthesized in a dispersed mode*). The choice depends on the specific application and the required properties, for example, the BNC production using an agitated culture usually results in lower mechanical strength than the one synthesized by static culture. Usually, the agitated fermentation approach gives rise to a lower yield and a higher chance of mutation than those by the static fermentation method. The unique properties of BNC include pure cellulose and high-water holding capacity (up to 99%) in never dried and mechanical robust hydrogels. The gel bodies are generated in the planar form (pellicles) and can be molded into various shapes, depending on the templates. Drying of BNC can be accomplished by several approaches: air and press drying, lyophilization, and critical point drying (e.g., supercritical carbon dioxide drying), where dewatering of BNC can be attained by stepwise solvent exchange. Drying can irreversibly change the structure and property of the resulting BNC product. As a result, the pellicles are invariably difficult to disperse, which constitutes a problem for membrane production on large scale, whereas the solvent exchange treatment appears to be one of the limited ways to disperse the BNC pellicles.

2.4. Selective NC Fabrication Facilities at Commercial Scale

Large-scale NC fabrication basically creates only two classes of materials: CNC with high crystallinity and low aspect ratio, and CNF with relatively lower crystallinity and high aspect ratio. CNC only became commercially available in 2012 by CelluForce in Quebec. One example production facility is the Forest Products Laboratory (FPL) in Wisconsin. One process adopted by FPL involves sulfuric acid hydrolysis (e.g., 64 wt %) of machine dried prehydrolyzed Kraft rayon-grade wood pulps at 45 °C for 90 min. In this process, aqueous hypochlorite solution is used to quench the reaction, where neutralization is carried out by slow addition of 5−8 wt % sodium hydroxide in water. Finally, tubular ultrafiltration (UF) and reverse osmosis (RO) membranes are often used to perform the final purification and concentration enhancement process. The total time required for each batch CNC production is about 8 h for CNC main reaction and neutralization, 24−48 h for the initial workup, and another 24 h for the purification of the product.

- *Advantage*: This process uses the popular acid hydrolysis method, which has been well documented.
- *Disadvantages:* This process requires a long processing time and can be expensive due to the high cost of sulfuric acid, which is the main ingredient in reaction and is not recyclable, and large water consumption.

The University of Maine is one of the largest producers in the U.S., able to provide industrial-scale quantities of mechanically extracted CNF with the capacity of about 1 ton/day. Similarly, Innventia at Sweden can also supply mechanically/enzymatically provided CNF materials with about the same capacity.

- *Advantage*: A simpler and cleaner method compared to chemical treatments.
- *Disadvantage*: High consumption of energy and large distribution in fibers dimensions.

Around the world, there are numerous scaled-up pilot plants, as well as commercial scale manufacturing plants, such as Borregard (Norway), Namicell (France), and Stora Enso (Sweden/Finland), that can produce various CNF materials. However, their detailed processes have not been disclosed. The classes of TOCNF materials have long been produced using large-scale manufacturing in Japan by Nippon Paper and Oji Paper.

- *Advantage*: The TEMPO oxidation process produces the most refined thin nanofibrils with low polydispersity, where the produced CNF can be used to fabricate transparent gels and films.
- *Disadvantage*: The TEMPO agent is expensive and not easily recyclable, although Nippon paper has developed a process for recycling of TEMPO agents.

2.5. Emerging Low-Cost NC Production Technologies

As many people consider safe drinking water a basic human right, the advancement of NC technologies for water purification must start with low-cost NC that can be produced at large scale and in an environmentally friendly manner. No such production technology exists today. However, some emerging NC extraction technologies, especially those suitable to treat underutilized biomass feedstock at low cost, show great promise to achieve this goal. We will start this section by briefly reviewing the current-state-of-the art NC production technologies and facilities. Several recent technologies, actually based on old biomass processes demonstrated in the 1950s and 1960s, have emerged as new cost-effective methods that can produce NC at a large scale with significant savings in energy, chemicals and water. Two such technologies are exemplified as follows.

The nitro-oxidation process (NOP) demonstrated in our laboratory has been shown to be a simple and low-cost approach to extract CNF directly from untreated biomass, including both woody plants and nonwoody plants (e.g., jute, spinifex grass, bamboo, moringa, and sorghum stalk).[108,109,137−139] In this method, only two chemicals: nitric acid and sodium nitrite are involved; both are also ingredients that can be used to synthesize fertilizers. NOP combines the steps of pulping and cellulose oxidation. Nitric acid pulping has a long history, dating back to the 19th century, where the presence of nitrogen oxide species can depolymerize the lignin component by converting the syringyl units in lignin into soluble benzoquinone products, and the hemicellulose component can be broken down by nitric acid into xylose and other byproducts, both soluble in water. Despite extensive efforts,[140−143] this technology never became a successful pulping technology. There are several reasons for this, including the high cost of nitric acid (unless produced on-site), nonuniform pulping from wood chips, the need of good impregnation of starting wood chips, and deteriorated pulp strength properties due to cellulose hydrolysis and toxicity problems from nitrogen oxides.[144] Nonetheless, the reaction between nitric acid and sodium nitrite can generate HNO_2 and nitroxonium ions (NO^+), where the latter can selectively oxidize the primary hydroxyl groups of the cellulose to introduce a negatively charged surface to induce defibrillation.

https://doi.org/10.1021/acs.chemrev.1c00683
Chem. Rev. 2022, 122, 8936−9031

As NOP is a one-pot method, where simultaneous pulping of biomass and oxidation of cellulose fibers occurs, the approach greatly reduces the consumption of energy, water, and chemicals for CNF extraction. This process has been demonstrated at the lab scale, while large-scale production is still under investigation in our lab. This method appears to be more suitable to process nonwoody plants with a low degree of lignin content. However, the reaction conditions of NOP can be adjusted to treat different biomass feedstocks including woody plants. Importantly, the effluent from NOP can be easily neutralized into nitrogen-rich salts (i.e., plant fertilizer), which essentially eliminates the need for recovery of reacting agents and thus lowers the overall production cost. In 1961, Brink et al. investigated the use of the spent liquor as plant fertilizer.[145] Thus far, the demonstrated CNF products by NOP appear to have residual lignin and hemicellulose contents,[138] indicating the process is not yet optimized to produce pure CNF. Fortunately, our studies also showed that pure CNF is not necessarily required for water purification applications, indicating that NOP may play a key role to design a circular economy by upcycling underutilized agricultural residues into water purification materials.[108,139]

Another potentially low-cost large-scale NC extraction technology is thru the use of peracetic acid to defibrillate wood fibers, recently demonstrated by the Berglund group.[146−148] This method was first investigated in the 1950s by Rapson,[149] for the bleaching operation of biomass, where a good review of this technology was made by Suchy and Argyropoulus in 2002.[150] This method was found to be relatively expensive when compared to other methods because of the high chemical cost and transportation complexities, preventing the broad industrial utilization of peracetic acid for bleaching sequences.[150] Albeit the higher cost for bleaching, this process may be quite feasible for low-cost NC production, depending on the evaluation of the energy requirement for defibrillation. The advantage of this process is that the recycling of the spent liquor may be easier than other NC extraction methods since peracetic acid can be distilled and reused (e.g., by addition of peroxide to create more peracetic oxide). Perhaps, this approach will also be more suitable to process nonwoody biomass plants with lower lignin content, such as agricultural residues, than woody plants. Recently, a review on the peracetic acid bleaching technology by Sharma et al. indicates that the process can be environmentally friendly.[151]

2.5.1. Strategies to Develop Large-Scale Low-Cost NC Production from Diverse Biomass Feedstocks. We are confident that besides the two emerging low-cost NC production technologies discussed above (see section 2.5), more cost-effective NC extraction techniques will be developed. Although these techniques may exhibit good commercialization potentials on the lab scale, only a few will be suitable for real large scale yet low-cost operations that can extract NC from a variety of raw biomass feedstocks. In this section, some strategies, partially based on the experiences from CNF production using TEMPO oxidation and CNC production using acid hydrolysis of cellulose fibers (after pretreatment), are outlined below for the evaluation of the development of a successfully ascendable process that will be useful to produce low-cost materials for water purification. The plan is illustrated in Figure 3, where the key features of each element are discussed separately.

Biomass Choice. There is truly a wide range of biomass feedstocks, some are more suitable for low-cost NC extraction than others using the technologies illustrated in section 2.5.

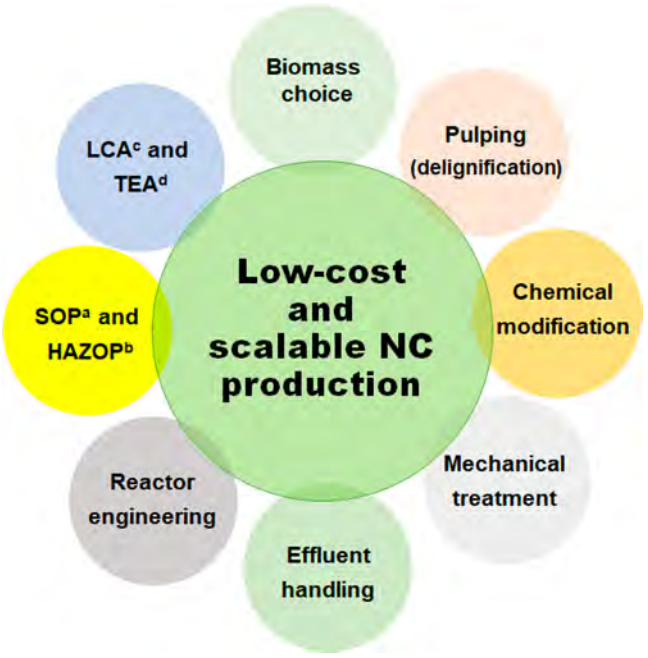

Figure 3. Overall strategic plans for the development of low-cost and large-scale NC production from diverse biomass feedstocks. Here, (a) SOP, standard operating procedure; (b) HAZOP, hazard and operability study; (c) LCA, life cycles assessment; and (d) TEA, techno-economic analysis.

Generally, biomass sources with lower lignin content and more porous cell wall structure, such as most nonwoody plants, will suit this purpose (nonwoody plants usually possess lower amounts of lignin than woody plants; see Table S1). Interestingly, some studies have shown that NC extraction can be achieved in the pretreatment steps. For example, the high-aspect ratio of NC from untreated *Triodia pungens* (spinifex grass) can be easily produced after a mild pulping process using sodium hydroxide, followed by passing through a high-pressure homogenizer at low pressure for 1 cycle.[152] Hence, the appropriate biomass choice is highly critical to evaluate the NC production scalability and its economic returns. Some key features, such as availability and flow of locally available biomass feedstocks, handling, supply chain, and storage operations should be considered while planning for scale-up production of NC.

Pulping. The most popular pulping process adopted today is Kraft pulping, which includes the use of chlorine dioxide, oxygen, ozone, peroxide, and also alkaline extraction in various different stages on wood fibers.[153] The pulping of fibers is usually followed by the bleaching step, which includes the use of chlorine dioxide oxygen or ozone peroxide, or alkaline extractions.[154] Another pulping process involves sulfite pulping, where the wood chips are first digested using sulfite or bisulfite liquors.[155] The yield in this process may be low for certain acidic pulping procedures but can be very high when alkali is combined with an acidic stage, delivering high hemicellulose yields. In the case of nonwoody plants, the delignification may require less chemical consumption, for example, nonwood biomass plants can be pulped with simple chemical systems using only caustic soda. This step can be considered if the NC extraction step is mainly effective on cellulose fibers (i.e., pulps).

Chemical Modification. Commonly adopted chemical modification schemes for defibrillation of cellulose fibers involve

https://doi.org/10.1021/acs.chemrev.1c00683
Chem. Rev. 2022, 122, 8936−9031

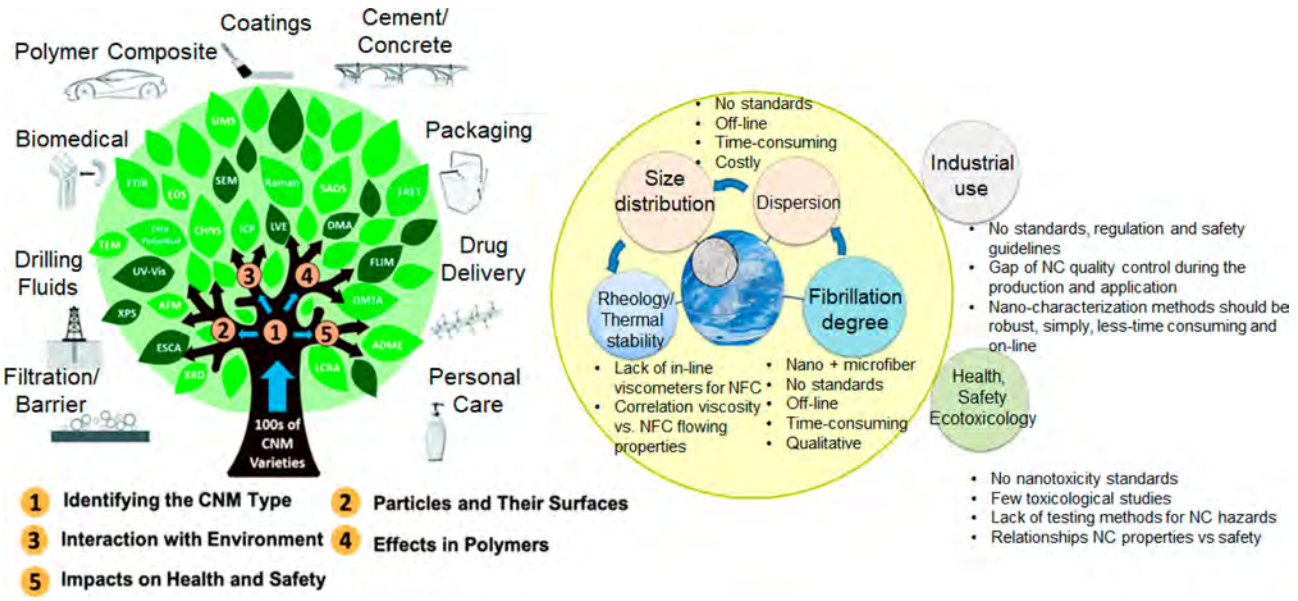

Figure 4. Current status (left) and challenges (right) of NC characterization. Reprinted with permission from ref 7. Copyright 2018 The Royal Society of Chemistry (left). Adapted from ref 161. Copyright 2021 NC State University (right).

oxidation (e.g., periodate oxidation, TEMPO oxidation, nitro-oxidation, and carboxymethylation), sulfonation, and phosphorylation.[23] Chemical modification of the cellulose fibers approach is the easiest pathway to reduce the energy consumption of the defibrillation process, becoming the foundation for low-cost and scalable NC production. The proper choice of modification schemes can combine the processes of pulping and cellulose oxidation and significantly reduce the preparation steps for NC extraction directly from raw biomass. (a) NOP: The mixture of nitric acid and sodium nitrite in NOP significantly reduces the consumption of water, chemicals, and energy to produce carboxycellulose nanofibers or CNF as compared to TEMPO oxidation or carboxymethylation approaches.[109] (b) Sodium hypochlorite oxidation: Highly concentrated NaClO, followed by low energy mechanical treatment, can also extract NC with high content of carboxyl groups and good aspect ratio from untreated biomass.[156] We note that TEMPO oxidation uses the combination of sodium hypochlorite/sodium bromide/TEMPO to produce carboxyl NC from treated cellulose fibers. It was also noted that the NaClO treatment can greatly reduce the consumption of water and energy, as well as enable the easy recovery of the reactant. The disadvantage of NaClO oxidation is that the use of sodium chlorite has been abandoned from pulping by most pulp mills in the world because of its high toxicity.

Mechanical Treatment. Most NC production processes require the use of different mechanical treatments to defibrillate unmodified cellulose fibers or chemically/enzymatically modified cellulose fibers. The energy needed to defibrillate the unmodified cellulose fibers is much higher than those to defibrillate the modified cellulose fibers. For example, the energy consumption reported for MFC production from the Kraft and sulfite pulp is 12000−70000 kwh/t, enzymatic/refining of sulfite pulp is 1500 kWh/t, and carboxymethylation of sulfite pulp is 500 kWh/t.[70] Hence, this fact should be considered while choosing the suitable mechanical treatment for the process development of NC scale-up production. Typical treatments include ultrasonication, high-pressure homogenization, and microfluidization, to name a few.

Effluent Handling. Effluent is a key component in NC extraction, and it can greatly impact the final production cost and the environmental friendliness of the pulping process. For instance, the process will be less cost-efficient and not environmentally friendly if heavy water consumption for washing and purification is required. Since the effluent will contain a large amount of reacted/unreacted chemicals and degraded biomass components, it must be properly treated before it can be discharged. Optimum effluent treatment would be to reuse unreacted chemicals and to convert/recycle effluent (e.g., by neutralization) into valuable byproducts. In addition, the process should involve a small set of reactants to ease the recycling or neutralization steps. In section 2.5, the NOP approach is appealing for commercialization because the effluent can be converted into nitrogen-rich salts (as plant fertilizer) by simple neutralization, whereas the effluent from other approaches, such as TEMPO oxidation, requires a reduction treatment or ion-exchange resin treatment followed by electrodialysis.

Reactor Engineering (Reactor Design and Reaction Optimization). To perform NC extraction from a diverse source at a large scale, a robust and leak-proof reactor system design is necessary, along with the presence of subject expertise to execute the process safely under proper operational procedures and reaction capacity. As the available biomass feedstocks contain a wide range of compositions with different cellulose, lignin and hemicellulose contents; the optimal operational conditions to treat different feedstocks will be quite different. As the matrix of sample compositions, reaction parameters, product structure, morphology, and functionality will be messy in this task, one logical approach is to use machine learning and data mining to help analyze extensive experimental results to identify the cause-effect relations and key feature parameters for the optimal control of the process and make new predictions.

Standard Operating Procedure (SOP) and Hazard and Operability (HAZOP) Study. The development of thorough SOP and HAZOP documentation is crucial for operating the NC extraction process safely and efficiently, and for maintaining

https://doi.org/10.1021/acs.chemrev.1c00683
Chem. Rev. 2022, 122, 8936−9031

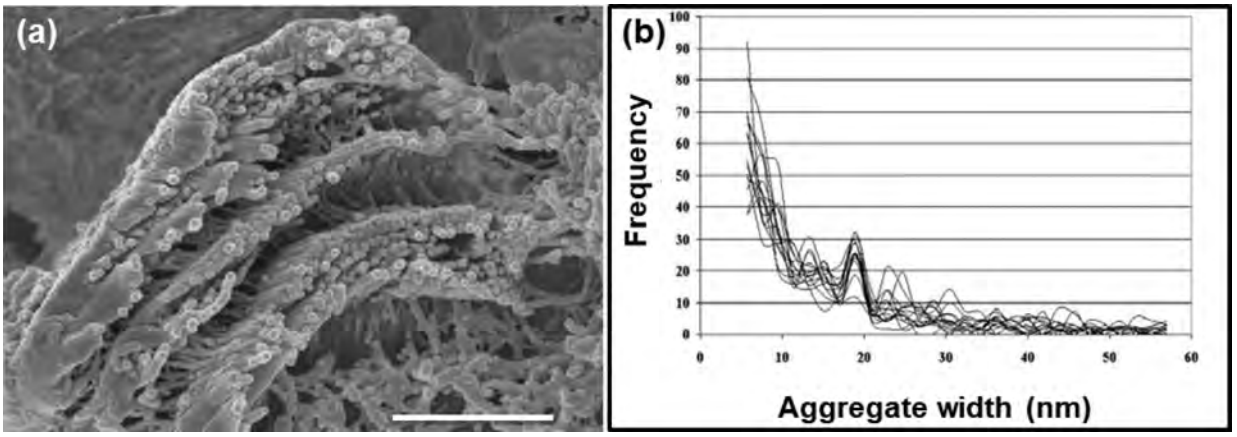

Figure 5. (a) Electron microscopic image of a Norway Spruce wood fiber. It shows the aggregated CMF (macrofibrils) (scale = 1.38 μm) (Courtesy: Geoffry Daniel, Swedish University of Agricultural Sciences, Uppsala, Sweden). (b) Frequency distribution curves of widths of CMF found in the secondary cell wall (i.e., S2 layer) of pulp fibers (Norway Spruce). Around 300 measurements on the cell wall layer/pulp are taken and displayed. One can see the common sharp peak between 18 and 20 nm. The figure is reproduced with permission from ref 174. Copyright 2018 Walter de Gruyter GmbH.

consistent output and uniform performance. These documentations can simultaneously decrease the risk of miscommunication and ensure the required industrial compliance. In specific, the proper SOP compilation will permit the operator to follow step-by-step instructions to carry out routine operations, where the HAZOP study will allow a systematic approach to identifying possible hazards associated with each step and each variation during the scale-up NC production.

Life Cycles Assessment (LCA) and Technoeconomic Assessment (TEA). For the NC scale-up production, process-based LCA should be carried out to study the cumulative energy, economic flows, and greenhouse gases impacts associated with the process from varying biomass feedstocks, especially those from underutilized sources such as agricultural residues, wood waste, and recycled cellulosic materials. Such LCA will provide a thorough understanding of the environmental impact by the extraction process, covering the complete life cycle of NC, from different sources of feedstock. This type of analysis can form the foundation for the success of sustainable long-term process development. Meanwhile, TEA will allow the examination of production costs, benefits, risks, uncertainties, and time frames for NC production. There are several reports on the LCA analysis of NC production based on different processes.[157−160]

3. NC PROPERTIES AND ITS CHARACTERIZATION PRIORITIZING CRITICAL PROCESSING PARAMETERS

In this section, we discuss the typical techniques for characterization of the two major forms of NC materials including CNF and CNC. Several recent reviews have addressed the challenges, standards, status, and guidelines on this subject.[7,161−163] A schematic overview of NC characterization is shown in Figure 4. This figure reveals some major applications of NC, which are well corroborated in the Supporting Information (section S1). It also shows some safety and ecotoxicological impacts of NC. Some authors analyzed these facts and observed low biological impacts and environmental risks of NC.[164,165] However, a recent review by Foster et al.[7] highlighted a state-of-the-art summary of characterization techniques for NC. The report was aimed to bridge the scientific knowledge gaps between academic research projects and industrial applications for the development of NC-based products. This work laid a solid foundation of the guidelines and protocols for structural, morphological, physical, and chemical characterizations of NC. Balea et al.[161] and also identified the critical challenges associated with the characterizations of NC materials that prevent their upscaling and commercial applications. An emerging aspect of NC characterization is to deal with their structure, molecular interaction, colloidal behavior, self-assembly, and morphological features in the wet state or in the dispersion form, preferably in real-time. For example, characterization of NC materials in their "never dried" state is critical for understanding the impacts of various drying techniques (air drying, freeze-drying, spray drying, etc.) on structure changes.[166] On this subject, morphological characterization was carried out by high-resolution electron microscopic techniques using samples prepared during varying dehydration processes. Characterizations of the chiral nematic liquid crystal phase and structure alignment of NC materials with short aspect ratios in the dispersion state, enabling photonic, and biomedical and sensing applications, have also been discussed.[167−170]

In this section, we emphasize the recent development of characterization strategies and tools that have been developed specifically for the understanding of the processing effect. This section is meant to complement the next, section 4, on the subject of "structure and property" relationships. First, we highlight some characterization results of NC properties and discuss NC characterization from the perspective of critical processing parameters, that is, what kind of characterization techniques need to be chosen based on different feedstock selection, or processing history. Second, some recent advances on the characterization of NC are reviewed. Finally, a special focus is given to the solution small-angle X-ray scattering (SAXS) for NC characterization and its implications for morphology, self-assembly and ordering, and colloidal behavior in the dispersion state.

3.1. Structural Features of Cellulose and NC Properties

Cellulose is a polymer chain, consisting of β-1,4 linked glucose repeat units, in a nearly flat ribbon-like shape, and its native molecular weight can exceed 10 000 g/mol. In the chain conformation, the glucose unit is linked with a β-1−4-glycosidic bond, where all hydroxyl groups are equatorial to the pyranose ring plane and considered the hydrophilic plane (the

https://doi.org/10.1021/acs.chemrev.1c00683
Chem. Rev. 2022, 122, 8936−9031

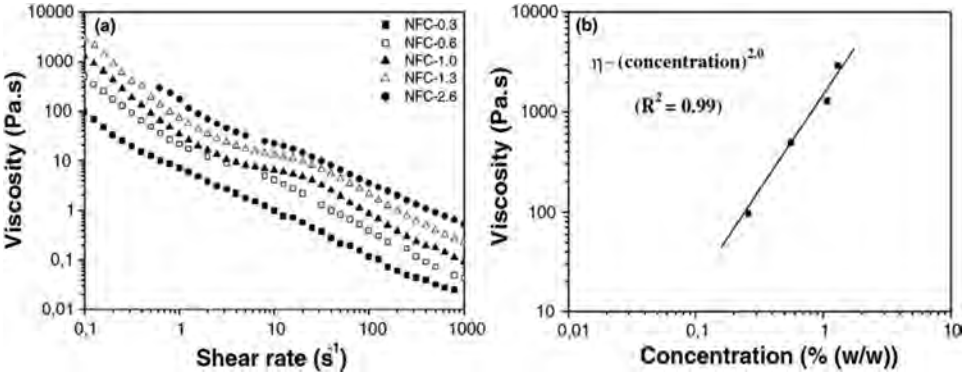

Figure 6. (a) Relationship between shear viscosity and a shear rate of carboxymethylated CNF with various dry contents. (b) The power law of the shear viscosity of the CNF consistency is given (measured at 0.1 s^{-1}). Reprinted with permission from ref 200. Copyright 2014 Springer Nature.

perpendicular plane is considered the hydrophobic plane). The cellulose microfibril can be considered as an amphiphilic moiety.[171] A recent study by our group indicated that the liberated elementary microfibril in NC is hydrophilic in nature,[172] where secondary aggregation or assembly of elementary microfibrils can take place after the biosynthesis through Rosette complex.[173−176] The aggregate dimension can reach the order of 10−20 nm. For example, an electron microscopy graph of a Spruce tree fiber is shown in Figure 5a, exhibiting aggregated cellulose micro/macro-fibrils (CMF). Figure 5b reveals the size distribution of the microfibril in the same Spruce fiber in Figure 5a. Furthermore, the subsequent assembly of cellulose chains is always associated with other matrix polysaccharides (such as hemicelluloses, lignin, and pectin) in the cell wall during biosynthesis in higher plants. As a comparison, cellulose biosynthesis in *Gluconacetobacter xylinus* is free from hemicellulose or pectin interference, although some other exopolysaccharides (such as mannan-based) have been reported to affect the crystallization or cocrystallization process.[177] The cocrystallization of CMF results in larger crystal size (6−8 nm) and higher crystallinity (75−85%) for BNC.[177]

3.1.1. Crystallinity in Cellulose. The crystalline structure of cellulose can be categorized into several polymorphs (I, II, III, and IV), all of which have been studied in depth in the Supporting Information (section S2). The crystal structure of natural cellulose fibers has high complexity. First, the crystal structure of CMF depends on the deposition pattern and the interactions with other cell wall matrix polymers (lignin and hemicellulose), which are very different depending on the plant species, growth conditions, and environment.[178] Second, it is important to recognize that the assignment of the crystallinity appears to depend on the instrumental selection and the corresponding data analysis method. The common techniques to determine crystallinity include X-ray diffraction (XRD), infrared (IR), Raman, nuclear magnetic resonance (NMR), and sum frequency generation (SFG) (a nonlinear laser spectroscopic technique) spectroscopy. Among them, XRD is the most broadly used technique to estimate the crystallinity index (CrI) and crystal size information of cellulosic materials, based on the total volume fraction of crystalline or ordered cellulose chains. However, various analytical techniques[179] (e.g., the peak height method, peak deconvolution method, and amorphous subtraction method) can lead to different values of CrI even for the same material, and further obscure the fundamental understanding of the degree of crystalline in various cellulosic or NC materials that are subjected to different chemical pretreatments or defibrillation processes. In contrast, the NMR technique only detects cellulose molecular chains that exist within the interior regions of CMF and usually yield a lower CrI value as compared to XRD method. An emerging quantification of cellulose crystallinity is determined using SFG based on its non-centrosymmetric, allowing measurement of ordered cellulose regions in various biomass feedstocks without interference from noncellulosic polysaccharide components in cell walls. Considerations for the various analytical methods have been discussed by Kim et al.,[180] and the determined crystallinity by the different methods should be considered qualitative and not quantitative.

A central problem in the determination of crystallinity is the ambiguity of the crystalline (or ordered) and paracrystalline/amorphous (or disordered) content. Over the years there have been long discussions regarding the early fringe-micellar model,[181] which suggests that the cellulose fibrillar aggregates contain alternating regions of crystalline and amorphous domains. The amorphous regions are thought to contain disordered cellulose chains, but a study indicated that these disordered cellulose chains might be more complicated than one thought, and the exact arrangement of these chains has not been totally understood.[182] For example, Heise et al.[183] argued that these amorphous domains should be called disordered or defects regions, where very short (1−2 nm) defects exist, rather than the presence of totally disordered chains in the bulky amorphous regions, based on a neutron scattering study.[184] Furthermore, different kinds of chain disordering have been detected by different experimental methods.[185,186] Thus, the crystallinity concept is best expressed in a variety of ways appropriate to different end uses. For example, the cellulose morphology has recently been subjected to statistical analysis, exhibiting a distribution of non-Gaussian kink angle, where the investigators argued that the alternating structure of disordered/amorphous and crystalline regions should be replaced by the process-induced kink formation in cellulose fibers.[187] This study supports the concept of microfibrils with a single crystalline core proposed by Nishiyama et al.[188] and is more consistent with the biosynthetic mechanism. Such a conclusion has also been derived in a study dealing with the nanostructure of CMF and the issues of estimating crystallinity by Fernandez et al. using the wide-angle X-ray scattering (WAXS) technique.[185]

3.1.2. Rheology of NC Suspensions. *Rheology of CNF Suspensions.* The rheology of CNF suspensions is relatively complex, exhibiting both sheer-thinning, thixotropy and rheopexy behaviors.[189−192] Due to the complex viscoelasticity, protocols for the rheological measurements should be carefully

https://doi.org/10.1021/acs.chemrev.1c00683
Chem. Rev. 2022, 122, 8936−9031

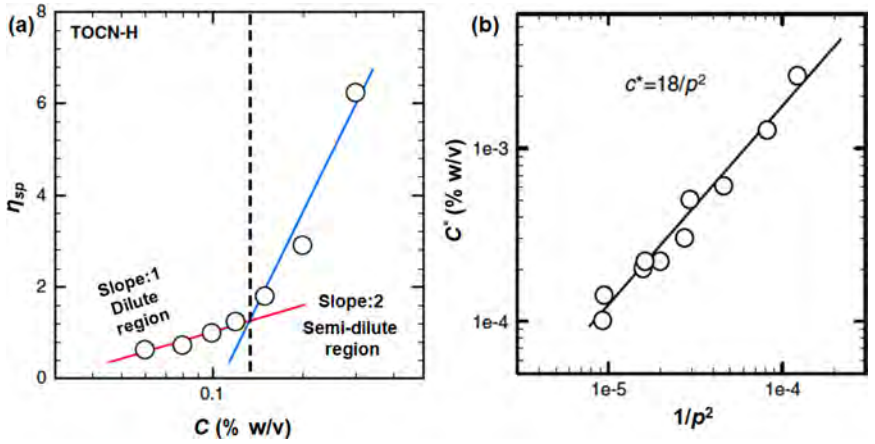

Figure 7. (a) Specific viscosity of TOCNF suspensions as a function of the CNF concentration. (b) The critical overlap concentration versus the inverse square of the aspect ratio of the CNF suspension. Reprinted with permission from ref 208. Copyright 2014 Springer Nature.

followed. However, there are no universally accepted protocols for this purpose at the moment, and thus the rheological studies of CNF suspensions can sometimes lead to confusing results. Moreover, there are many different types of CNF materials with different rheological features in suspension, further complicating the subject. In the reported studies, different rheological protocols discussed included gap-size, surface depletion, shear banding, serrated geometries, etc.[193−196] Additionally, a variety of CNF materials with different nature of inhomogeneity (individual nanofibrils versus microfibrous/nanofibrous network) were also reported which could exhibit inherent instability and thus required specific protocols. For example, it has been demonstrated that it is a necessity to use preshearing[195] and serrated geometries to avoid the slip effects[196] to produce reproducible rheological results in some CNF suspensions. It has also been suggested that one should combine optical coherence spectroscopy,[193,197] or ultrasonic speckle velocimetry,[198] with rheology to investigate unstable or inhomogeneous CNF suspensions. Despite such issues, the complex rheology and their proper characterization are very important in order for the practitioner to process samples for practical applications. Generally, CNF materials and their stability is governed by the anisotropic colloidal interactions between adjacent fibrils,[199] where a small number of ionic groups on the fibril surface can stabilize the homogeneity of the dispersion and their charge interactions, with the addition of counterions, can decrease the homogeneous dispersion and induce local aggregation (or microscopic gelation).

Figure 6 illustrates the shear viscosity of a stable (carboxymethylated) CNF suspension with various concentrations (a) and power-law modeling of the shear viscosity of the CNF consistency is given (b). In this figure, the exponent of the power-law (β) is 2.0, and the same exponent has been observed by Tatsumi,[201] for noncharged CNF in suspension for a variety of different fibers. The same low exponent has also been reported for TOCNF suspension at high shear rates.[202] It has also been reported that there is a power law (α) relationship for the evolution of the storage modulus ($G' = C^{\alpha}$) in CNF suspension, where C represents the solids content of CNF. As discussed by Nechyporchuk et al.[191] some exponent values are higher than the theoretical values for semiflexible networks, which are between 2 and 2.5.[203,204] It is thought that the deviation is due to the arrested state of the CNF suspension after dilution, which was reported by Naderi et al.[200,205] The correct exponent value of a homogeneous and well-dispersed CNF suspension should be 2.4,[200] where the higher value is presumably due to insufficient dispersion. It should be noted that Hill proposed a new scaling theory[206] to describe the rheology of enzymatic treated CNF in suspension using the data from the studies of Pääkkö et al. in 2007[91] and of Jowkarderis and van de Ven in 2015.[207] However, we noticed that the rheological data by Pääköö et al. could also be possibly caused by insufficient dispersion. In the dilute region with insignificant interactions between the fibrils, the slope of the viscosity versus CNF concentration was found to be 1.0.[205,208]

The transition point between the specific viscosity in the dilute CNF concentration region and that in the semidilute concentration region can be defined as the critical overlap concentration (Figure 7a). This value has practical importance to the sample preparation. For example, if the CNF suspension at concentrations above the critical overlap concentration is centrifuged, then the entangled dispersion is aggregated in the bottom of the vial; only if the centrifugation of CNF suspensions with concentrations below the critical concentration takes place can the apparent CNF yield be determined.[205] As expected, the critical overlap concentration is closely related to the fibrillar aspect ratio, where the relationship is shown in Figure 7b. It was found that the macroscopic concept, such as the crowding factor, works well to explain the transition from dilute to semidilute transition for CNF in suspension.[110] The ionic strength and valency of the counterions have a strong effect on the rheological behavior. For example, the initial electroviscous effect can give rise to an elevated intrinsic viscosity of NC suspensions. In addition, if the surface charge is fully shaded, there can be a good concurrence between the intrinsic viscosity and the viscosity predicted by the traditional theory for dispersions of rod-like particles at low shear rates.[209,210] At high electrolyte concentrations, coagulation generally would result in a higher intrinsic viscosity. Thus, there is a minimum value in the intrinsic viscosity versus ionic strength profile, where the intrinsic viscosity can be well fitted with the theoretical prediction. Finally, it should be noted that flow fields can also dictate the formation and configuration of nanostructure in semiflexible fibrous networks.[211] As reported in the literature,[191] the network properties of chemically pretreated CNF materials are usually stronger than enzymatic and mechanically delaminated CNF materials in spite of the fact that oxidation

https://doi.org/10.1021/acs.chemrev.1c00683
Chem. Rev. 2022, 122, 8936−9031

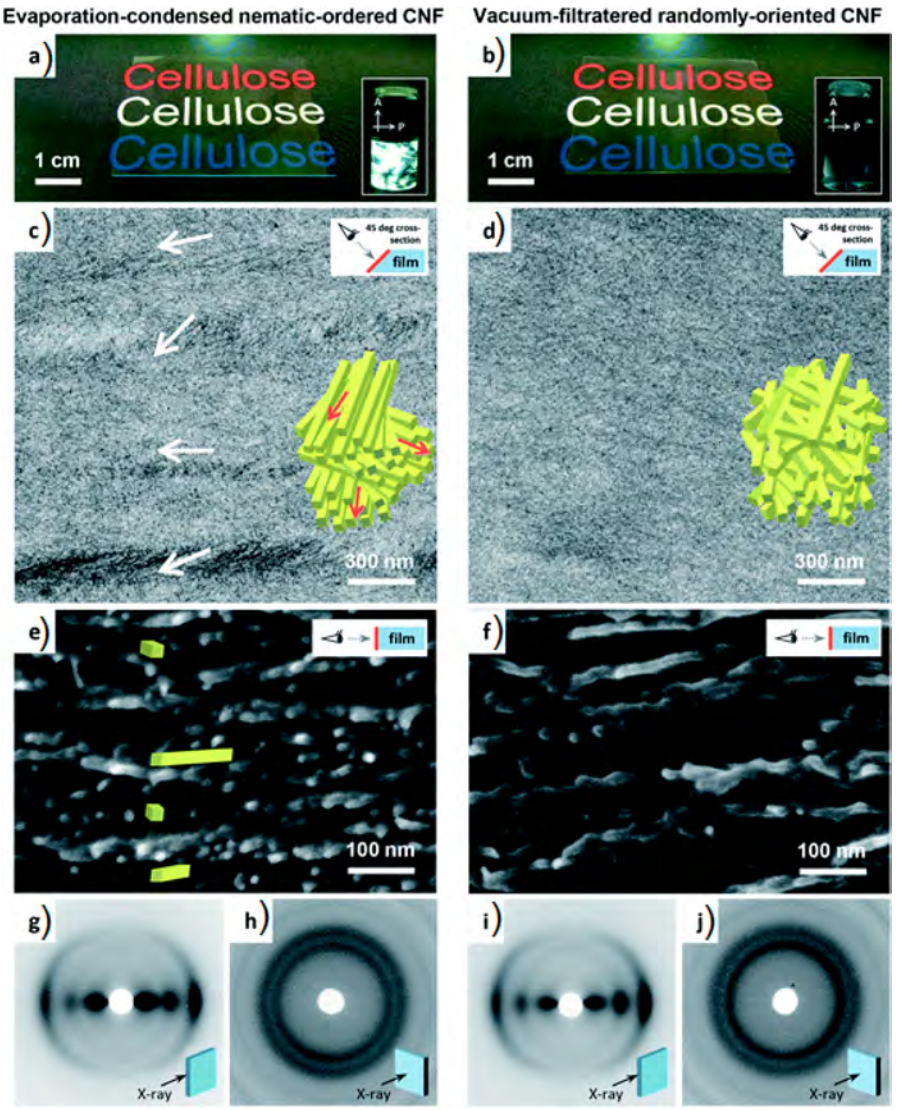

Figure 8. Structural characterization of CNF films prepared at varying conditions. (a and b) CNF films prepared by evaporative condensation (solvent cast) of a nematic CNF suspension (0.4 wt %) and vacuum filtration of an isotropic CNF suspension (0.05 wt %), respectively. The inset images show the birefringence formed in the CNF suspensions at 0.4 (a) and 0.05 wt % (b), respectively. These suspensions indicate the polydomain-type nematic to an isotropic phase transition. (c and d) Cross-sectional (45°) transmission electron microscope (TEM) images of CNF films in (a and b), respectively. (e and f) Scanning electron microscope (SEM) images of CNF film surfaces (a and b), respectively (the film is freeze-fractured). (g–j) XRD diagrams of the respective CNF films (the incident X-ray beam is parallel or perpendicular to the film plane). Reprinted with permission from ref 227. Copyright 2018 The Royal Society of Chemistry.

may also decrease the length and degree of polymerization (DP) of the fibrils.

Rheology of CNC Suspensions. There has been a great deal of attention in literature given to the subject of rheology for CNC suspensions because of its complex phase behavior. Generally, the CNC suspension has a much lower viscosity than the CNF suspension[212] because of its shorter fibrillar length (or aspect ratio), which becomes the key advantage in the manufacturing of CNC-based composites. Sulfated CNC has been the dominant class of CNC materials studied with respect to rheological features. This is because colloidal stability has a profound effect on the rheology of CNC suspensions. As typical sulfated CNC materials are electrostatically stable due to the high charge density (typically 0.2−0.35 mmol/g), their rheological behavior has been characterized in great detail.[213,214] The results have been modeled by the DLVO theory to address the colloidal stability and corresponding critical coagulation concentration (CCC)[214] with respect to different counterions (e.g., with varying valences).[215] However, the DLVO prediction is not ideal according to the Shulze−Hardy rule (i.e., CCC $\sim Z^{-6}$ and Z is the valency of the counterion). This is because, at low concentrations, CNC suspensions form an isotropic phase. With the increase of CNC concentration, the isotropic phase can transition into the liquid crystal phase. This phase transition behavior was predicted for liquid crystal molecules by Onsager and Flory.[216,217] Dong et al.[119,120] investigated the phase transition of CNC suspensions as a function of electrolyte and counterion type and found that the results could be well fitted by the so-called SLO theory,[218,219] which is an extension of the early Onsager theory.[216] This subject has also been discussed by Hu et al.[220] The reader can be referred to some more detailed investigation on the rheology of CNC suspensions published by Shafeiei-Sabet et al. and Ureña-Benavides et al.[221−224]

https://doi.org/10.1021/acs.chemrev.1c00683
Chem. Rev. 2022, 122, 8936−9031

3.1.3. Nonergodic States of NC Gels and Glasses. The isotropic to the nematic liquid crystal phase transition is well-known for CNC suspensions but can also occur for CNF suspensions. This behavior can be explained by the Onsager theory for free energy considerations for hard convex solids.[225] By slow evaporation of a CNF suspension, a transition from the gel to glass state (both states are disordered) can take place followed by the formation of a nematic liquid phase (an ordered state),[226] which has been further investigated recently.[227,228] The glass state is also called a volume-spanning arrested state, which can be formed at a relatively low concentration when the aspect ratio is high. The cellulose hydrogel in the glass state is mechanically rigid and transparent and has a high shear stiffness. The structure and orientation of such a gel or glass can be controlled by varying processing pathways under flow or nonflow conditions.[228] For example, the morphological and structural differences between the solvent-cast nematic CNF suspension and vacuum-filtrated isotropic CNF suspension under nonflow conditions[227] is displayed in Figure 8. In this figure, several structural discrepancies were identified. For example, the film produced from the nematic phase exhibited a higher density (1.54 g/m^{-3}) than the vacuum-filtrated film produced from the isotropic phase (density of 1.41 g/m^{-3}). The strength of the nematically structured film also displayed higher Young's modulus and tensile strength and superior light transmission and oxygen gas permeability than the film from the isotropic phase.[227]

The differentiation between the gel and glass state is not straightforward, as both exhibit a solid-like character and do not flow in the inverted cuvette test.[229] The glass state is established mainly because of the high packing density and strong particle−particle repulsive interactions, a phenomenon also referred to as caging.[228,230] These transitions have been discussed from both experimental (i.e., via the inverted cuvette test of varying NCs and other rod-like nanoparticles, such as CNTs and virus) and theoretical considerations using the concept of rod aspect ratio (r) and rod volume fraction (ϕ). The critical points (the threshold volume fractions) for transitions in different samples and the theoretical lines for suspension, gel, and glass transitions are shown in the Supporting Information (section S3). The theoretical upper limit can be described by the equation of $\phi \approx 5.4/r$ (above this line, the ordered liquid crystal phase occurs; below this line, the disordered glass state occurs). The transition line between the gel and glass state can be described by the equation of $\phi \approx 0.7/r$. If attractions between the rod are insufficiently strong, then a suspension to gel transition line can exist, following the Equation of $\phi \approx 24/r^2$.

3.2. Characterization of NC for Consideration of Critical Processing Parameters

Starting from various lignocellulosic biomass feedstocks, extraction and processing of NC can include a multitude of chemical, mechanical, or biological pretreatments coupled with different mechanical defibrillation processes. The resulting NC in the dispersion state will often undergo complex dehydration and dewatering processes for storage and transportation purposes, or surface modification processes to enable additional functionalities for multiple end-use applications. In this subsection, we identify several key processing parameters in the extraction and postprocessing of NC materials and present the appropriate characterization strategies and tools that one should consider.

3.2.1. Diverse Biomass Feedstocks as Starting Materials. With residual lignin, hemicellulose, or other cell wall components in the resulting NC materials, quantitative characterization of chemical compositions is critical for the understanding of the individual role of each noncellulosic component on the structure−property relationship of lignocellulosic nanomaterials (LCNMs). For this purpose, characterization of lignin (e.g., Klason lignin and acid soluble lignin), structural carbohydrate (e.g., glucose, xylose, galactose, mannose, and arabinose), ash, and extractives based on standards using accepted laboratory analytical protocols is necessary. For instance, a series of Laboratory Analytical Procedures (LAPs)[231−233] from the National Renewable Energy Laboratory (NREL) for the general chemical composition analysis of lignocellulosic biomass, are also applicable to LCNMs. Briefly, LCNMs can be subjected to sequential water and solvent extraction by a Soxhlet extraction apparatus or an accelerated solvent extractor (such as Dionex ASE 350) to determine the content of extractives. After the removal of nonstructural components, a two-stage acid hydrolysis (typically sulfuric acid) can be performed to decompose the structural carbohydrates into sugar monomers. Subsequently, the amounts of neutral sugars and acid soluble lignin can be determined by ion chromatography and UV−vis spectrophotometer, respectively. The insoluble residues from the acid hydrolysis process can be dried (typically at 575 °C, 3 h in a muffle furnace) and weighted to obtain the contents of Klason lignin and ash. Alternatively, the content of Klason lignin, extractives, and ash can be determined based on TAPPI T222 om-02,[234] ASTM E1690-08,[85] and ISO 1762,[235] techniques, respectively. Considering the rising interest in isolating and developing LCNMs through various sustainable and cost-effective approaches, a comprehensive characterization of the chemical composition of LCNMs is, therefore, required and should be always investigated when comparing structure and property with other lignin-free or hemicellulose-free NC materials.

3.2.2. Effects of Nanofabrication Processes. With different nanofabrication processes using different solvents, the resulting NC can possess different surface chemical groups, thermal stability, crystalline structure, colloidal stability, and degree of nanofibrillation. Reid et al. investigated the structure and property comparison of sulfuric acid extracted CNC (s-CNC) made in a lab to CNC made from major industrial facilities.[236] They carried out the comprehensive characterization of some key properties in various CNCs, including surface chemistry, morphology, colloidal, thermal stability, crystallinity, and liquid crystalline self-assembly behavior. Generally, even with different extraction and purification processes used, lab-made s-CNCs correlated well with those industrially produced. However, some variations in the sulfate group content, crystallinity, and morphology were still observed for s-CNCs made from different sources. The authors suggested that these key properties of CNCs must be appropriately characterized prior to their use. To ensure consistent performance, it is recommended that the end-users adopt electron microscopy, conductometric titration, XRD, and zeta potential measurement techniques as basic tools for characterization. As noted by these authors, the surface chemistry of CNC is a critical factor in determining their colloidal behavior affecting potential applications.[236] Interestingly, CNCs produced by unconventional approaches, such as those from API (SO_2−ethanol−water along with mechanical delamination) and Blue Goose Biorefineries (metal-catalyzed oxidative approach), showed

https://doi.org/10.1021/acs.chemrev.1c00683
Chem. Rev. 2022, 122, 8936−9031

significantly different nanoparticle morphology (e.g., a combination of CNCs and CNFs), aggregation and colloidal behavior and thermal stability. These samples all had high crystallinity but unmodified surface chemical groups (i.e., hydroxyl groups), instead of the grafted sulfate half-ester groups from the sulfuric acid hydrolysis route.[236] Vanderfleet et al. reported that the monoacid hydrolysis, such as sulfuric acid, hydrochloric acid, and phosphoric acid, could lead to different surface functional groups at the C-6 position of cellulose backbone in CNC extraction, while the mixed-acid hydrolysis, such as mixed sulfuric and phosphoric acids, could result in coexistence of two functional groups grafted on CNC.[237] Because of the differential hydrolysis, these CNCs varied in surface chemistry (charge type, density, and counterion type), dimensions, crystallinity, DP, and thermal stability. By adjusting the counterion type, grafted surface functional groups (sulfate groups are the least thermally stable), and DP, the authors were able to enhance the thermal stability of CNC.

For CNF extraction,[102,112] the sizes (i.e., length, width, aspect ratio, etc.), network structure, branching, and kinks of the produced CNF can vary significantly, depending on the pretreatment chemical (e.g., grafted charge density) and mechanical conditions (e.g., time, cycles and pressure). In the case of TOCNF, it generally exhibits a uniform nanofibril size distribution, where the individual CNF morphology shares some similarities with that of CNC. A recently published ISO standard—ISO/TS 21346:2021 Nanotechnologies—Characterization of individualized CNF samples—describes the detailed methods to characterize individual CNF in different forms (i.e., powder and dispersion states) and specifies the characteristics that are required to be evaluated prior to the application. For the majority of CNF materials (including mechanically defibrillated CNF), the lateral aggregation or bundling of fibrils can lead to heterogeneous distributions of length and diameter, as well as different degrees of branching and interconnected fibrillar network. As a result, the most challenging but paramount characterization of any resulting CNF is to determine its level of nanofibrillation, branching, and network structure. For the characterization of individual CNF, such as TOCNF, high-resolution microscopic characterization techniques, for example, atomic force microscopy (AFM) or TEM, are well suited to determine its morphology and sizes. However, for the aggregated, bundled, or branched CNF samples, these characterization techniques are not so useful to reveal their true state in suspension, as the sample preparation can inevitably cause aggregation and dehydration-caused artifacts (e.g., residual stress). For this purpose, characterizations, such as turbidity, light scattering, and viscosity, are often carried out to correlate with the particle size and aggregation state in CNF suspension with rheological behavior and even water retention value in the wet state.[162,163,238]

3.2.3. Functionalization of Cellulose Surface and Reducing Ends. The hydroxyl groups on the NC surface can be readily modified to introduce other functionalities through varying chemistries, resulting in tailored surface polarity or interfacial compatibility for different applications. The inherent differences (i.e., crystallinity, DP and chain rigidity) between CNC and CNF require different functionalization schemes with acceptable reaction efficiency. Thus, surface modified NC should be characterized to confirm the functionalization efficiency by determining the amount of grafted or adsorbed functional groups, and the impact of modification (especially the covalent modification) on the property changes. Ideally, the surface modification should only tailor the surface chemistry without deteriorating the inherent properties, such as morphology, DP, and crystallinity of NC. However, in certain chemical modifications, both the crystalline and chemical structure of NC can be affected because of excessive reaction time or harsh reaction conditions.[239] The major characterization techniques for surface functionalized NC include Fourier-transform infrared spectroscopy (FTIR), zeta potential, and elementary analysis. However, depending on the type of modification (physical or chemical), other analytical techniques are also necessary. For example, X-ray photoelectron spectroscopy (XPS), solid-state NMR techniques are frequently used to characterize covalently modified NC; while surface adsorption tools, such as isothermal titration colorimetry, quartz crystal microbalance with dissipation measurement, and Langmuir isotherm, are more sensitive and efficient to characterize physically adsorbed polymers.[7] In addition, to disperse functionalized NC in organic solvents, their dispersion is often characterized by UV−vis technique to confirm the nanodispersion state prior to processing.

In the past few years, there have been increasing trends in the study of reducing end modification, specifically for CNC.[240−244] In specific, directional, terminal, and regioselective chemical modifications have been demonstrated as important functionalization routes to modify CNC for new applications, where the materials modified by conventional surface functionalization routes cannot achieve. For example, fluorescently labeled CNC on its reducing end has found unique biomedical applications.[245] The precise manipulation of reducing end functionalized CNCs can further yield novel morphological features (e.g., star-shaped, end-to-end, hairbrush-like) due to the unique assembly, allowing expanded applications.[242] The origin of the reducing end modification comes from the directionality of cellulose chains in the crystalline assembly, where the hemiacetal groups are often present at the reducing end and the pendant hydroxyl groups are present at the other end. The reducing end modification also allows CNC to maintain its initial surface chemistry and anisotropic feature. Compared to the conventional surface modification, the reducing end modification of CNC differs in the amount, accessibility, and reactivity of reducing end's aldehyde groups. The latter can be performed through two major routes, that is, aldimine condensation and carboxyl-amine condensation, leading to different functional groups at the reducing end.[242] However, there are still challenges for the reducing end modification of CNC. For example, different methods: direct methods such as Fehling test and formazan method and indirect methods such as colorimetric assays and potentiometric titration, can result in different amounts of terminal hemiacetal groups formed.[242] In addition, the characterization techniques for verification and quantification of reducing end modification are generally insufficient and not sensitive because of the small reaction sites when compared to the abundant surface hydroxyl groups on the CNC surface. For example, typical quantification techniques for surface modification, such as elementary analysis and XPS, are not sensitive enough to detect the low amount of grafted functional groups at the reducing end. FTIR is only able to identify newly formed covalent bonds at the reducing end and its accuracy can be significantly affected by the low grafting density in reducing end functionalized CNC. NMR, in particular solution-state NMR, can be a direct and accurate technique to characterize the changes in chemical bonds at the reducing end. But this would require the dissolution of CNC in an ionic liquid electrolyte.[241]

https://doi.org/10.1021/acs.chemrev.1c00683
Chem. Rev. 2022, 122, 8936−9031

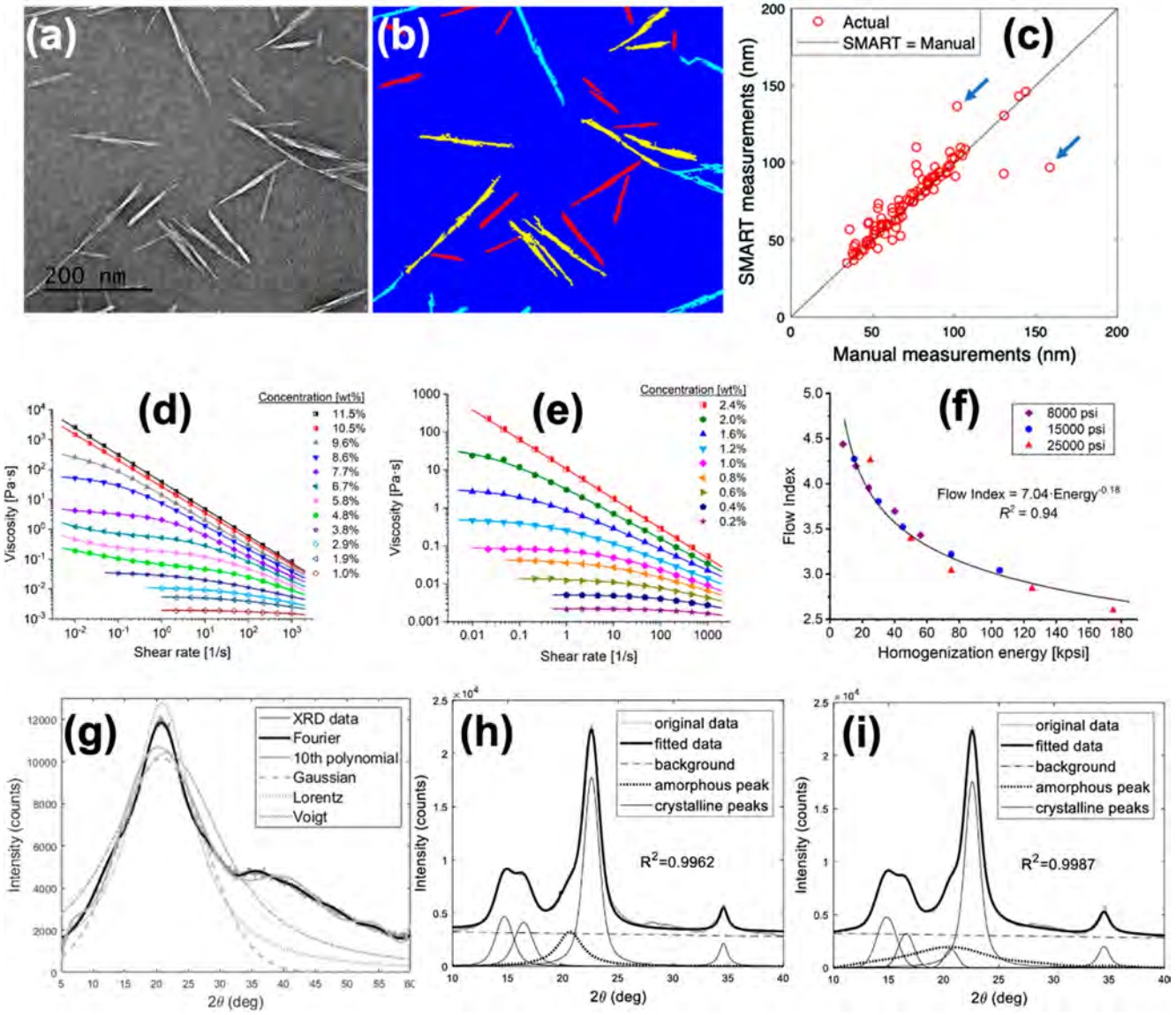

Figure 9. (a–c) Recent progress on semiautomated microscopy image analysis. Reprinted with permission from ref 250. Copyright 2021 Springer Nature. (d, e) The unified rheological modeling. Reprinted with permission from ref 254. Copyright 2020 Springer Nature. (f) Correlation of the "flow index" with a degree of defibrillation. Reprinted with permission from ref 255. Copyright 2021 Springer Nature. (g–i) CrI estimation using the XRD peak deconvolution method with improved amorphous profiling of NC materials. Reprinted with permission from ref 257. Copyright 2020 Springer Nature.

Other indirect characterization techniques, including microscopy techniques (AFM or TEM),[241,242] rely on the chemical interactions between grafted functional groups at the reducing end and metallic nanoparticles that take advantage of high interaction potential with the electron beam. In most cases, complementary analyses, including direct and indirect characterization of reducing end modified CNC, are simultaneously performed to validate the reducing end modification. It is envisioned that more accurate and reliable characterization techniques will be developed in the future for better study of reducing end modification in CNC.

3.2.4. Dewatering and Drying Processes. From the perspective of end-users, having readily redispersible NC materials with consistent properties is very important in practical applications. The production of NC always involves a large amount of water for various chemical, mechanical, or biological pretreatment processes. Therefore, understanding the NC-water interactions, colloidal stability and chemical accessibility in suspension is critical for the development of NC-based materials in different forms (e.g., hydrogels, aerogels, and foams). The processing of NC materials to create products in the condensed form also includes hydration, rehydration, dewatering, drying, or solvent exchange steps. For this purpose, the water retention value measurement is necessary to quantify the water holding capacity of CNF, which is related to the degree of nanofibrillation.[162] Dynamic vapor sorption is another approach to understand the water activity in NC materials. More advanced techniques, X-ray or neutron scattering, NMR, thermophotometry, and molecular dynamic simulation, can also be used to investigate the above subjects.[183]

In the commercial development of NC products, the processes of dewatering and drying are essential to reduce the high transportation cost of diluted NC suspensions and to meet specific end-user requirements (e.g., melt compounding of

https://doi.org/10.1021/acs.chemrev.1c00683
Chem. Rev. 2022, 122, 8936−9031

polymer nanocomposites), respectively. In both scenarios, the dehydration treatment should not change the initial nanoscale features of NC, where the processed NC should be able to redisperse easily back to the dispersion state in water. Several drying methods, including spray drying, freeze-drying, supercritical CO_2 drying, and oven/air drying, have been reported in the literature.[246] To understand the effect of various drying processes on the property changes in NC, proper characterization methods should be applied. Some typical methods are as follows: Electron microscopy characterization of oven-dried and freeze-dried NC materials can reveal the different nanoparticle morphology and the network structure caused by particle aggregation driven by the enhanced interactions of hydrophobic attractive forces during dehydration.[166] These results allowed for the selection of appropriate drying methods to process NC to create consistent structure and property. On the other hand, dewatering of NC is often performed to reduce the particle agglomeration (especially in drying), as well as the transportation cost. Dewatering is a relatively mild process that can remove a large amount of water (especially free water) from NC systems using physical, chemical, and mechanical methods. As described by Zhu et al.,[247] these methods include solvent evaporation, vacuum/pressure filtration, centrifugation, incorporation of counterions, polymers and other additives, as well as adjustment of ionic strength. A straightforward example is by adding sodium chloride solutions into NC suspensions. Using counterions, such as sodium ions, to shield the negative charges on the NC surface, can significantly reduce the electrostatic repulsion and increase hydrophobic interactions between NC particles, leading to aggregation of NC and dewatering of the system. As a result, the freeze-drying of such a system does not affect much of its redispersion capability. To characterize such a process, techniques for characterizing the colloidal behavior and stability of the suspension prior to freeze-drying and after redispersion under different counterion (e.g., H^+ and Na^+) conditions and with NC materials of different surface charges are essential.

3.3. Recent Progress on Characterization of NC

To address the challenges in different characterization techniques for NC materials, extensive efforts have been made to minimize the artifacts due to sample preparation and enhance the consistency of analytical procedures for various forms of NC materials.[161] Some of the characterization techniques are complex, time-consuming and require specific expertise. Hence, straightforward and easily applicable characterization methods and data analysis protocols are desired and critical. In this section, we highlight several recent advances on the characterization of NC materials, including microscopic imaging, rheology modeling, crystallinity estimation, particle anisotropy, and self-assembly behavior.

3.3.1. Microscopy Techniques. High-resolution imaging of NC materials and the corresponding analysis to reveal their geometric dimensions can suffer from inhomogeneous distribution of particles due to the tendency of aggregation, and sometimes from subjective/biased analytical procedures. This problem has been seen in AFM, TEM, and SEM studies, where the results from different research groups can be quite different.[248,249] Yucel et al.[250] demonstrated a semiautomated image analysis protocol, termed Standardized Morphology Analysis for Research and Technology (SMART) that can improve the reliability and grouping of NC (i.e., CNC) from AFM and TEM imaging. In their demonstration, the raw AFM or TEM image of CNC is first processed in grayscale (Figure 9a), the different types of particles can then be segmented and grouped using different color codes (Figure 9b) with the assistance of the built-in MATLAB function "*regionprops*". They reported that isolated CNC particles identified by SMART analysis can yield more consistent results of geometrical dimensions than those extracted by the manual approach (Figure 9c), allowing the high throughput analysis of multiple microscopy images. Chen et al.[251] investigated the cross-section shape and dimensions (width and height) of CNC by AFM imaging, and performed an in situ calibration of the AFM probe using codeposited gold nanoparticles to exclude the tip broadening effect. Specifically, the gold nanoparticles, acting as internal standards, allowed the calibration of the AFM probe tip radius. Their results indicated that a portion (approximately one-third) of CNC possessed symmetric cross sections, while asymmetric lateral aggregation containing two or three CNC crystallites was also observed.

In the microscopic characterization of CNF, Ang et al.[252] discussed the likely effects of the measurement statistics and operator factors on the determination of the cross-sectional dimensional distribution of CNF, for example, coarse and heterogeneous versus fine and homogeneous fibers. On the basis of SEM imaging, they proposed that the width measurement of CNF in a reduced area could alleviate the operator bias and produce a more representative distribution of the nanofibrillar width (based on the Kruskal–Wallis statistical analysis), as compared to measurement on integral SEM images with a selection of 100 fibers. They provided a rapid analysis to determine the average CNF cross-sectional dimension and argued that this approach is also applicable for the measurement of geometrical dimensions from AFM or TEM imaging. To improve the bulk morphology characterization of NC materials by TEM, Campano et al.[253] demonstrated an imaging technique to investigate the agglomeration state and degree of defibrillation for CNF and CNC. In their study, different TEM grids (i.e., holey and Formvar/carbon) and fixing agents (i.e., glow discharge, UV light irradiation, and poly-L-lysine (PLL)) were compared, where the Formvar/carbon grid coupled with PLL coating on the mica substrate yielded the best TEM image quality and highly reproducible results, based on the Fractal dimension and lacunarity analysis. They further concluded that the dispersion state of NC can be accurately characterized by TEM using these sample preparation protocols.

3.3.2. Rheological Techniques. The rheological behavior of NC suspensions is closely related to the morphology, surface chemistry, geometric dimensions and defibrillation level of the constituting fibrils, as well as their network structure. As a result, the diverse forms of NC, with different characteristics, can make the corresponding flow behavior of their suspensions very complex. Understanding the structure and rheological property relationship is essential for the use of NC as a rheological modifier in the formulation of inks, personal care products, emulsions, coatings, and paints.[121] The knowledge of the fibrillar interactions, network formation, flocculation, and self-assembly behavior of NC in suspension underflow is also essential for the processing of NC materials. However, the lack of standard protocols and empirical models for the analysis of complex flow behavior and network structure in NC suspension is still a major challenge. In addition, artifacts during measurement, such as wall slip, shear banding, and instability, can greatly impact the accuracy and reproductivity of the rheological characterization. There have been some attempts to develop robust protocols and

https://doi.org/10.1021/acs.chemrev.1c00683
Chem. Rev. 2022, 122, 8936−9031

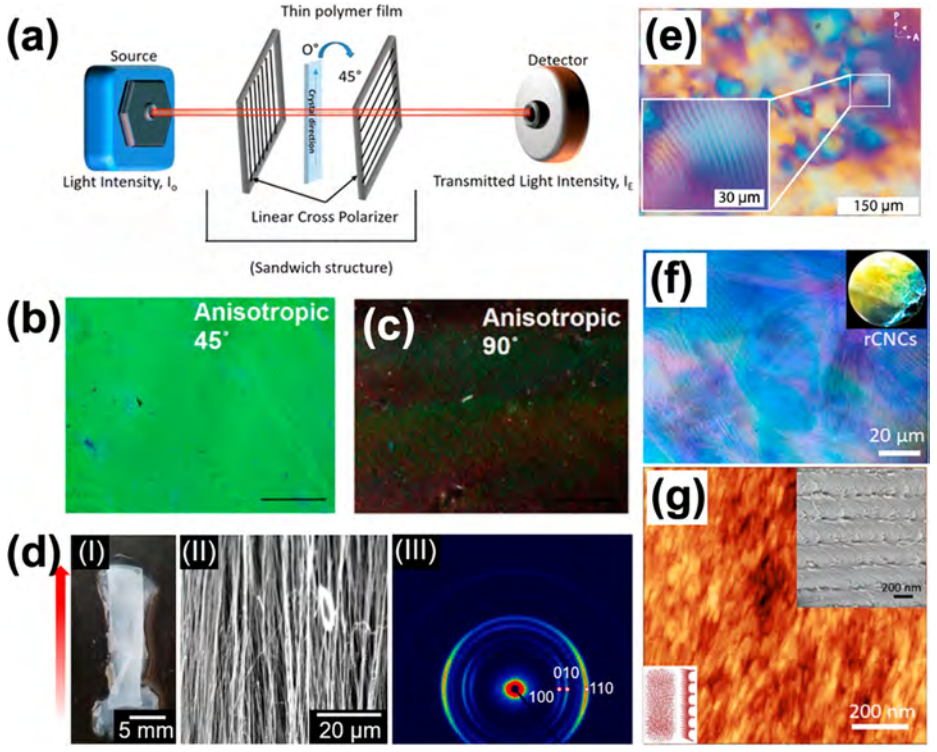

Figure 10. Representative characterization techniques to characterize the NC alignment and chiral nematic assembly of NC. (a) Schematic illustration of an optical birefringence technique. (b and c) POM imaging of anisotropic CNC films at 45° and 90° configurations. Reprinted with permission from ref 261. Copyright 2017 Springer Nature. (d) SEM images (II) and 2D-WAXS of shear-enabled alignment of BNC. Reprinted with permission from ref 262. Copyright 2021 Elsevier. (e) POM images of 8 wt % a CNC suspension showing an optical pitch of 8.7 μm and the "fingerprint" liquid crystal banded texture (zoomed image). Reprinted with permission from ref 263. Copyright 2020 The Royal Society of Chemistry. (f) POM images of iridescent CNC films. (g) AFM surface image and SEM cross-sectional image (top right inset) of CNC films with helicoidal nanostructure (left bottom inset). Reprinted with permission from ref 264. Copyright 2020 American Chemical Society.

rheology models to assist the quality control of NC processing.[7] For example, Liao et al.[254] reported the feasibility of using a unified rheological model, combining the power law (between viscosity and shear rate) and the cross model (which captures the flow curves in the isotropic and the chiral nematic phases), to characterize the entire flow behavior of CNC (Figure 9d) and CNF (Figure 9e) at various concentrations. This model, involving both considerations of phase transition and viscoelastic properties, has been found to be quite useful for the systems of commercially produced s-CNC and TOCNF. In addition, key model parameters of this model could be used to predict the solid content and salt concentration in NC suspensions with high accuracy. In their follow-up study,[255] the viscoelastic properties of TOCNF suspensions were investigated to shed more insight into the correlations between rheological properties, nanofibrils morphology, and surface chemistry. On the basis of the the flow curves fitted with the Cross model, they further established a rheological factor "flow index", which appeared to be closely related to the nanofibrillar network structure. Higher energy homogenization coupled with higher surface charge could lead to extensive defibrillation and a reduced flow index value (Figure 9f). The single parameter (flow index) derived from this rheological modeling of the viscoelastic responses of varying CNF suspensions enabled the identification of optimized processing conditions for processing TOCNF.

3.3.3. Determination of Crystallinity. As NC is a crystalline entity, the analysis of its crystallinity and crystallite dimensions is important for understanding the effects of various pretreatment conditions and achievable final properties. Over the past decades, various characterization techniques (e.g., XRD, NMR, and IR) and corresponding analytical methods (i.e., peak height, peak deconvolution, and Rielveld) have been established to estimate the CrI information from a vast array of cellulosic or nanocellulosic samples. These methods have been compared in several review articles.[7,179] In particular, XRD is the most widely used tool to evaluate the crystallinity information of NC materials. To analyze the XRD data, different analytical procedures possess different limitations. For example, the Segal peak height method often overestimates the CrI value, and while the peak deconvolution method and the Rielveld method can yield better estimates; they require careful fitting procedures and baseline determination. One approach to improve the peak fitting method is by considering the contribution of the amorphous phase in the overall diffraction profile.[256,257] It has been noticed that the shape of the amorphous peak in cellulose is often complex and should not just be represented by a broad Gaussian functioned peak as reported in some studies.[258] To tackle this issue, Yao et al.[257] and del Cerro et al.[256] constructed different expressions to represent the amorphous cellulose phase and discussed their appropriateness for fitting the experimental XRD diffraction patterns (along with the crystalline peaks). In the study of Yao et al.,[257] they noticed that there is a lack of a standard for amorphous cellulose modeling and the amorphous peak feature cannot be described by typically adopted mathematical functions (i.e., Gaussian, Voigt, and Lorentz) as seen in Figure 9g. To deal with this problem, they have constructed an eighth-order Fourier series equation to model the amorphous fraction of the samples

https://doi.org/10.1021/acs.chemrev.1c00683
Chem. Rev. 2022, 122, 8936−9031

(Avicel, pulp, BNC) prepared by varying ball milling techniques. The peak fitting of the experimental XRD profile (e.g., BNC) using the Fourier series equation to describe the amorphous fraction illustrated an accurate and easy-to-use procedure as compared to the use of Voigt function (Figure 9h). The use of the Fourier series equation also yielded more meaningful insights on the contribution of the amorphous cellulose phase, as well as reliable determination of CrI, than other peak deconvolution methods. Alternatively, the method of terahertz time-domain spectroscopy (THz-TDS) has been demonstrated by Wang et al.[259] as a new approach to estimate the CrI value. They reported that cellulosic samples exhibiting the characteristics peak at 3.04 THz can be analyzed by a min-max algorithm to normalize the integrated intensity between 2.79 and 3.32 THz into 1 to 0. With this approach, they proposed a new "index" for the crystallinity estimation of cellulose. The quick and easy sample preparation for the THz-TDS measurement may enable this technique to be a new standard for estimating the CrI value in NC materials.

3.3.4. Determination of Fibrillar Alignment. The alignment of NC has significant implications for the development of high-performance functional materials with fully exploited nanoscale properties. For example, the formation of aligned NC can enable anisotropic properties (e.g., birefringence), improve reinforcing efficiency in nanocomposites, and strengthen mechanical properties.[169] Recently, alignment strategies and the applications of aligned NC materials have been extensively reviewed,[169,170,260] and readers are encouraged to consider these articles as valuable sources for information. Some common analytical techniques that can quantitatively determine the NC alignment include microscopy (e.g., AFM, SEM, and polarizing microscopy (POM)), birefringence measurement, and X-ray scattering (i.e., WAXS and SAXS). For example, Chowdhury et al.[261] demonstrated a simple and low-cost optical technique (captured by POM) to determine the birefringence and CNC orientation in film, which was sandwiched between two rotating polarizers (Figure 10a). The transmitted light intensities in bright and dark fields could be used to estimate the linear dichroitic ratio for the determination of the order parameters in isotropic and anisotropic CNC films. In the 90° and 45° configuration between two polarizers, the sheared CNC film could exhibit noticeable differences in the transmitted light intensity (Figure 10b and 10c). The results from this method could be quantitatively compared with that of two-dimensional (2D) WAXS, which is more accurate in determining the crystal order parameter. Electron microscopy, such as SEM (Figure 10d-II), and 2D WAXS pattern (Figure 10d-III), has been used to determine the degree of CNC (same as crystal) alignment. In the WAXS analysis, the CNC alignment is related to its diffraction peaks and azimuthal spreads. For NC materials, the (200) diffraction peak is often adopted to extract the azimuthal intensity distribution, which can be used to calculate the Hermans' order parameter (ranging from 0 to 1, with 0 representing the isotropic state and 1 representing the full alignment state).[169,260]

3.3.5. Investigation of Chiral Nematic Liquid Crystal Assembly. The most intriguing behavior of CNC in suspension is their self-assembly tendency to undergo a phase transition from isotropic to chiral nematic liquid crystal phase with increasing concentration. This behavior has enabled a range of unique optical and electronic applications for CNC materials. At the low concentration range, rod-like CNC particles are dispersed in an isotropic state, where above a critical concentration; CNC can start self-assembling into ordered tactoids that are discrete domains of the liquid crystalline phase. The dispersed tactoids in the isotropic phase are often referred to as the biphasic phase, where both isotropic and liquid crystalline domains are in equilibrium with each other.[168] The solvent evaporation method can be used to initiate the bottom-up assembly process, where the solvent evaporation rate can fine-tune the CNC organization, yielding a photonic structure at various hierarchical levels. In the liquid crystalline phase, CNC suspensions can also display characteristic pitch as observable by polarized optical microscopy (Figure 10e). This isotropic to cholesteric liquid crystal phase depends on the interparticle interactions (e.g., hydrogen bonding, van der Waals force, and electrostatic), inherent features of CNC (e.g., aspect ratio, surface functionality and charge density), and external conditions (e.g., incorporation of polymers, pH, and ionic strength).[265] For example, CNCs with different crystalline allomorph structures (cellulose I and II) could exhibit variations in the pitch of the chiral nematic texture.[263] After drying, solid CNC films can display an iridescent structure color due to the retention of the chiral nematic phase, resulting in new applications of materials, such as optical displays and biosensors. To characterize the microstructure and surface features of iridescent CNCs films, various microscopy techniques including POM (Figure 10f, showing vivid iridescent colors), AFM and SEM could be used. The chiral nematic texture in CNC films can also be confirmed through SEM cross-section imaging (Figure 10g, top right insert), while the AFM image reflects locally aligned CNCs with discrete tactoids.[264] In addition, to better understand the structure development at varying hierarchical levels during the chiral nematic liquid crystalline assembly in CNC suspensions, Kádár et al.[168] demonstrated the following characterization methods to analyze the phase changes during solvent evaporation. These methods included rheological analysis, SAXS and small-angle neutron scattering (SANS), POM, NMR, FTIR, and Raman spectroscopy techniques, especially ones monitoring the in situ structure development during self-assembly from the liquid to solid state.[168]

3.4. Small-Angle X-ray Scattering (SAXS) of NC Suspensions

The SAXS technique has been widely used to characterize the supramolecular structure of cellulose crystallite assembly and the pore structure within the cellulose fibers (e.g., after the enzymatic hydrolysis pretreatment).[266] The sensitivity of SAXS is quite high for the analysis of nano-objects having a sufficient density contrast with respect to the surrounding medium, where the maximum spatial limit of SAXS can reach over 100 nm. SAXS analysis can provide critical information regarding the average cross-sectional dimensions, orientation, and spatial ordering of NC materials. Several comprehensive reviews regarding the SAXS technique and its principles for characterizing nanostructured materials are available.[267] However, its application in characterization of NC in the dispersion state has only been recently reported.[268−271] As mentioned earlier, the extraction and processing of NC often deals with the wet or dispersion state, in which the solution SAXS technique has turned out be uniquely suitable to study the morphological and cross-sectional features of individual NC particles, their colloidal and aggregation behaviors, and the flow-induced alignment phenomenon without the worry of sample preparation (e.g., drying).

The quantitative solution SAXS measurement of NC suspensions can yield average cross-sectional dimensions and

https://doi.org/10.1021/acs.chemrev.1c00683
Chem. Rev. 2022, 122, 8936−9031

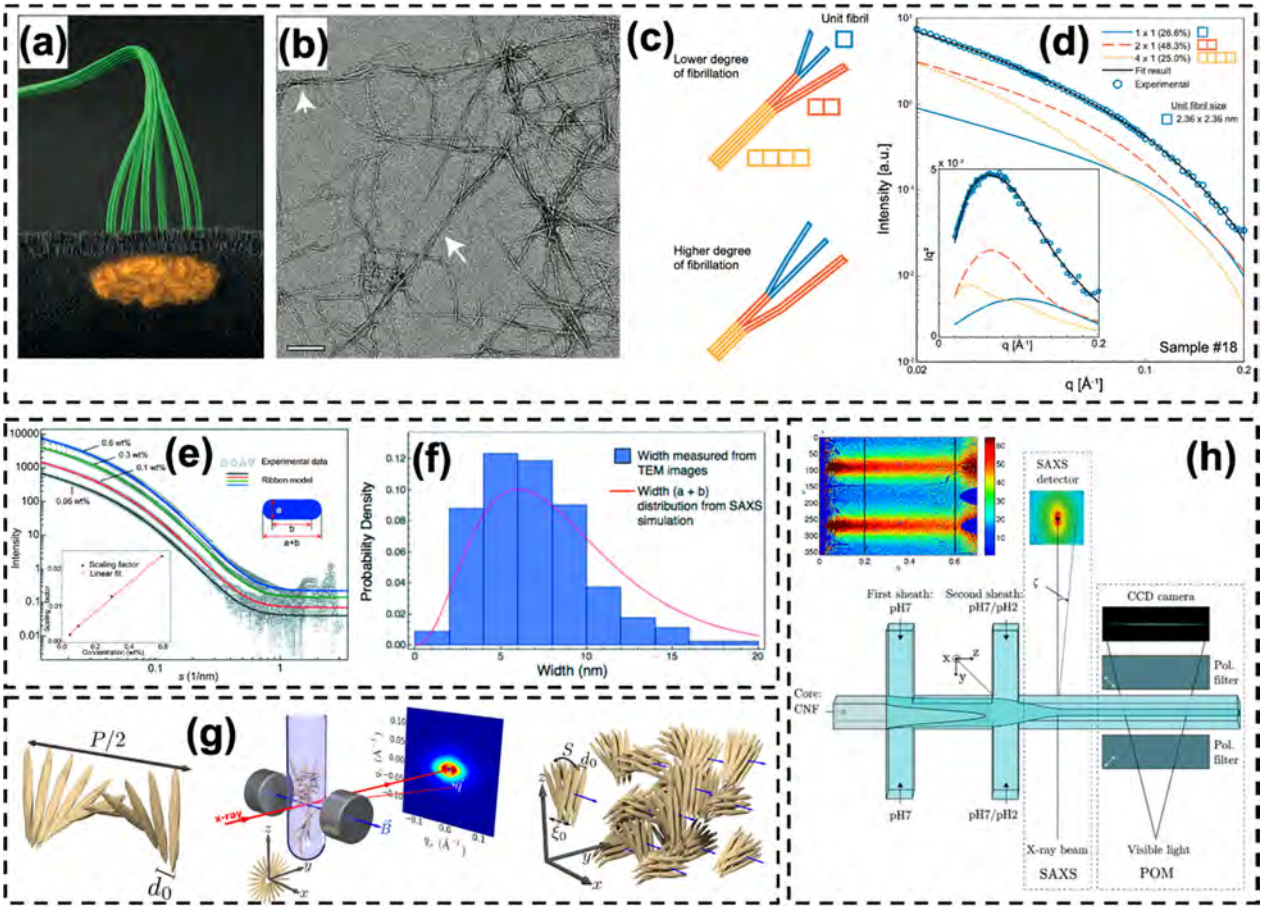

Figure 11. Application of solution SAXS technique for NC characterization. (a) Biosynthesis of cellulose chains and the formation of elementary microfibril. (b) TEM image showing the lateral aggregation of elementary microfibrils (indicated by arrows). (c) Schematic illustration of CNF with different degrees of nanofibrillation. (d) Solution SAXS profiles fitted with three types of elementary microfibril aggregation, resulting in different cross-sectional shapes and dimensions. Reprinted with permission from ref 172. Copyright 2020 American Chemical Society. (e, f) Experimental SAXS profiles of TOCNF suspensions fitted with a ribbon-shaped cross-section model (solid lines) and comparison with the width results from the TEM image analysis. Adapted from ref 271. Copyright 2014 IUCr/Wiley. (g) Schematic diagram of the in situ SAXS technique to characterize of the electromagnetic field-induced alignment and ordering of chiral nematic CNC. Reprinted with permission from ref 268. Copyright 2016 American Chemical Society. (h) Combined SAXS and POM techniques to characterize the flow-induced alignment of CNF during fiber spinning by the flow focusing technique (the inset images represent 2D SAXS diagrams with polar and Cartesian coordinates, respectively). Reprinted with permission from ref 269. Copyright 2015 The Royal Society of Chemistry.

distributions (Figure 11b), as well as the degree of defibrillation of NC particles (Figure 11c). This is because the spatial resolution of SAXS is ideally suited to extract statistical information regarding the cross-sectional dimensions (from the form factor) of NC in dilute concentrations. From high-resolution microscopic measurements, it has been reported that CNF's height is between 1 and 3 nm (by AFM) and its width is between 4 and 8 nm (by TEM).[271] However, these dimensions are inconsistent with the sizes of an 18-chain microfibril (Figure 11a), where cross-sectional dimensions should be between 2.3 and 3.6 nm.[234] Microfibril has been considered as the elementary building block of all NC particles. To gain more insights into the morphology and dimensions of extracted CNF, and its relationship with the lateral aggregation of elementary microfibrils, our group has recently performed additional WAXS and TEM measurements to complement the solution SAXS study, using elementary microfibrils as the foundation.[172] Assuming each elementary microfibril has a square-shape with an average cross-section size of 2.4 nm; multiple microfibrils can be assembled into a ribbon-shaped cross-section, consistent with the TEM observations. The experimental SAXS data were fitted by a quantized polydispersity method using elementary microfibrils (Figure 11d) to assemble into different-sized aggregates. By further defining the degree of defibrillation, we found that the aggregation has a preferred cohesion of phase boundaries parallel to the (110)-plane of the CMF. These findings are consistent with our earlier SAXS results of TOCNF in suspension,[270,271] which indicated that the individual CNF particle could be best described by a simplified ribbon model with nanoscale cross-sectional dimensions (Figure 11e). These dimensions and their size distributions were in good agreement with those estimated from the TEM image analysis (Figure 11f). The analysis of the solution SAXS data is model dependent. A different research group has used an elliptical cylindrical model to estimate the cross-sectional dimensions of CNC in dispersion, where the results were also consistent with the AFM data.[263] From these studies, we argue that the cross-section shape of NC is not round, where both ribbon and elliptical cylindrical shapes are possible. However, we also caution that the SAXS technique is a low-resolution technique and that precise measurements are not possible. In addition,

https://doi.org/10.1021/acs.chemrev.1c00683
Chem. Rev. 2022, 122, 8936−9031

there are always inhomogeneities of NC in lengths and widths.[172]

In addition, the SAXS technique can yield the structural information (e.g., spatial ordering and orientation) of NC in suspension during the phase transition (from isotropic into chiral nematic liquid crystalline phase)[272] or under externally induced alignment (e.g., electromagnetic field or extensional flow).[172,268] For example, the packing of CNC particles in the chiral nematic phase was investigated by Schütz et al.[272] using the solution SAXS technique. The average center-to-center separation distance between s-CNC in suspension was found to decrease from ∼51 nm (isotropic phase) to 24.5 nm (at fully liquid crystalline phase) with increasing CNC concentration (1.3−6.5 vol%). De France et al.[268] reported the real time change of CNC ordering/alignment at varying concentrations under a magnetic field using the in situ SAXS technique (Figure 11g). When the suspension was placed in the magnetic field perpendicular to the X-ray beam, anisotropic SAXS patterns could be observed, revealing the change in structure parameters, such as the packing distance, correlation length, orientation, and order parameter. In dilute concentrations, isotropic CNC suspensions were unable to orient noticeably. However, at high concentrations, the chiral nematic phase of the CNC suspensions exhibited two-staged ordering, with the fast partial alignment at the initial stage followed by the slow cooperative ordering at the later stage because of the influence of magnetic field. Another example of the in situ solution SAXS study involved the monitoring of structural change during the fiber spinning formation of NC (Figure 11h). It has been shown that NC-based fibers/filaments fabricated by the flow-focusing technique can create a new class of biobased high performance materials with the potential to replace petroleum-based synthetic fibers.[172] Careful characterization of nanoscale dynamics and structure during the flow process can lead to the optimized design of structure and desired properties. However, such characterization techniques need to be in situ, noninvasive and noncontact, where synchrotron SAXS seems to be a proper tool.

4. NC STRUCTURE PROPERTIES RELATIONSHIPS

4.1. Mechanical Properties of NC and Its Composite

CMF has very high crystal moduli (in the range of 130−150 GPa),[273−275] but the strength of this material is difficult to determine. The strength of TOCNF has been determined to be in the range of 1.6−3.0 GPa and the highly crystalline Tunicate to be in the range of 3−6 GPa.[276] It should be realized that the contribution of NC on the mechanical performance of NC-based composites or derived materials in varying forms, such as film, nanopaper, filament, foam, aerogel, or electrospun nanofiber, is different, depending on the formation method and process-induced structural variance. For example, Benítez et al. analyzed the impacts of several factors, including DP, moisture content, and porosity on the strengths of varying CNF products.[277] Because of the smaller porosity and fewer surface defects and internal stress, the fiber format generally has higher mechanical properties than the material in bulk format, depending on the processing conditions. However, it is somewhat difficult to investigate the surface defects of the fiber once its cross sections approach nanoscale, and there is little knowledge on the internal structural defects in these materials. There have also been very limited studies to explore the ultimate strength of NC films (especially CNF films). One issue is that there is a lack of globally accepted standards for sample preparation and testing protocols of CNF films. Typically, the community uses the standards for plastic and composite films, including ASTM D3039/D3039M-14, ASTM D 638-01, and ISO 527-1,[7] but these standards may not be completely applicable for CNF films, and may need modifications. Thus, a thorough investigation of the property space of different CNF products can be hampered by the use of different protocols. In spite of these limitations, some general conclusions can still be drawn. For example, Figure 12 illustrates

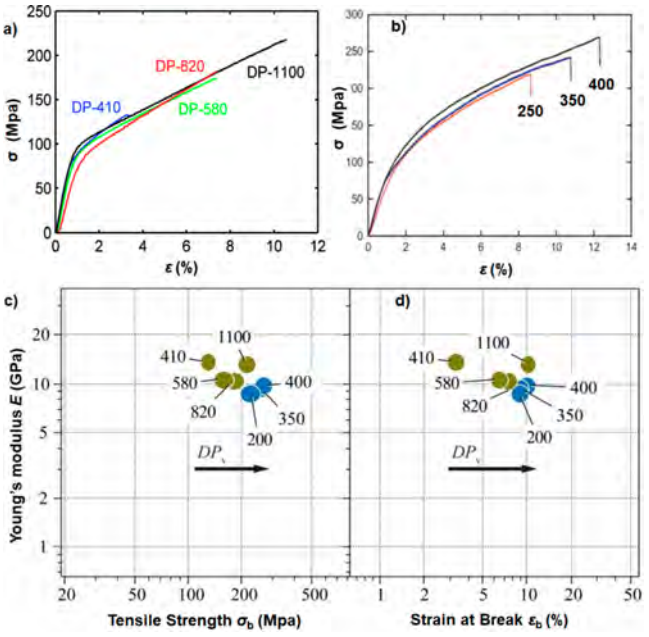

Figure 12. Effect of DP on the mechanical properties of CNF films. (a) Stress and strain curves of CNF films prepared by enzymatically extracted CNF from never dried sulfite pulps with different DP. Reprinted with permission from ref 278. Copyright 2008 American Chemical Society. (b) Stress and strain curves of CNF films prepared by TOCNF from never dried sulfate pulps of different DP. Reprinted with permission from ref 280. Copyright 2013 Elsevier. (c) and (d) Plots of Young's modulus comparison with tensile strength and strain at break, respectively, for CNF films of different DP (black arrows indicate the direction by increasing DP). Reprinted with permission from ref 277. Copyright 2017 The Royal Society of Chemistry.

the effects of DP on the varying mechanical properties with films prepared by CNFs extracted by two different methods: enzymatical treatment,[278] and TEMPO-mediated oxidation,[279] from never dried sulfate pulps of different DP. Figure 12a shows the stress and strain curves of CNF films prepared by enzymatically extracted CNF,[278] and Figure 12b shows the curves for CNF films prepared by TOCNF.[280] It was seen that all stress−strain curves exhibited the same trend, and with an increase in DP, the tensile strength and elongation at break generally all increased accordingly. This behavior was also confirmed by the correlations of Young's modulus with tensile strength or strain at break separately, using CNF films of different DP (Figure 12c and 10d). This can be explained by the notion that the fibril length generally decreases with DP, leading to notable decreases in mechanical properties. Figure 13 shows a linear relationship between the fibril length and DP for TOCNF,[279] which further confirms this explanation. In this figure, the theoretical chain length vs. DP is also illustrated. The

https://doi.org/10.1021/acs.chemrev.1c00683
Chem. Rev. 2022, 122, 8936−9031

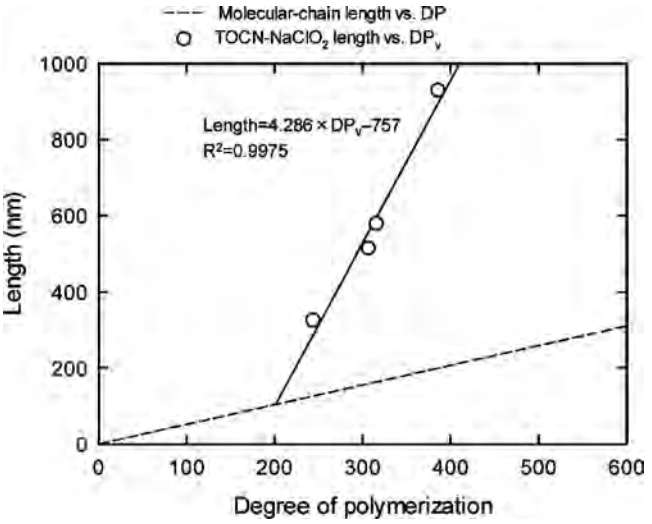

Figure 13. Fibril length of TOCNF (TOCNs−$NaClO_2$) vs the DP. The corresponding DP value of chain length is represented in the dashed line. Reprinted with permission from ref 279. Copyright 2012 American Chemical Society.

chain length is found to be substantially smaller than the fibril length, indicating that the fibril contains many chain ends. Unfortunately, the fibril length was not investigated by Henriksson et al. in the study of enzymatically prepared CNF film.[278]

Lindström et al.[112,281] argued that the tensile strength of CNF films can be deduced from the Page approach developed for paper property evaluation, by using the short-span tensile strength and an extrapolation procedure. This is because the strength of nonporous CNF film is not dependent on the bonding strength between the fibrils in the film. The tensile strength of the film with nonwoven structure can be estimated from the short-span strength of the CNF. In a recent review,[282] it was seen that even for various CNFs of different modifications, the properties became similar as soon as the fibers were sufficiently delaminated before making the film.

The porosity in CNF film can be increased by using the solvent exchange method involving a less polar solvent.[277,278] In general, increase in porosity leads to decrease in Young's modulus, yield strength and tensile strength but increase in strain at break. This was seen by the films with higher porosity prepared by the supercritical CO_2 drying method.[13] It has been seen that hydrogels could shrink significantly during supercritical CO_2 drying because of the hygroscopic properties of CNF.[283] To overcome this problem, the functionalization of CNF can be carried out to stabilize the fibrillar networks and reduce shrinking. The freeze-drying method has also been used to prepare porous CNF films, where ice crystals can act as a filler template for pore formation. It has been shown that one can fine-tune the porous network structure, such as lamellar-like or cellular-like structure, using different freezing or sublimation conditions.

The effect of humidity on the mechanical property of CNF materials is very strong. This is because the presence of water molecules can degrade the strong hydrogen bonding between the adjacent CNFs, resulting in formation of structural defects and degradation of mechanical properties. As seen in Figure 14, when the relative humidity increases, a clear transition can be observed during the CNF film deformation, that is, from brittle fracture to a ductile response (Figure 14a). During the ductile deformation, the fibril pull-out phenomena was found to be the dominant process (Figure 14b). It was interesting to find that there was virtually no change in the strain at break for all the samples tested, in spite of the varying different experimental conditions (different moisture contents) and different deformation mechanisms (brittle vs. ductile).

The presence of counterions can play a vital role to affect the dry and wet properties of CNF films. These effects have been investigated for various monovalent and multivalent metal ions and quaternary alkylammonium carboxylates during the preparation of CNF films.[277,285−288] Typical results are displayed in Figure 15. For monovalent ions, the larger size ions exhibited a slightly lower tensile strength but yielded an increased strain at break (Figure 15a). For the quaternary alkylammonium carboxylates, the higher hydrophobic chain length of the ammonium salt resulted in a larger strain at break (Figure 15b). In Figure 15c and Figure 16, the effect of multivalent metal ions on the wet tensile strength of CNF films is shown. It was found that all samples exhibited an increase in tensile strength over the pristine CNF film; however, the aluminum ion Figure 15c and iron ion (Figure 16) displayed particularly strong effects. Generally, multivalent ions behave like ionic cross-linking agents in the CNF scaffold, while monovalent ions merely act as a screening agent to shield the surface charge of CNF and, thus, only enhancing the hydrophobic interactions in the CNF scaffold.

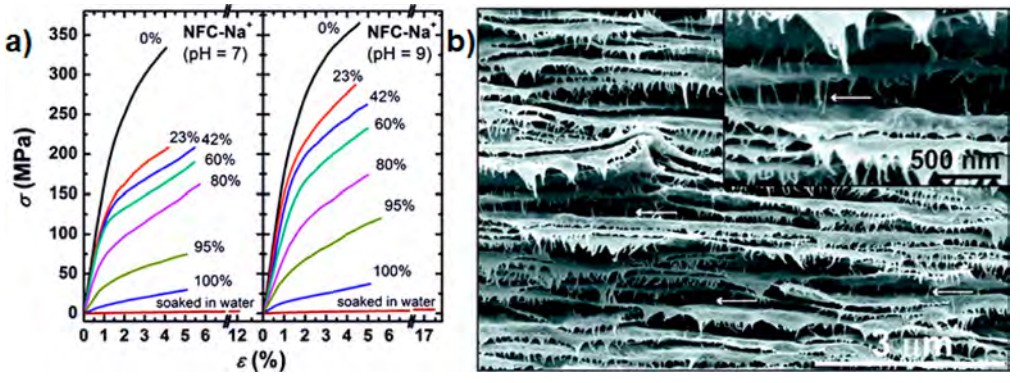

Figure 14. (a) Effect of relative humidity (RH) on TOCNF films at pH = 7.0 and 9.0, respectively. (b) SEM image of fractured CNF film's cross-sectional, indicating the likely deformation mechanism at 100% RH (the arrows indicating the pull-out of CNF fibrils). Reprinted with permission from ref 284. Copyright 2012 American Chemical Society.

https://doi.org/10.1021/acs.chemrev.1c00683
Chem. Rev. 2022, 122, 8936−9031

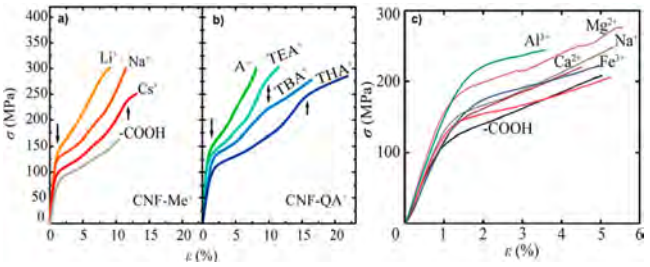

Figure 15. Mechanical properties of CNF films at 50% RH. (a) Tensile properties for various monovalent ions in CNF films in the protonated form. (b) Effects of ion-exchange to quaternary amines with different chain lengths, including A^+, ammonium; TEA^+, tetraethylammonium; TBA^+, tetrabutyl ammonium; and THA^+, tetrahexyl ammonium. Reprinted with permission from ref 288. Copyright 2017 American Chemical Society. (c) Effects of various multivalent metal ions on the wet tensile properties on CNF films. Reprinted with permission from ref 285. Copyright 2016 Elsevier.

Recently, Wågberg et al. investigated the wet tensile properties of TOCNF films with medium and high charge densities, where the films were treated with various multivalent ions.[289,290] The results of this study are shown in Figures 16 and 17. It was seen that Al^{3+} and Fe^{3+} are particularly effective cross-linking agents, leading to higher tensile strengths but also lower strain at break values. They proposed a semiquantitative model to explain the effects of varying multivalent counterions-induced attractive interactions on the wet modulus of the highly charged TOCNF scaffold, where this model contains four types of interactions: ion−ion interaction, metal−ligand complex formation, dispersion interaction, and local acid−base interaction. The contributions of these four interactions in the wet modules are shown in Figure 17. In this figure, each interaction is represented by a different color bar. In addition, the CNF scaffold and its physical entanglement are also taken into consideration, as represented by the gray area.

In Figure 17, it is seen that each interaction contributes to a specific portion of the wet modulus. For example, in the CNF−Mg^{2+} film, the ion−ion correlation is the mainly attractive interaction (besides the CNF network) due to a weak affinity of magnesium ions. For other ions, the additional contribution of each interaction is derived either from tensile data (such as Ba^{2+}, Ca^{2+}, Mn^{2+}, and Zn^{2+}), stability constants, or pH of solutions (in the case of Cu^{2+}, Al^{3+}, and Fe^{3+}). It was found that the metal−ligand complexes interaction plays a dominant role for CNF films associated with Cu^{2+}, Al^{3+}, and Fe^{3+} counterions, whereas the ion−ion correlation interaction is regarded as slightly less significant but can play an important role during plastic deformation.

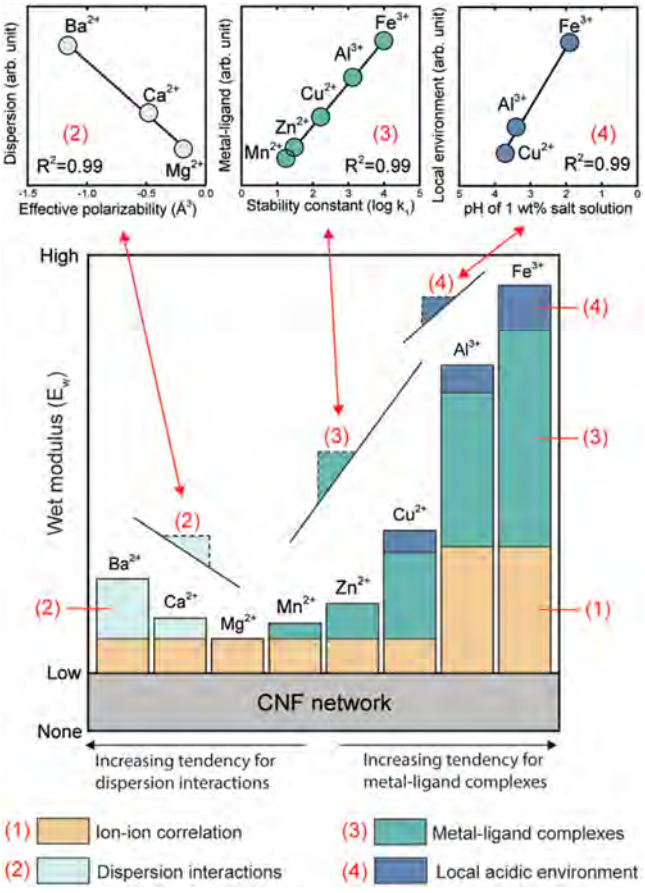

Figure 17. Analysis of the ion-induced assemblies of anisotropic CNF scaffolds, using a model describing the contribution of four different mechanisms, and their impact of wet modulus of CNF films. Reprinted with permission from ref 289. Copyright 2019 Wiley-VCH Verlag GmbH & Co.

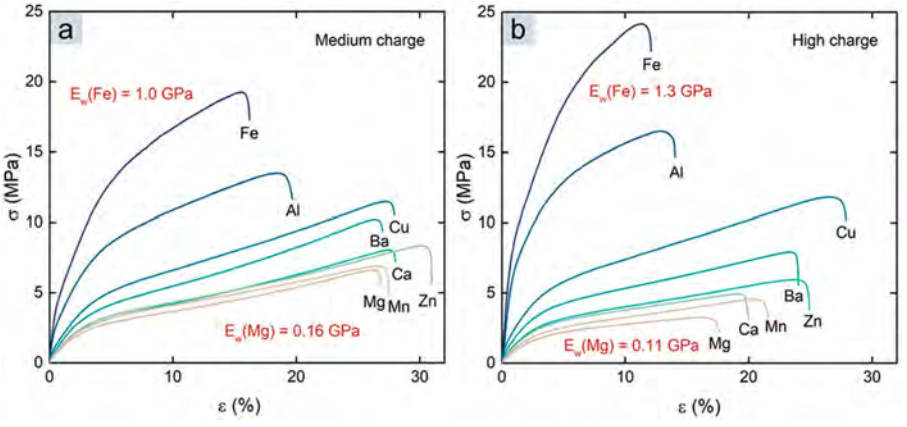

Figure 16. Typical stress−strain curves for wet TOCNF films with (a) medium and (b) high charge densities. TOCNF is treated with various multivalent ions, such as Mg^{2+}, Ca^{2+}, Mn^{2+}, Zn^{2+}, Ba^{2+}, Cu^{2+}, Al^{3+}, and Fe^{3+}. Reprinted with permission from ref 289. Copyright 2019 Wiley-VCH Verlag GmbH & Co.

https://doi.org/10.1021/acs.chemrev.1c00683
Chem. Rev. 2022, 122, 8936−9031

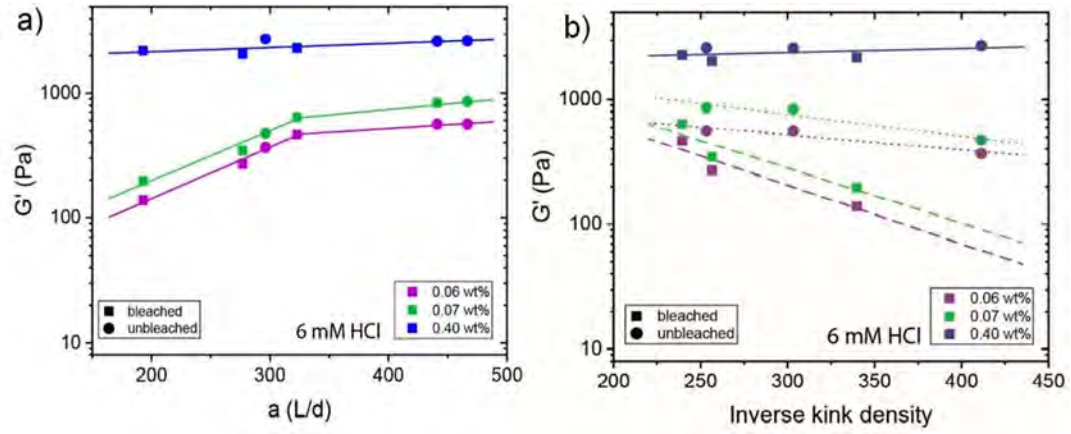

Figure 18. (a) Effect of CNF aspect ratio on the storage modulus (G') of the corresponding gel and (b) the relationship of G' of the gel and the inverse kink density in the network, after adding 6 mM HCl. The symbol with different colors indicates varying concentration, where the square and circle indicate CNF derived from bleached and unbleached pulps, respectively. Reprinted with permission from ref 283. Copyright 2020 The Royal Society of Chemistry.

NC-based aerogels/hydrogels are effective adsorptive media to remove varying pollutants from water. The effectiveness of the adsorption is directly related to the network formation of CNF scaffolds. Mezzenga and Nyström et al. investigated the self-assembled CNF structures in the varying form of gel network (aerogel/hydrogel).[283] They discovered that the aspect ratio of CNF could be used to control gel elasticity, where the results are shown in Figure 18. They reported that the threshold aspect ratio concerning the shear storage modulus (G') is 320, below which G' decreases with decreasing aspect ratio (Figure 18a). This is because smaller CNF cannot effectively entangle each other to form a stable network. They also suggested that the mesh size (ξ) of the CNF networks can be controlled by the CNF aspect ratio in this region, in which the plateau G' value is achieved when the aspect ratio becomes larger than 320. Theoretically, one can use eq 1 to calculate the mesh size of the gel, which is about 88 nm at the threshold aspect ratio.

$$\xi = \sqrt{\frac{2L_m^{\ 3}}{3L_p}} \tag{1}$$

In eq 1, L_m is the contour length (about 292 nm) of the CNF at the G' transition point (Figure 18a), and L_p is the persistence length of CNF (about 2.5 μm).[291] To form a network, each fibril has to make more than a single contact with another fibril. L_m, thus, represents the entanglement length of the fibrils that is longer than the ξ value at a certain concentration and can be presumed to be the fibril contour length (L) at the transition point of G' (Figure 18a). In general, longer flexible polymer chains can entangle more easily than smaller rigid polymer chains. CNF can be considered as a semiflexible polymer, where the observed kinks by TEM or AFM in CNF indicate that these sites can increase the interfibrillar entanglement. As shown in Figure 18b, the higher kink density in CNF produces stronger gel networks, attributing a higher degree of CNF entanglement. Interestingly, a correlation between the source of CNF, and the corresponding network elasticity was noticed in Figure 18. It was seen that CNF derived from the bleached pulp created a slightly weaker gel than that from the unbleached pulp at lower concentrations. This observation suggests the direct impact of the fibrillar properties on the corresponding gel properties.

Mechanical disintegration (defibrillation) of NC depends on its repulsive forces because of the surface charge. However, the concentration of NC also affects this process. It has been shown that the conversion of NC pulp to dispersed nanofibrils becomes more favorable at low cellulose concentrations (<0.1 wt %), whereas the higher concentrations (>0.6 wt %) promote the aggregation of nanofibers in the suspension.[283] This is because the interactions between dispersed nanofibrils at low concentrations are typically weak, but they can become relatively strong at higher concentrations due to hydrophobic interactions. The aspect ratio of NC, which also depends on the charge density, has a notable effect on the NC dispersion properties.[292] This indicates that the presence of charge density can also facilitate the mechanical defibrillation of the microfiber. It was interesting to note that Arcari et al. reported a nonlinear trend between the viscosity of the suspension and the aspect ratio.[292] Furthermore, it has been found that the branched CNF in suspension could only produce a small difference in viscosity as compared with the suspension of well-dispersed individual CNF. However, the increasing CNF concentration would increase the elasticity and produce a stronger fibrous network.[191]

While CNF films exhibit excellent mechanical properties, CNC products are generally weak and brittle, incapable of sustaining heavy stress transfer. Thus, several recent works have demonstrated to improve the mechanical properties of CNC films through interfacial engineering.[264,293−295] Hou et al. reported a humidity-mediated interfacial engineering pathway to toughen CNC films at the RH range between 10 and 90%.[293] In this scenario, the hydrogen bonding between CNC was partially replaced by hydrogen bonding of CNC−water−CNC, allowing better interfacial sliding and dissipation of localized strain during uniaxial tension. They observed a strain hardening state followed by the elastic stage in the stress−strain curves. The approach resulted in the increase of strain at break, in particular in the RH range of 30−50%. The highest tensile strength (~170 MPa) and toughness (~2.5 MJ/m^3) of CNC films were found at RH = 30%. In another approach, Adstedt et al. prepared CNC/polysaccharide films by intercalating amorphous polysaccharides (xylan, pullulan, and dextran) between nematic monolayers of CNC.[294] The free volume in the CNC network during the solution casting-induced self-assembly process was reduced by about 40% because of the presence of amorphous flexible polysaccharides. The resulting system exhibited a nearly 2-fold increase in modulus and toughness. CNC as a reinforcing nanofiller to produce stronger

https://doi.org/10.1021/acs.chemrev.1c00683
Chem. Rev. 2022, 122, 8936−9031

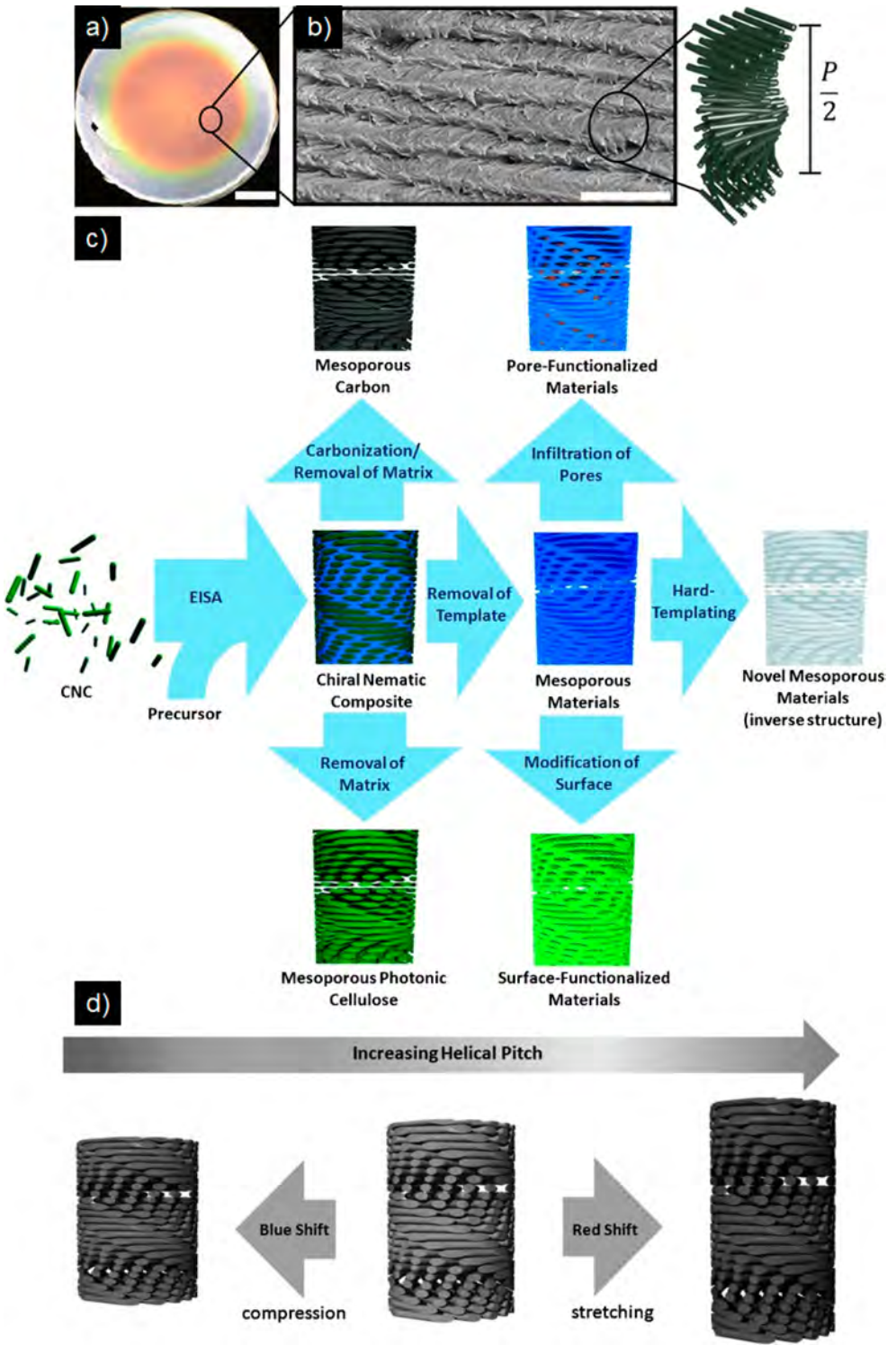

Figure 19. (a) Optical microscope image and (b) SEM image of CNC film with chiral nematic helical structure prepared by the EISA method. Reprinted with permission from ref 315. Copyright 2017 American Chemical Society. (c) Illustration of various hierarchical functional materials containing chiral nematic order that can be made by the EISA method, followed by varying postprocessing treatments. (d) Change of the chiral nematic pitch for sensing applications. Reprinted with permission from ref 316. Copyright 2015 Wiley-VCH Verlag GmbH & Co.

polymer nanocomposites has been an important application of interest. This application has been explored quite extensively by the French group since the 1990s[296] and later by the Dufresne group[22,297−299] and many others.[300,301]

The processes of nanocomposite preparation and the adoption of suitable modeling approaches to describe the varying nanocomposite systems using the concept of Halpin's mean field theory have been reported by Moon et al.[302] During the preparation of NC nanocomposites, it is usually important to have the nanofibrils fully dispersed to attain the maximum interfacial interactions with the surrounding matrix. However, the use of percolation theory to describe this system also

https://doi.org/10.1021/acs.chemrev.1c00683
Chem. Rev. 2022, 122, 8936−9031

requires that there are good mutual interactions between the interfaces of the individual fibril. Hence, there is the challenge to balance the complex interfacial interactions between NC and the matrix, especially to maintain the chemical modification of the NC surface (e.g., by grafting of hydrophobic polymers) without destroying the percolating NC network. This is because a high loading of grafted polymers on the NC surface can induce polymer aggregation, while the use of NC with a high aspect ratio can also induce flocculation and self-aggregation in the nanocomposite. Typically, the incorporation of CNF in the polymer matrix is a general hassle in manufacturing because even a low concentration can rapidly increase the viscosity of the system. There are various processing strategies to prepare nanocomposites,[303] some selective examples are (a) solution casting, followed by solvent evaporation, (b) freeze-drying/freeze-drying extrusion, followed by compression molding, (c) freeze-drying/freeze-drying extrusion, followed by a solvent exchange to produce high porosity products or by infiltration of a polymer resin to produce nanocomposites, (d) melt-compounding by incorporation of thermoplastic polymers, while avoiding degradation of NC or the polymer matrix, (e) the use of porous NC composites (e.g. aerogels, sponges, and foams) as scaffolding materials, (f) partial dissolution of cellulose, where a fraction of the NC is regenerated into a cellulose II structure, and (g) electrospinning to fabricate NC scaffolds. In this process, high voltage electricity is applied between the nozzle and a collector, where a nonwoven mat of submicron scale nanofibers is formed. A mixture of different NC/polymer compositions can be used as the feed.

4.2. Controlling Hierarchical Features of NC

It is important to note that the strong nanoscale materials, such as NC, do not always translate into strong bulk materials, unless they are processed into a structure with good fracture resistance and ability to dissipate high stresses. For example, stiff bulk nanomaterials are usually brittle with low strength.[304] Thus, strong biological-derived stiff nanomaterials are often toughened with low strength, flexible materials to improve the strain at break, by reducing the stress concentrations around the stiff nanomaterials and increasing the fracture toughness.[305,306] It is thought that the amorphous and flexible natural materials such as hemicelluloses or other polysaccharides can serve this purpose. Their presence can contribute to the gliding and interfacial sliding motions of stiff nanoparticles, thus promoting plastic deformation.

The self-assembly of nanoscale building blocks into higher-ordered architectures, stabilized by noncovalent interactions, including hydrogen bonding and van der Waal forces, can serve as excellent scaffolding templates to fabricate high performance nanocomposites. In particular, varying biological hierarchical structures that exhibit remarkable properties and functionality can be used as blueprints for this purpose. This is certainly the case for NC nanocomposite preparation and some examples are discussed below. For CNF, it has been reported in an isotropic nanocomposite system, containing 90% carboxymethylated CNF and 10% spider silk, exhibiting a tensile strength of 1015 MPa, a stiffness of 55 GPa and a tensile strain of 10%.[307] In another study, the hierarchical assembly made by flow-assisted alignment and interfacial complexation between a TOCNF and chitosan led to a tensile strength of 1289 MPa. When this system was cross-linked with Ca^{2+}, the tensile strength increased to 1627 MPa and simultaneously exhibited a high fracture toughness.[308] A different approach was conducted by Budtova et al.,[309] where hemicellulose rich (with an excess of 30% hemicellulose) bleached birch pulp was delaminated in a microfluidizer, followed by treatment with a water/ionic liquid (1-ethyl-3-methylimidazolium acetate) mixture. The mild post-treatment provided the swelling of the CNF scaffold without cellulose hemicellulose dissolution, where the process resulted in a highly disordered nanocomposite film exhibiting a tensile strength of 270 MPa and a strain at break value of 35% (nontreated CNF film exhibited a tensile strength of 100 MPa and strain at break of 7%).

One of the interesting features of CNC in water is its chiral nematic order, which has been previously known as the cholesteric liquid crystal order. By controlling this helicoidal order and using the evaporation-induced self-assembly (EISA) method, one can produce a variety of multifunctional materials with mesoporous networks (Figure 19). Revol et al. first demonstrated the EISA method, where the chiral nematic order could be preserved during the preparation of CNC films.[310] By adjusting the EISA parameters, such as ionic strength, substrate, and solvent evaporation rate, as well as the physicochemical properties of CNC, such as the aspect ratio and surface charge and functionality, one can fine-tune the final properties of the prepared films/materials, as well as the chiral nematic order.[167] For example, vacuum filtration has been used to increase the solvent evaporation rate and control the birefringence of the produced films.[311] The aspect ratio of CNC has a profound effect in preparing chiral nematic films. It has been shown that film prepared by CNC (tunicate) with a long aspect ratio exhibited both increases in tensile modulus and strength when compared with those by CNCs (wood pulp) with short aspect ratios.[312] Although there are many pathways to control the mechanical properties and characteristics of hierarchical NC structures to achieve the desirable features as shown in Figure 19, these practices have just begun to be considered for the applications of water treatments. Recently, MacLachlan group demonstrated the feasibility to incorporate both hydrophobic and hydrophilic CNC-based materials into an integrated system,[313,314] which facilitated the adsorption of both water-soluble and less water-soluble pollutants (although the challenges remained to remove multiple pollutants simultaneously). In addition, one component can be selectively removed from the integrated system to generate a mesoporous network. We believe this is a versatile and scalable strategy to obtain the desirable properties by manipulating the NC precursors with different types of surface charges (positive and negative) and modifications, as well as postprocessing and drying conditions.

4.2.1. Alignment of NC Materials. The mechanical performance of NC materials in varying forms (e.g., film, nanopaper, foam, aerogel, hydrogel, and filament) is intimately associated with the degree of alignment of the NC particles. The superior mechanical performance of NC building blocks is unable to guarantee the same performance in macroscopic NC materials, which is strongly dependent on the processing conditions, resulting structural features, and other factors (e.g., moisture). To overcome these challenges, the strategy of NC alignment can be used to achieve the desired properties, such as high tensile strength and toughness, of microscopic NC or NC-reinforced materials.[169] In general, NC alignment can be achieved by two pathways: the bottom-up approach such as the use of magnetic, electric and flow (shear and elongational) fields, and solid state stretching (uniaxial and biaxial), and the top-down approach, such as templating. Several reviews have

https://doi.org/10.1021/acs.chemrev.1c00683
Chem. Rev. 2022, 122, 8936−9031

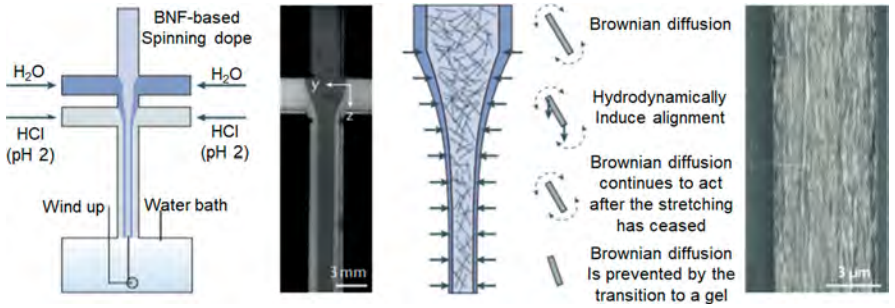

Figure 20. Regulating the alignment of CNC or CNF materials via microfluidic spinning processing. The nanofibrils are illustrated as rod-shaped and their fibril length associated with the channel width is exaggerated 300 times. The diffusion of sodium ions (blue) is incorporated in the form of NaCl solution. The colloidal surface charged nanofibrils are free to rotate in the spinning dope due to electrostatic repulsion and they can be aligned along the accelerating flow direction. Brownian diffusion (dashed arrows) and hydrodynamically induced alignment (solid arrows) are involved in the hydrodynamical, molecular and electrostatic processes. To the right, a resulting CNF filament is displayed. Reprinted with permission from ref 328. Copyright 2018 Springer Nature.

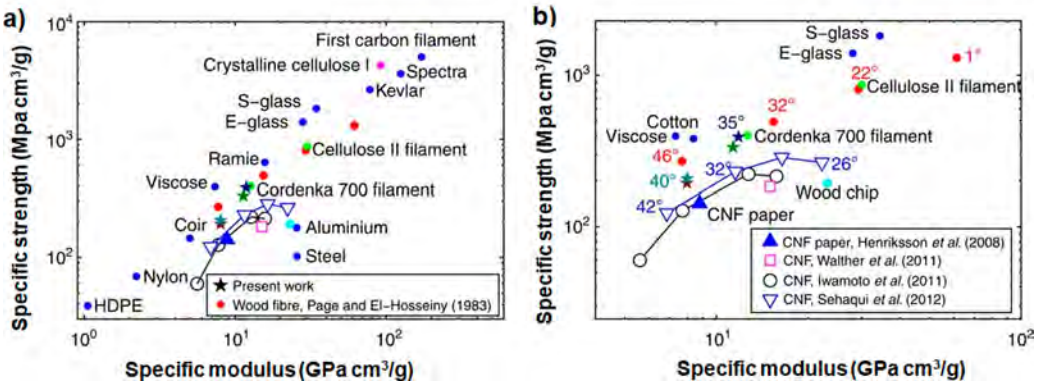

Figure 21. (a and b) Comparison of mechanical properties (i.e., specific ultimate strength and specific Young's modulus) of varying filament materials. Mechanical properties of wood-derived cellulose pulp fibers are represented by solid red dots, while films and filaments made from CNF materials using these pulp fibers are shown in open markers. The mechanical performances of different degrees (angles toward the flow direction) of alignment in these filaments are represented by filled stars. Adapted from ref 326. Copyright 2014 Springer Nature.

dealt with the topic of NC (CNC and CNF) alignment to improve the mechanical properties.[167,169,170,317]

A recent review has dealt with the challenges and opportunities in NC spinning (i.e., elongational flow induced alignment) to produce high-performance filaments.[318] It was interesting to note that the spinning of NC particles is quite different from the spinning of polymers from the molten, gel, or solution state. For example, there have been several reports on the production of self-assembled filaments using the dry-spinning approach,[319−321] but only with limited success. A more promising approach is the wet spinning of NC gels by extrusion through a spinneret into a coagulation bath. The orientation and alignment of NC could be fixated by solvent depletion, where several groups have successfully demonstrated this approach on a laboratory scale. For example, Iwamoto et al.[322] used TOCNF and coagulated a CNF filament in acetone. They found that, at their highest spinning rate, the resulting filament exhibited Young's modulus of 23.6 GPa, a tensile strength of 321 MPa, and elongation to break of 2.3%. Walther et al. also wet spun TOCNF in various organic solvents and reported the filament with Young's modulus of 22 GPa, a tensile strength of 275 GPa, and elongation to break of 4%.[323] Similarly, Lundahl et al. reported their CNF filament exhibited Young's modulus of 21.3 GPa, a tensile strength of 297 GPa and elongation to break of 2.8% when coagulated in acetone.[324] These observations indicate the challenges of using low CNF concentration in a conventional wet spinning setup, which always leads to inferior filament properties.

Microfluidic spinning has turned out to be a promising technique for spinning biopolymeric nanofibrils, including CNC and CNF. The major advantage of this technique is that the spinning channel and design can be adjusted to control the dope flow, and thus optimizing the processing conditions. In addition, the coagulation can be controlled by pH or electrolytes, while shear flow can be introduced to the spin channel to modulate the mechanical properties of the resulting filaments. In a recent design, the flow focusing arrangement (shown in Figure 20) has been demonstrated to fine-tune the alignment of both CNC and CNF.[325,326] The results of mechanical properties from the CNF filaments prepared by microfluidic spinning, together with several other filaments for comparison, are shown in Figure 21. The results indicate that the mechanical properties of the best performing NC filaments can rival the best high-performance polymer fibers. A recent review[327] of hierarchical nanostructured materials points out the possibility that the proper assembly of nanostructured materials in combination with multiscale modeling and machine-learning techniques can pave the path to overcoming the many bottlenecks for manufacturing high performance nanostructured materials.

We believe the newly developed flow-assisted assembly approach has a great potential to be used as a future manufacturing platform for creating 1D filaments, 2D films

https://doi.org/10.1021/acs.chemrev.1c00683
Chem. Rev. 2022, 122, 8936−9031

and membranes, and 3D-printed articles. The quantitative comparison of theoretically predicted and experimentally obtained orientation distributions of elongated nanoparticles in restricted flows can provide basic knowledge for projecting and controlling the development of new nanostructured materials.[329,330]

5. NC-ENABLED WATER PURIFICATION TECHNOLOGIES

5.1. Coagulation and Flocculation

Coagulation/flocculation is a simple and cost-effective method for solid−liquid separation, usually based on charge interactions between the colloids and the coagulant/flocculant. There are many different mechanisms on how to distinguish between coagulation and flocculation. The classical distinction is that flocculation is induced by long-chain polyelectrolytes, and coagulation is caused by simple electrolytes that are compressing the electrostatic double-layer that can be described by the DLVO-theory.[331,332] As hydrolyzed Al/Fe cannot be classified as either a long chain polyelectrolyte or as a simple electrolyte, the literature on water treatments usually uses the combined wording of "coagulation/flocculation" for whatever aggregation phenomena. More recently, there has been increasing attention toward natural coagulants/flocculants for wastewater treatments (e.g., recent reviews published by Othmani et al., Saleem and Bachmann, Gautam and Saini, and Mohd-Salleh et al.).[333−336] The application of natural coagulants is not new and has been used by mankind for more than 1000 years, but it has been displaced by inorganic salts (e.g., Al/Fe) and synthetic polymers during the last hundred years. Natural coagulants/flocculants are mostly obtained from various plants and animals and may be classified as polysaccharides, amino-polysaccharides and polyphenols (e.g., tannins and various proteins). Usually, common anionic/cationic polyacrylamides are used together with metal ions, such as Al/Fe ions. However, there are issues with these practices, including synthetic polymers are not readily biodegradable, and the use of metal ions is often not desired. There are also specific concerns due to varying environmental considerations.[334] For example, high carbon footprint can be associated with certain coagulants, negative human health effects can be associated with the residual Al in wastewater treatments, and environmental pollution is caused by improper disposal of raw Al-sludge. Therefore, the development of NC-based coagulants/flocculants is interesting because these materials are biodegradable, sustainable, and biocompatible. While there has been a strong research focus on NC adsorbents for heavy metal and dye remediation, there are only limited publications on coagulation/flocculation for wastewater remediation.[15,337,338] This section is intended to review the whole field of various coagulants/flocculants that are relevant to NC materials, which includes various charged CNC and CNF, as well as microparticulate materials that can be considered a separate class of coagulants/flocculants more or less unknown to the water remediation community. In spite of the complexity of the varying aggregation processes, it is convenient to classify the various aggregation mechanisms into different classes including charge neutralization and charge reversal, patch flocculation mechanism, heterocoagulation, bridging flocculation (monopolymer) systems (adsorption flocculation), and complex flocculation, as shown in Table 3. Detailed discussion of these aggregation mechanisms is given in section S4.

Table 3. Several Classes of Aggregation Mechanisms That Can Be Found in the NC Coagulation/Flocculation Process

	different classes of NC aggregation mechanisms	refs
(a)	charge neutralization and charge reversal	339−341
(b)	patch flocculation mechanism	342−345
(c)	heterocoagulation	346, 347
(d)	bridging flocculation (monopolymer) systems (adsorption flocculation)	348−350
	sensitization flocculation	348, 351, 352
(e)	complex flocculation	353
	dual polymer systems	354
	microparticle flocculation systems	353
	sweep flocculation	355
	network flocculation	356

5.1.1. Manufacturing of Charged CNC/CNF Materials.

Anionic CNC. The use of CNC in coagulation/flocculation operations requires an increased charge density compared to that of the traditional hydrolysis using H_2SO_4 in making CNC.[357] There are several post-treatments available, many of them being identical with those applied for pretreatments for fabrication of CNF or CNC, such as (TEMPO),[102,358] periodate−chlorite oxidation,[359,360] ammonium persulfate,[131] (on pulps), and carboxylation using citric acid/HCl (on MCC).[361] It should be recognized that carboxymethylation (using epoxypropyltrimethylammonium chloride (EPTMAC)) on MCC is an old commercial method to produce many different NC products, where EPTMAC is a valuable additive in pharmaceutical, food, cosmetics, etc. Additionally, van de Ven et al. have demonstrated another variation of the periodate-oxidation method.[362,363]

It has become apparent during the above processes that the reaction of cellulose takes place on the surface and in the paracrystalline regions of the fibrils. If the cleavage of the chains occurs in the paracrystalline region, this will induce the region to become more disordered and hence, more reactive. Kim et al. found that the dialdehyde group of cellulose in this region could be solubilized by hot water.[364] This discovery inspired a novel process development to fabricate sterically stabilized CNC,[365] resulting in a new class of NC termed hairy cellulose nanocrystalloids (HNC).[363,366]

Cationic CNC. There have been numerous efforts to prepare cationic CNC. The first attempt was demonstrated by Hasani et al. in 2008,[367] using an alkali (7% NaOH) mediated reaction with EPTMAC. The resulting crystal structure was still cellulose I, but the reaction could not reach a higher cationic value (i.e., 0.26 e/nm^2 or 0.12 mequiv/g), which is relatively low for strong charge interactions. The Suopajärvi group has manufactured cationic CNC using a two-stage process starting with periodate oxidation to produce dialdehyde cellulose, which is then treated with aminoguanidine hydrochloride to make aminated cationic CNC.[368] In a different approach by Eyley and Thieleman, CNC was treated with click chemistry to introduce imidazolium-grafted CNC.[369] This pathway involved the process of copper-catalyzed azide−alkyne cycloaddition in several steps and yielded a charge density of 1.17 e/nm^2. This group later demonstrated a simpler one-pot route, involving the process of pyridine-grafting using 4-(1-bromoethyl/bromomethyl)benzoic acid and pyridine, to produce cationic CNC.[370] They managed to exceed the surface charge in their previous demonstration under suitable cationization conditions. Another approach to produce cationic CNC was by the use of a one-step reaction

https://doi.org/10.1021/acs.chemrev.1c00683
Chem. Rev. 2022, 122, 8936−9031

involving 1,1-carboxyldiimidazole-mediated coupling with 1-(3-aminopropyl)imidazole, resulting in a CO_2-switchable CNC system.[371] In this system, CNC could be switched from a negative zeta potential value under alkaline conditions to a positive zeta potential value (i.e., cationic) under acidic conditions by changing pH, allowing the recovery and reuse of coagulants/flocculants. A similar approach to make pH-switchable CNC was also taken by the Cranston group using surface-initiated graft polymerization involving 4-vinylpyridine and ceric (IV) ammonium nitrate.[372] Finally, the van de Ven group demonstrated the system of hairy cationic CNC using a two-step reaction.[362,363] In this process, dialdehyde cellulose modified CNC was first prepared by periodate oxidation. Subsequently, dialdehyde cellulose was cationized by a reaction between (2-hydrazinyl-2-oxoethyl)-trimethylazanium chloride, known as Girard's reagent T, and aldehyde groups on the cellulose surface. The fibrous suspension was then treated with hot water at 60 °C, resulting in cationic nanocrystalloids. Cationic CNC can also be produced by physical pathways. For example, anionic CNC can be converted to cationic CNC by using the multilayer adsorption process, which can also be used to adjust the charge density on the CNC surface.[373,374]

Anionic CNF. Most CNF materials contain some level of negative charges, and thus can be considered anionic CNF. The introduction of surface charge in cellulose is essential for NC production as it reduces the energy consumption during delamination of cellulose fibers and prevents the aggregation of resulting CNF particles. There has been a multitude of methods demonstrated to incorporate charge groups on cellulose, including TEMPO-oxidation,[102,375] carboxymethylation,[106] phosphorylation,[111] sulphonation,[376] and periodate oxidation.[103,104] Recently, a unique method of nitro-oxidation was demonstrated by us where carboxylated CNF can be produced directly from untreated biomass.[108,109] This is because NOP combines the steps of pulping and cellulose oxidation, thereby saving a great deal of energy, water and chemicals. Because of the presence of a surface charge, anionic CNF is a natural coagulant/flocculant, capable of adsorbing positively charged contaminants in water. Of course, the higher the charge is, the more effective the coagulation/flocculation efficiency is.

Cationic CNF. Cationic CNF can be created by different pathways. In one simple approach, cationic CNF can be produced by reacting EPTMAC with carboxylated CNF under aqueous alkaline conditions, where high positive charge density can be achieved.[107,377] Another simple modification to create cationic CNF is by reacting carboxylated CNF with chlorocholine, albeit under nonaqueous conditions.[378] In other methods, many groups have used the periodate modification route to first produce dialdehyde cellulose and then reacted the aldehyde group with Girard's reagent T (2-hydrazinyl-2-oxoethyl)-trimethylazanium chloride) (the same as the cationic CNC production route by van de Ven's group), where the process can yield high positive charges on the resulting CNF.[379,380] The major difference between the CNC productions vs. the CNF productions is the processing temperature, where low temperatures favor the creation of cationic CNF. However, the periodate route often suffers from the slow reaction rate between cellulose and periodate, although the process can be improved by wet-milling,[381] the addition of lithium-ion, higher temperature operation,[360] and ultrasonification treatment[382] (although this is not very practical in scale-up production). Finally, there have also been some efforts made to use click-chemistry, a general approach for surface modification, to create cationic CNF containing amine functionalities.[383]

5.1.2. Coagulation/Flocculation Using Charged CNC/CNF Materials. All charged NC materials (CNC and CNF) can be used as coagulants/flocculants, where some examples and their performances are summarized in Table 4. In this table, the evaluation parameters include the residual turbidity and chemical oxygen demand (COD) of the treated water after coagulation/flocculation performed by NC materials, where most NC-based coagulants/flocculants show high turbidity and good COD reduction. Zhu et al. studied dicarboxylic NC for flocculation test, which showed a higher turbidity removal among all the tabulated flocculants.[16] Commercial coagulants often exhibited better turbidity reduction efficiency (14−40%) than dicarboxylic NC, but the latter also showed good COD removal (see Table 4).[384] Figure 22 shows the performance of a commercial coagulant ($CaCl_2$) and its mixture with dicarboxylic NC flocculant for coagulation-flocculation of kaolin suspension.[16] As the presence of dicarboxylic NC can also cause electrostatic interactions with cationic kaolin, the use of $CaCl_2$ and dicarboxylic NC mixture did not follow the adsorption/bridging or sweeping mechanisms. It has been proposed that the coagulant $CaCl_2$/other salts can create a cationic patch-up on the surface of kaolin particles. Subsequently, the carboxyl groups on dicarboxylic NC can connect the kaolin particles through cationic patches that lead to their precipitation.[16] The $CaCl_2$ and dicarboxylic NC mixture treatment, therefore, can produce larger flocs, which would ease the flocculation post-treatment.

Compared with carboxyl groups on dicarboxylic NC, it has been reported that sulfonic groups would have a higher affinity toward iron patches of coagulant.[386] In addition, the electrostatic affinity of the sulfonic group toward certain metal ions may be higher as compared with carboxyl or hydroxyl groups. Thus, the sulfonic groups containing NC may more likely have a larger degree of ionization and projected better turbidity and COD removal. However, in practice, we did not notice any significant differences between anionic dialdehyde and sulfonated NC and dicarboxylic NC in Table 4. In the following, we discuss the performance evaluation of the mono and dual systems in better detail.

Monocomponent Systems Based on CNC. The van de Ven group demonstrated an anionic CNC material via periodate-oxidation, chlorite, and TEMPO-oxidation, which was termed electrostatically stabilized nanocrystalline cellulose (ENCC),[389] and compared it with a sterically stabilized nanocrystalline cellulose (SNCC).[390] They found that ENCC functioned as charge neutralization flocculant, whereas SNCC functioned as a bridging flocculant, even though SNCC required higher CNC doses. In other studies, hairy cationic CNC has recently been reported as a powerful retention additive in a recycled paper (negatively charged) by Blanco and Negro in conjunction with the van de Ven group.[391] They found that optimum flocculation occurred at the isoelectric point and that the reflocculation efficiency was high (although the extent of reflocculation was not investigated), a telling sign for microparticulate additives. The group of Thieleman has successfully reported flocculation experiments using pyridine grafted nanocrystals (cationic).[392] Their results demonstrated that highly cationically charged CNCs are excellent flocculants for freshwater microalgae. Microalgae could also be recovered from the water,[393] using the previously mentioned CO_2-switchable CNC technology.[371]

Dual Component Systems Based on CNC. In a model study, anionic CNC (from the classical hydrolysis process using

https://doi.org/10.1021/acs.chemrev.1c00683
Chem. Rev. 2022, 122, 8936−9031

Table 4. Varying Examples of Using NC for Coagulation/Flocculation Applications and Their Performance

coagulant/flocculant (dosage)	charge	reaction parameters	water sample	turbidity reduction (%)	COD (%)	ref
$Fe_2(SO_4)_3$ (coagulant) (25−37.5 mg/dm^3)		stirring (200 rpm, 3 min, room temperature (RT))	municipal wastewater	50−80 (250 mg/L)	50 (250 mg/L)	384
dicarboxylic NC/(2.5−5 mg/dm^3)	anionic (0.38−1.75 mmol/g)	40 rpm, 15 min, settling time 30 min, RT		40−80	40−60	
				60 (pH 8)	42 (pH 8)	
$CaCl_2$/(100 mg/L)		stirring (200 rpm, 3 min)	simulated wastewater (kaolin) 1000 mg/L	81.3		385
polyetherimide (PEI) grafted pomelo-CNF (20−80 mg/L)	cationic	settling time 40 min		92.6		
$CaCl_2$ (300 mg/L)		settling time 30 min, pH 7	kaolin (500 mg/L)	66		16
dicarboxyl NC/(25 mg/L)	anionic (2.57 mmol/g)			99.5		
$Fe_2(SO_4)_3$ (coagulant)/(25 mg/dm^3)		settling time 30 min, 200 rpm, 3 min, RT	municipal wastewater	62−75	52	386
anionic dialdehyde/sulfonated NC/(2.5 mg/dm^3)	anionic (0.36−0.51 mmol/g)	40 rpm, 15 min, settling time 30 min, RT		48−55	32−35	
poly(acryloyloxyethyltrimethyl ammonium chloride)-grafted CNC/(40 mg/L)	cationicity (α = 31.2%)	200−500 rpm, 5−10 min, pH 7, 25 °C	neutral reactive blue 19 (100 mg/L)	color removal (95%)		387
hexadecyltrimethylammonium bromide functionalized CNC/(10 mg/L)	cationic (ζ = +22 mV)	200−65 rpm, 2−15 min, setting time 30 min, pH 7	kaolin (50 NTU)	98		388
			real wastewater (TB Hall dam, 13.96 NTU/Bronkhorstspruit WTW 13.99 NTU/Weltered WTW, 34.5 NTU)	96		

H_2SO_4) was used as a bridging flocculant for polyethyleneimine-functionalized latex particles.[394] Although these authors referred to them as microparticles, the data failed to confirm any relevance to microparticulate systems, probably due to the low charge density (0.33 e/nm^2) of the CNC. Recently, two dual component systems were reported for retention and drainage of pulp suspensions, involving CNC (H_2SO_4 hydrolyzed)[395] and TEMPO-oxidized CNC (TOCNC),[396] combining either with cationic polyacrylamide or cationic starch. They demonstrated that these mixtures behaved as typical microparticulate retention systems, where TOCNC exhibited better performance than acid hydrolyzed CNC (lower surface charge).

Monocomponent Systems Based on CNF. The retention of fillers, such as precipitated $CaCO_3$ or kaolin clay to a paper pulp by using different CNF materials has been investigated in both monocomponent systems and dual systems.[397] It was found that CNF-materials must have a high charge, being either anionic or cationic, to function as an efficient retention system. Both TEMPO-modified and carboxymethylated CNF-materials were very functional. One study has noted the marked flocculation reversibility, which is a key property of microparticulate systems. Another study[398] also reported the retention of ground $CaCO_3$ (its charge is controlled primarily by Ca ions), where two types of CNF were used: TOCNF and periodate−chlorite oxidized CNF. Basically, the authors came to the same conclusions as to the group of Koronen and Laine,[397] that both chosen CNF materials exhibited a powerful ability to cause agglomeration of ground calcium carbonate. Cationic monocomponent systems have also been used to treat municipal activated sludge. For example, the group of Sirviö modified periodate oxidized CNF with aminoguanidine hydrochloride to create aminated cationic CNF. They claimed that its performance on turbidity reduction was very near that of the referenced synthetic polymer.[368] Another group has also demonstrated that cationic CNF prepared by using EPTMAC was very efficient in flocculation and removal of an azo dye.[399]

Dual Component Systems Based on CNF. There are numerous papers dealing with the combination of cationic polyelectrolytes and anionic CNF. For example, Koronen and Laine also reported that the addition of a cationic polyelectrolyte (e.g., C-polyacrylamide) to negatively charged CNF exhibited strong synergistic effects on the retention property,[397] which has also been verified by several other groups.[400−402] One study also noted a significant reflocculation capability in both mono-systems and dual-component systems, as expected by the microparticulate systems.[402] Anionic CNF complexed with certain metal ions, such as Al and Fe ions, has also been investigated. For example, Niinimäki et al. investigated the flocculation of municipal wastewaters using periodate treated CNF that was sulfonated using ferric sulfate as a cross-linker. They noted that the flocs formed with this anionic NC material system were more stable than those formed by the referenced polymer.[386] In another study of flocculation of municipal wastewater, the same group used a periodate-chlorite-treated CNF (carboxylated CNF), together with ferric sulfate, and they came to a similar conclusion as using the sulfonated CNF system.[384] These researchers also investigated the combination of nanoparticles (from dialdehyde cellulose) or soluble anionic celluloses on coagulation/flocculation with aluminum sulfate. They concluded that NC particles were more powerful in coagulation/flocculation than soluble anionic celluloses, strengthening the idea of microparticulate particles for coagulation/flocculation operations. Finally, a different group

https://doi.org/10.1021/acs.chemrev.1c00683
Chem. Rev. 2022, 122, 8936−9031

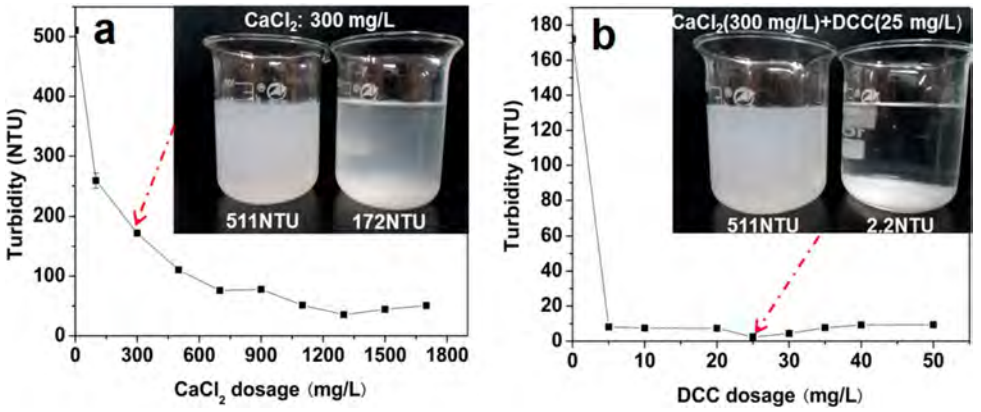

Figure 22. (a) Performance of only $CaCl_2$ and (b) its mixture with dicarboxylic NC (DCC) as coagulant/flocculant to the kaolin suspension (concentration = 511 NTU). Their corresponding digital photos are given as insets. Reaction parameters: pH = 7.0 and settling time 30 min. As seen, a small amount of DCC (25 mg/L), along with coagulant $CaCl_2$ (300 mg/L), secure very minimal residual turbidity (2.2 NTU). Reprinted with permission from ref 16. Copyright 2015 American Chemical Society.

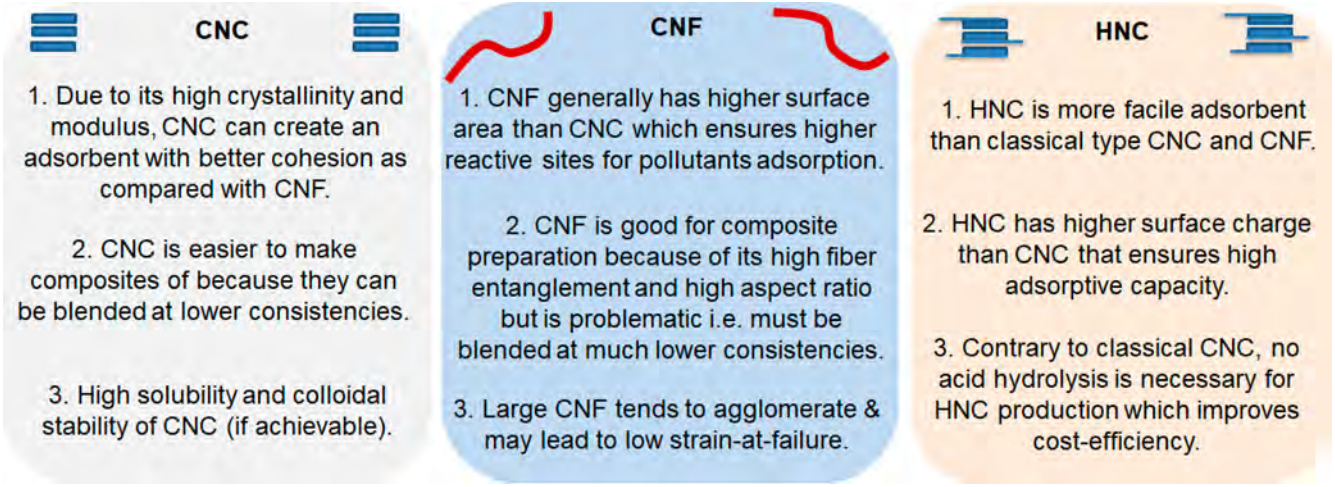

Figure 23. Features of CNC, CNF, and HNC that determine the adsorption properties for water purification.

investigated the combination of TOCNF in combination with cationic polyacrylamide.[403] These authors concluded that post addition of CNF, even after strong shear, could result in strong flocculation, and the system behaved like a typical micro-particulate system.

5.2. Adsorption

Adsorption is an effective method for water remediation due to its simplicity, scalability, and cost-effectiveness to remove pollutants. Many varying adsorbents, such as activated carbon, CNT, carbon nanowires, graphene, their derivatives, and zeolites have been extensively investigated and used for solute adsorption.[404] With the growing interest of developing sustainable adsorption technology, there is an increasing demand for using NC for adsorption operations. Because of its relatively low cost (≈4380 USD/t),[405] high surface area,[13] high aspect ratio, decent modulus, good crystalline degree,[15] hydrophilicity, low mass density, high surface energy, and biodegradability; this could greatly reduce environmental threats. There are multitudes of NC surface modification routes that can further tailor the adsorption efficacy and ensure solute selectivity. However, since different types of NC can possess different adsorption properties, it is often difficult to determine which NC system is the best adsorbent candidate. To deal with this issue, we summarize the advantages and disadvantages of using CNC-, CNF-, and HNC-based adsorbents for water purification in Figure 23. This figure was composed based on several studies. Liu et al. reported that, with almost the same specific surface area between CNC (138−226 m^2/g) and CNF (146−219 m^2/g), CNC exhibited a higher Ag(I) adsorption capacity of 34.4 mg/g as compared with CNF of 15.5 mg/g.[406] This difference in adsorption capacity might be due to the different pH values (6.4 for CNC, 5.5 for CNF) and different preparation schemes (H_2SO_4 for CNC, grinding for CNF) adopted during NC production, which resulted in different negative charges (230 μmol/g for CNC and 100 μmol/g for CNF). As can be seen from Figure 23, we also included the class of HNC materials. HNC contains amorphous hairy regions from both ends, which dictate the colloidal/steric stability when suspended in water. There are also different types of HNC, with neutral, positive, and negative charges.[407] In terms of dimension, they are similar to conventional CNC but have high charge content because of the carboxylated groups in the amorphous regions. Tavakolian et al. prepared HNC for the adsorption of methylene blue (MB).[408] That HNC had a negative charge density from 3.95 to 4.90 mmol/g and the dye removal capacity of HNC was considerably higher as compared with conventional CNC-based adsorbents. The difference between HNC and conventional CNC charge density could be due to the presence

https://doi.org/10.1021/acs.chemrev.1c00683
Chem. Rev. 2022, 122, 8936−9031

Table 5. Decontamination of Organic and Inorganic Water Pollutants Using NC-Based Adsorbents

Adsorbent	Cellulose source/Types	Preparation methods	Tested pollutants	Reaction media	Surface area (m^2/g)	Adsorption capacity (mg/g)	Ref.
Organic Pollutants Adsorption							
NCPPY[a] (Composite)	Cotton linter/CNC	Sulfuric acid hydrolysis/Stirring	Congo red (CR)	Adsorbent (10-30 mg), CR and Cr(VI) (10-50 mg/L), binary mixture, 150 rpm, 3 h and 25°C	CNC (197) NCPPY (488)	CR(74.87)	410
SA-PAM[b]			Methylene blue (MB)	Adsorbents (800 mg/L), MB (5-500 mg/L) and 25°C	-	43.1	411
SA-PAM-CNC (Hydrogel)	Bleached wood pulp/CNC	Sulfuric acid hydrolysis and mechanical process/Stirring				47.6	
SA-PAM-BC[c] (Hydrogel)	BC					47.8	
SA-PAM-TOCN[d] (Hydrogel)	CNC	TEMPO /Stirring				57.1	
NC-Graphene oxide (GO) (Aerogel)	*Amorpha fruticosa*/CNF	Homogenizing/Ultrasonication	MB CR Waste oil	Adsorbent (10 mg/L), MB and CR (10 mg/L), 120 rpm/min, 24 h and room temperature (RT)	-	265.6 21.5 25.6 g/g	412
PVA[e]-CNC (Microgel)	Cotton straw /CNC	Acid hydrolysis/Grafting	Chlorpyrifos (CP)	Adsorbent (200-1000 mg/L), CP (10-40 mg/L), 15 ± 2 °C and 48 h	CNC (27.237) PVA-CNC (32.17)	98.12	405
NCPPY (Composite)	-/CNC	Sulfuric acid hydrolysis and mechanical breakdown/Stirring	Direct blue 6 (DB 6)	Adsorbent (250 mg), DB 6 (10-500 mg/L), pH 7.0, 50°C, 140 rpm and 3h	-	760.81	413
			Bromophenol blue (BB)	Adsorbent (350 mg), BB (10-500 mg/L pH 9.0, 50°C, 140 rpm and 3h	-	689.56	
			DB 6+ BB	Adsorbent (250 mg), pH 3.0, 50°C, 140 rpm and 3h	-	846.98	
NB-DANC-CMC[f] (Aerogel)	-/CNC	Sulfuric acid hydrolysis /Stirring and sonication	BB	Adsorbent (5.0 mg), BB and DB-6 (0.5-8.0 g/l), pH 2.0 and 40°C (BB) and pH 4.0 and 50°C (DB-6)	-	29.84	414
			DB-6		-	20.92	
NCA-OA[g]-Fe_3O_4 (Aerogel)	-	Blending/Mixing/Stirring	Cyclohexane	RT for 5 min	NCA-OA-Fe_3O_4 (397.5)	68.06 g/g	415
NCA			Ethyl acetate		NCA (47.5)	81.12 g/g	
NCA-OA			Vacuum pump oil		NCA-OA (21.0)	60.50 g/g	
CC[h]	Corncob/CNC	Sulfuric acid hydrolysis/H_3PO_4	Methyl orange (MO)	CC, FCC, CCNC, (0.5 g), pH 3.01, 4.11, 2.09 respectively, MO (10-50 mg/L), 30°C, 300 rpm and 30 min	-	17.86	416
FCC[i]						60.82	
CCNC[j]						206.67	
NAF/SDS[k] (Aerogel)	Cotton/-	Commercial NC/Blending and mixing	Cyclohexane	RT for 5 min	NAF/SDS (151.2)	206.79 g/g	417
			Ethyl acetate		NAF (47.5)	194.75 g/g	
			Vacuum pump oil			145.20 g/g	
DNC[l]	Date palm/-	Acid hydrolysis/Oxidation	Gentian violet	Adsorbent (10 g/L), pH 8, 20°C, 100 rpm and 70 min	-	11.71	418
MNCC[m]	*Eichhornia crassipes*/NCC	HCl/Citric acid/Stirring	Reactive blue 21 (RB21) and Crystal violet (CV)	Adsorbent (17.5 g/L), RB-21 and CV (5-100 mg/L), 5-120 min and RT	-	44.05	419
						263.2	
Material Institute de Lavoisier (MIL-100(Fe)-BC (Composite)	-/BC	Refluxed/Stirring	Rhodamine B (RhB)	Adsorbent (0.18 g), RhB(10 mg/L), 35 h, and room temperature	BC (159) MIL-100(Fe)-BC (47.13)	2.77	420
DANC-PVAm[e] (Hydrogel)	Kraft pulp/CNC	Sulfuric acid hydrolysis/Periodate oxidation/Mixing	CR	Adsorbent (0.5 g/L), CR (65 mg/L) and 180 rpm		1469.7	421
			Acid red GR	Adsorbent (0.5 g/L), Acid red GR (350 mg/L) and 180 rpm	-	869.1	
			Reactive light yellow (RLY) K-4G	Adsorbent (0.5 g/L), RLY (375 mg/L) and 180 rpm		1250.9	
Universitetet i Oslo (UiO)-66/NC (Aerogel)	Bleached softwood kraft pulp/CNF	Mechanical fibrillation/ Homogenizing/Stirring and sonication	MO	Adsorbent (1 g/L), MO (50 mg/L) and 250 rpm	CNF (29) UIO-66 (1064) UiO-66/NC (826)	UiO-66 (68.4) UiO-66/NC (71.7)	28
			MB			UiO-66 (30.4) UiO-66/NC (51.8)	
CNF	Rice straw/CNF	TEMPO mediated oxidation/Sonication	MB	Adsorbents (250 mg/L), 25°C, 120 rpm, MB (10-1000 mg/L), CR (10-2000 mg/L) and 16 h	CNF (3220) CNF-GnP (3036)	GnP (567) CNF (1387) CNF-GnP (1178)	422
CNF–CNT (Aerogel)							
CNF–GnP[n] (Aerogel)			CR			GnP (1787) CNF (351) CNF-GnP (585)	

https://doi.org/10.1021/acs.chemrev.1c00683
Chem. Rev. 2022, 122, 8936−9031

Table 5. continued

Adsorbent	Cellulose source/Types	Preparation methods	Tested pollutants	Reaction media	Surface area (m^2/g)	Adsorption capacity (mg/g)	Ref.
O-CNCs-IIP[o] O-CNCs-NIIP[o] O-CNCs/O-MWCNT-IIP O-CNC/O-MWCNT-NIIP O-CNC/GO-IIP O-CNCs/GO-NIIP	Cotton/CNC	Sulfuric acid/TEMPO/Sonication	Dysprosium Dy(III)	Adsorbents (1 mg/ml), Dy(III) (0-200 mg/L), pH 4 and 100 rpm	3.32 2.99 5.71 5.08 9.06 6.91	30.47 25.70 38.26 35.94 48.14 39.62	423
NCPPY (Composite)	Cotton linter/CNC	Sulfuric acid hydrolysis/Stirring	Cr(VI)	Adsorbent (10-30 mg), CR and Cr(VI) (10-50 mg/L), binary mixture, 150 rpm, 3 h and 25°C	CNC (197) NCPPY (488)	Cr(VI) (12.67)	410
MIL-100(Fe)-BC (Composite)	NG/BC	Refluxed/Stirring	As(III)	Adsorbent (0.18 g), As(III) 20 mg/L, 72 h and room temperature	BC (159) MIL-100(Fe)-BC (47.13)	4.81	420
ZIF-67[q]-BC-Chitosan (Aerogel)	*Gluconacetobacter xylinus*/BC	Physical mixture, *In situ* synthesis, and lyophilization	As(III) Cr(VI) Fe(III) Mn(II) Ni(II)	Cu(II) and Cr(VI) (1 g/L), pH 6.0 and 24 h	BC aerogel (18.8) BC/Chitosan (8.4) ZIF-67-BC-Chitosan (268.7)	4.81 152.1 ≈ 160 ≈ 180 ≈ 224	424
CNC IACNC[r] SINC[s] UiO-66 EDTA[t]/CNF/CMC (Aerogel)	Jute/CNC Douglas fir pulp/CNF	Pretreatment and Probe sonication in water /Esterification Grinding>TEMPO>Homogenizing/Stirring and Sonication	Pb(II) Mn(II) Cr(III) Cu(II) Co(II) Ni(II) Mn(II) Zn(II) Fe(III) Zr(IV)	pH 5.5, 125 min and 25–30 °C Adsorbent (0.4 g/L) 120 h	3.6813 0.2244 0.05332 -	10 58 85 396 104 307 120 251 215 115 165	425 426
Spun-TCNF-PEI[u]	Tunicate/CNF	TEMPO/Stirring	Pt	Adsorbent (200 mg/L), Pt (100 mg/L), Single/binary (automobile) solution, 24 h and RT	150.93 (TCNF) 106.07 (TCNF-PEI)	417.6 (Single) 120.2 (binary)	427
Chitosan-g-poly(acrylic acid)-NC (Hydrogel)	Cotton/CNC	HCl hydrolysis/Stirring/ free Radical polymerization	Pd(II) Cu(II)	Adsorbent (20 mg), pH 4, Pd(II) and Cu(II): 1 g/L, 100 rpm and 25°C	-	818.4 325.5	428
CNF-COOH-Dopamine (DP) CNF-COOH-Dopamine-Fe (DF) CNF-COOH-Fe (FE) (Hydrogel) CNF-COOH-Hematite-Fe (FF) (Hydrogel)	Coffee filters/CNF	TEMPO/ Homogenization/ amidation reaction/ 0.75 g/L	As(V) Cr(VI)	Adsorbent (0.75 g/L), As–Cr (1–100 mg/L), pH 3.34 and 24 h	192.4 192.1 310.8 218	As(V) 13.47 Cr(VI) 25.95 As(V) 19.85 Cr(VI) 10.01 As(V) 28.96 Cr(VI) 5.75 As(V) 48.92 Cr(VI) 7.48	409

[a]Nanocellulose polypyrrole. [b]Sodium alginate polyacrylamide. [c]Bacterial cellulose. [d](TEMPO)-oxidized cellulose nanofibers, [e]Polyvinylamine. [f]Nanobentonite-dialdehyde nanocellulose-carboxymethyl chitosan. [g]Nanocellulose aerogel-oleic acid. [h]Corncob. [i]Functionalized corncob. [j]Corncob nanocellulose. [k]Nanocellulose aerogel foam-sodium dodecyl sulfate. [l]2,3-Dialdehyde nanocellulose. [m]Modified nanocellulose crystalline. [n]Graphene nanoplates. [o]Ion-imprinted polymer. [p]Nonimprinted ion-imprinted polymer. [q]Zeolitic imidazolate framework-67. [r]Nanocellulose itaconate. [s]Sodium itaconate grafted nanocellulose. [t]Ethylenediaminetetraacetic acid disodium salt. [u]Tunicate cellulose nanofiber-polyethylenimine.

of amorphous polymer chains, having more accessible carboxylate groups.

There are many different types of NC-based adsorbents, including binary or multilayered composite, membranes, electrospun mat, hydrogels, beads, aerogels, etc. We summarize the advantages and disadvantages of different forms of NC-based adsorption materials and their preparation methods in Supporting Information (Table S2). There are several relevant reviews on this subject. For example, NC could offer opportunities to adsorb endocrine-disrupting chemicals, which was reviewed by Tapia-Orozco et al.[20] They also sorted out the pros and cons of using raw materials for NC adsorbent

https://doi.org/10.1021/acs.chemrev.1c00683
Chem. Rev. 2022, 122, 8936−9031

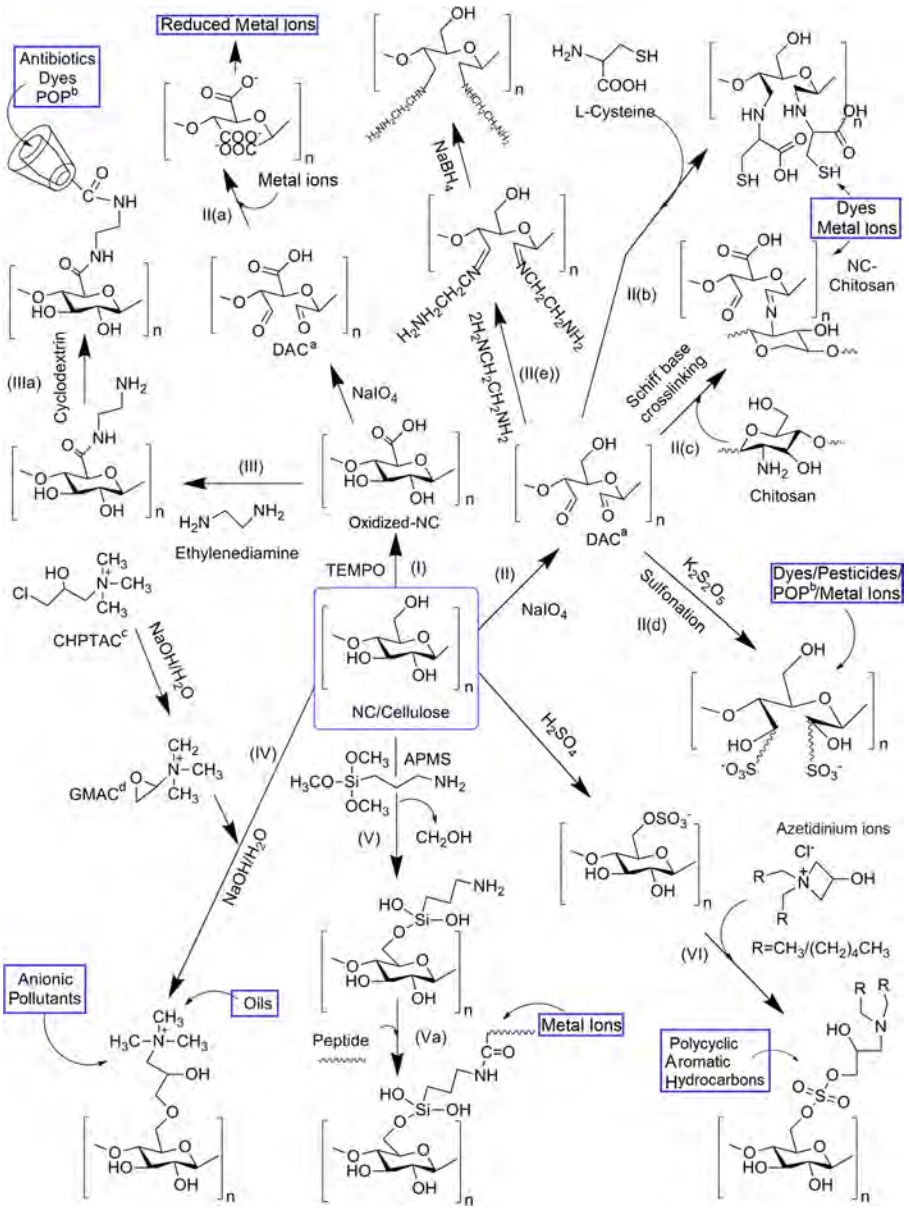

Figure 24. Derivatization of common functional groups of NC for varying adsorption applications ([a]dialdehyde nanocellulose, [b]persistent organic pollutants, [c]3-chloro-2-hydroxypropyl trimethylammonium chloride, and [d]glycidyltrimethylammonium chloride). As can be seen, derivative functionalities could be generated either directly from NC or its oxidized form (e.g., through TEMPO oxidation) and periodate-chlorite-oxidized NC (i.e., dialdehyde nanocellulose (DAC)). Pollutants that are entitled to be adsorbed are highlighted by blue color boxes.

production. Mahfoudhi and Boufi prepared an updated review,[21] focusing on varying NC functionalization schemes and conveying untreated and/or modified NC as adsorbent materials. Voisin et al. dealt with NC-based membrane processing, while a section was devoted to the adsorption of heavy metal ions and organic pollutants by functionalized NC.[17] Abouzeid et al. highlighted the NC preparation and their uses in adsorption and membrane separation.[22] Köse et al. reported the surface functionalization of NC and outlined their adsorption behaviors.[23] They compiled a detailed list of merits and demerits for adsorbent preparation methods, excluding the use of membrane and aerogels/foams. In a book chapter, Gopakumar et al.[37] reviewed the relevance of NC to adsorb toxic textile dyes and heavy metals.

The preparation of this section begins with the compilation of adsorption data in Table 5 from many independent recent studies, considering their methods of sorbent preparation and reaction media that were greatly varied. We mainly focus on the performance evaluation from different types of NC adsorbents, for example, classical-type composites, aerogels, hydrogels, and others where a range of reinforcing materials, such as polymers, metal−organic frameworks (MOFs), CNT, graphene, etc., were added to enhance the pollutants removal capacity. Readers who are interested in organic and inorganic pollutants adsorption are encouraged to scan the rows of two different colors: light-blue (organic) and light-red (inorganic), respectively. By using Table 5, readers can also identify the performance of NC-based adsorbents, with the rating of good > efficient > effective, for a large range of organic contaminants, such as dyes, oils, organic solvents, and pesticides, as well as inorganics (mainly heavy metal ions) adsorption.

https://doi.org/10.1021/acs.chemrev.1c00683
Chem. Rev. 2022, 122, 8936−9031

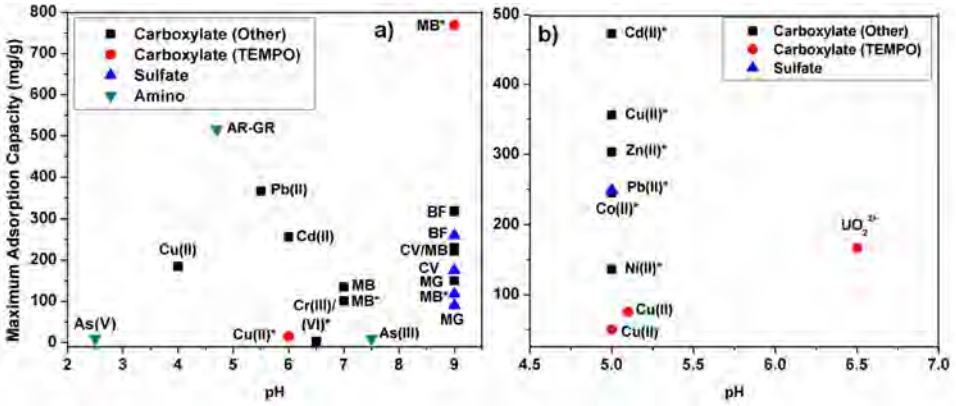

Figure 25. Effects of selective important functional groups and pH on the maximum adsorption capacity of varying water pollutants for (a) CNC and (b) CNF. The carboxylate (others) class includes succinic anhydride, maleic anhydride, sodium periodate/chlorite, ammonium persulfate oxidations, etc. *The values estimated by the Langmuir isotherm modeling, and abbreviations AR-GR (acid red GR), MB (methylene blue), BF (basic fuchsin), CV (crystal violet), and MG (malachite green) are used. Reported values are used for plots generation from refs 130 and 431−444.

5.2.1. Functionalization of NC to Improve Adsorption Efficacy. NC functionalization is an important step to fabricate adsorbents with high adsorption capacity. For example, Dwivedi et al. prepared CNF-COOH-dopamine and CNF-COOH-Hematite-Fe^{3+}, which showed higher Cr(VI) and As(V) removal efficiency of 76% and 100% than the granular activated carbon (68%) and powder activated carbon (51%), respectively.[409] Different oxidation, sulfonation, phosphorylation, polymer grafting, silylation methods have been used to synthesize NC with specific types (e.g., cationic, anionic, hydrophobic, etc.).[23] In Figure 24, we illustrate the derivative functionalities that can be created on NC once they have the OH, COOH, and CHO groups. These derivatives can electrostatically bind, chelate and ion exchange or a combination thereof, with water pollutants. Detailed discussions of these reactions are given in Supporting Information (section S5), and their adsorption performances are shown in Figure 25. These derivative reactions have been found responsible to enhance the NC adsorption property through the alteration of surface charge density, hydrophobicity, reactivity, and selectivity.

The subject of NC functionalization has been reviewed by Mahfoudhi and Boufi,[15] Voisin et al.,[17] and two other groups.[429,430] The advantage and disadvantage of these functionalization procedures were also compiled by Köse et al.[23] These reviews tabulated the adsorption capacity of NC with different functional groups and grafted polymers[15,17] however is difficult to understand the actual NC contribution to achieve the maximum adsorption capacity. This is because comparing one type of adsorbent with others (e.g., beads vs paper vs membrane vs aerogels vs foams, etc.) having different batch adsorption setups is not straightforward. However, the effectiveness of several important functionalized NC (CNC and CNF) materials on the adsorption capacity of varying charged pollutants under different conditions can be summarized in Figure 25. In Figure 25a, it was seen that carboxylated CNC produced by periodate and chloride oxidized CNC−COOH methods showed higher Cu(II) adsorption capacity than that of TOCNC. A similar observation was also observed for CNF (Figure 25b). Overall, non-TEMPO-oxidized NCs exhibited higher metal ion adsorption capacity than TEMPO-oxidized NC (TONC). On the contrary, TONC displayed higher MB adsorption than non-TONC at the pH condition (pH 9.0, Figure 25a). This figure also indicated that most of the dye adsorption was dominated by CNC rather than by CNF. It was also seen that functionalized NC materials generally showed a higher maximum adsorption capacity than pristine NC. For example, succinic anhydride functionalized CNC showed maximum adsorption capacity of Cd(II) and Pb(II) of 256.3 and 365.9 mg/g (Figure 25a) as compared with pristine CNC showing maximum adsorption capacity of 2.0 and 25.0 mg/g, respectively.[431] A similar observation was also reported for CNF in a different publication.[432]

In addition to carboxylate, sulfate, and amino functional groups as shown in Figure 25, phosphorylated NC was also found to be effective for adsorbing varying water pollutants. For example, Liu et al.[445] prepared phosphorylated NC that could adsorb Ag(I), Fe(III), and Cu(II) (≈ 100%) from water with simultaneous improvement of the velocity and sorption capacity because of the presence of phosphate groups. This system was effective to treat industrial effluent. Similarly, as shown in Table S2, phosphorylated NC (made by electrospinning) has been used together with chitosan for Cd(II) removal. The phosphate group was found to be uniformly deposited on electrospun nanofibers, and the system exhibited the maximum adsorption capacity of 232 mg/g (Langmuir analysis) because of the high affinity among the phosphate group on NC and the amine group of chitosan with Cd(II).[446] These observations confirmed the importance of NC functionalization as a viable route to produce adsorbents with high adsorption capacity and high selectivity against different pollutants.

5.2.2. Design of NC Composite Adsorbents. Because of its abundant functional groups, high aspect ratio, high mechanical strength, and high surface area; NC can also serve as a protective scaffolding material to host inorganic and organic nanomaterials. This ability can offer new properties from both components with synergistic effects. NC materials can serve as the primary matrix or the secondary reinforcing nanofillers. Several reviews and book chapters are available, and they deal with the preparation of NC-based nanocomposites materials and their applications in water purification.[301,447,448] In this section, we provide the assessment of whether NC and nanomaterials can "actually leverage" the best adsorption capability of their composite. As shown in Figure 26, it was seen that the loading of different nanomaterials, such as ZnO, Fe_3O_4, thiourea-functionalized Fe_3O_4, and graphene oxide (GO) nanoparticles onto NC could result in a higher adsorption capacity of the composite. Clearly, there is a synergistic action, contributed by both primary and secondary components. For

https://doi.org/10.1021/acs.chemrev.1c00683
Chem. Rev. 2022, 122, 8936−9031

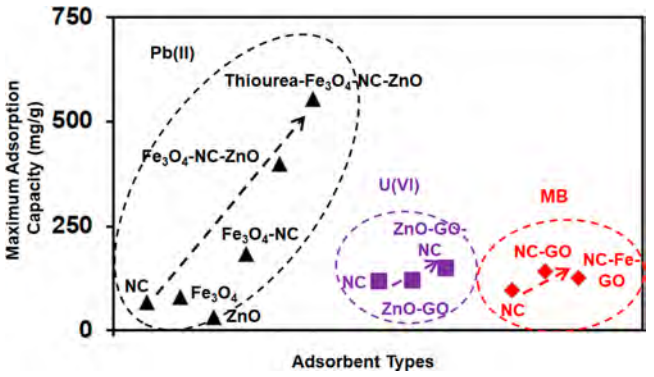

Figure 26. Performance comparison of the maximum adsorption capacity of pristine NC and its nanocomposites containing different nanomaterials (ZnO, Fe_3O_4, thiourea-functionalized Fe_3O_4, and GO nanoparticles) against three different pollutants (Pb(II), U(VI) and MB). It is apparent that the tricomponent nanocomposites show higher maximum adsorption capacity than dual- and monocomponent systems. Reported values are used for plot generation from refs 449−451.

example, NC exhibited comparable maximum adsorption capacity against Pb(II), similar to those of Fe_3O_4 and ZnO, but the composite of Fe_3O_4−NC−ZnO showed significantly higher maximum adsorption capacity (Figure 26). Such synergistic effects were also observed in the systems of ZnO−GO−NC and NC−Fe−GO against the adsorption of U(VI) and MB.

Some NC-based nanocomposites are found to be efficient to adsorb both organic and inorganic pollutants. For example, high cation exchange cetyltrimethylammonium bromide modified montmorillonite (CTM) has been used as an additive for CNC scaffold, where the composite was effective for adsorption of diuron—a potential carcinogenic herbicide.[452] Pristine CNC displayed a surface area of 27.23 m^2/g, which was increased to 39.51 m^2/g in CNC/CTM composite. It was found that around 70 mg/L of the composite was needed to adsorb 6.0 mg/L of diuron, which was below the permissible level of diuron in drinking water (100 mg/L) set by the US Environmental Protection Agency. In another study, zeolite and cationic surfactant poly(diallyldimethylammonium chloride) (PDADM) modified CNF composite has been used to remove black anionic reactive dye. Even though plenty of efforts have been made to prepare the composite, its adsorption performance was still not satisfactory. Only 11 and 30 mg/g of dye adsorption was noticed using both native and PDADM-coated P371 zeolites, respectively. This is because these composites are not capable of adsorbing organic pollutants with low polarity. Efforts have been made to modify NC using varying functional elements that showed some improvements. For example, Herrera-Morales et al. prepared block copolymer (BCP) Jeffamine ED 600 functionalized TOCNC composite (CNC−Jeffamine) for the adsorption removal of acetaminophen (paracetamol), sulfamethoxazole, and *N*,*N*-diethylmeta-toluamide (DEET) from water.[453] After modification, the BET (Brunauer, Emmett, and Teller) surface area was found to increase from 8.4 (TOCNC) to 15.1 m^2/g (CNC−Jeffamine). The increased surface area might be due to the new BCP functionalities. Nevertheless, the CNC−Jeffamine has shown very low adsorption capacity for acetaminophen (Freundlich, nearly 0.3 mg/g), sulfamethoxazole (Langmuir, 0.6 mg/g), and DEET (Freundlich, 0.6 mg/g) at pH 9. In another study, Wang et al. used magnetic GO-grafted CNC as supporting materials for molecularly imprinted polymerization (MIP).[454] MIP has become a popular method to design cavities with different shapes and sizes, where the cavity can act as an excellent binding site for pollutants adsorption. However, MIPs have some drawbacks, such as low binding affinities, limited site availability and high diffusion barriers. To overcome these drawbacks, a composite (Mag@GO-*g*-CNCs@MIPs) was developed which was very effective for fast adsorption of fluoroquinolones from river water (74 mg/g achieved within 5 min). An external magnet has been used to separate the composite, where only a 13% drop in the adsorption capacity was noticed after seven consecutive cycles of operation.

Similar to organic pollutants, some inorganic metal pollutants can also be successfully removed by NC-based composites. Nath et al. prepared the ZnO−CeO_2−NC−polyaniline composite by the in situ polymerization approach, where both polyaniline and NC could act as polymer supporting matrices. Although they claimed 95% of As can be removed using this composite, no control experiment was performed to check if the individual component can also be effective for the As adsorption. In

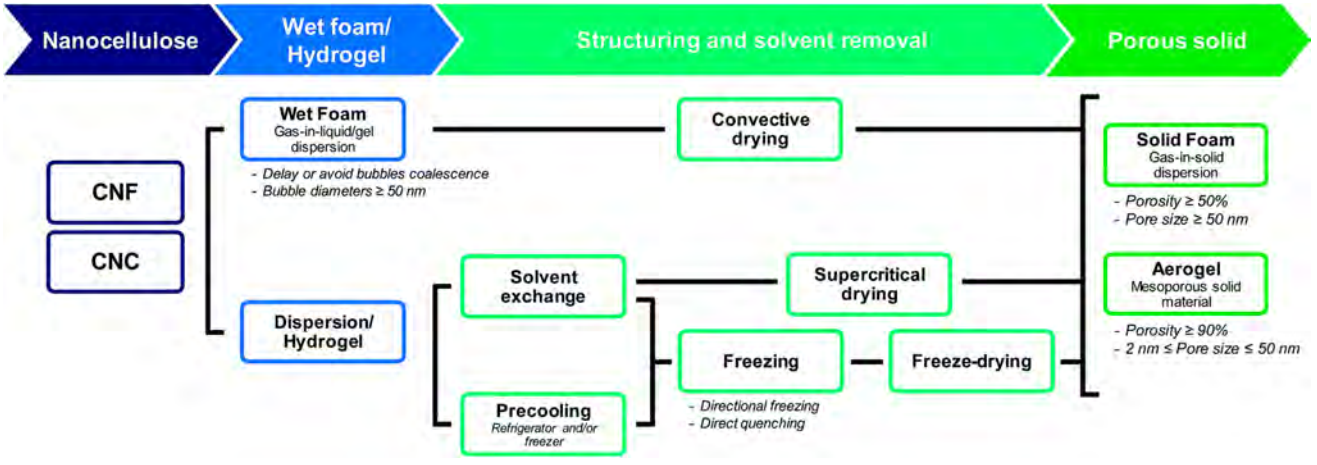

Figure 27. Schematic illustration of NC-based aerogels/hydrogels/foams processing. The end products are NC-based mesoporous aerogels with an average pore size between 2 and 50 nm and overall porosity >90%, whereas NC-based foams have an average pore size >50 nm with porosity >50%. Adapted from ref 458. Copyright 2017 Royal Society of Chemistry.

https://doi.org/10.1021/acs.chemrev.1c00683
Chem. Rev. 2022, 122, 8936−9031

addition to As, this composite exhibited a good antibacterial activity, which was higher than native ZnO and CeO_2 nanoparticles.[455] In another study, the adsorption efficiency of CNC against Ni(II) was found to be around 30%, whereas it increased to more than 50% by making the composite of CNC−GO.[456] This improved efficiency can be attributed to the synergistic effects due to high density of oxy-functionality, large surface area and presence of $\pi-\pi$ bonds in CNC/GO composites. However, 50% adsorption efficiency is still considered low, where significant efforts have been made to fabricate composite materials in the forms of aerogels/hydrogels/foams aiming to achieve adsorption efficiency >90%.

5.2.3. Hydrogel and Aerogel Composite Adsorbents. The application of three-dimensional (3D) hydrogels, aerogels, and foams has been escalating recently because of their lightweight and very high surface area, which is especially suitable for hosting pollutants. Many nanomaterials such as graphene have difficulties for hydrogel/aerogel fabrication due to their hydrophobicity, weak supporting tendency and poor mechanical strength.[457] The entanglement nature of fibrous NC particles, their versatile functional groups and their ability to cross-link with a range of reactive components make them an ideal candidate to form hydrogel and aerogel composite adsorbents. To fabricate NC-based macroscopic 3D materials, different methods have been demonstrated, where the schematic illustration of NC-based aerogels/hydrogels/foams processing is shown in Figure 27. This topic has recently been reviewed by Lavoine et al.[458] and their various applications have been discussed by De France et al.[459] NC-based macroscopic 3D materials cross-linked with suitable nanomaterial can result in a highly porous structure with excellent mechanical performance and controllable high absorbent efficiency.

CNF not only can offer functional groups, such as −COOH and −OH, to initiate gelation by chelating with metal ions through strong bonding interaction but also can serve as a stable scaffold due to its high surface area, large aspect ratio, cross-linked structure and mechanical flexibility to promote the growth of inorganic nanocrystals. For example, Zhu et al. used TOCNF as a template for in situ growth of MOF to form aerogel by freeze-drying (Figure 28a and b).[460] The TOCNF template could simultaneously initiate the nucleation and growth processes as well as decrease the aggregation of MOF, that is, zeolitic imidazolate framework-8 (ZIF-8) to form nanoscale crystals (18−65 nm, Figure 28c). ZIF-8 exhibited a surface area of 273−891 m^2/g, mesopores with a size between 7 and 40 nm and an average porosity (99%), resulting in a very high maximum adsorption capacity and rapid adsorption kinetics for pollutant removal. As seen in Figure 28e, the Langmuir adsorption capacity of the CNF−ZIF-8 composite against rhodamine B (RhB) was 81 mg/g, which was around several times higher than that of neat ZIF-8 powder. The distribution coefficient (K_d), calculated by ($K_d = q_e/c_e$), indicated its adsorption affinity was 8800 mL/g at 2.5 mg/L (i.e., the equilibrium concentration, c_e). The observed maximum adsorption capacity and K_d values of the CNF−ZIF-8 composite surpassed those of the reported adsorbents (Figure 28e). Furthermore, ZIF-8 showed good MO selectivity during mixing with methyl violet (MV). Besides batch adsorption, Zhu et al. also tested the adsorption efficiency during the continuous filtration process. As shown in Figure 28f, after three consecutive cycles of filtration, the dye concentration rapidly fell to 2.0% with the permeance flux of 2.31−4.72 × 10^3 $L{\cdot}m^{-2}{\cdot}h^{-1}$. It was interesting to note that when Zhu et al. used conventional ZIF-8

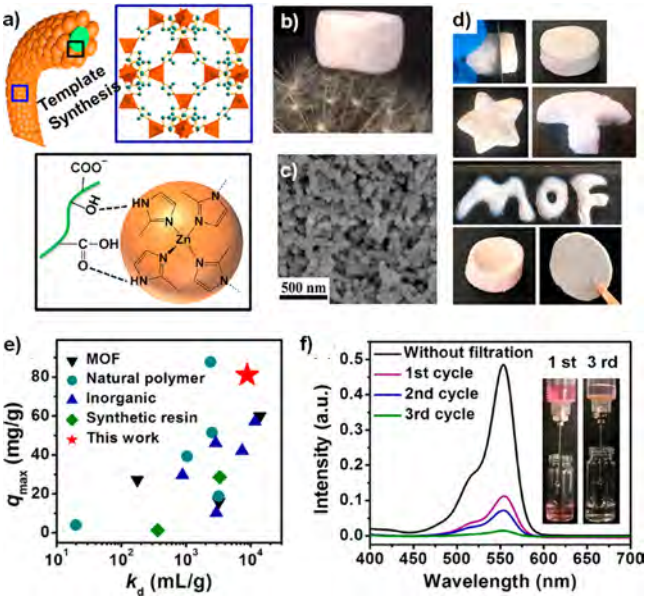

Figure 28. (a) CNF−M^{2+} as a template for MOF (ZIF-8) crystals growth. (b) Freeze-drying and (c) SEM images of CNF−ZIF-8 aerogel. (d) Shaping of CNF−ZIF-8 for cutting, molding and patterning. (e) Maximum dye (RhB) uptake amount and K_d values compared with other porous absorbents. (f) Shaping CNF−ZIF-8 aerogels for classical filtration setup with adsorption capability. Reprinted with permission from ref 460. Copyright 2018 American Chemical Society.

powders without the CNF template, they noticed immediate run-away of MOF in the filtration setup resulting in very low adsorption efficiency. This study also demonstrated that the CNF−ZIF-8 composite aerogel could be molded into different shapes (e.g., plate, cylinder, and 3D complex, as seen in Figure 28(d)) for diverse applications. The demonstration of CNF−ZIF-8 aerogel appeared to overcome the current challenge of forming MOF-based aerogels, due to the intrinsic rigidity in MOF and weak interparticle interactions.

In another study, Sajab et al. prepared a dual functional GO−Fe−CNF aerogel for MB adsorption and subsequent Fenton oxidation, where its structure and performance relationship is shown in Figure S5.[451] The authors reported that the synergistic effect of the GO−Fe−CNF was essential for the Fenton decomposition of the dye. For example, CNF aerogel only exhibited the maximum adsorption capacity of 97 mg/g against MB, but the maximum adsorption capacity was sharply increased to 126 mg/g in GO−Fe−CNF aerogel. More importantly, GO−CNF showed no oxidation capability for MB degradation, but the oxidation occurred notably by using GO−Fe−CNF (Figure S5c). Therefore, adding Fe in the composite was the key to activate this multicomponent composite to treat complex wastewater. However, this Fenton reaction in the GO−Fe−CNF system appeared to be too slow to decompose the dye solution, especially at a high concentration.

On the basis of the above observations, it is clear that the maximum adsorption capacity of NC is generally low, but it can be increased significantly by incorporating other functional nanomaterials. Compared with classical composite materials, NC-based composite hydrogels and aerogels could yield high performance adsorbents with desirable properties. In Table 6, we summarize several NC-based composite aerogels, their density and porosity, as well as maximum adsorption capacity against varying pollutants. It was seen that NC−GO aerogel

https://doi.org/10.1021/acs.chemrev.1c00683
Chem. Rev. 2022, 122, 8936−9031

Table 6. Comparisons of Density and Porosity of NC-Based Composite Aerogels and Their Maximum Adsorption Capacity (MAC) against Varying Pollutants

aerogels	density (g/cm^3)	porosity (%)	pollutant	MAC (mg/g)	ref
PDA[a]−CNF−PEI[b]	25	98.5	MO	265.9	461
			Cu(II)	103.5	
NC−GO	0.00215	99.88	MB	265.6	412
			CR	21.5	
DFNS[c]−BHNC[d]	0.107	93	MB	270	462
			MO	300	
PDChNF[e]/TOCNF	0.0082	99.44	As(III)	217	463
			MB	531	
Si−CNC[f]/RM[g]	0.018	99	2,4-dichlorophenol	6.25	464
PMVEMA[h]/PEG/CNC	0.0877	86.83	MB	116.2	465
Universitetet i Oslo (UiO)-66-EDTA[i]/CNF/CMC[j]	0.005	99	Cu(II)	104	426
			Cr(III)	396	
			Co(II)	307	
			Ni(II)	120	
			Mn(II)	251	
			Zn(II)	215	
			Fe(III)	115	
			Zr(IV)	165	
			Fe(III)	115	

[a]Polydopamine. [b]Polyethylenimine. [c]Dendritic fibrous nanostructured (colloidal) silica. [d]Bifunctional hairy NC. [e]Partly deacetylated chitin nanofiber. [f]Silylated CNC. [g]Red mud. [h]Poly(methyl vinyl ether-co-maleic acid). [i]Ethylenediaminetetraacetic acid. [j]Carboxymethyl cellulose.

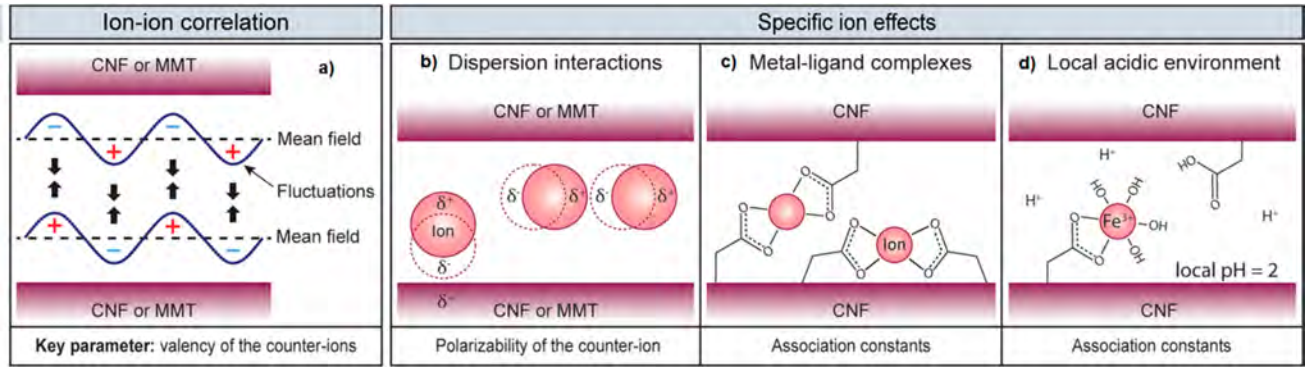

Figure 29. Simplified illustration of the interaction between anisotropic nanoparticles, such as CNF or montmorillonite clay (MMT), and metal ions using different interaction forces. Adapted from ref 290. Copyright 2019 Royal Society of Chemistry.

exhibited a lower density (i.e., lightweight material) and higher porosity as compared with other composites. One can control these aerogel properties by adjusting the initial material concentration, the expansion and shrinkage of aerogel at the dispersion during aerogel formation or solvent removal processes.

5.2.4. Mechanistic Explanation. Most of the literature uses kinetics and isotherm modeling to explain the nature of pollutant adsorption by NC and its composites. These mathematical expressions are essential for adsorption optimization and process design. Detailed discussions of these modeling theories have been reviewed by Hubbe et al.,[466] Chen,[467] and Tan and Hameed.[468] On the experimental side, some authors have used extensive characterization tools, such as XPS, extended X-ray absorption fine structure, X-ray absorption near-edge spectroscopy, etc., to investigate the reaction mechanism between pollutants and the NC derivatives.[409,469] In these reviews, semiquantitative models have not been evaluated, which are important to explain the binding between metal ions and NC. These models could explain the anionic and cationic polymer assemblies with specific counterions. These models include ion−ion correlation and specific ion effect models, involving dispersion interaction, metal−ligand complex and local acidic environment as shown in Figure 29.[290] The effect of ion−ion correlation resembles the London dispersion force, which is temporary because of its weak intermolecular forces, especially in the van der Waals theory. Such forces are often referred to as induced dipole−induced dipole attraction. Thermal energy causes the irregular rising and falling in the number of molecular electrons or ions in the counterion cloud. It leads to the formation of instantaneous dipoles as shown in Figure 29a. As seen in this figure, ion−ion correlation occurs upon the dipole emergence, when counterion clouds or molecules are contiguous. It has been shown that CNF has a charge density (0.07−0.13 Cm^{2-}),[290] which is sufficient to overcome the double-layer repulsive forces of divalent metal ions.[470] In general, the extent of fluctuations in the counterion cloud increases due to the less crowded ion cloud caused by the higher valence of the counterion. As shown in Figure 29b, dispersion interaction is controlled by the polarizability of counterions which typically interact with CNF through van der

https://doi.org/10.1021/acs.chemrev.1c00683
Chem. Rev. 2022, 122, 8936−9031

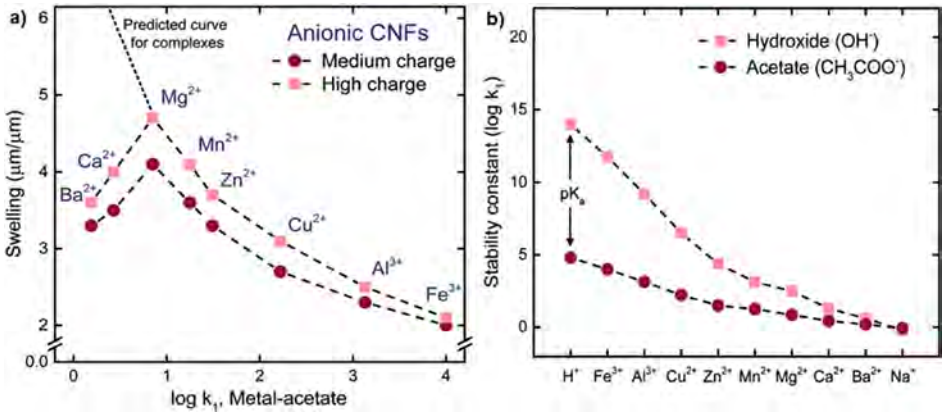

Figure 30. (a) Correlation between the stability constants (log k_1, metal−acetate) and swelling of CNF film. (b) Plot of stability constants (log k_1) against different ions. Here, hydroxide and acetate groups are used as models for water and the surface of CNF. Reprinted with permission from ref 290. Copyright 2019 Royal Society of Chemistry.

Waals forces. Such interaction defeats the CNF surface charge and diminishes the double-layer repulsion.

It was found that the high polarizability of larger ions, such as Ca^{2+} and Ba^{2+}, because of their loosely bound electrons, decreased the swelling of CNF films (Figure 30a).[290] In general, monovalent counterions follow the dispersion interaction pathway as they have fewer tendencies to form metal−ligand complexes because of their low effective polarizability. Metal−ligand complexes typically follow the coordination chemistry pathway, such as Cu^{2+}, Fe^{3+}, Al^{3+}, etc. However, polarizable ions, such as Ba^{2+} and Ca^{2+}, typically follow the ion−ion correlation model. This is because most of the transition metal ions naturally attract ligands to fulfill their *d*-orbitals using shared electrons such that these ions can reach the noble gas states. The binding force in the metal−ligand complex is quite strong.[471] The stability constant log k_1, the first association constant in the logarithm scale, is commonly used to define the strength of these interaction forces. Figure 30b shows the stability constant of the interactions between hydroxide or acetate ions (as models for water and the surface of CNF) with various metal ions. It was seen that the metal ions exhibited higher log k_1 for hydroxide ions than for acetate ions. Interestingly, monovalent ions, such as Na^+ displayed less affinity than multivalent ions, such as Cu^{2+}, Al^{3+}, and Fe^{3+} (Figure 30b).[290] As shown in Figure 29d, in the ion-induced local acidic environment, acidic ions, such as Cu^{2+}, Al^{3+}, and Fe^{3+}, can form strong complexes with CNF. The charge of CNF is directly related to the amount of the carboxylate group, which is proportional to the ion concentration in the CNF film. Therefore, the local acidic environment depends on the concentration of CNF, as well as their surface charge density.

Pollutants can be adsorbed into NC-based adsorbents through varying pathways such as ion exchange, chemical complexation, hydrogen bonding, van der Waals interaction, hydrophobic interaction, reductive adsorption, diffusion, electrostatic interaction, covalent bonding, etc. Some examples illustrating the dominant binding forces between pollutant and NC-based adsorbents are shown in Figure 31, and they are briefly discussed as follows: (a) *Ion Exchange*: Most of the inorganic metal/metal ions are commonly adsorbed through the ion exchange mechanism as shown in Figure 31a. It occurs through the replacement of undesired ions, such as Na^+, K^+, H^+, etc., at the acidic active sites of an adsorbent with the target pollutants, such as Cu^{2+}, Fe^{3+}, Ni^{2+}, and so on. Succinic anhydride functionalized CNC (SCNC) and $NaHCO_3$-treated SCNC (NaSCNC) can remove Pb^{2+} and Cd^{2+} from water based on this pathway.[431] While adsorption of these metals occurs on SCNC through chemical complexation, NaSCNC mainly follows the ion exchange mechanism for the removal of Pb^{2+} and Cd^{2+}. (b) *Complexation*: Chemical complexation or coordination occurs between metal ions and ligands (a molecular or ionic entity) that contains at least one atom with an unshared pair of electrons. As shown in Figure 31b, the hydrated metal adsorbed through bidenate complex formation. In addition, a coordination complex between the metal ions and the functional groups of a hydrogel matrix is shown in Figure 31c. These complexes often rely on the size of the metal pollutants and the matching of their sizes with the symmetry of its valence electrons orbitals to the functional groups' position on the adsorbent. Details of these interactive mechanisms have been discussed by Lawrance et al.[473] They argued that the adsorbent, having six COOH groups in a specific arrangement, could be an effective chelating agent to form a coordination complex with certain metal ions. (c) *Coordination complexation*: The hard−soft acid−base theory is another model that can explain why certain functional groups have a great affinity to certain metals. For example, there is a high affinity of binding between the −SH (soft base) group and Hg(II) ions (soft acid).[474] Soft ions are those whose outer electrons are polarizable and are loosely held. These ions allow the formation of a covalent complex between these ions (e.g., Pb, Hg, etc.) and the surface functional groups (mostly S and N atoms) on NC. On the other hand, the outer electrons of hard ions are less polarizable and more closely held (e.g., Ni). In this scenario, they need to be complexed electrostatically with functional groups, such as O-atoms[475] on NC. (d) *Hydrogen Bonding*: The density-functional theory (DFT) calculation can be used to describe the complex interaction between pollutants and NC. For example, DFT calculation has been carried out to explain the acetaminophen adsorption onto NC−Jeffamine composite, involving multiple intermolecular interactions such as hydrogen bonds (hb1 and hb2) and van der Waals forces with binding energy (BE = 14.549 kcal/mol) (Figure 31d). Similar interaction bonding has been observed for sulfamethoxazole (hb1 and BE = 7.21 kcal/mol) and DEET (BE = 5.70 kcal/mol).[453] (e) *Hydrophobic interaction*: As shown in Figure 31e, the adsorption of diuron onto CNC/CTM, followed the pathway of hydrophobic interactions (i.e., between diuron and the alkyl chains of CNC/CTM), hydrogen bonding (i.e.,

https://doi.org/10.1021/acs.chemrev.1c00683
Chem. Rev. 2022, 122, 8936−9031

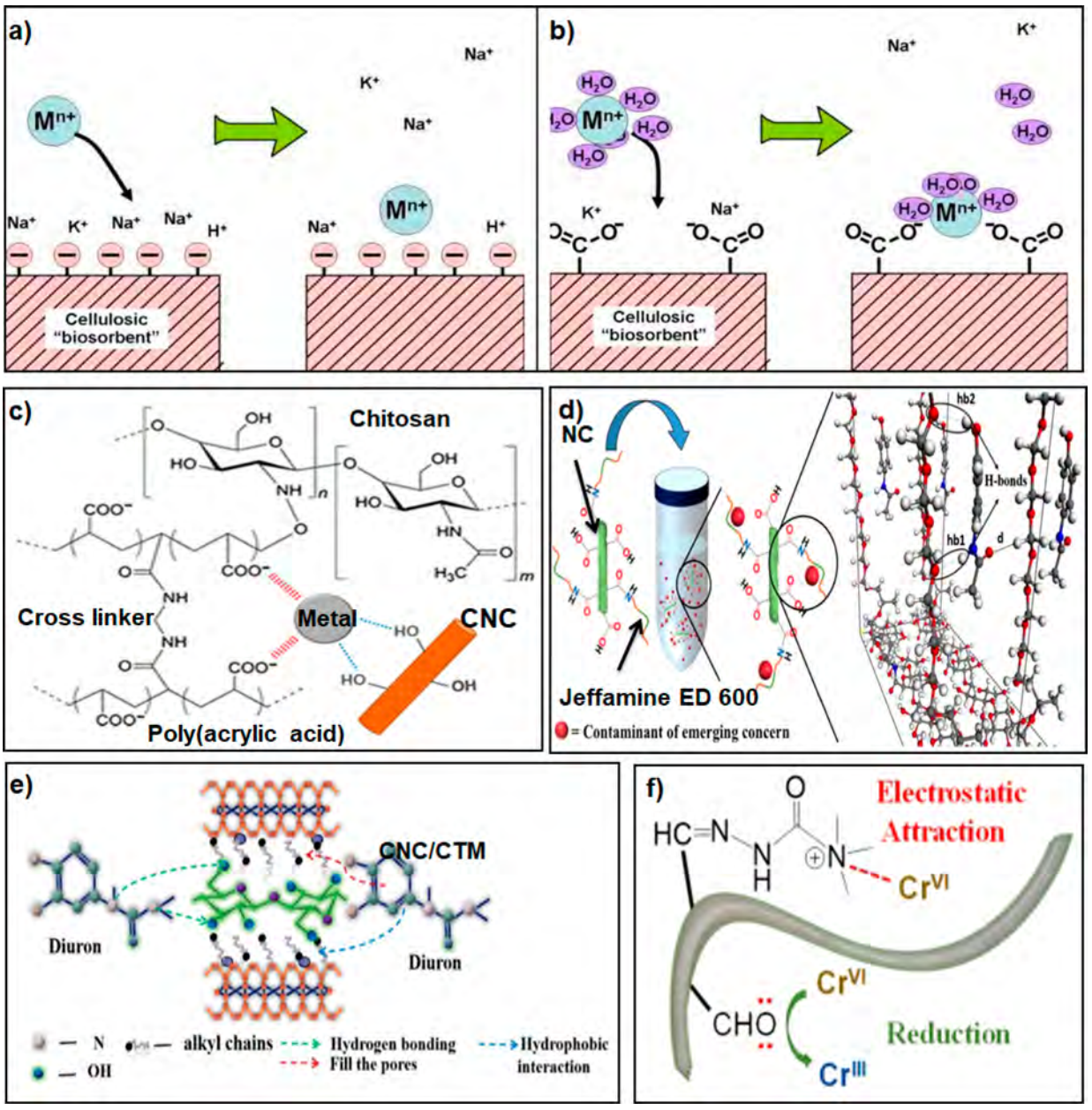

Figure 31. Illustration of some important pollutant binding forces to NC-based adsorbents. (a) Ion exchange and (b) complexation. Adapted from ref 466. Copyright 2011 NC State University. (c) Coordination complexation. Reprinted with permission from ref 428. Copyright 2019 Springer Nature. (d) Hydrogen bonding. Reprinted with permission from ref 453. Copyright 2017 American Chemical Society. (e) Hydrophobic interaction. Adapted from ref 452. Copyright 2020 Royal Society of Chemistry. (f) Electrostatic attraction. Reprinted with permission from ref 472. Copyright 2020 American Chemical Society.

between −OH groups of CNC/CTM and N atoms of diuron) and electron sharing or exchange. (f) *Electrostatic attraction.* Huang et al. used Girard's reagent to prepare cationic DANC, which electrostatically binds hexavalent Cr(VI) ions as presented in Figure 31f. In addition, the CHO group could reduce Cr(VI) to Cr(III), which is less carcinogenic than Cr(VI).[472]

5.2.5. Assessment of Adsorbent Stability, Regeneration Ability, and Fate. Because of the hydrophilic character of NC, which becomes soft and unstable when surrounded by water, Herrera-Morales et al. functionalized the CNF surface with a hydrophobic functionality called alkoxysilane trimethoxy-(2-phenylethyl)silane (TMPES).[476] Subsequently, a BCP compound termed poly(4-vinylpyridine-b-ethylene oxide) (P4VP−PEO) was used to modify the TMPES−CNF film, which has been used to remove sulfamethoxazole (SMX), an emerging organic contaminant (Figure S6). It was seen in Figure S6b, despite the hydrophobic modification, the film could still hold water after immersion. In contrast, when the pristine CNF film was immersed in water, the film would be broken and begin to disperse into suspension, whereas TMPES−CNF films could stay intact. The TMPES and BCP modified CNF film could be successfully reused up to five cycles after desorption of the film with ethanol with a very negligible loss of the adsorption capacity. Herrera-Morales et al. also prepared an NC composite system by grafting BCP for adsorption of emerging organic contaminants. Unfortunately, this system was found to be unstable and could be easily dissolved in an aqueous solution,

https://doi.org/10.1021/acs.chemrev.1c00683
Chem. Rev. 2022, 122, 8936−9031

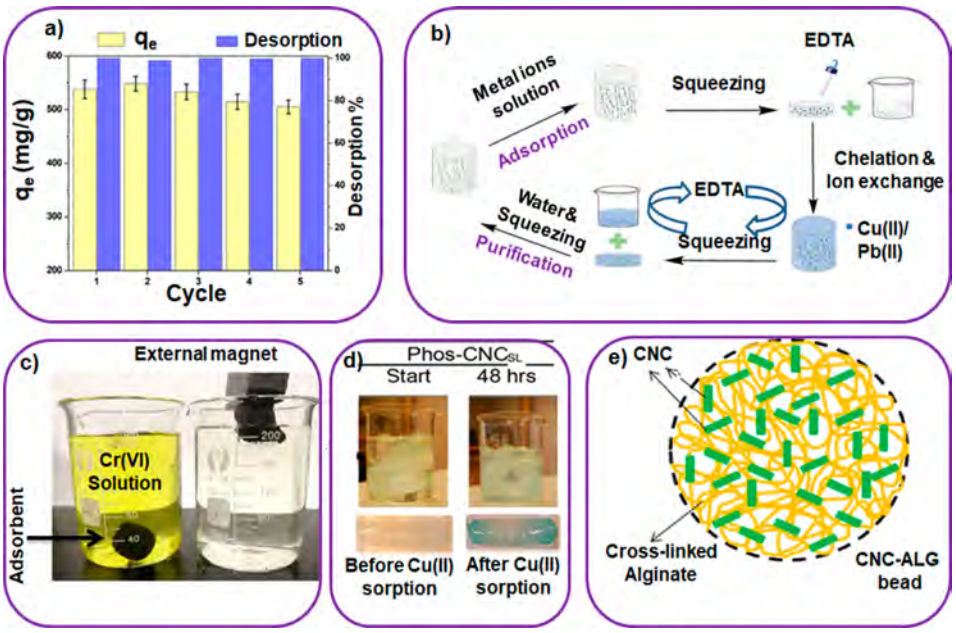

Figure 32. (a) Recycling stability and regeneration of TOCNF−nanochitin-based aerogels for the removal of MB (C_0 = 200 mg/L, pH = 10 and T = 25 °C). Reprinted with permission from ref.[463] Copyright 2019 American Chemical Society. (b) Processing routes for desorption and recycling of NFC/PEI aerogel. Reprinted with permission from ref 478. Copyright 2018 Elsevier. (c) Digital photograph showing the removal of aerogel using an external magnet after Cr(VI) adsorption. Reprinted with permission from ref 479. Copyright 2019 Springer Nature. (d) Image showing the NC inside a dialysis tube before and after Cu(II) sorption experiments. Reprinted with permission from ref 445. Copyright 2015 Elsevier. (e) Illustration of external and internal networks of an NC-based bead (here CNC is cross-linked with alginate in the presence of Ca(II) ions). Reprinted with permission from ref 480. Copyright 2016 Elsevier.

which makes the separation of the composite difficult after adsorption.[453]

In most of the studies, centrifugation methods and a range of eluents have been utilized to remove and wash the contaminated NC adsorbent. For example, carboxylate-functionalized CNC was isolated by centrifugation after adsorption of cationic dye CV.[433] Then, the authors used 50% ethanol solution (pH 3.0) to desorb the dye from the used CNC after being heated for 4 h. Although the rate of desorption was good (80%) and the CV removal after four cycles was >90%, there is no clear explanation by what mechanisms the ethanol solution can desorb the adsorbed dye. Besides ethanol, it has been shown that methanol and water were also good to desorb organophosphate insecticide from the used CNC. Although many other eluents have been tested, including H_2SO_4, NaOH, CH_3COCH_3, and $CaCl_2$:MeOH, their desorption results are often unsatisfactory. In addition, extensive CNC mass loss has been noticed upon washing with these solvents.[477] Distilled water has been used to wash the MB-adsorbed sodium alginate/polyacrylamide−TOCNF hydrogel, but the adsorption efficiency was not good after three adsorption−desorption cycles (i.e., 55% of MB desorption).[411] Several types of acids were also tested for the desorption study. For example, Zhang et al. used HCl for desorbing MB from TOCNF- and nanochitin-based aerogel.[463] They reported that HCl could protonate both carboxylate groups of TOCNF and amine groups of nanochitin, where the sorption of MB could be reversed (i.e., >99% of MB desorption). The aerogel exhibited a high MB adsorption capacity of 505 mg/g after five consecutive cycles of test, as shown in Figure 32a. HCl has also been used along with thiourea to desorb Hg(II) ions from SH-modified NC under stirring conditions.[474] Other acids such as HNO_3 have been employed as the eluent to desorb Cu(II), Pb(II), and Cr(VI) from tannin-DANC composite, followed by centrifugation of the mixture.[442] It was found that regeneration of the composite was effective for adsorption of Cu (II) and Pb (II), where their adsorption capacities could remain almost the same even after five cycles of test. However, regeneration of the composite was ineffective for Cr(VI). After the desorption treatment, the composite's adsorption capacity was significantly reduced in the second cycle. The authors explained this behavior as follows. In general, Cr(VI) is reduced to Cr(III) by the OH group on an adsorbent and consequently, the OH group is oxidized into COOH group. As a result, these COOH groups cannot adsorb $HCrO_4^-$, CrO_4^{2-}, or $Cr_2O_7^{2-}$ ions. It has been shown that HNO_3 can be a suitable washing agent for metal desorption from NC, while the method may need ultrasonic treatment for effective regeneration. This has been demonstrated for the succinic anhydride mercerized NC system.[443] In contrast, some weak acids (e.g., ascorbic, formic, and acetic acids) could not regenerate the metals adsorbed on this system. It has been noted that using acids in the absence or presence of ultrasonic treatment could both be problematic. The use of acid solution without sonication could stimulate hydrogen bond formation between NC fibers and the amorphous regions resulting in the decrease of the available surface area. However, the use of high-power ultrasonic treatment in regeneration could lead to the degradation of the NC fibers.

Very often, desorption and regeneration processes for the consumed adsorbents require tedious steps. They include soaking of contaminated adsorbent into a desorption solution, followed by several times of washing with the aqueous solution. Some authors also used heating as a tool to remove residual contaminants. However, such methods are not always practical and economic. To overcome these limitations, a simple recovery method has been introduced by Li et al.[478] They prepared nanofibrillated cellulose/polyethyleneimine (NFC/PEI) aero-

https://doi.org/10.1021/acs.chemrev.1c00683
Chem. Rev. 2022, 122, 8936−9031

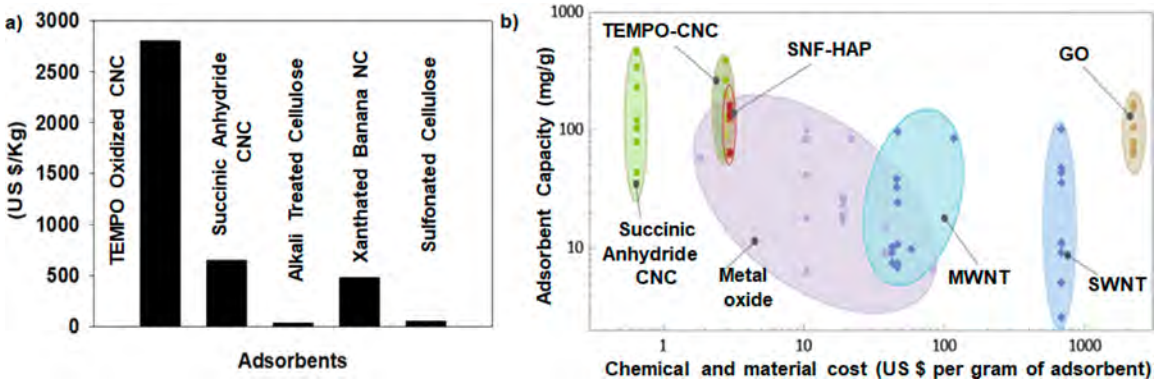

Figure 33. (a) Estimated total cost to prepare 1.0 kg of adsorbent from cellulose materials. Reported values are used for plot generation from ref 481. (b) Cost and adsorption capacity estimates for the most studied adsorbents. Reprinted with permission from ref 482. 2017 American Association for the Advancement of Science.

gel with wet-end and shape recovery properties. As shown in Figure 32b, Cu(II) and Pb(II) contaminated water in the NFC/PEI aerogel was first mechanically squeezed by hand. Then, an EDTA solution was subsequently added to the aerogel until it recovered to the original shape to exchange the metal ion with a chelating agent. These steps were repeated several times to remove all the residual metal ions. Finally, an aqueous solution was used to wash the aerogel. This method appears to be economical and more practical as compared with other methods because of the following: (a) the mechanical squeezing method was used to replace the more energy-consuming steps, such as centrifugation, sonication, shaking, or filtration, and it also reduced the amount of washing agent; and (b) the adsorption capability remained at the same value after three cycles, indicating the good regeneration ability. In another study, the preparation of magnetic NC aerogel by incorporating magnetic nanoparticle in the NC scaffold could ease the recovery process (Figure 32c).[479] Alternatively, one can consider the strategies given by Liu et al.[445] and Mohammed et al.[480] (Figure 32d and e, respectively). As presented in Figure 32d, a dialysis bag was used as a reactor where an NC gel was trapped inside the tube. In this setup, metal ions could pass through the dialysis bag without obstruction, where the color change of NC could indicate the process of adsorption or desorption. In another study, gel beads containing cross-linked alginate and CNC were investigated (Figure 32e). Both of these methods can retain NC without losing them during regeneration and be easily implemented in practical conditions.

5.2.6. Cost Estimation, Greenness, and Acceptability. Since NC is a renewable biomaterial that can be extracted from inexpensive and abundant biomass feedstocks, the cost to produce these products is expected to be low. However, the cost-effectiveness is often compromised by the expensive and energy-intensive defibrillation and modification processes as shown in Figure 33a. It is discernible that xanthated NC isolated from banana is considerably cheaper as compared with TEMPO and succinic anhydride treated NC. Low-cost NC can be produced only if the production process can be carried out at a large scale and cheap, and environmentally sensible NC processing schemes are implemented. Figure 33b shows the relationship between the cost of some most studied nanoadsorbents and their adsorbent capacity. The cost of CNC materials is between US $0.65/g and US $2.80/g and their adsorption capacities are comparably better than other inorganic nanomaterials. However, this price does not accurately reflect the actual price of NC-based composites, which usually have better adsorption capacity as compared with oxidized NC. Researchers have used expensive nanomaterials as reinforcing fillers, which should be used in small quantities to impose a minimal cost on the final product. Also, measuring energy/electricity consumption to prepare NC or its composites is important. Scientists often use methods, such as sonication, stirring, vacuum filtration, etc., which are not always energy efficient. One has to perform the optimization of materials processing to reduce the energy cost. Furthermore, the transportation costs for the production and the application of NC-based adsorbents can be significantly reduced if we consider strategies from point-of-make to point-of-use in treating local water problems.

The greenness of an adsorbent can be evaluated by the assessment of environmental impacts at both qualitative and quantitative levels. Such assessments can help the stakeholder to evaluate the manufacturing cost and determine the benignity of the material used. These measuring parameters are calculated using eqs 2−6 below.[483]

$$\text{mass intensity} = \frac{\text{mass of all reactants used excluding water}}{\text{mass of product}} \left(\frac{\text{kg}}{\text{kg}}\ \text{product}\right) \tag{2}$$

$$\text{water intensity (Wp)} = \frac{\text{mass of all water used}}{\text{mass of product}} \left(\frac{\text{kg}}{\text{kg}}\ \text{product}\right) \tag{3}$$

$$\text{reaction mass efficiency (RME)} = \frac{\text{mass of product}}{\text{mass of all reactants}} \times 100\% \tag{4}$$

$$\text{energy intensity} = \frac{\text{amount of nonrenewable energy used}}{\text{mass of product}} \left(\text{kW}\cdot\frac{\text{h}}{\text{kg}}\right) \tag{5}$$

$$E\text{-factor} = \frac{[\text{kg(raw materials)} - \text{kg(desired product)}]}{\text{kg(total product including water)}} \tag{6}$$

Mukherjee et al. calculated the mass intensity, solvent intensity, reaction mass efficiency (RME), energy consumption, and *E*-factor for CNF-PANI-templated ferrihydrite (CNPFH) nanocomposite,[469] which were 1.84, 38.80, 54, 1.78, and 0.6, respectively. The overall cost of this technology was $0.70 to produce 1000 L of F^- free water. The mass intensity (1.84) could be further reduced to <1.0 if one could avoid the leaching/losing of CNPFH during washing and filtration steps. We think the solvent/water intensity of this study was very high because of the large amount of water used for reagent processing. This water loss can be offset if the composite can produce a much larger volume of clean water (i.e., efficiency of the pollutant

https://doi.org/10.1021/acs.chemrev.1c00683
Chem. Rev. 2022, 122, 8936−9031

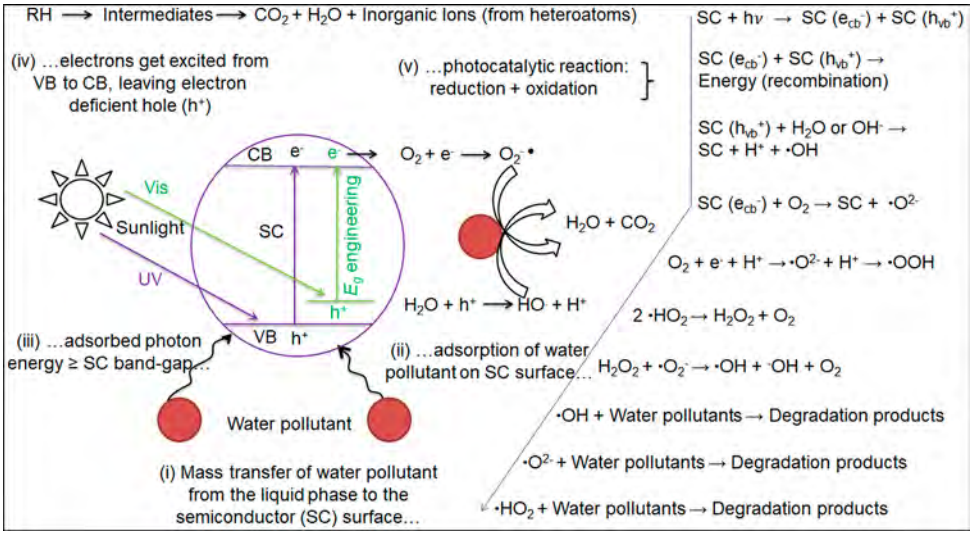

Figure 34. Illustration of fundamental steps and photocatalytic reaction equations over a semiconductor that is used for degradation of water pollutants to CO_2 and H_2O.

adsorption capacity needs to be very high). For example, the author needs 1.0 L of water for preparing the nanocomposite, which can effectively produce 200 L of F^- free water (Wp, 1−2 orders of magnitude). Similarly, RME can be improved by avoiding the excessive usage of reagents and by optimization of the reactant concentrations. The overall energy consumption (1.78 kW·h/kg) is relatively good, which is comparable with 2.8 kW·h/kg, required for MFC manufacturing at an industrial scale. A low environmental (E) factor suggests the minimal emission of harmful byproducts. Some other parameters are needed to assess the greenness. For example, (a) leaching of harmful byproduct/solvents during adsorbent processing and testing should be minimal to ensure low emissions to the environment; (b) replacement materials/reagents/chemicals, having low-toxicity, can be considered according to the guideline of the European Chemicals Agency and/or other standard regulatory authorities; and (c) regeneration of the adsorbent for subsequent testing using acidic/alkali treatment needs special attention as these strong acidic and basic solutions alter the surface water pH value upon leaching. The solvents/adsorbent should be deposited in leach-free landfills. In summary, NC, either as the freestanding or composite material as adsorbent, has good social acceptability. This is because they are simple and easy to recycle (depending on the type of adsorbents) and environmentally benign. Most of the NC-based technology does not demand trained manpower for their field-level implementation and maintenance.

5.3. Photocatalytic Applications

Photocatalysis is an oxidation process, where the acceleration of the reaction can take place in the presence of a catalysts and light. There are two types of photocatalysts, depending on the phase of the catalyst: homogeneous and heterogeneous. A homogeneous photocatalyst indicates that both the catalyst and reactants are in the same phase. Typical examples include photo-Fenton and ozone-mediated reactions. A heterogeneous photocatalyst indicates that both the catalyst and reactants are not in the same phase. Semiconductors and transition metal oxides are the most common examples of heterogeneous photocatalysts, which have been popular in wastewater treatment because of their high pollutants removal efficiency in the presence of light (UV or sunlight).[484] Photocatalysts are capable of absorbing light quanta of a specific wavelength. It depends on their band gap, which is an energy difference between the top of the valence band (VB) and the bottom of the conduction band (CB). Since 1972, after Fujishima and Honda discovered the water-splitting phenomenon by TiO_2,[485] various semiconductors have been investigated. Readers who are interested in understanding the band gap property of some popular semiconductors are encouraged to study an earlier report.[3] In addition, we discuss some limitations of precise measurement of band gap energy (E_g) in the Supporting Information (section S6).

Despite some drawbacks of pristine NC, such as electrically nonconductive, photocatalytically inert,[5] and low UV permeability;[486] other properties, such as scaffolding ability, functionalities, and large surface area, are very unique for water applications. With the rise of green and sustainable chemistry concepts, many investigators have made great efforts to investigate the use of NC either as a template for nanoparticle growth or a scaffolding material to create composite photocatalysts. The use of NC can improve the cost-effectiveness and decrease the utilization of toxic reagents and chemicals necessary for catalyst preparation, thus greatly reducing the environmental footprint. Fine-tuning of the size of nanoparticles (from macro- to nanoscale), crystallinity, porosity, etc., is possible by adjusting the physicochemical properties of NC (i.e., surface area, pore size and functionality). For example, the highly accessible surface area of NC could provide a large substrate for uniform nucleation and growth of inorganic metal nanoparticles. The unique charge property of the NC scaffold can enhance the distribution of electrons and transfer them to the catalyst surface leading to good photocatalytic activity.[487] In addition, oxy-functional groups of NC could anchor different nanoscale photocatalysts that would offer similar photodegradation mechanism of different solutes over semiconductors surfaces (see Figure 34).

We summarize the photodegradation performances of NC photocatalysts for pollutants removal in Table 7. A closer examination of this table suggests that NC can be found in two forms of photocatalytic reaction: (a) as a template in the final composite and (b) as a carbon residue, since the template is subsequently removed by calcination/pyrolysis (the hydrothermal method is widely used for such photocatalysts

https://doi.org/10.1021/acs.chemrev.1c00683
Chem. Rev. 2022, 122, 8936−9031

Table 7. Summary of NC-Based Photocatalysts That Are Used for Water Pollutant Removal

photocatalyst (g/L)	NC source/methods	bandgap (eV)	light source/power	pollutants (mg/L)	degradation (%)	reaction rate (min^{-1})	ref
TiO_2 (1.5)	macroalgae/ultrasonication		mercury (Hg) lamp (UV)/450 W	mefenamic acid (1−3)	68 (60 min)	0.028	487
NC−TiO_2 (1.5)					89 (160 min)	0.083	
Ni−Fe (0.50)	pine needles/Hydrothermal		Xe lamp (visible)	remazol black 5 (50)	73 (120 min)	0.0122	488
CNF−Ni−Fe (0.50)					97 (120 min)	0.0343	
silanated (S) CNF−Ni−Fe (0.50)					98 (120 min)	0.0345	
BC−SiO_2	*Komagataeibacter xylinus*/hydrothermal		Xe−Hg lamp (UV)	CV (10)	56 (50 min)		489
BC−SiO_2−TiO_2					97 (50 min)		
ZnO−NFC (0.5)	−/hydrothermal method	3.16	UV lamp/36 W	tetracycline (25)	87 (120 min)		490
Fe−ZnO−NFC (0.5)		2.95			90 (120 min)		
cotton fabrics Cu_2O−NC	−/precipitation		Xe lamp/350 W/ >400 nm	MB (200)	98.32 (60 min)		491
				cationic yellow (200)	∼60 (300 min)		
				cationic red (200)	∼72 (300 min)		
				anionic red (200)	∼92 (300 min)		
				anionic yellow (200)	∼95 (300 min)		
				neutral red (200)	∼85 (300 min)		
CNC/Fe_3O_4	filtering paper/coprecipitation		Hg-lamp/250 W/ 365 nm	RhB (400)	50 (300 min)		492
			visible/55 W		20 (60 min)		
(straw cellulose) SC-CeO_2 (0.3)	straw pulp/hydrothermal method		halogen lamp/400 W/ 420 nm	Cr(VI) (3−5)	95 (60 min)		493
CNF-doped BiOCl (0.5)	hydrothermal method	2.92	xenon lamp/300 W/ 420 nm	RhB (20)	100 (16 min)		494
				tetracycline (10)	41 (16 min)		
Ag_2O−NP (0.5)	filter paper/layer-by-layer surface sol−gel (NC is removed by calcination at 450 °C for 6 h)	1.46	Hg lamp/300 W	MB (10)		0.16	495
TiO_2−nanotube (NT) (0.5)		3.04				0.24	
Ag_2O−NP/TiO_2−NT (0.5)		2.08−2.67			99 (6 min)	0.62	
Ag_2O−NP (0.5)				RhB (10)		0.04	
TiO_2−NT (0.5)						0.17	
Ag_2O−NP/TiO_2−NT (0.5)					98 (10 min)	0.37	
Ag_2O−NP (0.5)				norfloxacin (10)		0.07	
TiO_2−NT (0.5)						0.28	
TiO_2−NT (0.5)					98 (8 min)	0.39	
Ag/CCN (g-C_3N_4 doped by both Ag and CNF) (0.5)	eucalyptus wood/Wet−drying (CNF is removed by calcination at 550 °C for 4 h)	2.30	xenon lamp/300 W/ ≥420 nm	RhB (20)	100 (21 min)	0.127	496
				tetracycline (10)	75 (15 min)		
P25 (0.001)			xenon lamp/300 W/ 420 nm	MO (20)		0.0104	497
CdS (0.001)	hydrothermal					0.00013	
CdS/BC (0.001)	*Acetobacter xylinum*/hydrothermal					0.012	

https://doi.org/10.1021/acs.chemrev.1c00683
Chem. Rev. 2022, 122, 8936−9031

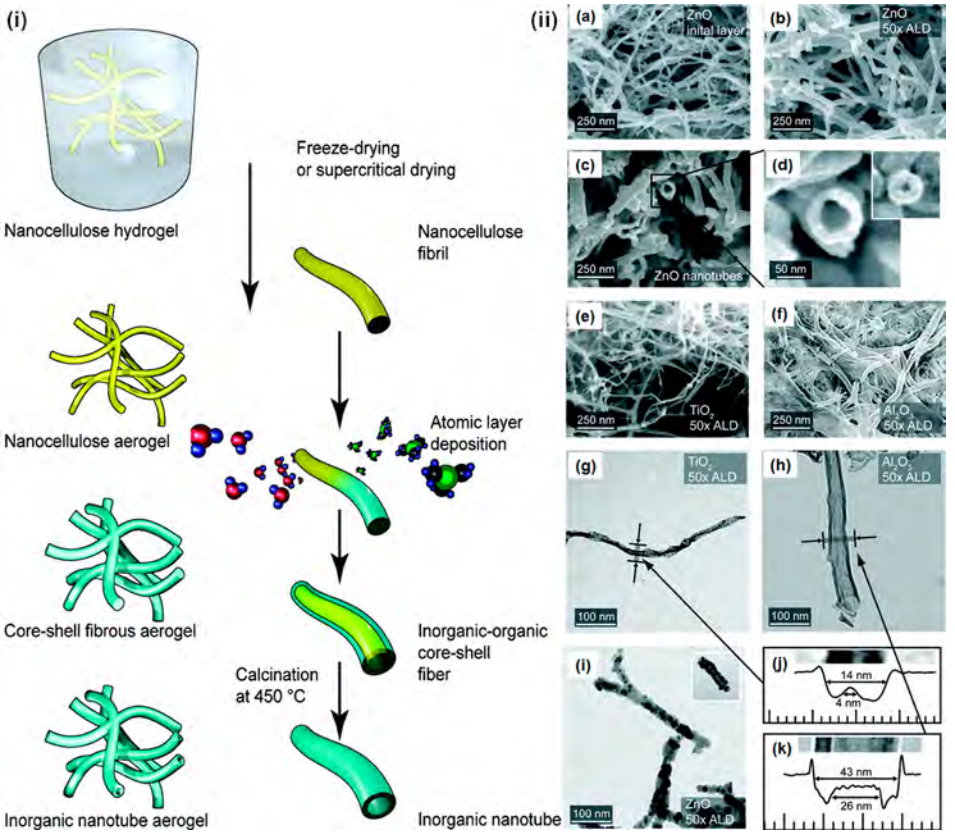

Figure 35. (i) Schematic illustration of the synthesis route to fabricate inorganic 1D nanotubes. (ii) SEM and TEM images of NC aerogels where different nanoparticles are grown as shown in panels a–f and g–i, respectively. (a) ZnO is used to deposit on CNF after the initial cycle of ALD reaction, followed by 50 cycles of reaction to increase the thickness of the tube as depicted in panel b. (c) Rough surface of the ZnO nanotube area after calcination and its hollow morphology is shown in panel d. (e) TiO_2 nanotube and (f) Al_2O_3 nanotube aerogels. (g) Crystallization-induced rough TiO_2 surface. (h) Al_2O_3 hollow nanotube with a smooth and uniform coating. (i) After calcination, the ZnO hollow nanotube becomes crystalline. (j and k) Intensity profiles across TiO_2 and Al_2O_3 hollow nanotubes, respectively. Reprinted with permission from ref 506. Copyright 2011 American Chemical Society.

preparation). The data gathered in Table 7 clearly suggests the system of (b) exhibited higher photodegradation efficiency over NC-based catalysts (the a system) for removal of different dyes, antibiotics, and inorganic metal ions under both UV and visible light irradiations. Overall, NC is a new family of sustainable and environmentally friendly templates or scaffolding materials to improve the photocatalytic performance of inorganic metallic nanoparticles.

The varying subjects of NC–nanoparticle hybrid photocatalysts have been reviewed in the literature.[5,447,498−502] Our goal in this section is to outline some essential fundamental knowledge based on a comprehensive literature search that is relevant to the relationship between efficient photocatalysts and water purification. We also try to address several questions: (a) Is NC a feasible template for nanoparticle growth? (b) Are these structures suitable in terms of high surface area and reactive sites to ensure sufficient photodegradation efficiency? (c) Is it possible to synthesize NC-based visible light active photocatalysts? (d) Can we report the appropriate photocatalytic mechanisms? (e) Is the system stable enough to regenerate? For brevity, we would like to declare that this section overlooks some NC-based catalysts, which are activated by reducing agents (e.g., $NaBH_4$, H_2, etc.).

5.3.1. Tailoring NC as Building Block in Nanocomposite with Inorganic Photocatalyst. A variety of natural templates, including cellulose, lignin, chitosan, chitin, silk, collagen and alginate fibrils, etc., are commonly used to host a variety of nanoparticle growths. While recognizing the quality of NC, although it is a renewable and low-cost biomaterial with good mechanical properties (toughness and strength), it is not photoactive, despite containing abundant active sites to anchor and interact with other functional components. Therefore, one may ask why NC is so important for template-directed nanoparticles synthesis? We believe this is because of the nanoscale dimension of NC that would have size-dependent characteristics (e.g., decreasing its dimension will increase the surface area and crystallinity, as well as accelerate reactivity leading to improved mechanical, thermal, and chemical properties). These size-dependent effects of NC were reported by Li et al.[503] For example, they prepared three types of micro-/NC-fibers, such as MNCF-10, MNCF-20, and MNCF-30 (produced by varying the grinding time), which exhibited mean particle sizes of 100, 58, and 31 nm, respectively. With decreasing MNCF sizes, the diameter of the ZnO nanoparticle decreased because of the increase in porosity and surface area. Because of the decreasing size, more hydroxyl groups in MNCF were exposed, promoting the in situ nucleation of Zn(II). Moreover, it has been shown that negatively charged NC greatly facilitates its electrostatic interactions with the positively charged Zn [001] planes. Wei et al. used NC to protect this 001 plane in hexagonal wurtzite ZnO crystals using the hydrothermal route.[504] They noticed that aggregated ZnO

https://doi.org/10.1021/acs.chemrev.1c00683
Chem. Rev. 2022, 122, 8936−9031

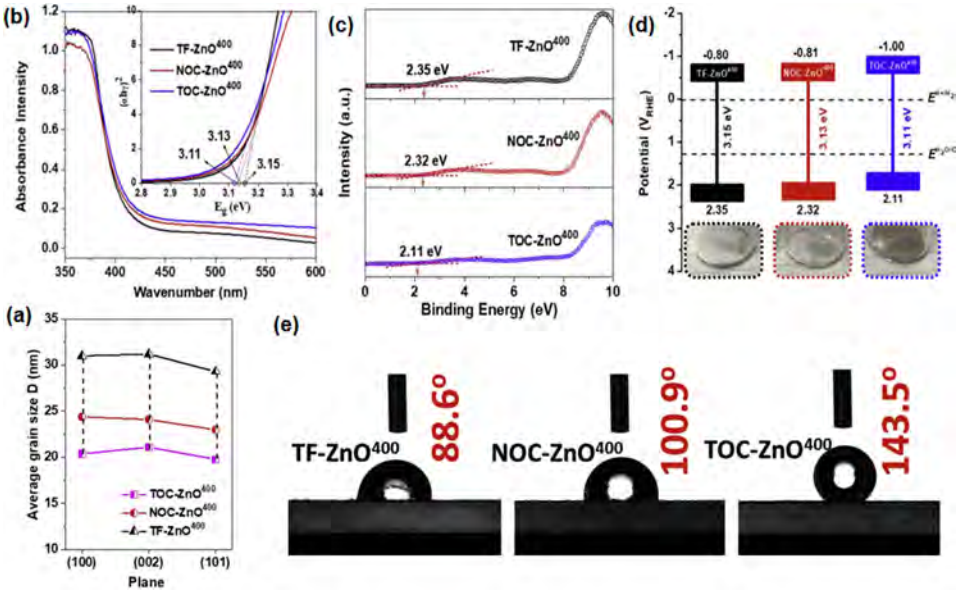

Figure 36. Characterizations of TF−ZnO^{400}, NONC−ZnO^{400}, and TONC−ZnO^{400}. (a) Calculated mean grain size from different crystal planes. (b) UV−vis diffuse reflectance spectra (DRS) for E_g calculation. (c) XPS spectra for elucidating the positions of VB. (d) Calculated VB and CB positions. (e) Image of contact angle measurements (NONC or NOC, nonoxidized nanocellulose; TONC or TOC, TEMPO-oxidized nanocellulose; TF, template-free). Reprinted with permission from ref 511. Copyright 2020 Elsevier.

flakes were produced without NC, whereas well-dispersed flakes distribution is found with NC. In another study, Lefatshe et al. pretreated cellulose fibers using acid and alkaline media to increase their CrI, which generates roughness on the surface, where anchoring of ZnO is favorable.[505] They noticed that acid hydrolysis is more efficient to increase the CrI of NC as compared with the alkaline treatment.

The unique scaffolding properties of NC enable the synthesis of nanoparticles (in 1D-3D nanostructures) with different catalytic properties. It has been shown that the increase of CNF content reduced the size of BiOCl nanosheets, which eventually assembled into a 3D flowerlike feature after the hydrothermal treatment. This might be due to the increase in viscosity, which could slow down the growth rate of nanocrystals and prevent their aggregation on CNF.[494] Korhonen et al. used the atomic layer deposition (ALD) method to incorporate Al_2O_3, ZnO, and TiO_2 in the NC aerogels, which could result in 1D hollow nanotubes (Figure 35),[506] using the following procedures. The NC template was used as the inner core, on which the nanoparticle precursor was deposited as the outer layer. This step was repeated many times to achieve the desired thickness of nanocrystal. The approach could generate a core−shell nanostructure, where the CNF core could be removed by calcination or other treatments to form hollow inorganic nanotubes with compositions, such as Al_2O_3, ZnO, and TiO_2 (Figure 35).[506] Often, the temperature-mediated removal of the NC template could collapse and break the skeleton of these nanotubes. This was seen by the shrinking of interwoven TiO_2 nanowires after NC removal by calcination (Figure 35g).[507] The diameter of these hollow structures can be controlled by the behavior of individuals or aggregation of NC fibrils in the suspension. It was seen that the resulting ZnO nanotubes exhibited a rough surface in Figure 35a−c, where the roughness could increase by calcination (Figure 35i). With ALD, a uniform Al_2O_3 coating was always formed on the fibril surface, where the nanotube structure could be maintained after calcination (Figure 35f). Alternatively, TiO_2 nanocrystal-based nanofibers were obtained by calcination because of the collapse of the skeleton core (Figure 35g).

Many different methods for the synthesis of NC-templated nanoparticles have been demonstrated. These methods include hydrothermal, sol−gel, ALD, chemical vapor deposition (CVD), dip-coating, sol-spray, sputtering, vapor deposition, coprecipitation, spray pyrolysis, thermal decomposition, and so on. Among them, both the sputtering and sol−gel methods are considered as the low-temperature methods to immobilize nanoparticles onto the NC substrates.[484] However, a scalable, ecofriendly, and low-cost preparation approach, enabling the nanoparticle growth in the NC scaffold to reach the desired properties, is still highly attractive, especially for large-scale production. Electrospinning could be an alternative pathway that can fabricate multistructure nanofibers on a large scale.[502] Such nanostructures would have huge advantages in the field of photocatalysis, where a very high electroactive surface can be generated. These hierarchical NC-enabled photocatalyst systems may simultaneously promote the trapping of pollutants, enhance photodegradation efficiency, and create excellent recycling stability of the system, which will be an interesting research topic.

5.3.2. Photocatalytic Properties Influenced by NC from Different Biosources. As seen in Table 7, different raw materials, such as woody and nonwoody lignocellulose biomass, as well as microbes, are used to extract NC for the preparation of different photocatalysts. However, different biosources can produce NC of different properties. Shi et al. compared the effects of NC (from cotton) and BC as templates on the physicochemical properties of the two resulting SiO_2−$(WO_3)_xTiO_2$ photocatalyst samples.[508] As shown in Figure S7, both samples showed mesoporous pores, but the photocatalyst with NC showed a significantly smaller pore size compared with the BC-based system. However, there are no noticeable differences in surface area between these two samples. Both NC- and BC-templated composite samples exhibited higher adsorption capability (followed by photocatalytic degradation)

https://doi.org/10.1021/acs.chemrev.1c00683
Chem. Rev. 2022, 122, 8936−9031

against RhB than that of the template-free $(WO_3)_xTiO_2$ powder. Although the adsorption of RhB into the BC-templated sample was faster than that of the NC-templated sample, the photodegradation efficiency of the latter one was slightly higher than the former one under visible light irradiation.

Some researchers hypothesized that NC with high CrI can favor the growth of nanoparticles because of the high surface roughness.[505] Such a hypothesis prompted the selection of BNC as a template because of its high crystallinity. However, this hypothesis was not supported by the study of Zheng et al.,[509] who functionalized BNC using amidoxime groups as they argued the initial interactions between unmodified BNC and nanoparticle are weak, leading to low-yield and nonuniform distribution of nanoparticles on the BNC surface. The amidoxime modification favored the immobilization of metallic ions on BNC because of its 3D tunneling structure that also thwarted the aggregation of ZnO during crystal growth in a polyol medium. The BNC−ZnO nanocomposite showed MO photodegradation efficiency of 92% after 120 min of UV light irradiation. Similarly, almost the same MO photodegradation efficiency was reported in another study, where BC−ZnO composite was prepared without functionalization.[510] This raised an essential question of whether such complicated amidoxime-functionalization of BNC is "truly" needed for template-directed nanoparticles synthesis. Although not explicitly discussed in these two papers, it is our opinion that a key control experiment (without functionalization) was missing in the study of Zheng et al.[509] We do not think the increase in crystallinity can substantially enhance the nanoparticle growth on the NC surface. Based on our experience, we believe the amorphous region may often be more active for metal ion adsorption because of the higher content of exposed functional groups when compared with the crystalline region. However, this argument is also not conclusive nor supported by evidence. As a result, more study is needed to verify these hypotheses in the future.

The amidoxime-functionalization is a complex process to modify the NC surface, and there are abundant simpler functionalization routes that one can consider for the preparation of NC-based photocatalysts. Xiao et al. investigated two types of NC, including nonoxidized nanocellulose (NONC) and TONC as templates to support the growth of ZnO nanocrystals using the solvothermal process.[511] A control experiment was also carried out using the template-free (TF) ZnO system. All the samples were calcined at different temperatures to remove the templates, where the calcination temperature at 400 °C was found to produce the best performing samples for photodegradation of MO. The mean grain sizes of NONC−ZnO^{400} and TONC−ZnO^{400} (the superscript 400 represents the calcination temperature) calculated from crystal planes as shown in Figure 36a, were significantly lower (by 22 and 33%, respectively) than that of TF−ZnO^{400}, which was ≈30 nm. The results indicated that NC played a vital role in decreasing the agglomeration of ZnO nanocrystals. This effect was particularly notable in TONC−ZnO^{400} because of the large amount of carboxylate group in TONC. Such functional groups could facilitate the Zn(II) adsorption by increasing the number of nucleating sites. Higher nucleating density can decrease the particle size and the agglomeration of ZnO crystals. In this study, all the samples showed a mesoporous structure, especially the TONC−ZnO^{400} sample. It was found that the average surface area, pore volume and pore sizes were significantly higher in TONC−ZnO^{400} as compared with TF−ZnO^{400} and NONC−ZnO^{400}. These properties in TONC−ZnO^{400} would facilitate the higher mass transfer rate of the solute during the photocatalytic process. Figure 36b shows UV−vis diffuse reflectance spectra indicating the band-gaps of TF−ZnO^{400}, NOC−ZnO^{400}, and TOC−ZnO^{400} were 3.15, 3.13, and 3.11 eV, respectively. In addition, the XPS spectra revealed the VB potentials and the positions of CB and VB. The straight line in the XPS spectra in Figure 36c indicates that the values of VB were 2.35 (TF−ZnO^{400}), 2.32 (NOC−ZnO^{400}), and 2.11 eV (TOC−ZnO^{400}). Given these values, the CB values could be calculated from $E_g = V_B - C_B$, which were −0.80, −0.81, and −1.0 eV, respectively (Figure 36d). The results indicated that the NONC and TONC templated ZnO nanoparticles have shifted their band gap to lower potentials. Accordingly, TONC−ZnO^{400} exhibited the photocatalytic rate for MO of 2.2 and 2.9 times higher than those of TF−ZnO^{400} and NONC−ZnO^{400}, respectively, under the same UV light irradiation. Another significant change found was related to the hydrophobicity of these photocatalysts. For example, as shown in Figure 36e, the contact angle of TONC−ZnO^{400} (143.5°) was higher than those of TF−ZnO^{400} (88.6°) and NOC−ZnO^{400} (100.9°). The hydrophobic photocatalysts will have superior performance over hydrophilic samples in removing pollutants with low water solubility.

5.3.3. NC-Enabled Photocatalysts for Water Purification. *Titanium Dioxide (TiO_2).* TiO_2 is a common photocatalyst because of its high catalytic activity, photochemical resistance, and chemical stability. It contains anatase, brookite, and rutile crystal polymorphs. The physicochemical properties of the prepared TiO_2 are dictated by their overall morphology, size, and crystal structures, which can be controlled by varying preparation methods. Rutile is more stable at the bulk phase, whereas the preparation of TiO_2 through the solution phase typically favors the formation of anatase structure. The surface free energy/surface stress and precursor chemistry can play a vital role in determining these nanostructures. In specific, the surface free energy controls the phase stability, especially at the nanoscale confinement. For example, anatase TiO_2 is more stable than rutile when the particle size is <14 nm.[512] It has been demonstrated that the surface free energies of rutile and brookite are higher than that of the anatase. As the nature of reactants determines the TiO_2 chemistry, understanding the reaction mechanisms is essential. However, these mechanisms are difficult to fully understand because of the varying routes of TiO_2 synthesis, in which a great deal of parameters are involved. It has been shown that increasing acidity of the reaction media and concentration of precursor ($TiCl_4$) facilitates the rutile phase, whereas the usage of $Ti(OBu)_4$ at pH 7 can result in the anatase phase at the low-temperature synthesis of TiO_2.[513] Readers interested in understanding the effects of reactant chemistry and mechanisms of the phase formation should refer the work by Reyes-Coronado et al.[514] They calculated the E_g values of 3.21, 3.13, and 3.00 eV for the anatase, brookite and rutile phases, respectively. Because of such high E_g values, TiO_2 is not capable of utilizing the visible part of the solar spectrum. In addition, pristine TiO_2 tends to recombine photoinduced charges, resulting in low quantum efficiency. However, during the literature review, we notice that most of the TiO_2 photocatalytic activity is governed by the presence of both anatase and rutile phases. It has been shown that pure anatase TiO_2 possesses high catalytic activity, while pure rutile TiO_2 is more stable.[515] For the mixed crystalline phase, it is seen that the optimal photocatalytic activity can be achieved when the anatase

https://doi.org/10.1021/acs.chemrev.1c00683
Chem. Rev. 2022, 122, 8936−9031

content is more than 60%. Commercial P25 usually consists of both anatase and rutile phases with ∼80% and ∼20% contents, respectively.

When the TiO_2 film is grown on NC, it usually exhibits a very low photocatalytic activity.[516] Although no notable band gap differences can be found between such TiO_2 synthesized in the NC scaffold and conventional TiO_2, NC can offer some unique advantages, including the better control of TiO_2's porosity and crystal structure. For example, Ivanova et al. synthesized CNC-templated anatase TiO_2 composite film on the glass substrate.[517] The composite was calcined at 450 °C to remove the CNC scaffold, to produce highly porous crystal TiO_2 with well-defined and narrow pore size distribution. With the increasing NC concentration, both pore volume and surface area of TiO_2 could increase gradually. The process produced a polycrystalline TiO_2 structure with a very small crystallite size (∼9.0 nm). It is thought that the nucleation of TiO_2 crystals occurs simultaneously during calcination. In this step, one can fine-tune the pore size of the composite. If a large pore size is desired, the NC integrity has to be maintained or preserved as long as possible during calcination. Meanwhile, the TiO_2 nucleation and crystal growth need to be slowed down. Alternatively, if NC is swollen (especially under hydrothermal conditions), that could facilitate the formation of a large pore. Therefore, NC could offer dual functions in the TiO_2 formation, that is, tuning the crystal growth process and controlling the porosity of the nanoparticle. The fundamental knowledge behind this process thus relies on the scaffolding structure and properties of NC, including porosity, functionalities and thermal stability. First, the porous NC can provide accessible surface sites that facilitate the growth of TiO_2 precursors.[518] Second, the surface functionalities of NC can play an important role in the synthesis of TiO_2 nanoparticles. It has been reported that a uniform distribution of TiO_2 can be produced in the CNC scaffold because of the sulfuric groups, which can bind to positively charged TiO_2, leading to the decrease in the surface energy of NC and preventing the occurrence of TiO_2 aggregation.[519] It has also been reported that the hydroxyl groups of NC are accountable for TiO_2 crystal growth and Ti^{4+} nucleation,[520,521] because these functional groups of NC could transfer oxygen atoms to a metal ion.[522] Finally, the high rigidity and thermal stability of NC can act as a thickener and facilitate the formation of TiO_2 films.[518]

Various methods are available to synthesize NC-templated TiO_2 photocatalysts. ALD has been used at high temperatures to replicate CNF using TiO_2.[522,523] In addition, CVD, sol−gel, microemulsion, and hydrothermal routes have also been demonstrated for the in situ/ex situ growth of TiO_2 onto NC. These methods are complex and time-consuming and require toxic reagents. We have demonstrated a simple hydrolysis method of titanium oxysulfate, a potential precursor for TiO_2 synthesis at low temperatures.[524] The process enabled the formation of TiO_2 on CNC with a narrow size range 3−5 nm, which exhibited both high MB photodegradation and bacterial inactivation capability under UV light irradiation. Comparing our observation with previous studies, it was seen that only a few studies had success in fabricating TiO_2 nanocrystals with size <10 nm onto NC. Such a composite system exhibited very good photocatalytic performance enabling both high dye removal and bacteria reduction applications. Therefore, this hydrolysis method is more efficient than the ALD, CVD, and other hydrothermal methods because of its simplicity in synthesis. It should be noted that commercial antimicrobial UV light typically has a short wavelength of 254 nm, which was extended to a mild UV light wavelength of 400 nm to irradiate the CNC−TiO_2 system.[524] This adjustment can improve the cost-effectiveness in terms of energy reduction and lowering the potential radiation hazards. In another study, ultrasonication was used to prepare NC−TiO_2 composites at low temperatures.[487] The adsorption capacity of this composite system was decreased due to the increase in TiO_2, (having reduced porosity). On the other hand, the photocatalytic efficiency of NC−TiO_2 was increased by elevating the concentration of TiO_2, but decreased at a very high concentration. This was explained by the behavior of TiO_2 sedimentation and aggregation.[525] Nunes et al. used the simple microwave irradiation method to grow TiO_2 on BC, paper, and polyester substrates at low temperatures.[516] Their objective was to achieve high photocatalytic activity though low-cost synthesis routes. The resulting composites showed higher RhB degradation efficiency when NC was used as a substrate than those with the substrates of polyester and tracing paper under solar radiation, even though they formed TiO_2 containing both brookite and rutile phases. This might be due to the high surface area of NC and flower-like TiO_2 structure (facilitated by the NC-template), yielding a higher content of reactive sites as compared with paper and polyester.

It has been shown that mesoporous TiO_2 exhibited higher photocatalytic activity than typical TiO_2 nanoparticles due to its high surface area and porous networks.[526] This observation has drawn several follow-up investigations. Wang et al. used NC as a template to fabricate mesoporous TiO_2 using the hydrothermal and calcination methods for photocatalytic application.[527] The resulting TiO_2 exhibited a single anatase crystal and its surface area and pore volume was higher than the commercial TiO_2 (P25). The mesoporous TiO_2 sample showed better RhB adsorption capacity than P25, where its photocatalytic degradation performance was also improved (e.g., 97% and 77% for mesoporous TiO_2 and P25, respectively) after 1 h of UV light irradiation. Similarly, Zhang and Qi used BNC as a template to grow TiO_2 nanowires with the anatase phase, where the sample also exhibited a mesoporous structure.[507] TiO_2 nanowires showed higher photodegradation activity against RhB than TiO_2 microfiber. In another study, the NC-templated mesoporous TiO_2 also showed higher photocatalytic activity than the eggshell-templated TiO_2 because of the high surface area of NC.[528]

Some authors functionalized NC to increase the adsorption capacity of the photocatalyst and hence the photodegradation efficiency. For example, Chen et al. used surface-quaternized nanocellulose (Q-NC) to prepare N-doped TiO_2 cryogel, which was used for adsorption and mineralization of MO.[529] Although the adsorption of MO was increased on Q-NC because of its positive charge, this efficiency is decreased upon N and TiO_2 doping because of the shielding of some surface cationic groups of Q-NC. However, N doping is essential, since pristine TiO_2 can absorb UV light that is only 4% of the total solar radiation. This limitation hinders the widespread applications of pure TiO_2 in photodegradation applications under sunlight irradiation. Doping of the N atom inside the lattice of TiO_2 (Ti−O−N/Ti−N−O) will decrease the band gap, which can effectively absorb the visible light. As shown in Figure 37(a), N-doping improves the photomineralization of MO using TiO_2-supported Q-NC. As seen in Figure 37c, the deep orange color of 10N10Ti−NC, which was obtained after MO adsorption in 30 min, became lighter after sunlight irradiation for 90 min.

https://doi.org/10.1021/acs.chemrev.1c00683
Chem. Rev. 2022, 122, 8936−9031

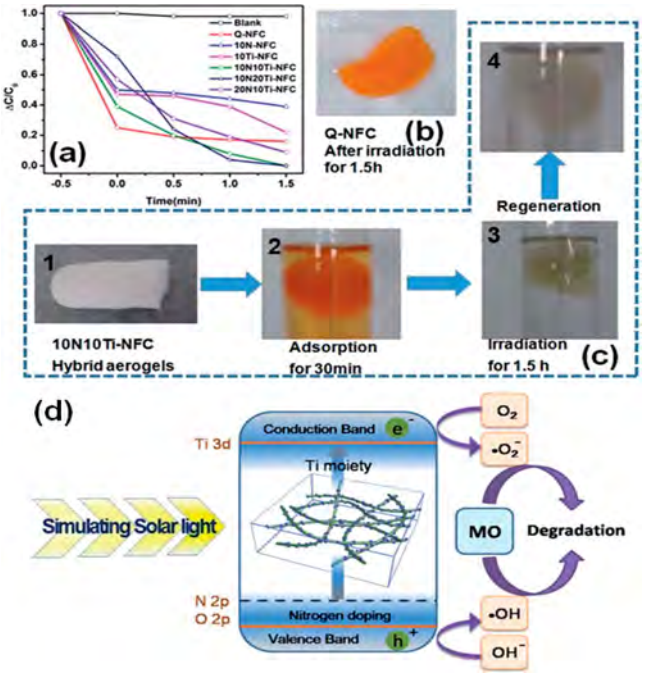

Figure 37. (a) Performances of photocatalytic applications of varying surface-quaternized nanocellulose (Q-NC) samples under sunlight irradiation. (b) Pristine Q-NC as a reference after solar irradiation for 1.5 h. (c) Adsorption > degradation > regeneration steps of Q-NC samples. (d) Proposed photocatalytic mechanism of N-doped TiO_2/Q-NC. Reprinted with permission from ref 529. Copyright 2017 Royal Society of Chemistry.

Zinc Oxide (ZnO). ZnO is an alternative to anatase TiO_2 because of its comparable band gap (~3.2 eV). It has versatile morphology, antimicrobial activity, lower cost, and low toxicity. However, the major limitation for photocatalytic applications of ZnO is its demand for UV-light excitation. Therefore, efforts have been made to fabricate ZnO-based composite materials with enhanced light absorption capability in the visible spectral range.[530] Some other drawbacks of this material include the aggregation of ZnO due to high surface charge,[531] high recombination rate, and the occurrence of photocorrosion that often leads to the formation of Zn−OH. To overcome these limitations, many strategies have been undertaken, including tuning its nanosizing and doping elements, such as carbon or other metals into the ZnO crystal phases.[511] ZnO's photocatalytic efficiency directly depends on the surface area and active crystal planes. Wei et al. prepared ZnO in the NC-template by the hydrothermal route followed by calcination. The sample exhibited many active and exposed (001) planes, but its surface area was only 21 cm^2/g, which is not so high.[504] ZnO crystals possess both positive and negative polar planes of Zn (001) and O (001), respectively. To reduce the surface energy, these polar planes tend grow rapidly due to their thermodynamic instability. Thus, these 001 planes often diminish, which results in needle-like (sharp-end) ZnO nanoparticles. It is thought that the ZnO polar (001) planes would act as the optimally active sites to increase the photocatalytic performance. So, it is important to develop a large number of 001 facets that are free, open and active during the ZnO growth. Because of favorable electrostatic interactions between positively charged Zn (001) planes and negatively charged NC, most of these (001) planes could be covered by NCs. This would significantly decrease the surface energy of Zn and O (001) planes, thus reducing the ZnO crystal growth along the (001) direction and resulting in the flake-like structure. After that, calcination can remove the (001) plane-covered NC and expose a high-energy surface with active 001 facets. This pathway can result in excellent photocatalytic activity as compared with commercial TiO_2 (P25).[504]

While many chemical methods have been extensively tested for ZnO nanoparticle synthesis, the NC-based composite approach seems to offer many promising features of green chemistry. For example, Nahi et al. used NC extracted by the *Tinospora cordifolia* plant using simple sonication treatment as a template to synthesize ZnO.[532] The ZnO−NC composite photocatalyst showed the enrofloxacin degradation efficiency of 97% after 120 min under sunlight irradiation. The authors also used these catalysts for the photodegradation of aureomycin (a widely used antibiotic in poultry). The photodegradation efficiency against this antibiotic was 93.5% for ZnO−NC, 72% for ZnO, and 52% for NC, respectively, after 120 min of sunlight irradiation.[533] In another study, Modi and Fulekar used *Allium sativa* skin for the preparation of ZnO and cellulose composites.[534] Later, they prepared CNC chemically and used a simple sonication method for ZnO−CNC composite preparation. Similar to typical chemical routes, ZnO showed a polycrystalline wurtzite structure and possessed rod- and hexagonal-shaped morphology. ZnO−CNC exhibited a large surface area of 32 m^2/g, where that for ZnO was 13 and 19 m^2/g for CNC. The pseudo-first-order reaction rate of MB degradation using ZnO/CNC was 0.020/min (the photodegradation efficiency was 88.62%), while it was only 0.011/min (the photodegradation efficiency was 65.87%) for ZnO under sunlight irradiation.

In the literature, different morphologies of ZnO have been observed, including porous, nanorods, and flower-like, which exhibited different properties.[535] For example, Ning et al. synthesized sphere-, rod-, and needle-like ZnO with and without the TONC template.[531] Only the sphere-type morphology showed a homogeneous distribution in TONC because of the lesser aggregation of ZnO crystals. With sphere-type ZnO, MB could be removed completely after 20 min, but the removal time was 100 min for other types of ZnO under the same UV light irradiation. Therefore, sphere-type ZnO was more catalytically active as compared with rod- and needle-like ZnO. Similar to this study, Abdalkarim et al. used the hydrothermal method to prepare different types of ZnO crystals within the CNC scaffold at three different $ZnCl_2$ precursor concentrations.[486] The resulting structures included hexagonal nanorod, flower-like, and hexagonal disk with sheet-like structures of ZnO formed at low, medium and high $ZnCl_2$ concentrations, respectively. It is important to mention that at very high precursor concentrations, some impurities might also be incorporated in the final catalyst, which would be difficult to trace. For example, with excess Zn^{2+} ions not anchored to the CNC surface (because of the saturation of OH groups), these ions might yield some impurity phase. In addition, Abdalkarim et al.[486] showed that by simply changing the pH value and temperature during reaction, one can change the ZnO structure between flower-like nanorod (pH 11 at 100 °C) and rod-like nanohybrids (pH 9.3−10.5 at 90 °C) in the CNC scaffold.[536] The flower-like nanorod structure showed excellent photodegradation against MB and better antibacterial activity than the nanohybrid structure. This confirms that the precursor concentration, as well as the reaction conditions, could play vital roles to affect the overall composite structure and, thus, their photocatalytic properties.

https://doi.org/10.1021/acs.chemrev.1c00683
Chem. Rev. 2022, 122, 8936−9031

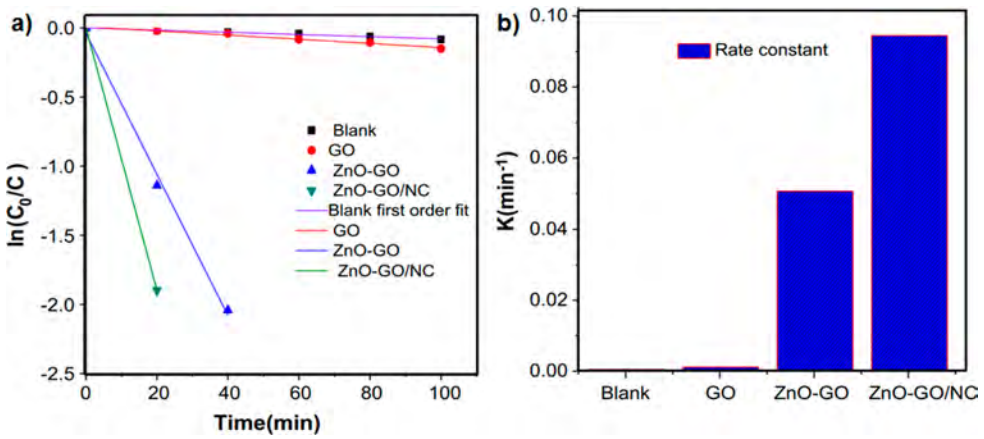

Figure 38. (a) Linear kinetic plots of photodegradation of ciprofloxacin using photocatalysts based on ZnO, GO, and NC components. (b) Reaction rates of blank, GO, ZnO−GO, and ZnO−GO/NC composites. Reprinted with permission from ref 538. Copyright 2017 Elsevier.

Engineering the band gap property of ZnO using the NC template method is still an inconsistent topic in the literature. For example, Jamal et al. prepared ZnO−NC composite using a simple sonication approach. They observed that the band gap decreased from 3.3 (ZnO) to 2.75 eV (ZnO−NC), while NC itself had a band gap of 3.8 eV.[537] However, they did not explain how NC could decrease the band gap of ZnO. The lower band gap ensured the visible region excitation of the composite. About 98% of photodegradation of CR was obtained by using ZnO−NC, while it was only 72% and 52% for NC and ZnO, respectively. Since the composite also had a significantly higher BET surface area (184 m^2/g) than that of pristine ZnO (82 m^2/g), it was difficult for us to judge whether the enhanced photocatalytic activity in ZnO−NC was due to a smaller band gap or larger surface area or both. In contrast, Anirudhan and Deepa used NC-based ZnO-doped GO composite for the adsorption and subsequent photodegradation of ciprofloxacin—an antibiotic commonly found in wastewater.[538] Adding NC into the ZnO−GO hybrid has shown to increase the band gap from 2.4 to 2.8 eV. The photodegradation of ciprofloxacin follows the first-order kinetics in visible light (with a solar simulator). The ZnO−GO could degrade ciprofloxacin almost completely after 60 min, while the degradation was reduced to 40 min with the NC incorporation. The photodegradation rate for ciprofloxacin using varying photocatalysts based on ZnO, GO, and NC components are shown in Figure 38, It was seen that all data points for each photocatalyst could be fitted with a linear relationship, suggesting the photocatalytic reaction followed the first-order reaction kinetics (Figure 38a). The first-order reaction kinetics can be expressed as $Ln(C_0/C_t) = kt$, where C_0 is the initial concentration of solutes, C_t is the concentration of the solute at reaction time t, and k is the reaction rate constant. The k values for ZnO−GO and ZnO−GO−NC composite were 5.1×10^{-2} and 9.49×10^{-2} min^{-1}, respectively (Figure 38b). The results showed that ZnO−GO−NC possessed very high photodegradation efficiency, which could be explained as follows. The incorporation of NC into the ZnO−GO system can increase the oxy-functional groups (e.g., COOH and OH groups), which would lead to higher adsorption efficiency of ciprofloxacin by ZnO−GO/NC than by ZnO/GO. Because of the high electrical conductivity of GO, which often acts as an electron sink halting the recombination of photogenerated electron and hole (hence the accumulation of hole on the CB value). The authors hypothesized that the photodegradation mechanism of ciprofloxacin was not due to photolysis of ciprofloxacin, since the drug is found to be stable in sunlight, but mainly occurred through the photocatalytic reaction process. However, ciprofloxacin has photosensitizing ability, and it can eject electrons onto the CB of the composite after the visible light excitation. The proposed reaction mechanism is shown in eqs 7−14 below:

$$\mathrm{ZnO{-}GO{-}NC} + h\nu \rightarrow \mathrm{ZnO{-}GO{-}NC}\ (e^-_{(cb)}{+}h^+_{(vb)}) \quad (7)$$

$$\text{ciprofloxacin (CF)} + h\nu \rightarrow {}^1\mathrm{CF}^* \text{ or } {}^3\mathrm{CF}^* \quad (8)$$

$${}^1\mathrm{CF}^* \text{ or } {}^3\mathrm{CF}^* + \mathrm{ZnO{-}GO{-}NC} - \rightarrow {}^1\mathrm{CF}^* + \mathrm{ZnO{-}GO{-}NC}(e^-\mathrm{cb}) \quad (9)$$

$$\mathrm{ZnO{-}GO{-}NC}(e^-_{cb}) + O_2 \rightarrow O_2^{\bullet -} + \mathrm{ZnO{-}GO{-}NC} \quad (10)$$

$$\mathrm{ZnO{-}GO{-}NC}(h^+_{vb}) + H_2O \rightarrow \mathrm{ZnO{-}GO{-}NC} + H^+ + OH^- \quad (11)$$

$$O_2^{\bullet -} + H^+ \rightarrow HO_2^{\bullet +} \quad (12)$$

$$\mathrm{ZnO - GO - NC}(h^+_{vb}) + OH^- \rightarrow \mathrm{ZnO - GO - NC} + OH^{\bullet} \quad (13)$$

$$OH^{\bullet} + \mathrm{CF} \rightarrow H_2O + CO_2 \quad (14)$$

NC often acts as a carbon (C) source to dope/coat ZnO. It can facilitate the photocatalytic activity of ZnO through band gap engineering, as well as through tuning of size and other morphological properties. Because of the suitable electrical and photophysical properties of C, which acts as a reservoir for photogenerated electrons, the C atom can thus participate in the shuttling of electrons from the catalyst. Furthermore, C has the potential to increase the adsorption efficiency. If one can uniformly deposit C on the surface of a ZnO nanoparticle, the C coating can also increase the chemical stability against photocorrosion. The source of C can come from carbon nanomaterials, such as CNT, GO, and fullerene, which are not exactly safe or low-cost materials. In this case, NC can be a better alternative, offering a C source to improve the photocatalytic performance of ZnO. For tuning the ZnO morphology, porosity, and crystal growth behavior, Xiao et al. used a solvothermal process to coat/dope the ZnO surface with C, as shown in

https://doi.org/10.1021/acs.chemrev.1c00683
Chem. Rev. 2022, 122, 8936−9031

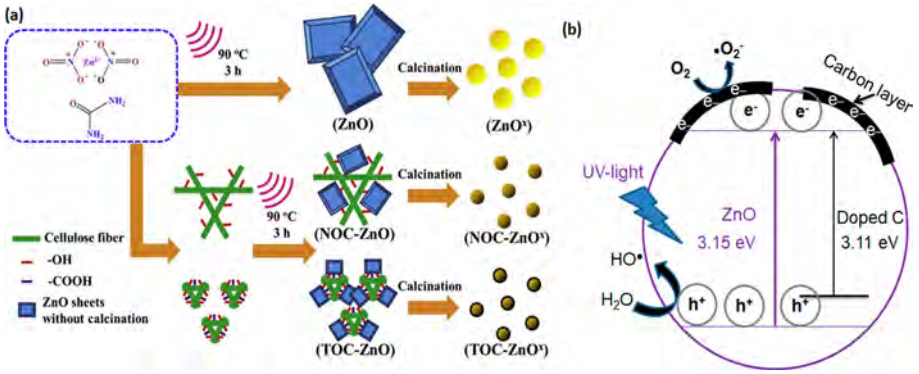

Figure 39. (a) Illustration of fabrication methods of C-coated ZnO using two types of NC materials. Reprinted with permission from ref 511. Copyright 2020 Elsevier. (b) Simplified illustration of the pseudo-first-order photocatalytic reaction mechanism of C-coated ZnO; doping of C creates sub-band gap, which helps to reduce the E_g value of ZnO.

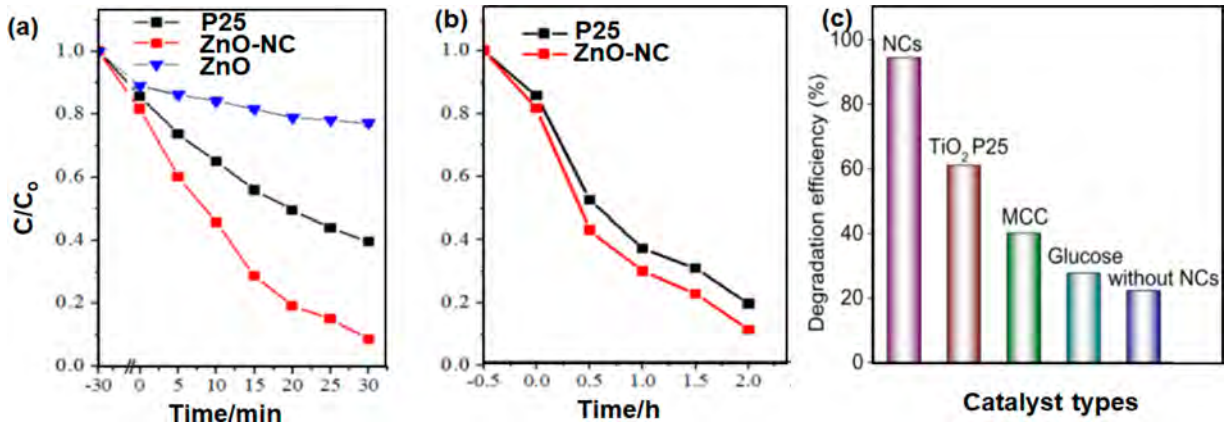

Figure 40. MB photodegradation under the irradiation of (a) UV and (b) visible lights and (c) MB photodegradation efficiency with and without NC. Adapted from ref 504. Copyright 2016 NC State University.

Figure 39a.[511] They used two types of NC templates NONC and TONC as C sources to assist the ZnO synthesis through calcination. They reported that calcination at a temperature of 400 °C was effective to preserve the thin C-layer on the surface of ZnO nanocrystals with a hexagonal wurtzite structure. The authors also introduced urea into precalcined ZnO to generate CO_2 gas, which increased the porosity of ZnO after calcination. The doped/coated C in ZnO decreased the band gap and increased the surface area, especially for TONC−ZnO^{400} that facilitates MO photodegradation, and its rate constant was 0.0254, which is 2.2 and 2.9 times higher than those of TONC−NOC^{400} and TF−ZnO^{400} under the same UV light irradiation. The proposed mechanism for the first-order photocatalytic reaction of C-coated ZnO is illustrated in Figure 39b.

In another study, Wei et al. used NC to prepare a hexagonal wurtzite ZnO structure, similar to the system prepared by Xiao et al.,[511] but with a hydrothermal route.[504] In addition, they carried out calcination at a higher temperature of 550 °C to remove NC. The resulting ZnO exhibited an average size of around 32 nm. It was shown that the intensity ratio between 100 and 002 peaks in XRD of this ZnO was smaller than the bulk sample, suggesting the ZnO nanoparticles prepared by Wei et al. possessed a high content of polar facets. The mean pore diameter in this ZnO−NC sample was nearly 9.0 nm. The photodegradation efficiency of ZnO−NC for MB was nearly 95%, which was higher than ZnO without NC (23%) and Degussa TiO_2 P25 (60.5%) after 30 min of UV light irradiation (Figure 40a). On the other hand, ZnO−NC showed a 10% higher photocatalytic performance than P25 when using visible light irradiation (Figure 40b). To justify the photocatalytic efficacy of this ZnO−NC composite, the authors compared their degradation efficiency with those of other ZnO systems using different templates where the results are shown in Figure 40c. In this figure, ZnO−NC showed the best photodegradation efficiency (a significantly faster rate for MB degradation, that is, over 90% within 30 min) than the ZnO without NC and ZnO with other additives, under the same experimental conditions. These observations indicate that the use of NC as a template can directly assist ZnO to achieve better photocatalytic activity and a faster degradation rate as compared with other ZnO prepared by conventional means.

Bi/Trimetallic Nanoparticles. Although TiO_2 and ZnO have been extensively studied for a range of photocatalytic applications, the judicial choice of preparing bi/trimetallic nanoparticles onto NC is to achieve multifunctional properties. In the case of TiO_2, Nair et al. used the low-temperature growth method to prepare TiO_2 nanorod (NR) at varying temperatures (90 and 150 °C) on functionalized CNC, having sulfonic, carboxyl and phosphoryl groups together; the resulting composites were termed CNC/TiO_2−NR(90) and CNC/TiO_2−NR(150) with NR grown at 90 and 150 °C, respectively. These systems were further doped with plasmonic Au nanocrystals as shown in Supporting Information (Figure S8a).[539] The presence of Au nanocrystals on TiO_2 narrowed its band gap from 3.15 eV (CNC/TiO_2−NRs(90)) to 3.11 eV (CNC/TiO_2−NRs(90)/Au). However, this effect did not occur

https://doi.org/10.1021/acs.chemrev.1c00683
Chem. Rev. 2022, 122, 8936−9031

for CNC/TiO_2−NR(150). In addition, the BET surface area was significantly higher in CNC/TiO_2−NR(90) than CNC/TiO_2−NR(150), where the former also showed a higher content of anatase phase than rutile phase. On the contrary, the CNC/TiO_2−NR(150) had a higher degree of crystallinity dominated by the rutile phase. These observations clearly suggest that the demonstrated photocatalyst synthesized at a low temperature (90 °C) exhibited better physicochemical properties required to achieve a good photocatalytic activity than when synthesized at a high temperature (150 °C). Unfortunately, CNC/TiO_2−NR(90) showed much lower photocatalytic activity for RhB degradation than CNC/TiO_2−NR(150) as shown in Supporting Information (Figure S8b) under sunlight irradiation in the presence of H_2O_2. The author hypothesized that this was due to a lower number of defects in CNC/TiO_2−NR(150), which might decrease the charge carrier recombination (usually occurred at defect sites). In principle, the presence of Au could generate the local surface plasmon resonance (LSPR) effect that should ensure good photocatalytic activity in the visible light region. Unfortunately, the Au addition did not significantly change this photocatalytic activity in the photodegradation of RhB study. It was surprising to see such low photocatalytic performance in the presence of Au and H_2O_2. In general, H_2O_2 is often used to decrease the recombination of electron−hole, which can act as a scavenger of electrons, i.e., hosting of photoinduced electrons from the CB of the semiconductor ($H_2O_2 + e^-_{CB} \rightarrow {}^{\bullet}OH + OH^-$). In this case, the reaction can accelerate the formation of hydroxyl radicals. As a result, H_2O_2 is a powerful oxidizing agent for dye degradation. This study should be investigated further to reveal other mechanisms that hinder the expected photocatalytic performance in the presence of Au and H_2O_2.

In another study, Liu et al. used NC as a template to prepare Ni−NiO/TiO_2 composites with a hollow structure having a large number of pore and pore volumes.[540] To accomplish this structure, the electroless plating technique was used to deposit Ni−NiO uniformly on the NC surface, followed by a sol−gel method to prepare TiO_2. NC was removed by calcination at different temperatures. At the calcination temperature of 600 °C, TiO_2 showed the anatase phase which was then transformed to the rutile phase at 800 °C. The threshold wavelength of the absorption spectrum of the Ni−NiO/TiO_2 composite was found to be shifted to 66 nm (band gap was 2.55 eV). The final product exhibited 86% of Pb(II) degradation after 120 min of UV light irradiation. Generally, doping of Ni/O would bring some level of impurity to TiO_2 crystals which might help to absorb photons at lower energy. Therefore, we expect photodegradation of pollutants by the Ni−NiO/TiO_2 composite could occur by visible light irradiation, however, this was not checked in the study.

Al has been used to dope into ZnO crystals synthesized in the templates of MNCF, where the resulting composite was termed Al-doped ZnO/cellulose (AZOC) and tested for photodegradation of MO under visible light irradiation.[503] Due to its smaller size, Al can substitute the regular lattice sites of ZnO and does not destroy its crystal structure. Depending on the MNCF diameter, the mean pore diameters of AZOC-10 were 536 nm, AZOC-20 was 396 nm, and AZOC-30 was 285 nm), where the corresponding surface areas of these three composites were 20, 24, and 27 m^2/g, respectively. It was seen that doping of Al into ZnO/MNCF resulted in a red-shift of the absorption peak. Consequently, the band gap differences of ZnO/MNCF-30 (without Al doping) and AZOC were 2.97 and 2.92 eV, respectively. Moreover, the crystallite size of ZnO in ZnO/MNCF-30 and AZOC-30 was 15.91 and 14.21 nm, respectively. As a result, AZOC exhibited higher photocatalytic activity of MO photodegradation (89%) than ZnO/MNCF-30 (53%) under visible light irradiation. The first-order kinetics model was well suited to fit the catalytic efficiency data, where the rate constant followed the order of AZOC > ZnO−MNCF > Al−ZnO > ZnO > MNCF under the same experimental conditions. These findings clearly indicated the effect of the template morphology (MNCF in this case), as well as demonstrated that Al doping could play a vital role in achieving good photocatalytic efficiency of ZnO-based composite. An illustration of the overall mechanism of MO photodegradation using AZOC composite is given in Figure 41a. The doped Al element into ZnO crystals

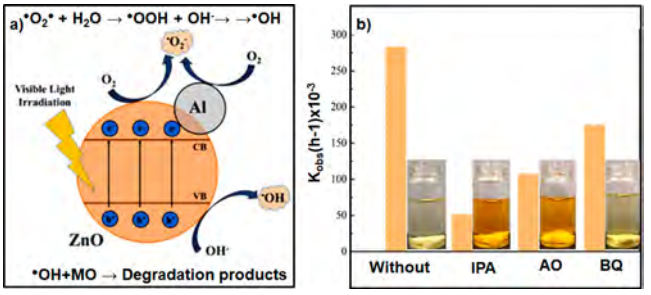

Figure 41. (a) Illustration of tentative photocatalytic mechanism for MO degradation using AZOC under visible light irradiation. (b) Reaction rate constant for degradation of MO during the radical capture experiments. Reprinted with permission from ref 503. Copyright 2020 Elsevier.

favors the transfer of photogenerated electrons from the surface of AZOC to the dissolved oxygen molecules that can accelerate the photocatalytic activity of the AZOC composite. To explore the actual mechanisms of photoinduced h^+, $^{\bullet}OH$, $^{\bullet}O^{2-}$, and $^1O_2$ in the photocatalytic degradation of pollutants, radical capture experiments can be carried out using standard chemical probes as scavengers to rummage these reactive oxygen species (ROS). These probes include potassium iodide/ethylenediaminetetraacetic acid disodium/ammonium oxalate (AO), isopropanol (IPA)/dimethyl sulfoxide, benzequione (BQ), and sodium azide, respectively.[541] The results from the radical capture experiments to explore the photodegradation mechanism of MO by AZOC are illustrated in Figure 41b. It was seen that the addition of IPA, AO and BQ could significantly decrease the photocatalytic efficiency of the AZOC composite. Since IPA exhibited a drastic decrease in photocatalytic activity (followed by AO), it can be concluded that the $^{\bullet}OH$ and $^{\bullet}O_2^-$ are the two main active ROS that participate in the MO degradation. The hole may also play a small but essential role in the MO photodegradation process. Similar to MO, other azo dyes, containing (—N═N—) bonds, can undergo photocatalytic degradation. The (—N═N—) bonds are generally oxidized by hydroxyl radicals and the positive hole or the electron of the conduction band could reduce this double bond. Breaking of (—N═N—) bonds can result in the discoloration of dyes.[542] These observations were seen not only for organic dyes but also for inorganic heavy metal ions using NC-based photocatalysts.[543]

On the basis of the above discussions, it is clear that the use of NC to host varying inorganic photocatalysts could be useful for water remediation. It is possible that with different forms of nanoparticles (from monometallic to bimetallic or even

https://doi.org/10.1021/acs.chemrev.1c00683
Chem. Rev. 2022, 122, 8936−9031

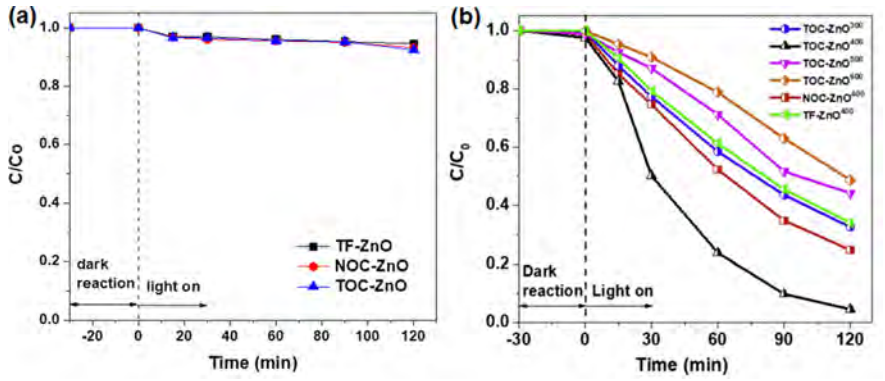

Figure 42. MO photocatalytic degradation curves by different ZnO samples: (a) before and (b) after calcination. Reprinted with permission from ref 511. Copyright 2020 Elsevier.

Table 8. Reusability Performances of NC-Based Photocatalysts for Water Purification

name	pollutants	light source	washing agent	recollecting	recycling efficiency	remarks	ref
N−Ti−NFC	MO (10 mg/L)	sunlight (300 W)			>98% (90 min, 3 cycles)	MO adsorption decreased by 25% at third cycle	529
TiO_2/CNC	MB (6.67 mg/L)	UV		centrifugation	>98% (3 cycles)	lack of characterization after regeneration	524
NC−TiO_2	mefenamic acid (1−3 mg/L)	UV/450W	0.1 M NaOH	filtration	85.39% (5 cycles)	7.0% decreased after the first cycle; small loss of catalyst	487
TiO_2−NFC (NC removed by calcination)	MO (5 mg/L)	UV (36 W)		filtration	90% (60 min, 5 cycles)	lack of characterization after regeneration	521
ZnO−GO/NC	ciprofloxacin (0.4 g/L)	sunlight	water	ultracentrifugation	84.3% (5 cycles)	about 14% decreased after first cycle due to catalyst weight loss	538
ZnO/CNC	MB (10 mg/L)	solar irradiation		centrifugation	~82% (120 min, 5 cycles)	suspected photocorrosion decreased efficiency due to MB accumulation over the catalyst surface	534
CNC−ZnO	MB (0.00001 mmol/L)	UV			95% (3 cycles)	SEM image shows no significant change of catalyst morphology after recycling	486
ZnO (NC removed by calcination)	MB (5 mg/L)	UV (6 W/365 nm)	no wash	centrifugation	92% (6 cycles)	lack of characterization after regeneration	504
AZOC	MO (10 mg/L)	visible light 420 nm/500 W	water		86.2% (10 cycles)	decreased by ~4% to the first cycle; lack of characterization after regeneration	503
Ag_3PO_4/NC	MB (0.03 g/L)	direct sunlight			>99% (90 min; 3 cycles)	lack of characterization after regeneration	546
BiOBr/CCNF-900	RhB and Cr(VI) (simultaneous)	LED lamp visible light/200 W			~96% (MB after 5 cycles) ~80% (Cr(VI) after 5 cycles)	XRD shows the catalyst reserves its crystalline structure after reuse	543

trimetallic) synthesized in the NC scaffold, the hybrid nanocomposite can exhibit different photocatalytic properties (e.g., photodegradation rates). In addition to the above examples, we discuss the performances of NC-based silver phosphate (Ag_3PO_4) and bismuth oxybromide (BiOBr), which also show good potential for photodegradation of some pollutants in Supporting Information (section S7).

5.3.4. Role of Calcination on NC-Based Photocatalysts. Calcination/pyrolysis is an important step in the fabrication of NC-templated photocatalysts as it can play a direct role in controlling the overall morphology of the produced metal oxide nanoparticles. For example, ZnO synthesized without a template could show a flake-like shape having disorder aggregates in the size of 2−4 μm (Figure S9a). In contrast, uniform deposition of ZnO flakes with relatively smaller in size (1 and 1−2 μm) when NC templates (TONC and NONC) were used (Figure S9b and S9c). The corresponding ZnO morphologies after the template removal by calcination are shown in Figure S9d−f). It was found that the increase in calcination temperature could cause distinct changes in morphology, that is, from flakes to nanorods/coarse rounded macro- and/or nanoparticles (Figure S9g−i). The increase in calcination temperature also gradually increased their sizes.[511] Figure 42 shows the MO photodegradation activity of different TONC−ZnO photocatalysts under UV light irradiation prepared before and after calcination. It was seen that the samples without calcination show very low photodegradation compared to samples undergoing calcination. The study indicated that appropriate calcination temperatures could substantially improve photocatalytic activities. This could be due to the increased crystallinity in ZnO or stimulating the conversion of its precursor into ZnO.

For TiO_2 to achieve a highly active crystalline phase, selecting an appropriate calcination temperature is important. Xiao et al. investigated the effect of different calcination temperatures using the NFC-templating method to fabricate TiO_2 for photocatalytic degradation of MO.[521] The degradation efficiency of these catalysts was notably decreased by increasing the calcination temperature. This behavior was also found in ZnO.

https://doi.org/10.1021/acs.chemrev.1c00683
Chem. Rev. 2022, 122, 8936−9031

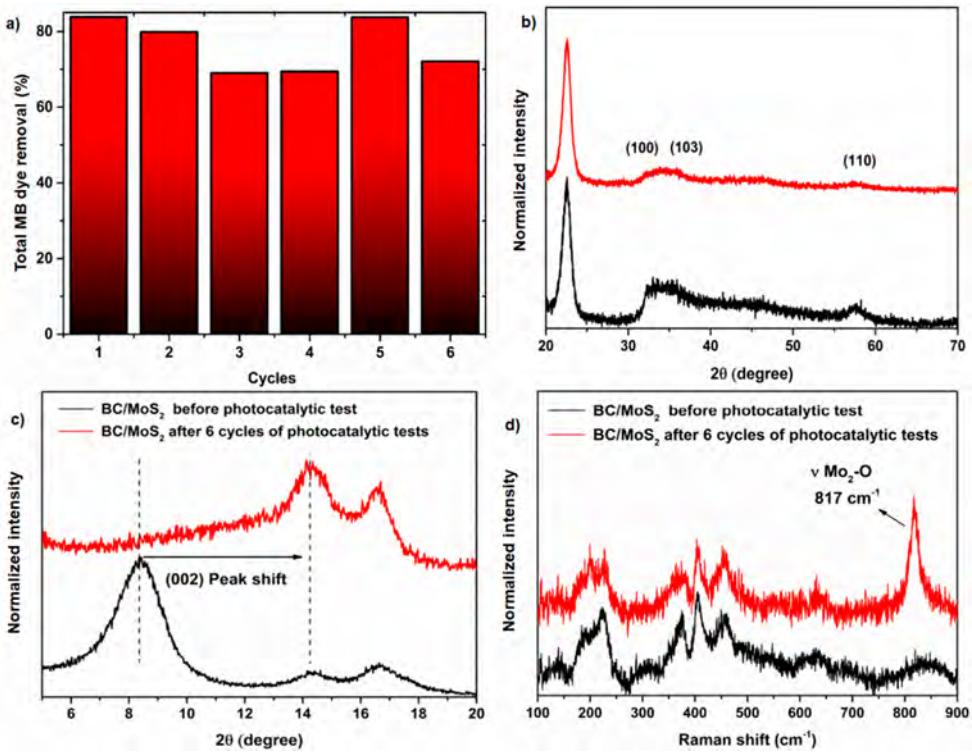

Figure 43. (a) Recycling stability of MB photodegradation under UV−visible light irradiation. (b) XRD characterizations (2θ range from 20 to 70°) of BC/MoS_2 before and after recycling tests. (c) 2θ range from 5 to 20°. (d) Raman spectroscopy of BC/MoS_2 before and after recycling tests. Reprinted with permission from ref 545. Copyright 2020 American Chemical Society.

Although the authors did not mention the reason for this behavior, we think it could be due to the increasing TiO_2 crystal size, which greatly decreased the surface area with the increasing calcination temperature. Similarly, Melone et al. used TOCNF to nucleate TiO_2 or TiO_2/SiO_2 using a sol−gel method to fabricate catalysts for adsorption and photocatalytic degradation of MB and RhB.[544] They calcined CNF−TiO_2 (T) and CNF−TiO_2/SiO_2 (TS) aerogels at two different temperatures: 600 and 800 °C, respectively. The TS aerogel generally showed higher MB adsorption capacity than T aerogel, and the adsorbed MB was completely degraded after 2 h of UV light irradiation at 366 nm. TS aerogel (800 °C) showed higher RhB adsorption capacity as compared to others that are mineralized by UV light irradiation. It should be noted that T (800 °C) was scarcely photoactive for MB, while T at both 600 and 800 °C exhibited negligible catalytic activity toward RhB. Although such photocatalysts could be useful to regenerate the contaminated adsorbent, there are several uncertainties in this study. First, little explanation was given to explain the varied adsorption capacities and photocatalytic activities. Second, the presence/absence of SiO_2 on the catalyst could influence the crystallinity of the final product that might in turn influence the pollutant degradation efficiency.

5.3.5. Stability and Recyclability of NC-Based Photocatalysts. Evaluating the stability of a given photocatalyst through regeneration study is important for practical applications. The high stability of a photocatalyst, which can exhibit high catalytic activity after each regeneration cycle, can greatly enhance the cost-effectiveness in large-scale industrial operations. Since most of the powder photocatalysts are soluble in water and have the tendency to undergo photocorrosion, immobilizing them in a NC scaffold can be a good option to increase their stability and improve their recyclability. As summarized in Table 8, only small fluctuations of the photocatalytic efficiency were observed among the different NC-based photocatalysts, while a notable decrease in the pollutant removal ability was not observed even after several cycles of tests. This suggests that most of the NC-based photocatalysts have good stability, which can be attributed to the lack of surface poisoning by intermediates/final products of the reaction, lower photocorrosion and/or decreased catalyst leaching effects. Nevertheless, there is always the possibility that photocatalytic reactions can degrade the molecular structure of the NC scaffold. This would result in the collapse of the NC template and decrease in the catalytic performance and lifespan. To explore such a possibility, we expect that the characterizations, such as SEM, XPS, XRD, and Raman spectroscopy, of the samples before and after the recycling can shed some insights. Ferreira-Neto et al. have carried out such a study, and the results are shown in Figure 43, which offered us some important knowledge.[545] In Figure 43a, the BC/MoS_2-based photocatalyst showed only a 10% decrease in MB removal efficiency after six cycles under UV−vis light irradiation. According to the XRD spectra (Figure 43b), BC exhibited almost the same spectra before and after the use, suggesting that their crystalline lattice remained unchanged during the recycling processes. This observation was also true for the NC functional groups as observed by FTIR, where no apparent peak changes regarding the polysaccharide structure were seen. These findings indicated that the NC scaffold could maintain its network structure even after several consecutive cycles of regeneration.

A significant change in XRD, that is, the sharp shift of the 002 peak (from 8.4° to 14.2°), was observed in MOS_2 (Figure 43c). This suggested the interlayer distance of MOS_2 2D nanosheets was expanded from 0.62 to 1.05 nm after six cycles. Interestingly, the authors found this change was quite beneficial as it enhanced

https://doi.org/10.1021/acs.chemrev.1c00683
Chem. Rev. 2022, 122, 8936−9031

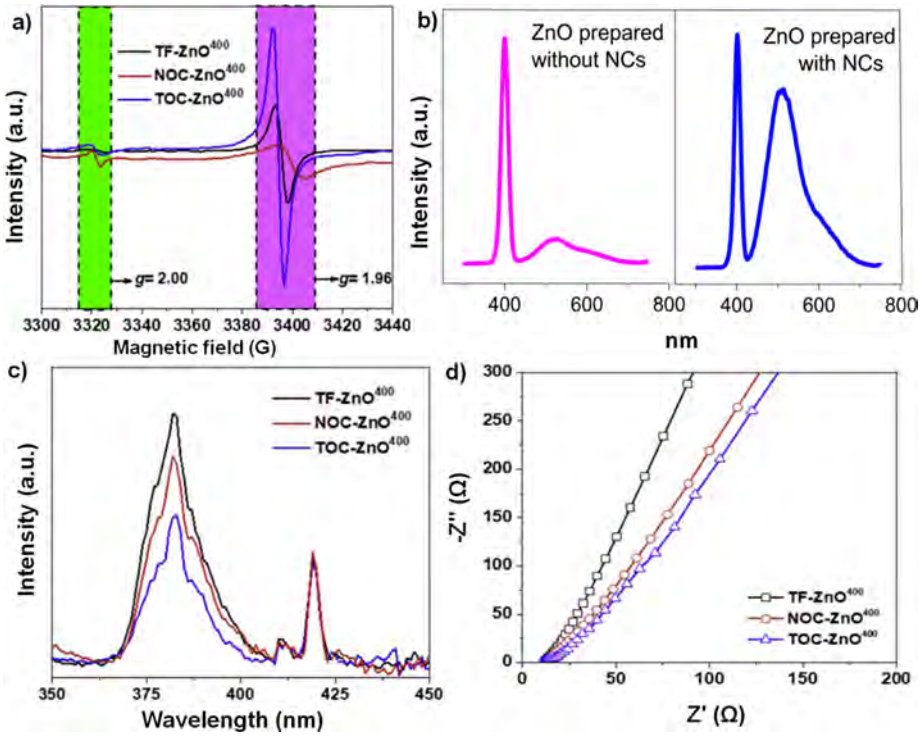

Figure 44. (a) EPR spectra, (c) PL spectra, and (d) EIS Nyquist plot of ZnO photocatalyst with NC (NOC−ZnO and TOC−ZnO) and without NC (TF−ZnO) after calcination at 400 °C. Reprinted with permission from ref 511. Copyright 2020 Elsevier. (b) PL spectra of ZnO with and without NC after calcination at 550 °C. Adapted from ref 504. Copyright 2016 NC State University.

the MOS_2-mediated dye/Cr(VI) removal efficiency. The new band peak at 817 cm^{-1} in the Raman spectrum of the recycled BC/MoS_2 shown in Figure 43d could be due to the surface passivation layer of MoO_3. However, their formation on MOS_2 clearly did not influence the overall photocatalytic performance of BC/MOS_2. The authors also measured the Mo concentration to determine whether Mo could be leached from the photocatalyst. They estimated that there was only about 0.3 wt % of loss in Mo, which was negligible. The above observations clearly suggest that NC is a suitable and stable scaffold for the fabrication of metal-oxide nanoparticle composite photocatalysts, where the NC scaffold is photostable and recyclable.

5.3.6. Characterizations to Further Understand NC-Based Photocatalytic Mechanisms. An overall fundamental photodegradation mechanism of water pollutants for a semiconductor is illustrated in Figure 34. Earlier, we discussed the radical capture experiments in Figure 41b to disclose the actual mechanisms of photoinduced ROS on pollutants mineralization. In this section, we highlight some other characterizations, which could provide further mechanistic insight into the physicochemical properties of an NC-based photocatalyst. First, electron paramagnetic resonance (EPR), also known as electron spin resonance (ESR) spectroscopy, is commonly used to understand the electron spins (unpaired electrons) of metal complexes/organic radicals. EPR spectra are useful to divulge defects/vacancies and interstitials of photocatalysts. In preceding discussions, we noticed that some of the photocatalysts have oxygen vacancy, which occurs through surface defects.[511] In addition, some nanoparticles show other defects such as interstitials. These defects have the potentiality to modify photocatalytic activities and also may play a vital role in the adsorption process, which is not well studied. However, as shown in Figure 44a, Xiao et al. found two kinds of defects in NC-templated ZnO followed by calcination at 400 °C.[511] These defects are oxygen vacancies (V_o, g = 2.00) and Zn interstitials (Zn_i, g = 1.96). According to Figure 44, the NONC−ZnO^{400} and TONC−ZnO^{400} may have higher intensities of oxygen vacancy than TF−ZnO because of the deposition of C from NC after calcination. These V_o defects/vacancies might be the reason for the lower band gap of these samples as shown in Figure 44c and d. Some reports claimed that the abundant V_o and Zn_i increased the reactive sites and boosted sufficient vacancies to increase the photocatalytic activities.[547,548] Besides tracking these properties, EPR was also used to detect photoinduced radicals in the Cu_2O/NC/cotton fiber photocatalytic system.[491] Second, photoluminescence (PL) spectroscopy is also an important tool to characterize the optical properties of NC-based photocatalysts. In Figure 44b, ZnO without NC showed two classical PL bands at 400 and 400−700 nm.[504] The first intense peak near 400 nm was due to the exciton emission. It originated from the direct recombination of the photoinduced electrons and holes of CB and VB, respectively. On the other hand, the wide emission at 400−700 nm was due to the visible emission. It came from the transformation of photoinduced electrons of CB of a given nanoparticle to their defects. This later peak was very intense in ZnO prepared with NC as compared to without NC (Figure 44b). This suggests a defective state of ZnO prepared with the NC template, which would ensure the high photocatalytic property. One can understand a low recombination rate when the PL intensity is weak. However, increasing the dopant contents and defect percentage in a catalyst can also be a reason to decrease PL intensity.[549,550] In Figure 44c, ZnO grew without NC template showed the strongest PL intensity, which was decreased in NONC- and TONC-templated ZnO after calcination at 400 °C. This could be due to the Zn- or O-defects, as well as deposited C that seemed to decrease the

https://doi.org/10.1021/acs.chemrev.1c00683
Chem. Rev. 2022, 122, 8936−9031

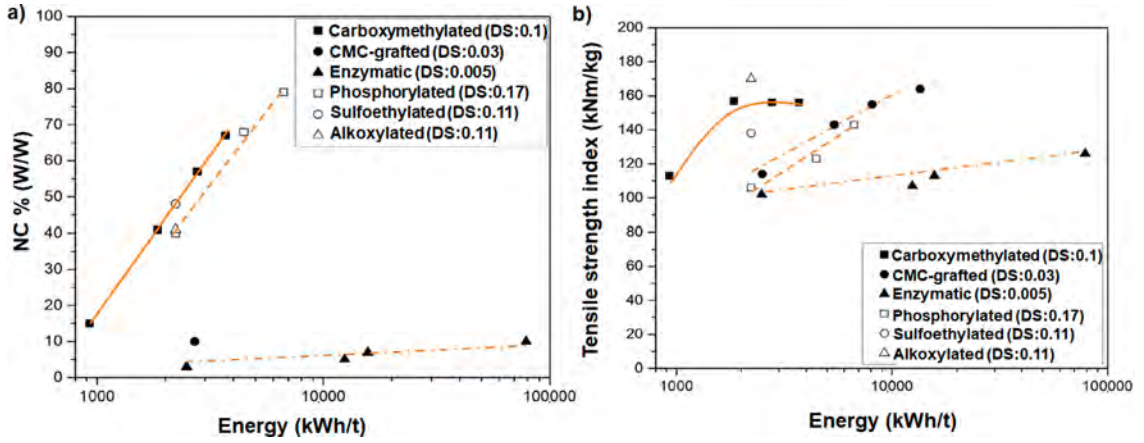

Figure 45. (a) Apparent evolution of the NC content of the various CNF materials. (b) Effects on the tensile strength of the CNF films by variously charged CNF materials versus energy of delamination during high-pressure delamination. All films were in their Na^+ form. Adapted from ref 282. Copyright 2021 Multidisciplinary Digital Publishing Institute.

recombination rates, which might be the possible reason for the increase in photocatalytic performance.[511] However, these hypotheses are not conclusive.

To understand the mechanism at a deeper level, several authors performed electron conductivity tests using the electrochemical impedance spectroscopy (EIS) method. This method can help us understand the electron transfer behavior of a photocatalyst. In Figure 44d, TONC−ZnO^{400} exhibited a lower slope of the EIS spectrum as compared to those for NONC−ZnO^{400} and TF−ZnO^{400}. It suggests TONC−ZnO^{400} could transfer photoinduced electrons more efficiently than the other two systems because of the deposited C layer on ZnO. This observation supports the PL intensity results. Typically, the C coating can absorb more light (both UV and visible), which can subsequently increase photoinduced electrons and holes. Alternatively, the doping of C in the ZnO lattice results in the formation of a new midgap/localized energy level. Because of the presence of oxygen vacancies, this new energy state locates just above the valence band of O_{2p} orbitals of ZnO. It causes a reduction of VB position. Some studies claimed that during photodegradation, C−ZnO-mediated charge generation that is fast and can be quickly transferred and devoured by reactant, and therefore, the quick utilization of surface charges thwart the charge of recombination.[551] These results clearly answer why the NC-templated photocatalysts could accelerate photodegradation of water pollutants as compared with the template-free sample.

5.4. NC-Based Membrane Filtration

There are many studies on the development and applications of NC-based membranes for wastewater treatment during the past decade,[22,337] including a perspective from our group[18] and a recent review published by Ahankari et al.[19] Several excellent reviews on the state-of-the-art of water purification membranes are also available, but they do not cover the subject of NC-based membranes.[552−554] In this section, we focus on the tailoring of the properties of NC membrane for water remediation and then provide an overview of the most important NC families for the water purification application. For water filtration, there are several critical properties of the NC membranes: (a) dry strength of the membrane, (b) wet membrane strength, (c) porosity and pore structure of membranes, and (d) suitable composite format for high flux and good selectivity performance. When it comes to their dry strength properties, CNC materials are inherently weak due to their short fibrillar length and high crystallinity, which make the resulting membrane stiff and difficult to consolidate. BNC materials are also not a great choice as they have thick microfibrils and high crystallinity, which also results in high stiffness and low porosity in the resulting membranes, not suitable for water purification.

5.4.1. Considerations of NC Membrane Fabrication.

Mechanical Strength for Handling. Several studies on the highest toughness and rigidity of CNF films have been reported, as were substantial modeling efforts made in France during the 1990s on this subject.[555,556] There are some more recent reviews on NC mechanical strength.[277,557] Lindström has proposed a reliable procedure,[112] to estimate the film/membrane strength properties based on the Page Equation.[558] As shown in Figure 45, for sufficiently delaminated CNF films, the maximum tensile strength is in the region of 160−180 N m/g, a value that can be derived from the short span strength of the pulp (from which the CNF materials were made). The extent of delamination must, however, be in the region of about 60−70% apparent content of NC (Figure 45a) to attain the maximum tensile strength. The NC content of the various CNF materials is given in Figure 45b. Interestingly, the different surface charging (except for the enzymatic CNF) and the various charge modifications are not critical. This suggests that the extent of hydrogen bonding and van der Waal forces are not seriously affected by the surface charging and charge density. The addition of counterions, however, has a significant effect on the mechanical properties of film/membrane, as they may aggregate the CNF-dispersion. In this case, the film and its mechanical properties can be greatly deteriorated, especially in the presence of multivalent counterions.[288]

Wet Strength for Operation. Cellulose films/membranes are extremely sensitive to moisture, and the films will lose their integrity when used in water filtration operations. Measuring the wet strengthening is an important characterization to determine the moisture sensitivity of the films. Many different wet-strengthening agents have been used over the years in the paper industry, such as alkaline polymeric amidoamine epichlorohydrin resins, urea-formaldehyde and melamine resins, and glyoxalated polyacrylamide resins,[559] and they can also be used to enhance the wet strength of the CNF films/membranes. Nowadays, secondary amines are the most important resins, which contain 3-hydroxy-azetidinium rings as their main

https://doi.org/10.1021/acs.chemrev.1c00683
Chem. Rev. 2022, 122, 8936−9031

Table 9. Compilation of Three Major Classes of NC-Based Membranes, Their Method of Preparation, and Their Role in Water Purification

NC type	composition	preparation method	water pollutants	rejection/reduction (%)	membrane type	ref
		CNF-based membranes				
CNF	micro/CNF grafted with zwitterionic PCysMA[a]	vacuum filtration	BSA[b]	84		602
			S. aureus[c]	86.92		
CNF	TEMPO−CNF and PVA[d] coated on PES[e] membrane	coating	BSA	75	UF	579
			E. coli[f]			
			Victoria blue	97		
			MO	6		
CNF	TEMPO−CNF grafted with PVA	casting of CNF/PVA on ePAN[g]/nonwoven PET[h] support layer	bacteriophage (MS2)	log removal values: 4	UF	603
			Cr(VI)	100 mg/g		
			Pb(II)	260 mg/g		
CNF	CNF membrane cross-linked with PAE[i]	papermaking	BSA	79.7	UF	604
			lime nanoparticles	99		
CNF	CNF and GO membrane	vacuum filtration	Victoria blue B	98.8	UF	605, 606
			methyl violet 2B	97.6		
			R6G	92.3		
CNF	tissue paper coated with ODA[j]/GA[k] modified TEMPO−CNF	coating	MO	∼99		607
			toluene	90−99		
			chloroform hexane			
			heptane			
			dicholoroethan			
			kerosene diesel			
			silicon oil			
			soybean oil			
CNF	CNF aerogel membrane cross-linked with PEI[l], decorated with Ag	freeze-drying	MB	97−99		608
			CR	96.4		
CNF	ZIF-8 in situ synthesized at CNF membrane	grafting	Janus green B	98.9		609
			MB	93.8		
			orange G	8.1		
			MO	5.8		
			bromothymol blue	1.3		
CNF	CNF and PCL[m] membrane	electrospinning	Fe	38−75	UF	596
			Cr	42−99		
CNF	TEMPO−CNF dipped coated on cellulose microfibers membrane followed by solvent exchange	coating and vacuum filtration	Ag(I)	100	UF	574
			Cu(II)	19		
			Fe(II)/Fe(III)	30		
CNF	thiol-modified CNF	infusion of modified CNF into ePAN/nonwoven PET support layer	Cr(VI)	87.5 mg/g		610
			Pb(II)	137.7 mg/g		
CNF	TEMPO−CNF on ePAN membrane	coating	silica nanoparticle	>99.8	NF	611
			oil	>99.5		
CNF	TEMPO−CNF coated with titanate-bismuth oxide	vacuum filtration	Cs(I), Sr(II), Pb(II), and anions	100	MF	612
			oil/water	>99.8		

https://doi.org/10.1021/acs.chemrev.1c00683
Chem. Rev. 2022, 122, 8936−9031

Table 9. continued

NC type	composition	preparation method	water pollutants	rejection/reduction (%)	membrane type	ref
		CNF-based membranes				
CNF	CA-NF[n] membrane	electrospinning	mineral oil	99.9		613
			kerosene	99.75		
			hexane	99.8		
			petroleum ether	99.5		
CNF	CNF fibers prepared in NMMO[o] supported on alumina (200 nm thick)	solvent casting	ferritin nano Au (10 nm)	93.8	UF	614
				82.6		
CNF	CNF fibers prepared in NMMO supported on 200 nm pore filter, performed interfacial polymerization using PEI and TMC[p]	solvent casting followed by interfacial polymerization	$MgCl_2$	89.7	NF	615
			$MgSO_4$	65.3		
			NaCl	43.6		
			Na_2SO_4	39.1		
		CNC-based membranes				
CNC	CNC incorporated with chitosan, cross-linked with GA	vacuum filtration	Victoria blue 2B	98	UF	616
			methyl violet 2B	84		
			R6G	70		
CNC	amine functionalized CNC and PES	casting	direct red 16	99		617
			Cu(II)	90		
CNC	APTES[q] modified CNC and PES	electrospinning	industrial colored compounds (COD[r])	94		618
				88		
CNC	CNC as support layer and CNC/gelatin as barrier layer	vacuum filtration	Cu(II)	36	MF	619
			Ag(I)	13		
			Fe(III)/Fe(II)	86		
CNC	CNC as support layer and CNC from BNC as barrier layer	vacuum filtration	Cu(II)	33	MF	619
			Ag(I)	14		
			Fe(III)/Fe(II)	74		
CNC	TiO_2 and CNC	vacuum filtration	hexadecane	99.60	MF	620
			soybean oil	99.48		
			pump oil	99.54		
CNC	tunicate CNC membrane	vacuum filtration	toluene	≥99.9		621
			isooctane	≥99.9		
			chloroform	93.3		
			n-hexane	≥99.9		
CNC	CNC as support layer and phosphorylated CNC as barrier layer	vacuum filtration	Cu(II)	100	MF	619
			Ag(I)	100		
			Fe(III)/Fe(II)	100		
CNC	CNC modified with BTCA[s] deposited on PVA-*co*-PE[t] nanofibrous membranes	coating	Cu(II)	95.8		622
			Pb(II)	52.1		
			Mn(II)	9.94		
			Cr(VI)	3.91		
CNC	PSF[u]/NC/Ag/Pt as a supporting layer for TFC polyamide membrane	NIPS[v] process	microorganism	67−80	FO	583
			wastewater			
			urea			

https://doi.org/10.1021/acs.chemrev.1c00683
Chem. Rev. 2022, 122, 8936−9031

Table 9. continued

NC type	composition	preparation method	water pollutants	rejection/reduction (%)	membrane type	ref
		BNC-based membranes				
BNC	cultivation of BNC followed by cross-linking with PMPC[w]	cultivation of BNC membrane followed by cross-linking	*S. aureus*	log CFU reduction		623
			E. coli	4.3		
			MB	1.8		
			MO	4.4 mg/g		
				4.6 mg/g		
BNC	BNC membrane and Ag nanoparticle	vacuum filtration	R6G	99		624
			MO	≥80		
			4-nitro phenol	90−100		
BNC	Pd/GO/BNC membrane	GO blending with BNC network and in situ growth of Pd nanoparticle	MO	>99	UF	625
			4-nitro phenol			
			MB			
			R6G			
BNC	BNC-MoS_2 aerogel membrane	cultivation of BNC membrane followed by growth of MoS_2 by hydrothermal process	MB	96		545
			Cr(VI)	88		
BNC	BNC embedded with mesoporous PDA[x] and decorated with Pd nanoparticle	cultivation of BNC membrane followed by in situ incorporation of mPDA followed by in situ Pd growth	MO	>99	UF	626
			4-nitro phenol			
			MB			
BNC	PDA and BNC membrane	cultivation of BNC membrane and in situ deposition of PDA	R6G	4.3 g/m^2	UF	627
			MB	3.8 g/m^2		
			Pb(II)	5.3 g/m^2		
			Cd(II)	2.1 g/m^2		
BNC	TiO_2/PDA on BNC membrane	coating of TiO_2/PDA	MO	95.1		628
			MB	100		
			rhodamine B	99.5		
BNC	silane modified BNC aerogel membrane	conventional drying	*n*-hexane	99.6		629
			hexadecane	98.3		
			kerosene	99.4		
			petroleum ether	99.8		

[a]Poly(cysteine methacrylate). [b]Bovine serum albumin. [c]*Staphylococcus aureus*. [d]Poly(vinyl alcohol). [e]Poly(ether sulfone). [f]*Escherichia coli*. [g]Electrospun polyacrylonitrile. [h]Polyethylene terephthalate. [i]Polyamide-amine-epichlorohydrin. [j]Octadecylamine. [k]Glutaraldehyde. [l]Poly(ethylene imine). [m]Polycaprolactone. [n]Cellulose acetate nanofibers. [o]*N*-methylmorpholine n-oxide. [p]Trimesoyl chloride. [q]3-Aminopropyl)triethoxysilane. [r]Chemical oxygen demand. [s]1,2,3,4-Butanetetracarboxylic acid, [t]Poly(vinyl alcohol-*co*-ethylene, [u]Polysulfone. [v]Nonsolvent induced phase separation, [w]Poly(2-methacryloyloxyethyl phosphorylcholine). [x]Polydopamine.

https://doi.org/10.1021/acs.chemrev.1c00683
Chem. Rev. 2022, 122, 8936−9031

reactive group,[560] to improve the properties of CNF films.[561] TOCNF can also be wet-strengthened by drying at high temperatures, where the aldehyde groups on TOCNF can form cross-linking reaction. In addition, the citric acid treatment has been demonstrated to improve the wet-strength and reduce the pore size for films made of *Cladophora* nanofibers.[562] The addition of multivalent counterions is another effective approach to control the cross-linking of TOCNF by electrostatic interactions. There are two ways to accomplish this: (a) the multivalent counterion can be added to the CNF suspension and control the gelation and property during the formation of the membrane or (b) initiate the cross-linking reaction through membrane post-treatment. Both methods can radically change the wet strength, but also the permeability and porosity of the membrane.[285] A more extensive discussion can be found in our previous review.[18]

Membrane Porosity. Porosity and pore size distributions are two essential parameters to control the performance of filtration membranes. For NC membranes, the pore size can be governed by the diameter (thickness) and shape of the nanofiber. For example, some wood-derived CNF and BNC membranes have shown higher permeances as compared to TOCNF and CNC membranes.[563] This difference could be attributed to the fiber diameter, where BNC and wood-derived CNF consisted of larger diameters than those of TOCNF and CNC. In general, the smaller diameter nanofibrils could accommodate more in per unit mass, which would increase the number of pores and decrease the average pore diameter. It has been shown that BNC with a large diameter resulted in a bigger pore size in nanopapers.[564] Therefore, one can control the membrane permeance by selecting the appropriate NC type. In addition, the crystallinity and swelling of the nanofibers will determine their bending by capillary forces, thus affecting the consolidation phase during drying. A good correlation has been observed among the mean pore size, maximum pore size and mean fiber diameter in a nonwoven nanofibrous framework of optimal filtration performance.[565] Zhang used computational modeling to confirm the structure−property relationship in nonwoven membranes.[566] It was observed that the diameter of a cylindrical fiber could directly affect the pore size of a packed fibrous network. However, this relationship may not be applicable for swollen CNF materials because of the flexible nature of CNF that may turn and bend the membrane during the action of capillary forces. Under normal conditions, the capillary forces between the nanofibers can be very strong, even down to the nanometers scale.[567] There are therefore important ramifications of the role of capillary forces interconnected with the membrane's thickness and the rate of drying. Sometimes, air percolation will occur in the course of drying thin nanofilms and can block the capillary forces and create a porous film. Thicker films are generally not permissible for air percolation to block the capillary forces, thus consolidation under such conditions can render the membrane to become nonporous.[568] In the fabrication of thicker CNF membranes, it has been shown that there could be a surface structure gradient along with the thickness.[569] The membrane thickness has a profound effect on the filtration performance (flux and rejection). The film thickness often can be controlled by the CNF concentration. Figure S10 illustrates the filtration flux and rejection of bovine serum albumin (BSA) for TOCNF membranes as a function of CNF concentration. It was found that the optimal filtration performance against BSA was found for the film prepared near the overlap concentration of CNF suspension.[570]

There are several other ways to control the membrane porosity. One is by the drying conditions. For example, during high-temperature drying, a slow drying rate usually consolidates the film more and creates a lower porosity, whereas fast drying can rapidly evaporate the water and block the capillary forces, leading to a higher porosity.[571] Also, the CNF-film can be incorporated with nanostructured materials that have suitable porous structures to enhance the total pore characteristics of the composite membrane.[572] The solvent exchange method is another method to create a greater porosity in the resulting membrane.[13,278,573−576] In this approach, various solvents have been tested including methanol, acetone, ethanol, etc. Basically, these solvents can reduce the adhesion forces between the fibrils and decrease the capillary forces. Additional useful methods to enhance the membrane porosity include supercritical drying and freeze-drying methods.[13,575] It should be noted that, when the porosity of the membranes is increased, the mechanical strength typically decreases. These factors should be considered carefully as a whole.

5.4.2. NC Membranes for Water Filtration. Current studies on NC-based membranes indicates that NC is an excellent building block material for the design and fabrication of almost all types of filtration membranes, such as (a) pressure-driven membranes for microfiltration (MF),[577,578] UF,[579] nanofiltration (NF),[580] and RO,[581,582] (b) concentration-driven membranes (ΔC) for forward osmosis (FO),[583] (c) temperature-driven membranes (ΔT) for membrane distillation (MD),[584] and (d) electric-driven membranes (ΔE) for electrolysis.[585,586] In these membranes, the separation performance is closely related to the structural and physical properties such as pore size, porosity, pore size distribution, tortuosity thickness, composition, hydrophobicity/hydrophilicity, and surface charge characteristics of the CNF either as a barrier layer or as a support. The manufacturing of these NC-based membranes under laboratory conditions is not complicated and can use conventional paper technology style equipment with proper modifications. However, the true upscaling of NC-based membranes for water filtration has not yet been demonstrated. Vacuum filtration of dilute CNF-dispersions, followed by drying, is probably the most popular method,[587,588] where laboratory papermaking equipment, such as Rapid−Köthen sheet former,[589] or the dynamic sheet forming equipment (e.g., Formette Dynamique[590]) can be used for this purpose. In fact, a simpler procedure by use of a Petri-dish and room temperature drying has been adopted in some studies.[569] Hot-pressing has also been employed by many groups,[591] using the high-temperature drying method that is commonly used to produce thick BNC films (with *Cladophora* fibers).[24] The casting of NC suspension can produce a barrier layer on the nonwoven substrates (e.g., electrospun mats) or porous supports (e.g., membranes made by phase inversion) for UF applications,[592] or as a support layer to host interfacially polymerized polyamide selective layers for NF/RO applications.[593,594] Detailed summary of these membranes has been given in an earlier review.[595] In Table 9, we compile some important NC-based membranes regarding three major classes (CNF, CNC, and BC), their preparation methods, and their role in tackling the multiple contaminants for water filtration. The key features of these three classes NC-based membranes are as follows.

CNF-Based Membranes. Using CNF as the barrier layer, our group has developed a new type of thin film nanofibrous composite (TFNC) membranes, as opposed to the conventional thin film composite (TFC) membranes, for high flux UF

https://doi.org/10.1021/acs.chemrev.1c00683
Chem. Rev. 2022, 122, 8936−9031

applications. The format of TFNC is shown in Supporting Information (Figure S11), where such a membrane contains a three-layered structure: (a) a nonwoven substrate of micrometer-size fibers to provide mechanical strength of the membrane, (b) a nonwoven middle layer support having submicrometer fibers, typically fabricated by electrospinning, and (c) a top CNF barrier layer to provide the filtration performance. There are several advantages to using this three-layered configuration for membrane design, including very high permeate flux because of the high porosity (~80%) in the electrospun support layer (e.g., polyacrylonitrile (PAN) electrospun nanofiber layer), and antifouling property of the CNF layer due to the hydrophilic and highly charged surface. The electrospinning technology for the production of polymeric nanofibrous membranes for filtration has been well established,[596] and this subject has also been reviewed recently.[597] The incorporation of CNF to form an interconnected fibrous network in the polymer nanocomposite barrier layer can introduce directional water passages, created at the interface between CNF and the polymer matrix, to facilitate the water transportation and enhance the permeate flux.[598,599] For example, using TOCNF thin film as a support layer to host the interfacial polymerization of polyamide (PA) on the membrane surface, the reaction can generate a thin CNF/PA nanocomposite barrier layer enabling the fabrication of a new type of TFNC membrane for NF/RO applications.[600] The flux performance of such a membrane can be fine-tuned by controlling the barrier layer thickness. As seen in Figure 46,

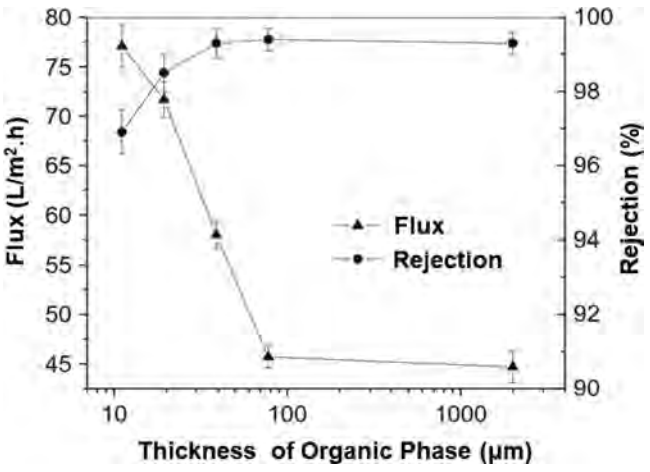

Figure 46. Effect of the thickness of organic phase on the membrane water flux and $MgSO_4$ rejection (2000 ppm). Reprinted with permission from ref 601. Copyright 2014 Elsevier.

the flux performance of an NF membrane having the CNF/PA nanocomposite barrier layer was controlled by the available thickness of the organic phase for interfacial polymerization. The performance of the optimized membrane exhibited the flux of 71.7 $L/m^2 \cdot h$ and rejection ratio (against 2000 ppm $MgSO_4$) of 98.5%, which were slightly superior to commercial NF membranes.[601]

In the Supporting Information (Table S3), it was noted that the CNF layer, whether it was used as a barrier layer for UF or FO applications, or as a support layer for NF and RO applications, had to be thin and uniform. To accomplish this feature, one can take advantage of the gelation behavior of CNF suspension in acidic conditions. In specific, a dilute CNF suspension can be uniformly coated (by using the knife-coating or spray-coating method)[630] on an electrospun support layer that was infused with an acid solution. The interaction between the CNF suspension (in the sol state) and the acid solution will form a thin and uniform gel of controllable thickness, as well as prevent the leakage of CNF suspension into the electrospun scaffold. The subsequent drying process can result in a uniform coating of a thin CNF barrier/support layer.

For MF applications, the infusion of CNF (which has cross-section dimensions of 2−10 nm and up to a few micrometers in length) into a fibrous scaffold of larger fiber diameters is an effective way to fine-tune the pore size of the membrane without significantly changing the porosity. The loading of CNF can be used to alter the mean pore size and the pressure drop of the membrane as well as to provide the adsorption capability due to the surface charge. For UF applications, the use of CNF as a barrier layer in composite format can also provide an additional advantage, that is, the low fouling tendency due to the hydrophilicity and charging nature of CNF. Some examples of the CNF-based membranes for MF applications are as follows. A composite nanofibrous membrane produced by infusing CNF into an electrospun PAN/nonwoven PET substrate exhibited a reduction in mean flow pore size from 0.66 to 0.32 μm. The resulting membrane enabled the retention of bacteriophage (MS2) with a logarithmic reduction value (LRV) of 4, as well as the removal capability against Cr(VI) and Pb(II) ions with the efficiency of 100 and 260 mg/g, respectively.[603] Such a strategy was also used to incorporate varying inorganic metal nanoparticles, such as Ag,[608] into CNF-based membranes, rendering the system to exhibit both photocatalytic and separation capabilities. For example, a CNF membrane cross-linked with PEI followed by the infusion of Ag nanoparticles showed continuous catalytic discoloration capability for both aqueous cationic and anionic dye molecules. The discoloration efficiency of this membrane was 98% even after 10 times reuse, while maintaining the water permeance of 5×10^4 $L/m^2 \cdot h$ (LMH).[608] In addition, the fabrication of the composite membranes with ultrathin GO coating on CNF, exhibited a significantly high water flux of 18123 ± 574 LMH/bar with the capability to remove both anionic and cationic dyes (removal capacity of 92−97%). The creation of nanochannels in the CNF/GO nanocomposite membrane due to the anisotropic layered arrangement of GO has enhanced its performance through the combination of electrostatic and hydrophobic interactions, as well as the size exclusion factors.[605] Song et al. demonstrated the in situ synthesis of ZIF-8 in the CNF scaffold, where ZIF-8 acted as a spacer and could successfully wrap around CNF due to their strong interaction. The effective anchoring of ZIF-8 in the CNF scaffold allowed the flux to be maintained at 85−92 LMH for 24 h and for the high selectivity for removal of cationic dyes among the multiple dye impurities.[609]

Some research groups have used the electrospinning method to prepare CNF-based nanocomposite membranes with control pore size and porosity for the removal of dye molecules.[618,631] For example, tissue paper when coated with TOCNF modified with octadecylamine/glutaraldehyde exhibited 99% of MO removal and showed 90−99% of efficiency to separate solvent and water mixture.[607] When TOCNF was coated on the electrospun PAN scaffold, the resulting NF membrane exhibited the removal efficiency >99.8% for silica nanoparticles, and >99.5% of oil recovery.[611] However, when TOCNF membrane was coated with titanate-bismuth oxide, the membrane showed 100% removal efficiency for Cs(I), Sr(II), Pb(II), and some anions, as well as >99.8% of oil recovery, indicating its capability

https://doi.org/10.1021/acs.chemrev.1c00683
Chem. Rev. 2022, 122, 8936−9031

to handle multiple water impurities.[612] The modification of CNF with amino functionality is another way to improve the performance of the membranes. The amino group at low pH appeared as the positively charged group, useful to trap negatively charged metal ions. With thiol-modified CNF, when infused into the electrospun PAN support layer, the resulting membrane exhibited high adsorption capacities for both Cr(VI) and Pb(II) with a maximum removal efficiency of 87.5 and 137.7 mg/g, respectively, because of the large surface area and high concentration of thiol groups (0.9 mmol of −SH/g of CNF).[610] Zhang et al.[614] demonstrated that the self-standing CNF membrane cast on alumina support exhibited the ultrafiltration capability for ferritin and Au nanoparticle with the removal efficiency between 82% and 93%. Such membranes have been modified by Soyekwo et al. into NF membranes by interfacial polymerization of poly(ether imide) and trimesoyl chloride. This process created interconnected nanochannels, responsible for the transport of water molecules. The resulting membrane with a thickness of 77 nm with a mean pore size of ∼0.45 nm exhibited a water flux of 32.7 LMH/bar, which is an order of magnitude higher than the reported values by similar NF membranes. Such membranes also showed the capability to remove a range of salt ions (i.e., $MgCl_2$, $MgSO_4$, NaCl, Na_2SO_4, etc.) with the removal efficiency between 39 and 89%.[615]

Cladophora-Based Membranes. Mihranyan and his group have carried out extensive investigations of UF membranes (or nanofilters) for virus removal. They used highly crystalline *Cladophora* algae (FMC Biopolymer) and fabricated membranes with papermaking techniques. Because of the high crystallinity (95%) and high thickness in *Cladophora* NC microfibrils (10−30 nm), the membrane exhibited a high porosity (∼40%) when not fully consolidated. As a result, the adhesion between the microfibrils was relatively weak in the membrane.[632] To gain some membrane strength, the membrane was subsequently dried under load using a heat-press and resulted in a flat sheet.[633,634] Because of its low strength (especially the weak wet-strength), the group cross-linked the microfibrils using citric acid and sodium-hypophosphite (catalyst) at high temperature in the hot press. The resulting membrane exhibited very good wet strength but was still harmed by the brittleness in the dry state (Figure 47).[562] The group also

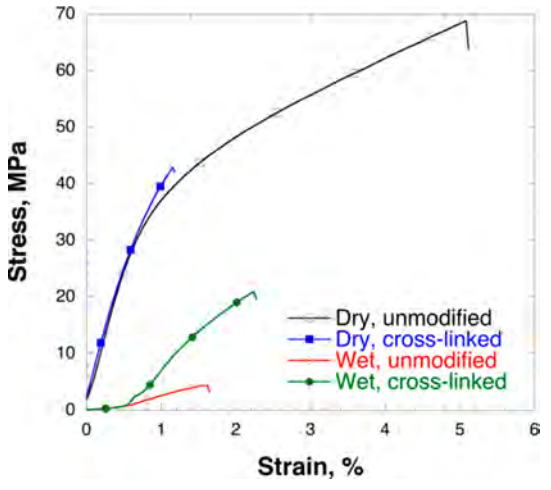

Figure 47. Typical stress vs strain for the dry and wet *Cladophora*-based membranes. Reprinted with permission from ref 562. Copyright 2015 American Chemical Society.

investigated the method to tailor the pore-size distribution,[571] by changing the thickness of the membrane.[635] A summary of the properties of these membranes, dried at different temperatures, is illustrated in Supporting Information (Figure S12). These membranes exhibited a pore size between 10 and 25 nm, surface area in the range of 70−100 m^2/g and porosity between 35% and 42%. The flux of these membranes at varying thicknesses and pore size distributions measured by the nitrogen gas isotherm (Barret−Joyner−Halenda method) are shown in Supporting Information (Figure S13). It was seen that the flux decreased with the increasing basis weight of the membrane, where the corresponding pore size distribution also became smaller. On the basis of these investigations, one can tailor the pore size distribution and the filtration performance of such membranes by careful selection of the algae nanofiber with different diameters and membrane thickness.

CNC-Based Membranes. Mathew and her group have made extensive efforts on the fabrication of CNF and CNC membranes using microfiber sludge from a sulfite mill in northern Sweden (Domsjö mill). CNC materials have poor mechanical strength and poor wet-strength, but the membranes can be reinforced using various composite mixtures, such as chitosan/CNC,[616,636] multiple NC components, such as CNF/CNC,[574,637] and other combinations.[619] Other groups also used a similar approach to enhance the properties of CNC membranes, such as infusion of TEMPO CNC into electrospun cellulose acetate scaffolds[638] or mixing of chitin nanocrystals.[639] A different group coated CNC and CNF onto a poly(ether sulfone) (PES) membrane and reported that the CNC coating layer could result in better antifouling properties than coating the CNF later due to the higher charge density in CNC.[640] A self-cleanable TiO_2/tunicate CNC membrane was fabricated by Zhan et al. using the vacuum filtration method for oil/water separation.[620] As seen in Figure 48, while the composite membranes generally exhibited good retention of varying oils, the UV-light irradiation significantly enhanced the permeation flux of the cross-linked membranes. The mechanism of the cross-linking reaction was offered. Upon UV light irradiation, the redox reaction can take place in Ti(IV) and O^{2-}, which would lead to the production of oxygen vacancies. These vacancies can react with water molecules and generate more adsorbed OH groups, thus making the CNC surface more hydrophilic with better antifouling properties.[641]

In the study of Mathew et al., the CNC/Chitosan nanocomposite membrane with a mean pore size of 10−13 nm was prepared by freeze-drying followed by compacting and cross-linking with glutaraldehyde. The membrane showed excellent removal efficiency of 98%, 84%, and 70% for Victoria Blue 2B, MV-2B and R6G, respectively, after a contact time of 24 h with a constant water flux of 64 LMH.[616] In the system based on the infusion of TOCNC in electrospun PAN scaffold, the resulting membrane exhibited effective removal of *E. coli* with LRV of 6, while the CNC infusion was also found to decrease the mean pore size of the membrane from 0.38 μm (without CNC) to 0.22 μm.[577] In the system containing infused CNC in the cellulose acetate scaffold, the composite membrane exhibited 89.92% removal of BSA with a water flux of 174 LMH.[642] In a separate system, a composite poly(vinylidene fluoride) (PVDF) membrane containing CNC was prepared by the phase inversion method and showed 92.5% removal of BSA with water flux of 230.8 LMH at 1.1 kPa.[643] In addition, the coating of modified CNC with 1,2,3,4-butanetetracarboxylic acid on the PVA-*co*-PE membrane was found to increase the adsorption

https://doi.org/10.1021/acs.chemrev.1c00683
Chem. Rev. 2022, 122, 8936−9031

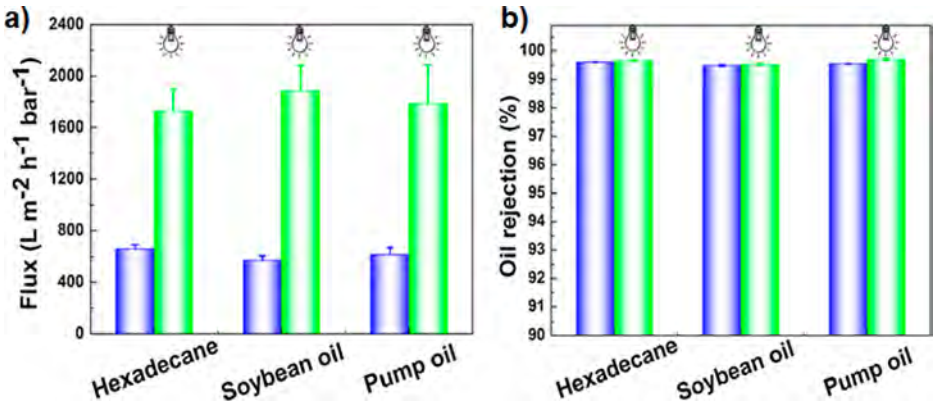

Figure 48. (a) Water fluxing and (b) oil rejection ratio of a self-cleanable TiO_2/tunicate CNC membrane for oil/water separation without and with UV cross-linking. Reprinted with permission from ref 620. Copyright 2018 Elsevier.

capability of the membrane for removal of multimetal ions, including Cu(II), Pb(II), Mn(II), and Cr(VI) ions, due to the higher negative charge on the membrane surface.[622]

CNC-based composite membranes containing Ag and Pt nanoparticles as additives have also been demonstrated in TFC format for FO filtration.[583] The fabrication of the CNC upper layer was accomplished by the nonsolvent induced phase separation technique, where the resulting membrane exhibited a diverse pore distribution with finger-like morphology. Interestingly, higher water flux of 11.5−11.8 MPH/bar and 3- to 8-fold improvement in bacteria reduction were observed when used to treat wastewater. In addition, the membrane was tested to treat urea and microorganism contaminated water, where it exhibited both improved electrochemical and antimicrobial properties.[583] It is known that the amino group at the low pH value is positively charged, which is useful to trap negatively charged metal ions. On the basis of this, amine-functionalized CNC was cast into the PES membrane, where the resulting system was able to remove the Cu(II) impurities with a removal efficiency of 90%.[617] Moreover, the addition of inorganic fillers, such as TiO_2, GO, titanate-bismuth oxide, silane, etc., has also been demonstrated to prepare NC-based membranes for separation of oil/water mixture. For example, TiO_2/CNC composite membrane showed the nanoporous morphology with super hydrophilic and underwater oleophobic property, resulting in effective separation of various surfactant-stabilized emulsions, including hexadecane/water, soybean oil/water, and pump oil/water with removal efficiency higher than >99.5%. These membranes showed even higher efficiency in the presence of UV-light irradiation.[612]

BC-Based Membranes. BC is produced from microorganisms, such as the genus *Gluconacterbacter*. Such NC is often synthesized into a gel body in planar form (pellicles/fleeces), following the same dimension as their cultivated reactor. BC can be manufactured into complex 3D shapes with various templates.[644] However, there are relatively fewer studies of using BC membranes for water remediation,[22,645−647] than those of CNF and CNC membranes. A recent review, including both bacterial and *Cladophora* nanopapers, was published.[648] This review can serve as a good reference for the subject of water purification. Interestingly, the use of BC membranes for water purification was investigated by two groups: one used BC-composites[649] and the other used regenerated BC.[650] The dimension of BC's cross sections is typically in the range of 20−100 nm, and this cross-section is inherently porous. The BC hydrogel pellicles after manufacture are difficult to disperse. Although the physicochemical properties of BC materials are attractive, their usage is often hindered by their propensity to aggregate because of the long length of the microfibrils enabling strong interfibrillar van der Waals-forces and hydrogen bonding interactions. Cutting the microfibrils can be one way to improve the dispersion of BC.[651] Inspired by the dispersion of CNT and nanowires using organic solvents of different surface energies, it was found that the optimal dispersion of BC could be achieved by using the solvent with a surface energy of 70 mJ/m^2 (see Figure S14: higher BC concentration indicates higher dispersion). Mautner and Bismarck also investigated the procedure of dispersing BC with several different solvents (acetone, tetrahydrofuran and ethanol) and fabricated NC membranes with basis weights between 15 and 85 g/m^2. These solvent-treated BC membranes are suitable for UF applications with over 40 times higher permeance than that of untreated BC membranes. These membranes' nanofibril diameter, mean pore size and specific area are shown in Table 10.[648]

Table 10. Summary of Nanofibril Diameter (from SEM), Average Pore Size, and Specific Area (Determined by N_2 Adsorption/Desorption Experiments) for Various BC Membranes Treated with Different Solvents[648]

material	fibril diameter (nm)	average pore size (nm)	specific surface area (m^2/g)
BC	56 ± 16	14.3 ± 1.1	22.8 ± 2.5
BC−ethanol	61 ± 17	15.3 ± 0.4	117 ± 7
BC−acetone	54 ± 15	18.4 ± 2.3	110 ± 13
BC−tetrahydrofuran	57 ± 15	17.6 ± 0.6	107 ± 1

The incorporation of inorganic nanoparticles, such as Pd,[626] TiO_2,[628] GO,[625] MoS_2, and SiO_2,[629] in the BC membrane could enhance the separation performance of the composite membrane, which would simultaneously adsorb and photocatalytically reduce the impurities by light irradiation. For example, a BC membrane cross-linked with polydopamine (PDA), BC/PDA, exhibited good filtration capability to remove R6G, MB and MO dyes. The integration of Pd nanoparticles into BNC/PDA further demonstrated the ability to reduce 4-nitrophenol (4-NP), while maintaining the high adsorption capability (93−99%) for MO and MB. Similarly, when TiO_2 nanoparticles were added to BNC/PDA, the composite membrane exhibited relatively fast photocatalytic degradation of MB, MO and RB within 60 min, having efficiencies between

https://doi.org/10.1021/acs.chemrev.1c00683
Chem. Rev. 2022, 122, 8936−9031

95% and 100%.[628] In addition, the mixing of GO into the BC network, followed by in situ growth of Pd nanoparticles produced a composite membrane system with capillary channels between the lamellar structure, where the resulting Pd/GO/BC membrane exhibited the fast and effective removal of MO with an efficiency of 99.3%, as well as the removal of a mixture containing 4-NP, MB and R6G with efficiency >99% while maintaining a stable flux of 33.1 LMH at 58 psi.[625] The addition of MoS_2 particle in a BC aerogel UF membrane could also introduce the photocatalytic degradation capability. It was noted that the embedded MoS_2 particles had the porous morphology and good photocatalytic activation ability allowing for the fast (within 120 min) and efficient removal of Cr(VI) with a capacity of 88% and removal of MB with a capability of 96%. The BC/MoS_2 membrane demonstrated in this study also exhibited good recyclability and high photostability.[545] Furthermore, the composite membrane based on BC incorporated with SiO_2 three-dimensional porous additives also showed good efficiencies for removal of several solvents, including *n*-hexane, hexadecane, kerosene, and petroleum, where the efficiencies were in the range of 98.3−99.8%, and the flux was also high (34000 ± 50 LMH/MPa).[629]

To remove organic, inorganic and biological pollutants from water, Singamaneni et al. published several research articles investigating the feasibility of using BC to develop biodegradable membranes.[584,626,627,652] In one study, they fabricated an interesting BC-based bilayer photothermal membrane, consisting of PDA, for solar-enabled photothermal membrane distillation (PMD) application.[584] As shown in the Supporting Information (Figure S15), the top photothermal layer consisted of light-absorbing PDA particles interlocked with BC, which was functionalized with tridecafluoro-1,1,2,2-tetrahydrooctyl)-trichlorosilane (FTCS) to make the membrane more hydrophobic. The bottom layer was made by porous BC, which can insulate heat as well as permeate vapor efficiently. One advantage of using the BC layer is that one can keep the membrane thickness thin (<300 μm), which was necessary for membrane distillation. The observed permeation flux values were 1.0 and 9.4 kg/m^2·h using 1.0 and 9.0 light power density (sun), respectively, even though their solar efficiency was nearly the same (i.e., the solar energy-to-collected water (SE/CW) efficiency was 68%). Such performance could be attributed to the membrane having very high light absorption (nearly 98%) and porosity (93%). The demonstrated FTCS-PDA/BC membrane exhibited high salt rejection rate >99.9% and excellent membrane stability (e.g., consistent performance of contact angle, permeation flux and salts rejection ratio) over five cycles of operation. The group also tested the chemical and mechanical stability of FTCS-PDA/BC membranes at acidic (pH 3.0), basic (pH 10.0) and neutral water under 30 days vigorous shaking. No leaching of PDA particles was observed, which could be explained by the strong entanglement in the BC fibrillar network. This very stable membrane system provides the pathway to overcome the environmental concerns of materials leaching during the operation.

5.4.3. Low Fouling Tendency of NC-Based Membranes. Membrane fouling is a phenomenon that occurs when a large number of pollutants, such as bacteria, biomacromolecules, colloids, salts, particles, other synthetic and biological molecules (e.g., proteins), start to accumulate on the membrane surface or internal pores. Because of its negative effects on water filtration, there are extensive publications and reviews dealing with this topic.[553,653−658] However, the information on antifouling strategies for NC-based membranes is still incomplete. There are several different types of membrane fouling, where the most critical one is the formation of biofilms. Membrane biofouling is when different types of biomacromolecules, such as carbohydrates, proteins, and cells, are colonized on the membrane surface. Extracellular polymeric secretions by microalgae, bacteria, and fungi can also cause microfouling issues. To alleviate these problems, several membrane systems have been demonstrated, in particular, the FTCS-PDA/BC membrane system.[584] This membrane exhibited a very good ability to destroy bacteria under sunlight through the interfacial photothermal disinfection mechanism. The mechanism not only decreases the tendency of biofouling but also disinfects wastewater. As shown in Figure 49, the fluorescence live/dead

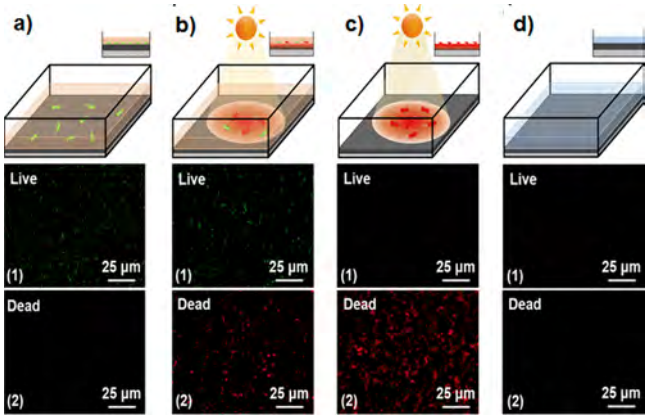

Figure 49. Fluorescence images of interfacial photothermal disinfection on FTCS-PDA/BC membrane surface. (a) Feeding of *E. coli* contaminated water to the membrane for an hour. (b) After exposure to the PMD operation, the membrane in the presence of *E. coli* contaminated feedwater was irradiated under sunlight for 60 min. (c) After exposure to PMD operation, the membrane was directly irradiated under sunlight for 10 min without feedwater. (d) After cleaning the membrane in (c) with deionized water. Panel 1 shows live bacteria; panel 2 reveals dead bacteria after the light exposure. Reprinted with permission from ref 584. Copyright 2021 Elsevier.

staining images showed that some dead bacteria (*E. coli*) were present on the membrane, when the membrane immersed in the *E. coli* contaminated feedwater was under one sun irradiation for 60 min. When the *E. coli* contaminated feedwater was decanted, the bacteria on the membrane surface were almost 100% dead under one sun irradiation for 10 min. These differences might be due to the different local temperatures near the membrane surface, that is, 33 °C (in feedwater) and 78 °C (without feedwater) under light illumination.

Generally, the aggregation of colloids through flocculation/coagulation is the most effective way to decrease the fouling tendency on the membrane surface. However, studies of this subject are usually empirical in nature because the system can be very complex. Let us start with the nature of the membrane surface regarding hydrophobicity. Most commercial membranes are hydrophobic, but there are also cellulose-based membranes, such as cellulose acetate, which are less hydrophobic. There is a consensus in the literature that hydrophobic surfaces will adsorb proteins and bacteria through hydrophobic interaction. Thus, surface modification of the membrane to make it more hydrophilic has become an important antifouling strategy. NC is hydrophilic, and this feature enables NC-based membranes to possess lower fouling tendency. In addition, if NC is charged, for

https://doi.org/10.1021/acs.chemrev.1c00683
Chem. Rev. 2022, 122, 8936−9031

example, TOCNF, the repulsion forces between the membrane surface and colloids of the same charge can create a barrier to further reduce the fouling tendency. This strategy has been adopted by our group for the application of TFNC membranes.[659−661] For example, TOCNF which has carboxylate functional group when coated as a barrier layer on the electrospun PAN support layer enabled the TFNC membrane to be able to achieve 97% removal of BSA—a model protein foulant.[661] This was also seen in another study, where the coating of TOCNF and PVA on a PES membrane showed good affinity for positively charged dyes but also with good antifouling properties. The individual filtration test showed 97% removal of Victoria blue, 6% removal of MO, and 75% removal of BSA.[579] Notably, the TOCNF coating provided a hydrophilic charged surface responsible for the removal of cationic dye and BSA. Poly(ethylene glycol) (PEG) has also shown a strong ability to thwart protein adsorption and cell adhesion due to its abundant oxy-functionalities.[662] Other hydrophilic polymers which have hydrogen bonding capability with water may also decrease the adsorption of proteins and cells to some extent. However, the foremost antifouling ability of any polymers strongly depends on their steric repulsions and surface hydration combined. In this regard, NC has the advantage of being easy to modify in many different ways.

There are several antifouling treatments that have been extensively investigated and they include two important classes of polymers: zwitterionic and hydrophilic polymers as shown in Figure 50. Common hydrophilic polymers, such as PA, PEG,

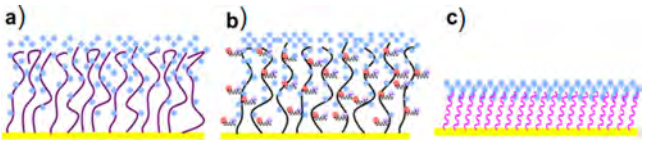

Figure 50. Schematic illustration of (a) hydrophilic, (b) zwitterionic, and (c) self-healing polymer-based materials showing their chain flexibility and chain hydration properties. These features could inhibit the nonspecific adsorption of different proteins due to surface resistance. Reprinted with permission from ref 653. Copyright 2010 Elsevier.

and polysaccharides are good examples for low-fouling coating materials as discussed above. These polymers share some common chemical features, that is, ability to form hydrogen bonds with water molecules (Figure 50a).[653] There are various ways to attach these polymers to the membrane surface, including plasma modification,[663] radiation grafting and surface coating,[664,665] as well as atom transfer radical polymerization (ATRP).[666] Zwitterionic polymers have also been known as low-fouling materials for polymer membranes. Some examples include 2-methacryloyloxylethyl phosphorylcholine-based,[667] sulfobetain-based,[668] and carboxybetain.[669] Recently, poly(cysteine methacrylate) was surface-grafted on NC by free-radical polymerization, where the coating of this modified NC on the membrane surface yielded excellent antifouling and antibacterial properties.[602] There are other examples of using zwitterionic materials to modify NC,[670] electrospun nanofibers,[671] and CNC,[672] to improve antifouling properties of varying membranes, such as PDVF,[673] and commercial cellulose membranes.[674] The use of zwitterionic polymers to prevent adsorption of proteins is a well-known strategy to reduce fouling, based on the ability of charge-neutral zwitterionic moieties to attract water, forming a hydration layer that thwarts the proteins adsorption (Figure 50b).[675−677] Self-assembled monolayers in Figure 50c are zwitterionic transplanted from the membrane surface through surface-initiated ATRP reaction by dip coating method or plasmas treatments.[653,678] It is known that micro/nanostructured surfaces also can reduce fouling and inactivate bacterial cells by physical means;[679] however, this topic is not included in this review.

6. RESEARCH GAPS AND PERSPECTIVES

In this section, we outline the research gaps, unsolved questions, and issues challenging us regarding the applications of NC for sustainable water purification, and also offer our perspective to overcome these challenges in the respective areas.

6.1. Low-Cost NC Production and Scalability Issues

Currently, NC can be produced on large scale (i.e., tons capacity per day) in many facilities in the USA, Canada, Sweden, Japan, etc. However, there is still a need to reduce the production cost of CNF and CNC materials for broader societal impacts. To achieve this goal, low-cost NC production may be possible by using nonwoody biomass feedstocks and thereby bypassing some treatment steps (such as pulping), as in the NOP approach as discussed in section 2.5. The challenges associated with adopting nonwoody biomass feedstock at the industrial scale include (a) the lack of consistent flow of biomass, (b) proper storage requirements, (c) transportation and collection, (d) large diversity in nonwoody biomass, and (e) variations in biomass composition. Some of these challenges can be readily resolved as many governments have already taken strategic actions and developed policies related to storage, handling, and transportation of a large source of nonwoody biomass feedstocks, that is, agricultural residues, for biofuel production. These strategic actions and policies can be readily modified for NC production using cost-efficient technologies. It is worth noting that in nonwoody biomass, the low lignin content, large hemicellulose content and loose cell wall structure may be particularly suited for emerging a low-energy, less water and less-chemical pathway for NC extraction. The adoption of machine learning will be a key tool to scale-up the different extraction conditions from varying biomass feedstocks. The modeling of LCA and TEA will also be essential to evaluate the environmental and economic impacts of large-scale NC production based on different processes.

6.2. Properties and Characterizations of NC

There are still many challenges that exist in characterization of the structure, property, and processing relations in NC materials, especially in the dispersion phase or the wet state. In the dispersion phase, the dynamics and colloidal behavior of charged anisotropic NC particles, such as CNC and CNF, can be complex and different. Furthermore, the small nanofiber cross sections and fast Brownian dynamics can make the network very difficult to characterize. However, the recent advances in the X-ray photon correlation spectroscopy (XPCS) technique may allow us to explore this subject. The proper analysis of XPCS can yield new information regarding the different diffusion modes under the confined Brownian dynamics in the network structure. We are confident that this will be a subject of growing interests. In the condensed wet state, the hydration and dehydration effect on the NC structure change is still not entirely clear. It has been hypothesized that NC materials can also undergo cocrystallization or hornification upon drying, where this process may be irreversible. To understand the structural change induced by water adsorption/desorption in NC thin films, in situ grazing-

https://doi.org/10.1021/acs.chemrev.1c00683
Chem. Rev. 2022, 122, 8936−9031

incidence (GI)SAXS/GIWAXS measurements can be carried out under different RH. These measurements can also generate new knowledge regarding the crystal structure changes, as well as interfibrillar interactions, simultaneously under varying moisture conditions.

6.3. Structure–Property Relationships of NC

The structure, property, and process relationship for cellulose products (e.g., paper and pulp industry) is well-known, but that for NC-based products is still in a relatively early stage. This may be partially related to the high production cost of NC materials. The different types of NC (i.e., CNC, CNF, and BNC) can offer different application opportunities, but their true values in commercialization applications are far from clear because of the cost issue of the starting materials. Currently, wood-based NC materials have been the primary subject for investigation, and it has been well demonstrated that the pathway to extracting NC from woody biomass feedstocks will always be energy, chemical, and water intensive. The ability to design and engineer desired architectures of using suitable NC building blocks will be essential for the manufacturing of NC-based products, such as composites, membranes, aerogels, hydrogels, foams, and fibers, for varying applications, especially water remediation. The stability of the various structures concerning their dry and wet mechanical properties will always be a central issue for applications. The ability to manipulate more complex structures with higher ordered hierarchical features in NC products is still relatively unexplored. For membrane engineering, even a high mechanical strength is not enough unless membranes have sufficient fracture resistance.

6.4. NC-Enabled Water Purification Technologies

6.4.1. Coagulation and Flocculation. Although natural polymeric coagulants have been used by mankind for many hundreds of years, they have been displaced by inorganic coagulants, such as Al/Fe salts, and synthetic polymeric coagulants during the last century. There is a renewed interest in using natural polymers for reasons of environmental sustainability. The current practice in the pulp and paper industry is to use microparticulate inorganic additives (such as colloidal silica/montmorillonite) for coagulation/flocculation in combination with cationic synthetic polymers because they can possess much higher reversibility of aggregation after shearing. However, the use of cationic synthetic polymers is not environmentally viable in the long run. Recently, it has been demonstrated that NC can exhibit similar characteristics to microparticulate inorganic additives (although NC is still far from being a commercial alternative), and it can also be combined with other additives, such as cationic chitosan, to form natural coagulants/flocculants. This may be one interesting direction to pursue.

To achieve successful coagulation/flocculation in practical wastewater treatment, NC has to resolve the issues of turbidity, microbes, algae, and others at a faster time frame. Therefore, thorough research activities to further understand the interactions between NC and fine particles/suspended solids need to be carried out. Interestingly, we notice a great deal of reports on the NC role in adsorption, photocatalytic, and membrane applications, but relatively few in coagulation and flocculation. For example, in Table 4, it was noticed that only a small amount of NC is needed to achieve the desired coagulation/flocculation performance as compared with commercial coagulants/flocculants. We recommend that the effective addition dosage should be optimized perhaps by in situ monitoring of the process. The knowledge obtained in the study not only can improve cost-efficiency but also can decrease time requirements for sedimentation.

As varying NC-materials can have different types of charge and charge density, it is difficult to assess whether CNC materials or CNF materials can provide the most suitable choice for coagulation/flocculation operations. It has been argued that CNC materials may be a better candidate for some reasons.[337] CNF has a lower critical percolation threshold than CNC, where CNF can form a gel relatively easily.[680−682] In this case, high CNF concentrations will be difficult to prepare or dilute because of the disentanglement tendency. The gelation behavior is generally not desired in coagulation/flocculation operations. On the other hand, it may be beneficial for network-induced flocculation at low solids concentrations. Thus, solid concentration can be a determining factor for the selection of CNF or CNC coagulant/flocculant. Finally, we caution that the application of natural coagulants as a primary treatment may not be sufficient because of the limited performance capability compared to synthetic coagulants/flocculants. Thus, combinations of NC-based dual or ternary systems may improve the performance of such systems, which need to be investigated in the future.

6.4.2. Adsorptive Removal of Water Pollutants. Although many studies rank the adsorption capability of NC and its composites for removal of different water pollutants in the scale of good, better and best; opportunities are available to further improve these materials to the level of superadsorbent with a better cost to performance ratio. We construct a decision tree diagram in Figure 51, where some important steps are highlighted for future research design.

On the basis of our literature survey, most of the NC materials used in the adsorption study are isolated from pretreated cellulose sources (e.g., pulp fibers). Typically, the starting materials have some hemicellulose content and a trace amount of lignin content. Some authors argued whether the residual

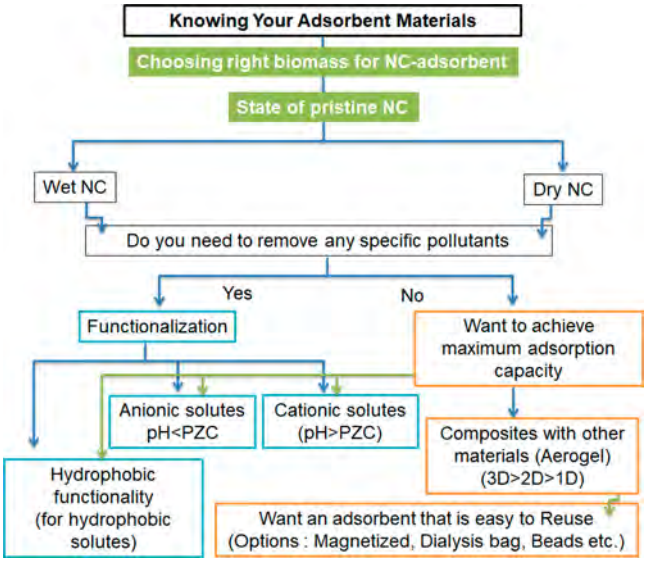

Figure 51. Simplified illustration of a decision tree showing major rate limiting steps of fabricating a NC-based bioadsorbent for effective water purification. Here, PZC indicates point of zero charge of NC-based adsorbents. Facilitates cation sorption (when pH > PZC) by increasing the negative surface charges of NC, postulating its positive surface charge for favoring anion sorption (when pH < PZC).

https://doi.org/10.1021/acs.chemrev.1c00683
Chem. Rev. 2022, 122, 8936−9031

lignin content could increase the adsorption capacity against certain pollutants.[683] Plenty of oxy-functional groups on lignin could be ideal adsorption sites for pollutants hosting. A study on lignin-rich sulfated wood nanofibers (isolated from groundwood and sawdust) showed higher Pb(II) and Cu(II) adsorption capacity as compared with lignin-free sulfated CNF. In addition, lignin-rich sulfated wood nanofibers exhibited higher stability at high metal concentrations as compared with typical CNF.[684] Therefore, less chemically treated lignin-rich lignocellulosic materials, for example, coconut fiber, softwood, pineapple leaf, etc., could be somewhat more promising in production of NC-based adsorbents. However, studies covering this subject are relatively rare, where most reports are focused on chemical modifications and preparations of composite materials to achieve desired pollutant removal. It, thus, makes sense to evaluate if lignin and hemicellulose-rich biomass feedstocks can have an important impact on the performance of final NC products.

Being a hydrophilic biomaterial, NC often faces problems to adsorb pollutants with low water solubility (e.g., with high octanol−water partition coefficient, K_{ow}), such as polychlorinated biphenyls, naphthalene, anthracene, *etc.*, and some of them are frequently found in petroleum or petroleum products spillage, pesticides, and pharmaceutical industries.[685] In fact, coremoval of both hydrophilic and hydrophobic water contaminants has been a major challenge, which is mainly due to the static character of NC. One possible solution to deal with this is by functionalizing NC using photochromic compounds that can reversibly adjust their physicochemical properties in response to environmental stimuli (e.g., pH, temperature, light, etc.).[686] Such multifunctional NC would have both hydrophobic and hydrophilic features, thus adsorption of both types of water pollutants is possible as compared to the single charged oxy-functional groups. Alternatively, one can graft dendrimer onto NC, which also has both hydrophilic and hydrophobic pockets. This system possesses high surface area and the elution of adsorbed pollutants is simple to desorb (e.g., by changing the solution pH level), suggesting the ease of reusability for this system.[3] Grafting of other polymers, such as polyacrylamide onto NC can be another solution to adsorb complex water pollutants, for example, humic acid consisting of many phenolic, quinone, catechol, and sugar moieties, which have not been studied in the literature. After adsorbing with humic acid pollutants, the NC-humic acid-pollutants complex could further be used to adsorb inorganic metal ions.[3]

NC-based composite with multiple (e.g., three/four) components has always shown better pollutants sorption performance, but its overall cost will differ substantially depending on the individual component used. Therefore, one has to be careful in designing the composite system and determining the exact amount of each composite required to reach the desired property. Anirudhan et al. devoted a great deal of effort in making poly(itaconic acid/methacrylic acid)-grafted-nanocellulose/nanobentonite (NC−NB) composite for removal of Th(IV) by adsorption.[687] However, the NC−NB composite only achieved a 10% increment of the adsorption efficiency with increasing temperature as compared with the system at 20 °C. Therefore, careful consideration and justification regarding the modification and material selection as well as the overall sample preparation strategies have to be considered. Also, in the design and construction of NC-based composite adsorbents, the interaction forces between NC and embedded nanomaterials are not always properly judged or considered by the investigators. For example, some authors mainly considered the use of physical entanglement and van der Waals interaction to fabricate NC-based composite materials. Such bonding forces are not suitable to make a stable composite, when the high loading of functioning agents is necessary. Cross-linking reactions, such as Michael-addition or Schiff-base reaction, have been proposed to make a stable aerogel composite.[461] But to accomplish such a system, one has to understand some fundamental issues, such as the interfacial bonding at the interface where stress transfer occurs between the reinforcement material and other polymers that can control the overall mechanical performance.

Understanding the bonding between the adsorbent and the pollutant is also essential before the consideration of using any kind of eluent agents for regeneration study. Some pollutants can adsorb through ion exchange, which will be easy to elute using cost-effective washing agents, such as NaOH/HCl. If ion exchange is a dominant mechanism for pollutant adsorption, we suggest the use of NaCl solution, which is a mild eluent and can replace the use of strong acids. Such solutions might not damage the adsorbent or block the active sites which are very common in the case of strong acidic and alkali eluents. In some studies, expensive eluents such as EDTA were used to disrupt the metallic pollutant that coordinately binds with NC-adsorbents; however some cheaper alternative eluents may also exist. Most of the organic pollutants with high K_{ow} could be adsorbed through hydrophobic interaction. In this case, they could be eluted by organic solvents, such as ethanol or others. Some authors argued that the diffusion of pollutants in NC-based composite also plays a role affecting the adsorption and regeneration performance. Yang et al.[688] reported that if the adsorption mechanism follows the diffusion pathway into the pores, this would make the material difficult to regenerate. Therefore, detailed studies of these mechanisms may shed light on our understanding regarding why a given adsorbent shows increased adsorption capacity toward some groups of water pollutants and why some adsorbents are prone to regenerate.

6.4.3. Photocatalytic Water Treatment. Commercialization of an NC-based photocatalyst can be realized by several combined properties: high photodegradation efficiency under near UV or visible light irradiation, ease of large-scale implementation, photostability (i.e., free from photocorrosion), less environmental impact, and low cost. However, most of the studies fall short of achieving all these features. To fabricate an ideal NC-based photocatalyst with inorganic nanoparticles for water purification, a simple design diagram, involving critical rate-limiting steps to be overcome, is illustrated in Figure 52. In every step, we identify potential knowledge-gaps in the literature, based on which we draw our perspectives for process optimization. First, we notice the use of three types of NC, including CNF, CNC, and BNC, to fabricate heterogeneous photocatalysts. In one study, it was shown that NC with high CrI could increase the surface roughness which would facilitate the anchoring of nanoparticles.[505] Accordingly, their synthesis should be more favorable along with the trend of BNC > CNC > CNF because of their high, medium, and low CrI. We found no evidence to support this hypothesis. In addition, these investigators grossly ignored the use of HNC, which has high-charge contents at the amorphous ends.[407] These ends are more accessible toward solutes as compared to crystalline parts which can make HNC more reactive.[408] Similarly, tunicate (T)NC possesses high porosity as compared with wood-based CNC and CNF,[689] but no study has been found using such NC for

https://doi.org/10.1021/acs.chemrev.1c00683
Chem. Rev. 2022, 122, 8936−9031

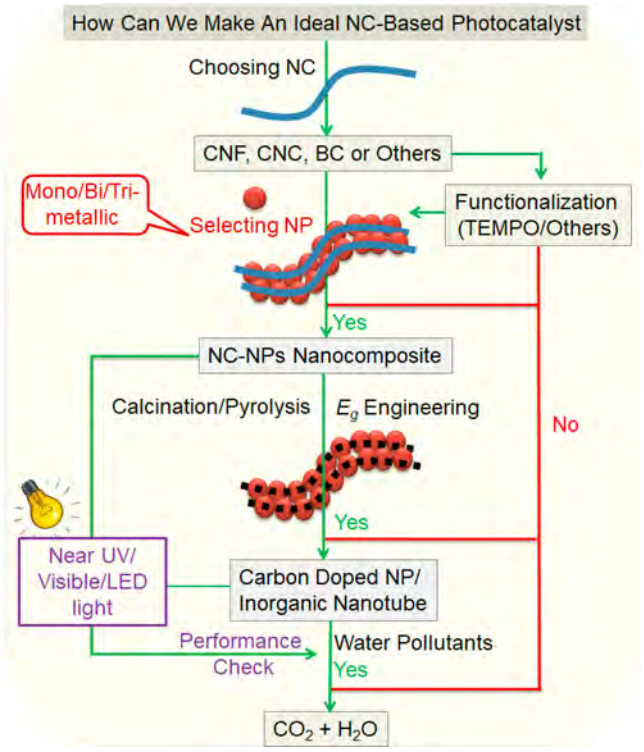

Figure 52. Schematic illustration of the key steps to be considered for fabricating an ideal NC-based photocatalyst with inorganic nanoparticles.

photocatalyst preparation. TNC could accelerate the light absorption, as well as ensure the good mass transfer of organic solutes into the catalyst, which may accelerate the reaction rate. However, if one wants to prepare 1D hollow inorganic nanotube photocatalysts, we encourage the use of CNF due to its high aspect ratio and high fiber entanglement. It has been shown that the rate of CNF degradation is low,[690] but some cellulose can be degraded notably by the photocatalytic reaction. The photodegradation of the NC scaffold may cause the leaching of immobilized nanoparticles during the catalytic reaction, which will be very undesirable.

Second, the functionalization of NC in the field of photocatalyst preparation is not well studied. This may be because of the abundant hydroxyl groups on the NC surface that can facilitate the nucleation of nanoparticles.[520,521] In one study, we notice that positively charged nanoparticles could electrostatically bind to negatively charged sulfate group.[519] In addition, there is also evidence that TONC containing carboxylate group promotes the binding of Zn(II) and increases the number of the nucleating site for ZnO nanoparticle growth.[511] Like this, Nair et al. used three types of functional groups (sulfonic, carboxyl and phosphoryl) on CNC to fabricate CNC−TiO_2 NR−Au photocatalyst, although they did not show the actual roles of these functionalities on the nanoparticle growth.[539] These studies inspire us to understand what type of functional groups will be truly important to fabricate an efficient photocatalyst for water purification. We think both the hard−soft acid−base theory and DFT could validate these hypotheses. Furthermore, it has been shown that NC often transfers oxygen atoms to a metal atom in TiO_2 photocatalyst.[522] This indicates that the sulfate, phosphate and carboxylate groups should be more efficient in transferring oxygen as compared with the hydroxyl group. However, no study has ever been carried out to test this hypothesis.

Third, selecting a suitable type of nanoparticle is an important step prior to the design of an ideal photocatalyst. Some authors have used plasmonic nanoparticles, such as Au, Ag, etc., in their studies, but these nanoparticles can undergo photocorrosion. For example, the formation of metallic Au°/Ag^{0} may increase light absorption due to the surface plasmonic resonance (SPR) effect. However, these Au°/Ag^{0} materials could trap electrons ($A_g^{+} + e^{-} + h\nu \rightarrow Ag^{\circ}$),[546] which would thwart the rate of carrier recombination. Excessive generation of Au°/Ag^{0} could have shielding effects and compromise the SPR effects, which would result in a decrease in photocatalytic rate. For the bi/trimetallic nanoparticles, one has to consider the concentration of these materials, which may create a thick coating on NC where absorption of the light energy would be diminished, especially at the inner layer that will thwart the decomposition of the pollutants in the underlying NC-nanoparticles interface. Although both TiO_2 and ZnO nanoparticles have been extensively tested, only a few studies dealt with the use of visible-light active magnetic nanoparticles, which should be investigated further as they have the advantages of easy regeneration and high recyclability. Another area of interest is that there has been an extensive focus on white TiO_2, whereas black TiO_2 is grossly ignored. Black TiO_2 nanocrystals could be prepared by hydrogen thermal treatment with defective surface layers. One of the major advantages to using such nanoparticles is its very narrow E_g, which can absorb light in both visible and near-infrared regions.[691] If black TiO_2 nanoparticles can be incorporated on NC, one can ignore the use of various dopants to engineer the band gap of white TiO_2 to improve cost-effectiveness in terms of energy-saving and also increase the photocatalytic efficiency for pollutant removal. Other less studied nanomaterials for NC-based photocatalytic application included 2D materials such as transition metal dichalcogenide (TMD or TMDC). These 2D nanosheets are very promising materials because of their very narrow band-gaps, which will show photoactivity within the visible spectrum, unlike most of the popular photocatalysts, such as TiO_2 and ZnO. For instance, the band-gaps of tungsten disulfide (WS_2), tungsten diselenide (WSe_2), molybdenum disulfide (MoS_2), and molybdenum diselenide ($MoSe_2$) monolayer nanosheets are 2.03, 1.67, 1.88, and 1.57 eV, respectively. These band-gaps could be varied depending on the thickness of TMD.[692] Moreover, these 2D nanosheets have suitable physicochemical properties, such as large surface area, reactive sites, and delocalized π-electrons, that could host a range of water pollutants through van der Waals, hydrophobic, electrostatic, and chemical complexation.[693] We also expect that 2D nanosheets could decrease the recombination of electron−hole by taking an electron from the CB and removing an electron from the recombination center. It has been seen that about 90% of photoinduced electron and hole is capable to recombine within 10 ns without prior modification of a photocatalyst.[694]

Fourth, many investigators used a table or a plot to justify the efficacy of their developed photocatalyst by comparing it with results from the literature. They typically utilized the percentage of photodegradation as a standard parameter, which can only show pseudoefficiency and does not accurately represent the experimental results. For instance, although TF−ZnO[400] showed an almost similar percentage of MO photodegradation to TONC−ZnO[300], their first-order reaction rate was quite different.[511] Such observations were also found for NC-

https://doi.org/10.1021/acs.chemrev.1c00683
Chem. Rev. 2022, 122, 8936−9031

templated Fe−ZnO and ZnO photocatalyst for tetracycline degradation.[490] Alternatively, the rates of the reaction for ZnO and CNC−ZnO were identical, but their MB photodegradation efficiency was very different.[534] We prefer the reaction rate constant for comparing such experimental data, where one has to consider the total amount of photocatalyst given in the reactor, as well as the relative ratio of the nanoparticles to the reactant. However, some other evaluation factors can also be used, such as the quantum yield and multiactivity assessment.

Fifth, the discrepancy in terms of hydrophobicity or hydrophilicity can be found in similar photocatalyst systems. For example, as seen in Figure 36e, TONC−ZnO showed a higher contact angle than the TF−ZnO and NONC−ZnO after calcination at 400 °C.[511] In a different study, it was shown that the TONC hydrophilicity did not change upon ZnO addition without calcination.[531] Such issues should be addressed carefully with a systematic study. The use of highly hydrophobic composite material in the photodegradation of some pollutants in water can be challenging. Although this material may be suitable for adsorption of less water-soluble organic compounds, it will repel water molecules thus thwarting the adsorption of water onto the catalyst surface. This step is essential to generate sufficient hydroxyl radicals upon reacting with photoinduced holes.

Finally, for industrial-scale applications, there are several important barriers that NC-based photocatalysts should overcome. (a) The photocatalysts should be able to work under sunlight—a renewable and unlimited energy source. Most of the authors used a higher energy radiation source, such as UV light to irradiate the photocatalysts, which would reduce the cost-effectiveness of the system. Besides sunlight, we recommend the use of light emitting diode (LED) lights as a viable light source. LEDs are inexpensive and can give a high current to light conversion efficiency with relatively small energy loss in heating (as compared with classical mercury lamps). These features will decrease energy consumption and improve cost-efficiency. (b) One has to check whether the prepared photocatalyst could completely degrade the tested pollutants and generate CO_2 and H_2O. There should not be any intermediary compounds that are more toxic than the initial compounds. Such byproducts can block the reaction sites of the catalyst and decrease the catalyst efficiency. Complete degradation of such byproducts can typically be confirmed by measuring COD,[538] a method to determine the organic loading of the water body. (c) The photocatalytic reactions should be selective where the radical anions should not degrade nontargeted molecules in the reaction mixture. It can be problematic for some applications when a controlled separation/degradation process of organic molecules is essential. For this purpose, one can improve the poor selectivity characteristic possibly by functionalizing the NC scaffold with a specific affinity toward certain water pollutants. (d) Since most industrial effluents are contaminated with varying pollutants at high concentrations, it is often difficult to tackle such a sample using a simple photocatalyst. To overcome such limitations, one can use ozonation treatment, which would help to increase the photodegradation rate (in the presence of ozone). However, this practice needs an extra setup for supplying ozone that will increase the total cost of the system. (e) Checking the feasibility of a photocatalyst to tackle real wastewater is important because many pollutant molecules can form complexes with other pollutant molecules or organic matter. (f) To achieve an optimum photocatalytic activity, one should fully understand the effects, such as pH, temperature, catalyst concentration, etc., on the reaction performance in the literature and identify the most essential parameters in process optimization.[3]

6.4.4. Membrane Technology. One strategy to incorporate water channels in the barrier layer is by using the concept of polymer nanocomposite. It is thought that water-channels can come from nanoporous fillers (e.g., zeolites or MOF) dispersed in the polymer matrix or from the interface formed between impermeable nanofillers and polymer matrix. It has been shown that NC, together with CNT and graphene can all behave as effective nanofillers to enhance the permeation flux of the nanocomposite barrier layer, if the filler structure can be arranged appropriately (e.g., interconnected network, and preferred direction). Our group has demonstrated the class of TFNC membranes, containing nanocomposite barrier layer based on TOCNF or oxidized CNT nanofillers, where the permeation fluxes of these membranes exhibited noted improvement when compared with commercial UF membranes.[695] Similar results were also found for filtration of high selectivity (i.e., NF and RO) using nanocomposite barrier layers such as CNF−GO for dye removal,[696] and CNC−CNT for salt rejection.[697] Despite these promising studies, the utilization of nanocomposite barrier layers to enhance the filtration performance is still in its infancy. We believe the incorporation of NC as a nanofiller is particularly promising because of its abundant surface functional groups and the many pathways to modify these groups to tailor the selectivity.

Although NC-based TFNC membranes have been proven to be a successful new membrane format to increase the permeation flux, manufacturing of these membranes at a large scale has not yet been demonstrated. There is also a need for the development of low-cost TFNC membranes without the use of synthetic polymer supports (e.g., electrospun PAN or nonwoven PET) and self-standing NC membranes on a large scale. In addition, there is a need for the selection of suitable biomass feedstocks from diverse sources to produce cost-effective NC scaffolding materials with various fibril thicknesses and crystallinity. Furthermore, there are many challenges in process selection, design and optimization, which can lead to the precise control of porosity, pore size distribution, and *Z*-scale pore size distribution at different thicknesses. For example, some ultrafine CNFs with high charge contents are difficult to separate by filtration. To overcome this problem, coagulants, such as multivalent ions, can be used before filtration.[563] In addition, membrane fabrication based on CNC using vacuum filtration is problematic but can be overcome by using flocculants.[563] The improper selection of coagulants/flocculants can alter the surface charges of the resulting NC materials. To resolve this issue, we can consider the covalent cross-linking approach instead of ionic cross-linking, which will change the charges of NC membranes that may compromise their ionic selectivity. For example, it was reported that TOCNF-based UF membranes exhibited low ion rejection performance (34% for Ca^{2+} and SO_4^{2-}) when $AlCl_3$ was used as a coagulant.[563] In this case, cross-linking agents, such as glutaraldehyde or compounds with siloxy groups, can be used to covalently attach NC without compromising the charge characteristics.

The reported ion rejection values of NC-based filtration membranes[563,697,698] are very low for water softening and desalination. This can be explained by considering the following two factors: electrostatic interaction between metal ions and NC, and pore size of the membrane. We believe that the initial pore size in the NC-based membrane is too large to exclude

https://doi.org/10.1021/acs.chemrev.1c00683
Chem. Rev. 2022, 122, 8936−9031

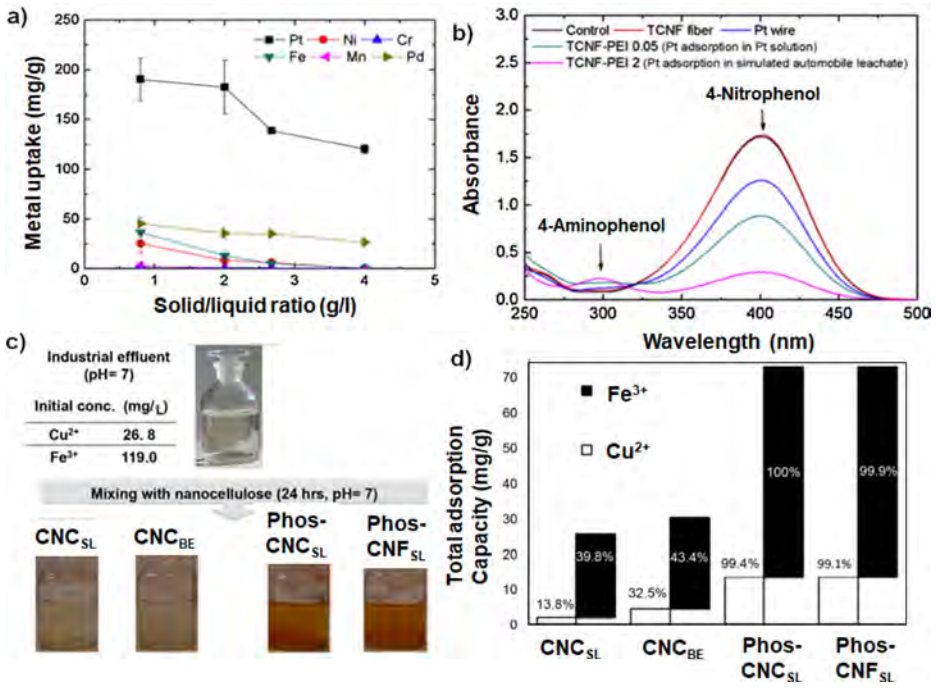

Figure 53. (a) Metal ion adsorption by TOCNF−PEI in simulated automobile catalyst leachate. (b) UV−vis spectra show the reduction of 4-NP to 4-AP catalyzed by a variety of NC-based materials (TOCNF is the same as TCNF). Reprinted with permission from ref 427. Copyright 2020 Elsevier. (c) Effluent treatment from the mirror industry using different types of NC-based materials. (d) Their metal adsorption capacity (Fe(III) and Cu(II)) is in complex metal ion mixture systems. Reprinted with permission from ref 445. Copyright 2015 Elsevier.

metal ions where electrostatic-induced adsorption of metal ions is the main mechanism. However, as progressive ion adsorption will cause the NC scaffold to collapse (i.e., by shielding with monovalent ions, or by cross-linking with multivalent ions), the NC-based barrier layer can become denser and eventually enable the diffusion control separation mechanism. However, these combined processes are not effective enough to remove metal ions practically. As discussed earlier, the nanocomposite barrier layer, based on NC and interfacially polymerized PA, can work well in NF/RO operation. We believe that the use of other polymers, such as cellulose acetate, a commonly used RO membrane material, can also be a good matrix to host the NC network. This approach may need some technology advancement regarding the homogeneous dispersion of hydrophilic NC in a relatively hydrophobic cellulose acetate matrix.

It is conceived, that a unique class of next generation filtration membranes will be based on NC hybrid composite membranes, tailored for various water remediation treatments, by creating effective water channels to increase flux, enhance surface charge density or produce zwitterionic characteristics to reduce fouling, using lower cost feedstocks to reduce the filtration cost. In addition, NC materials can be used as scaffolds to immobilize various enzymes, such as lysozymes, laccase, and others, thus can offer antibacterial ability. For example, Sampaioa et al. immobilized laccase in a BC scaffold, where the resulting membrane exhibited cytotoxicity toward Gram-positive and Gram-negative bacteria with efficiencies of 92% and 26%, respectively, for wound dressing application.[699] Such biohybrid membranes may also help recycling the enzymes, which can reduce the production need of enzyme molecules and result in more cost-effective antifouling NC membranes.

7. NC-BASED MATERIALS FOR MULTIPOLLUTANT REMOVAL SYSTEM DESIGN

Typical water contaminants include a multitude of impurities with variations in type, form, concentration, composition, and chemical environment. In the USA, it has been reported that more than 161 organic compounds are present in each of 38 studied streams.[700,701] This suggests the complexity of wastewater, which needs to be tackled by multiple technologies. Currently, most of the studies on NC-based materials for water purification dealt with the single pollutant removal, where works on simultaneous removal of multiple pollutants from water are relatively rare. Unfortunately, the results compiled in other reviews do not provide sufficient guidelines and strategies to tackle multiple pollutants removal using complementary NC-enabled technologies including adsorption, photocatalysis, and membrane filtration. In this section, we outline several strategies for simultaneous removal of multiple pollutants with good selectivity in both static and flow conditions.

7.1. System Design for Adsorption

The nature of multiple pollutant adsorptions in the field can be quite different from that in the lab, using simulated contaminated water. This is because a subtle change in the environment can strongly affect the pollutant of interest, and multiple pollutants may be competing with the same adsorption site. Nevertheless, evaluating the adsorbent selectivity toward multiple pollutants in the lab in a systematic manner will provide essential information for new material design to reach high removal/recovery efficiency of multiple pollutants, or a particular pollutant, from wastewaters.

Depending on the source (e.g., tap, industrial, mining, or agricultural water), one can tune the selectivity of adsorbents. For example, recovery of Au metals from its mining effluents, containing a range of other pollutants, requires highly selective

https://doi.org/10.1021/acs.chemrev.1c00683
Chem. Rev. 2022, 122, 8936−9031

adsorbents. Some assessment parameters can be used to evaluate the selectivity of an adsorbent. This adsorbent selectivity can be represented by the distribution coefficient, K_d (mL/g), where $K_d = V(C_0 - C_f)/mC_f$ with V being the total volume of the reaction and C_0 and C_f being the initial and final (residual) concentrations of each interfering pollutant, respectively. Zheng et al. attempted to increase the Dy(III) adsorption capacity by oxidizing CNC (O−CNC) using TEMPO-mediated oxidation method, where a great deal of −COOH groups were generated.[423] To increase the Dy(III) selectivity, they incorporated ion-imprinted polymers (IIP), non-ion-imprinted polymer (NIIP), CNT, and GO into O−CNC. The study also included other competitive interfering cations: Fe(III), Nd(III), Gd(III), and Pr(III). The highest K_d of Dy(III) was obtained for the O−CNCs/GO-IIPs composite (872 mL/g) as compared with O−CNC-IIPs. This was attributed to the appropriate size of imprinting in O−CNCs/GO-IIPs, which was not suitable for other cations. As a result, the adsorption capacity of O−CNCs/GO-IIPs exhibited the order of Dy(III) > Gd(III) > Nd(III) > Pr(III) > Fe(III). In another study, Shahnaz et al. used surface modified NC with polypyrrole to test the adsorption of a binary pollutant mixture: CR and Cr(VI) in the presence of other coexisting ions.[410] For CR, the removal efficiency followed the system without other salt ions (87%) > KCO_3^{2-} (86.33%) > $ZnSO_4$ (81.62%) > $FeSO_4$ (78%) > NaCl (77.53%) > $CaCl_2$ (76.53%) > $CuSO_4$ (74.08%) > KH_2PO_4 (73.52%) > $MgNO_3$ (71%). Similarly, for Cr (VI), the system without salt ions (87%) > NaCl (75.36%) > $CaCl_2$ (70.50%) > $ZnSO_4$ (66.26%) > $CuSO_4$ (60.81%) > $MgNO_3$ (60.90%) > KCO_3^{2-} (57.36%) > KH_2PO_4 (53.96%) > $FeSO_4$ (78%). The author claimed that the decreased removal efficiency of larger size CR and Cr(VI) ions was probably affected by the presence of smaller hydrated ionic radii of coexisting ions, which might be adsorbed more easily. We think this explanation may be too simple to explain the observed trend, as the hydrated ionic radii of NaCl should be very small as compared with the other ions. This implies that the adsorption of CR and Cr(VI) should be minimal in the presence of NaCl ions, which was not seen. In addition, some ions have nearly the same molar mass (e.g., $ZnSO_4$ and $CuSO_4$) even though their effects on the CR and Cr(VI) removal were quite different.

TOCNF−PEI has been used to adsorb multiple pollutants present in automobile catalyst waste leachate.[427] As shown in Figure 53a, the material could selectively adsorb Pt and Pd around 125 and 27 mg/g at a solid/liquid ratio of 4 g/L, respectively. Although other platinum group metals (PGM) were also present in the solution, their adsorption by TOCNF−PEI was minimal (Figure 53a). This selectivity toward Pt was completely due to its electrostatic interaction with TOCNF−PEI. Since the reaction environment was acidic, where Pt was present in the form of $PtCl_4^{2-}/PtCl_3^{/}$ $PdCl_4^{2-}$, this could be easily adsorbed with positively charged TOCNF−PEI. All other metals (Ni, Fe and Mn) were in the form of cation, which could not be adsorbed onto TOCNF−PEI. However, the more interesting aspect of this study was the use of the Pt/Pd adsorbed TCNF-PEI system as a catalyst to reduce a model organic pollutant 4-NP to 4-aminophenol (4-AP) (Figure 53b). In Figure 53b, the reduction process for 4-NP to 4-AP was found to be greater in Pt/Pd adsorbed TOCNF−PEI as compared with other catalysts; however, the reason for this observation was not entirely clear and warrants further investigation.

Liu et al. tested the adsorption of Fe(III) and Cu(II) by NC extracted from different sources: sludge (CNC_{SL}), bioethanol CNC (CNC_{BE}), phosphorylated CNC from sludge (phos-CNC_{SL}), and phosphorylated CNF from sludge (phos-CNF_{SL}).[445] Both phos-CNC_{SL} and phos-CNF_{SL} showed higher adsorption capacity values against both single and multiple metal ion systems than those of CNC_{SL} and CNC_{BE}. The adsorption capacity values of phos-CNC_{SL} and phos-CNF_{SL}, followed the order of Ag(I) > Fe(III) > Cu(II) in the case of a mixture of multiple ions. In an earlier study, it has been reported that the metal ion adsorption selectivity primarily relies on the electronegativity of each metal ion;[702] however, this hypothesis cannot explain these metal ion adsorption results in the complex mixture systems. Liu et al. also argued that the mechanism of such a sorption phenomenon have remained to be a scientific challenge and need future attention. It is known that the adsorption selectivity also depends on the nature and amount of different functional groups present and their dissociative pH values (i.e., the functional groups are pK_a dependent). Further research to tackle this challenge may include DFT calculations, where the results may yield some insights into the hidden mechanisms. As shown in Figure 53c and 53d, phosphorylated NC was more efficient in treating the effluent from mirror manufacturing at pH 7. These Phos-NC materials could successfully reduce Cu(II) and Fe(III) in the effluent to the levels of Cu(II) = 0.14−0.23 and Fe(III) = 0−0.05, meeting the national drinking water requirement (i.e., the United States National Secondary Drinking Water Regulation). In another pivotal study, NC-based composites exhibited excellent As(V) and Cr(VI) removal capacity (i.e., 100 and 99%, respectively) from contaminated groundwater, in which the treated water could also be below the permissible limit of the drinking water regulations.[409] The authors also tested the efficacy of this NC-based composite for As(V) and Cr(VI) removal from simulated wastewater, where peptone, meat extract, urea, anhydrous K_2HPO_4, NaCl, $CaCl_2{\cdot}2H_2O$, and $Mg_2SO_4{\cdot}7H_2O$ were added. The demonstrated NC-based composite also displayed good removal capacity with As(V) > 90% and Cr(VI) > 70%.

On the basis of the literature, NC-based adsorbents are capable of removing multiple pollutants from water, either in a simultaneous or sequential manner, due to abundant functional groups and straightforward modification schemes to create new functional groups on the NC surface. However, tuning of the selectivity toward one particular pollutant in a mixture of several interacting pollutants is still difficult, as the fundamental knowledge for adsorption of competing ions by NC remains lacking. Some authors claimed that the adsorption of targeted pollutant ions can be determined by their size, that is, the smaller ions possess higher adsorption capability. This behavior may be true in some situations, where the adsorption mechanism of targeted pollutant ions is determined only by electrostatic interaction. It is known that smaller ions act more ionic and they look big because of strong hydration, while large ions act more "nonpolar" and look smaller in water.[703,704] In other words, metal ions with a larger ionic radius decrease their electrostatic nature. This mechanism may not hold true if other interactions occur, such as covalent bonding. For example, it has been shown that the Pb(II) adsorption is unaffected by the presence of other metal ions, for example, Cd(II), Ca(II), Mg(II), and K(I).[431] In addition, the pollutant concentration can play a significant role on the adsorbent selectivity. If the targeted pollutant concentration is lower than those of coexisting pollutants, a more dominant adsorption effect of these coexisting pollutants can be seen.[472] Furthermore, the hard and soft acid concept, or the Pearson acid−base concept, has also been used to explain the

https://doi.org/10.1021/acs.chemrev.1c00683
Chem. Rev. 2022, 122, 8936−9031

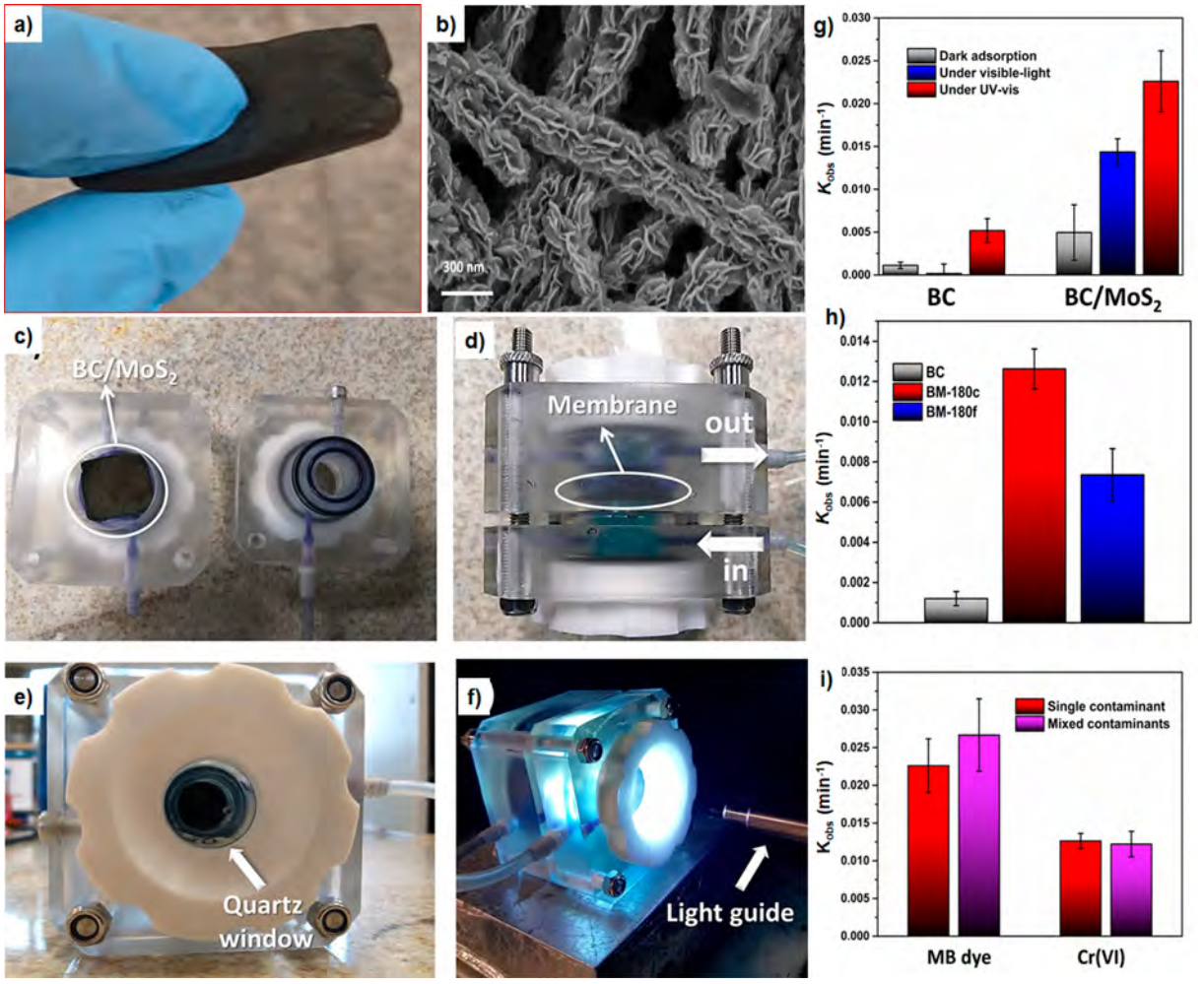

Figure 54. (a) Photograph of a BC/MoS_2 aerogel membrane after supercritical drying. (b) Field emission gun (FEG)-SEM image of the semivertical alignment of few-layer stacked MoS_2 nanosheets grown on BC. (c−f) Photographs of the experimental setup, where the BC/MoS_2 hybrid membrane is used as a photoreactor to evaluate the photocatalytic activity. (g and h) First-order decay kinetic constants for the single component removal processes for MB and Cr(VI) using BC and BC/MoS_2 membranes under different illumination conditions (visible light > 400 nm and UV−vis irradiation = 250−600 nm), respectively. (i) The first-order decay kinetic constants of photoassisted in-flow simultaneous removal of MB and Cr(VI) and their performance comparison with single component removal using BC/MoS_2 aerogel. Reprinted with permission from ref 545. Copyright 2020 American Chemical Society.

adsorption efficiency of NC for multipollutants removal. For example, Li et al. reported that L-cysteine-modified NC exhibited the pollutant removal efficiency of 87%, 2%, 19%, 6%, and 3% for Hg(II), Cd(II), Pb(II), Cu(II), and Zn(II), respectively. They argued that the higher Hg(II) removal was due to the soft Hg(II) acid nature, which is more inclined to bond with the soft thiol (SH) base of L-cysteine.[474]

7.2. System Design for Photocatalysis

There are very few studies dealing with the simultaneous photodegradation of multipollutants. Since some organic dyes and inorganic metal ions can utilize the same active radical species for photo-oxidative and photoreductive pathways, the mixing of these two different classes of water pollutants may positively or negatively affect their removal efficiencies. For example, the FBiOBr/CCNF-900 composite (cellulose carbon nanofiber incorporated with bismuth oxybromide) was found suitable for simultaneous photodegradation of RhB and Cr(VI).[543] However, the photodegradation rate for RhB was decreased to some extent in the presence of Cr(VI). This might be due to the reduced availability of photoexcited electrons for the production of $^{\bullet}O_2^-$. Nevertheless, RhB could still be completely removed within 90 and 50 min with and without Cr(VI), respectively. On the contrary, photodegradation efficiency for Cr(VI) was increased from 70 to 90% by the presence of RhB, which could act as a hole (h^+) consumer. This prolonged the lifetime of photoinduced electrons in the CB.[705] Such synergistic effect on the mixture of pollutants removal should be explored further in detail.

Evaluating the performance of a photocatalyst in the "continuous (in-flow)" system is challenging. Most of the photocatalysts discussed earlier are based on a "discontinuous" or "batch" system. The difference between discontinuous and continuous processes is to treat small vs large volumes of water and often, the treated water in the discontinuous process is contaminated with nanosized objects, whose removal is difficult and requires additional steps. Lucchini et al. prepared CNF/TiO_2 monoliths using the direct wet impregnation method for in-flow photodegradation of MO and paracetamol.[690] They observed a very low 21% and 30% of the MO and paracetamol removal upon irradiation with sunlight for 200 and 150 min, respectively. In another study, Ferreira-Neto et al. prepared BC-

https://doi.org/10.1021/acs.chemrev.1c00683
Chem. Rev. 2022, 122, 8936−9031

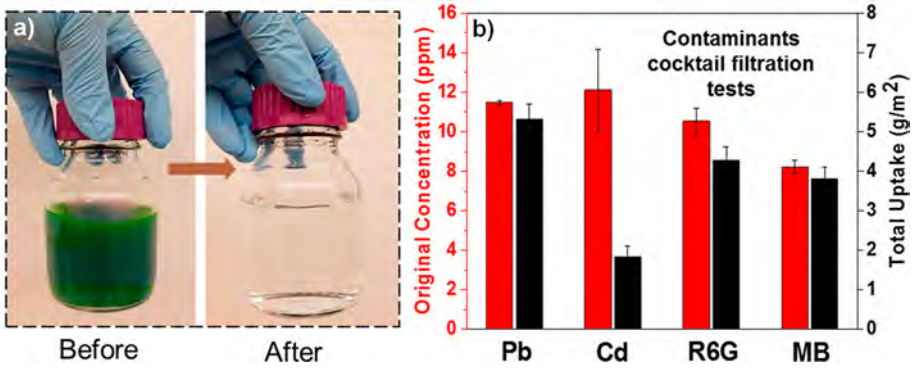

Figure 55. (a) Photographs of the cocktail solution before and after filtration using the PDA/BNC membrane. (b) Simultaneous pollutant removal capacity upon vacuum filtration. Reprinted with permission from ref 627. Copyright 2019 American Chemical Society.

templated MoS_2 (BC/MoS_2) hybrid aerogel membrane using the hydrothermal route for in-flow removal of both MB and Cr(VI) removal as shown in Figure 54.[545] They found a nanoscale size of MoS_2 crystallites (2−4 nm) on BC, which enabled the composite to possess a high surface area (97−137 m^2/g) and pore volume (0.28−0.36 cm^3/g). These values were higher than the previous study where CNF was cross-linked with MoS_2 aerogel.[706] They observed that the pore size of cylindrical mesopores could be controlled by the hydrothermal temperature. For example, the mean diameter of the pores fell between 20 and 60 nm at lower temperatures, and they became larger by increasing the temperature. The high temperature mediated hydrothermal treatment of the hybrid did not significantly change the morphology of the BC scaffold. The larger pores ensured better mass transfer, requiring less operational pressure (and hence energy) to pump the water flow through the hybrid photocatalytic membrane. The band gap range of the prepared samples varied between 1.73 and 2.15 eV, depending on the preparation conditions. For a single component removal, BC/MoS_2 exhibited a higher MB photodegradation rate (0.0225 min^{-1}) and Cr(VI) removal rate (~0.013 min^{-1}) as compared with BC, which was inefficient and kinetically sluggish under UV−vis illumination (Figure 54g and h). In the simultaneous in-flow removal of MB and Cr(VI), the BC/MoS_2 membrane showed a very good photocatalytic removal efficiency (Figure 54i) after 120 min of UV−vis light illumination. Interestingly, the reaction rate of MB in the presence of Cr(VI) was found to increase slightly, whereas the presence of MB did not affect the kinetic rate of Cr(VI). This observation is completely opposite to the results from the study of the BiOBr/CCNF-900 composite for simultaneous photodegradation of RhB and Cr(VI).[543] Without question, multiple pollutants can be removed simultaneously using NC-based photocatalyst in a turbulent in-flow system. However, we are expecting some challenges of using such a reactor for actual field application. Since the in-flow setup is relatively complex, one has to ensure whether the light can fully reach the entire area of the photocatalyst, or the solution can pass through the photocatalyst in a homogeneous manner to reach the best performance.

7.3. System Design for Membrane Filtration

NC-based membranes with tuned structure, chemical and physical properties to remove multiple contaminants from water have been relatively well investigated. For example, Singamaneni et al. carried out a cocktail filtration test, containing both inorganic ions (Pb(II) and Cd(II)) and organic dyes (R6G and MB) using PDA/BNC membrane (Figure 55).[627] It was seen that the color of this cocktail solution (green) became colorless upon being vacuum filtered by the PDA/BNC membrane (Figure 55a), which implies the efficacy of this membrane for simultaneous pollutants removal from water. More specifically, in Figure 55b, it was found that the Pd(II) uptake was better than Cd(II). This could be attributed to the less binding affinity between Cd(II) and carboxylic or phenolic groups on the PDA/BNC membrane as compared with Pb(II).[707] On the other hand, the uptake of R6G was slightly higher than MB (Figure 55b).

In another study, NC hydrogel was deposited on top of the titanate-bismuth oxide membrane using the layer-by-layer assembly method.[612] The final composite membrane was capable of removing a large variety of anions and cations in the presence of oils. Such membrane can be used to tackle complex sewage feed streams, especially in a situation where oil spillage is prominent. Mathew et al. prepared three different NC composite membranes, where CNC_{SL} (CNC isolated from cellulose sludge), CNC_{BE} (CNC extracted from bleached wood), or $PCNC_{SL}$ (CNC_{SL} were enzymatically modified to introduce phosphoryl groups on the surface) were used as a functional layer in a gelatin-matrix, whereas the support substrate was fabricated by cellulose microfiber sludge. They used these membranes for tackling industrial effluents where mixtures of Cu(II)/Fe(III)/Fe(II) ions were present (pH 2.3). The CNC-based membranes showed the Cu(II)/Fe(III)/Fe(II) removal capacity in the order of $PCNC_{SL}$ > CNC_{BE} > CNC_{SL} in the cross-flow mode, which could be mainly attributed to the functional groups' density present on CNC.[619] For the antifouling test, NC-based membranes also showed good selectivity against BSA in the mixtures of both fish and soybean polypeptides. Here, NC was deposited on top of electrospun PAN layer supported by the nonwoven PET substrate.[659]

The overall perspective of this section is that NC-based materials, whether they are in the form of adsorbents, photocatalysts, or membranes, are very well suited to tackle complex wastewater problems. Their performance can be fine-tuned depending on the required stability (i.e., form and structure) of the environment, and the necessary selectivity for single-component or multicomponent pollutants removal. For brevity, it should be noted that the simultaneous removal of multipollutants using NC-based coagulants/flocculants is not well studied in the literature. The concepts that we discuss for adsorption, photocatalysis, and membrane systems should bring sufficient scientific attention to using NC-based coagulants/flocculants for copollutants removal system designs.

https://doi.org/10.1021/acs.chemrev.1c00683
Chem. Rev. 2022, 122, 8936−9031

8. STRATEGY TO HANDLE THE USED NC-BASED MATERIALS

NC-based technologies will be sustainable only if one can ensure the regeneration/recycling or safe disposal of contaminated materials in an economic way. One major advantage in the treatment using NC-based photocatalysts is that the adsorbed water pollutants will be completely degraded, where the handling of the used NC composite materials will be relatively easier. In contrast, for the used NC-based coagulants/flocculants and membranes, where pollutants are retained in the NC scaffolds, one has to consider how to deal with the issue of possible secondary contamination. To deal with this issue, we can consider the following strategy to process the used NC materials (i.e., pollutants-loaded-sorbents/filters). These materials can be classified into two groups: post and spent materials. The former is the material where pollutants are most concentrated after the immediate collection and treatment, where the latter is the material regenerated through post-treatments, such as washing, neutralization, etc.[708] Although there are many papers investigating the use of NC materials in varying water treatments (optimization, mechanisms and their performance), disposal of the post and spent materials after the treatment is rarely addressed. To our knowledge, there are no reports or reviews discussing the possible management pathways of NC-based post/spent-materials. As a result, we outline our perspectives on the proper care of these used materials through some possible routes, as shown in Figure 56.

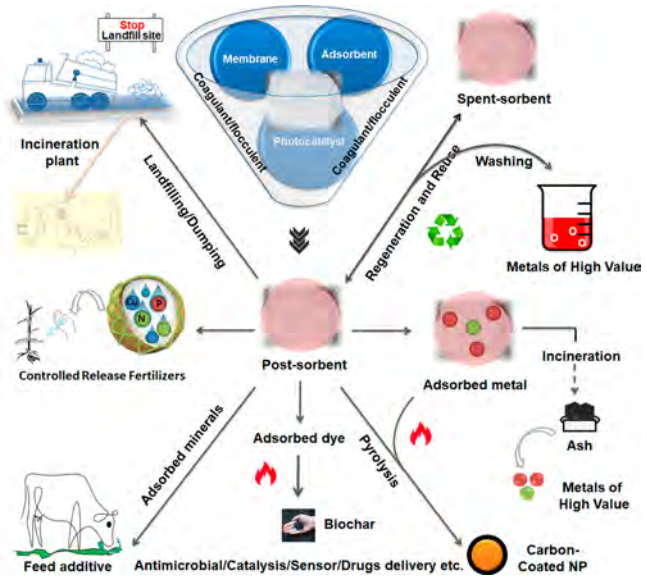

Figure 56. Schematic illustration of some possible routes for upcycling post and spent NC materials after water purification.

Generally, the management of postmaterials involves the recycling effort in collection and treatment followed by safe storage/disposal of the spent materials in landfills. Hubbe et al. reported an end-of-use analysis regarding the disposal of regenerated adsorbents in landfills,[466] where incineration and other chemical treatments were not carried out. The report indicated that such a practice could result in secondary pollution (i.e., contamination of soil and surface water) because of the leaching of toxic pollutants from the landfill area. Currently, environmental regulations prohibit the direct disposal of metal-loaded ashes from incineration by landfill dumping.[709] In addition, the operating and setup costs of an incineration facility can be very high. These limitations prompt us to propose the following strategies, where both post and spent materials could be upcycled and create new circular economic solutions (Figure 56):

(a) The adsorption of nutrient molecular ions, for example, ammonium, nitrate, phosphate, etc., and metal ions, such as K(I), Ca(II), Cu(II), Zn(II), Mn(II), etc., onto the NC scaffold can open up new economic opportunities to use post/spent materials as fertilizers or fertilizer supplements in agriculture. The sustained release of the nutrient components depends on the type of adsorbed pollutants and the suitability of NC scaffolding materials.[708] The slow release of a proper amount of fertilizer is essential to halt the rapid loss of nutrients, which can greatly damage the environment and also increase the cost of crop production by overusing fertilizers. The NC scaffold has been found as an effective medium in the control of the sustained release of different ions.[710] For example, the porous networks of NC from tunicate,[689] have been shown to possess good water retention capability, as well as suitable porosity and structure for releasing nutrients, minerals, and other agro-chemicals. Furthermore, decomposing the NC scaffold to organic carbon often can improve soil carbon insulation leading to the enhancement of soil quality.

Typically, NC materials possess negatively charged surfaces, which is ideal to adsorb cationic nutrients, such as K(I), Ca(II), Mn(II), Zn(II), and Cu(II). However, the primary form of nutrients, such as nitrate and phosphate, are negatively charged, which require the use of cationic NC materials. There are several easy and practical ways to convert the anionic NC surface to a cationic surface. One approach is by surface modification with cationic molecules, for example, quaternary ammonium compounds or by surface grafting with cationic oligomers/polymers (e.g., chitosan).[710] Another approach is by surface anchoring of metal oxide nanoparticles (e.g., ZnO and CuO). We prefer the use of NC-based organic nanocomposite to enhance the anionic nutrient adsorption, as this system usually possesses the slow-releasing behavior. The NC-inorganic nanoparticles composite systems, although effective, also run the risk of releasing nanoparticles that may not be safe to the environment.[711] To date, very few studies have been carried out to understand the pros and cons of NC-based nanofertilizers and their impacts on water contamination. Before the consideration of applying nutrients-adsorbed sorbents/filters for agriculture, one must ensure that the system should be free of other harmful organic (e.g., pathogens, polycyclic aromatic hydrocarbons, pharmaceuticals, etc.) and inorganic contaminants (e.g., toxic metal ions, such as Cd, As, and Pb, etc.), which can adversely impact food safety, plant growth, and microbial communities.[712]

(b) Since NC is capable of adsorbing many metal ions, it can be used as trace-minerals supplements and food additives, which are essential for the living system.[708] Since 1983, NC materials have been broadly used as safe food additives; this was the first application for NC.[713] As some metal ions, for example, Fe(II), Cu(II), Co(II), Mn(II), Zn(II), etc., are important to perform biological functions, one can consider loading the proper amount of these ions into the NC scaffolds as trace-minerals supplements in applications, such as nutrition for humans, cultivation for crop growth, and feed additives for animals. Since these minerals are required in small quantities, one has to ensure the minimal dosage of such additives. Additionally, antibiotics/other drugs and vitamins loaded NC systems will also be useful to maintain and improve the health of livestock.

https://doi.org/10.1021/acs.chemrev.1c00683
Chem. Rev. 2022, 122, 8936−9031

(c) Post-NC adsorbents loaded with metallic ions could offer some catalytic activities, where a redox reaction may take place that will be useful for reducing organic water pollutants. It has been shown that the TOCNF−PEI composite could adsorb Pt/Pd, which could be subsequently used as a catalyst to reduce organic pollutants such as 4-NP to 4-AP.[427] The photodegradation mechanism is due to the platinum groups in metal hydrides (with the addition of $NaBH_4$) that can simultaneously adsorb 4-NP ions and assist the electron transfer from $NaBH_4$ ions to 4-NP ions, leading to the reduction of 4-NP ions to 4-AP ions. It should be noted that pristine TOCNF could not reduce 4-NP.

(d) NC may be used to recover high-value heavy metal ions. Without calcination, it has been shown that the carboxyl (COOH) groups of NC could reduce the adsorbed metal ions to produce metallic nanoparticles, which have commercial values. For example, Liu et al. used TOCNF to adsorb Cu(II) ions, where the formation of Cu(0) or CuO nanoparticles could be subsequently obtained by reduction of Cu(II) ions and microprecipitation (Figure 57).[444] Such adsorbents can be

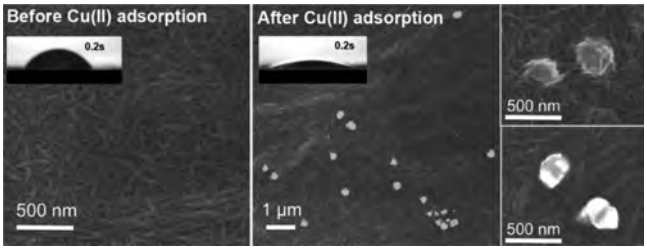

Figure 57. SEM images of TOCNF cast mats before and after the Cu(II) adsorption. The formation of nanosized Cu(II) clusters on the TOCNF is clearly visible after Cu(II) adsorption. Reprinted with permission from ref 444. Copyright 2016 Elsevier.

reused in other applications, such as the catalyst in hydrogen production,[714] conductive,[715] and antimicrobial materials. Another possible example is that after NC is used to adsorb $KAu(CN)_2$ that is commonly found in the effluent of the electroplating industry, one can use thermal or chemical treatments to recover valuable Au nanoparticles[716] from the used NC adsorbents.

(e) To encapsulate different nanomaterials with carbon coating, one typically synthesizes nanoparticles and carbon sources separately, and subsequently mixes them for post-processing. The procedures, involving multiple steps, are usually not cost-effective. To reduce the necessary steps, one can use the nanoparticle-adsorbed NC materials directly to produce carbon-coated metal nanoparticles by calcination. These nanoparticles are useful for sensing, magnetic resonance imaging, and plasmonic applications, to name a few. If nanoparticles have magnetic properties, they can be recovered rather easily using magnetic fields after usage. It has been shown that carbon coated magnetic nanoparticles have great application values in electronics, hyperthermia, drug delivery, catalysis, and more.[717,718]

With calcination treatments, one can encapsulate the adsorbed metal nanoparticles with carbon (from the NC scaffold). The reaction conditions, such as temperature and time can directly affect the porosity and available carbon content. Carbon encapsulation not only can protect nanoparticles from agglomeration and oxidation, but also can dope the carbon atom into the crystal lattice of metallic nanoparticles and decrease E_g of the catalyst in photocatalytic degradation of adsorbed contaminants. If such a photocatalyst can induce the reaction with visible light, it will greatly increase the cost-effectiveness of the operation. In a recent study, it has been reported that NC could act as a major carbon source for nanoparticles encapsulation, which has been used for H_2-enriched syngas production during the catalytic pyrolysis of biomass.[719]

(f) We have discussed the strategies for dye adsorption by NC-based materials in section 5.2. These dye-adsorbed NC can be converted to biochar by pyrolysis (Figure 56). Such biochar can be activated and form new water remediation materials (i.e., activated biochar or activated carbon) for removal of other dye molecules or contaminants through adsorption process. In one interesting study, MB was first adsorbed into CMC, in which the MB-adsorbed CMC was subsequently used for the removal of MO, which shows higher maximum adsorption capacity than those of CMC and unmodified cellulose.[720] Therefore, once used sorbents may also be effective for secondary adsorption, which will greatly improve the remediation performance.

(g) For high-value pollutants, for example, Au, PGM, and rare earth elements (REE), suitable recovery strategies need to be considered. Conventional recovery methods often include the use of a large volume of washing agents and multiple pH adjustments that can have negative environmental consequences.[466] One cost-effective and environmentally friendly approach to recover these materials involves the use of NC to first adsorb these metal ions followed by pyrolysis or incineration of the used adsorbents. In one example study, it has been shown that ashes, produced after burning of metal-laden cellulose-based biosorbent at 850 °C, possessed about 96% of Cu and Ni metal species.[721] Clearly, the same strategy can be used to recover valuable metal nanoparticles from the used NC-based adsorbents. For Pb recovery, it has been shown that the costs of the biosorption−pyrolysis and biosorption−desorption approaches are around $0.06 and $0.19 (using HCl) per ton of wastewater, respectively.[722] However, if one uses EDTA instead of HCl, the cost for the Pb recovery would increase from $0.19 (HCl) to $4.41 (EDTA) per ton of wastewater. Such cost analysis will be very useful for evaluating the feasibility of upcycling post/spent or exhausted NC materials for designing new circular economy solutions.

9. SUMMARY AND OUTLOOK

Although the practical usage of NC for water treatments is only in its infancy, the unique physicochemical properties of NC, such as high surface area, abundant functionalities, nontoxic and biodegradable characters, as well as scaffolding versatility and stability, make it an ideal candidate to enable new, sustainable and low-cost water purification technologies. Today, the major hurdle of applying NC-based materials for water purification is the relatively high cost for mass production of NC. As the current state-of-the-art NC (CNC or CNF) manufacturing processes are mainly based on technologies developed for wood-based biomass (containing a higher amount of lignin), they require intensive consumption of energy, chemicals and water. We believe NC can be produced in a much more cost-effective manner, if one considers (a) the use of underutilized nonwoody biomass plants, which are often considered low and no value, as feedstocks, (b) the low lignin content in these feedstocks can eliminate the pulping process, and (c) the role of surface functionality becomes more important than mechanical proper-

https://doi.org/10.1021/acs.chemrev.1c00683
Chem. Rev. 2022, 122, 8936−9031

ties in extracted NC, that is, the high degree of polymerization is no longer the primary concern for water purification.

Before engineering NC-based materials for varying water technologies, one has to understand the structure−functionality-property relationship thoroughly. With combined characterizations of spectroscopy, high-resolution microscopy and scattering (especially solution SAXS or neutron scattering), it is now possible to analyze the individual NC structure at the nanoscale and also its surface functionality. Such knowledge can help us to understand and design condensed and solid-state properties, such as CNC in the chiral nematic phase and CNF aerogels/films. To this end, new experimental techniques have been developed to further explore the NC structure and property relationship at the molecular level to bridge any knowledge gaps from single particles to assembled aggregates.[187] The fundamental knowledge obtained from varying structure−functionality-property relationship studies in NC is the foundation for the design of high-performing NC-based coagulants/flocculants, adsorbents, photocatalysts and membranes. These studies include the characterizations of amorphous and crystalline phases in NC and surface functionalities (e.g., the type of functional group, surface charge, charge density, etc.), investigation of deformation and flow behavior, as well as mechanical properties.

While we found a growing body of adsorption, photocatalysis, and membrane-based literatures on NC, the study of coagulation/flocculation is still very limited, but we believe the latter subject will be expanding soon. Surface-charged NC (anionic/cationic), by nature, is an anisotropic colloid in the dispersion state. The increase in the charge density of NC-based materials can replace synthetic polyelectrolytes, which are routinely used as coagulants/flocculants in varying kinds of wastewater treatments. However, synthetic coagulants/flocculants are not biodegradable, and often carcinogenic with genotoxic effects.[723,724] The development of NC-based coagulants/flocculants not only can reduce the adverse effects of synthetic polyelectrolytes but also may offer cost-saving benefits. Next, it has been demonstrated that NC-based materials work well as effective adsorbents for the removal of a large range of water pollutants. Studies showed that these materials possess excellent adsorption capabilities and fast kinetics that are often superior to commercial adsorbents. Because of these unique surface adsorption properties, NC materials have been used as effective scaffolds or templates for in situ growth or anchoring of metallic nanoparticles, allowing the creation of new kinds of NC-enabled photocatalysts. Such systems can be used to a degree for a multitude of water pollutants by visible light irradiation. This study, however, is at an early stage, as real wastewater systems can be extraordinarily complicated. For example, degradation of complex aromatic pollutants, such as persistent organic pollutants (POP), using photocatalysts, is often difficult because of the delocalized electron resonance of the aromatic ring. To tackle this problem, we propose the following strategy to design a suitable NC composite system as shown in Figure 58. After the construction of an NC-templated nanoparticle composite, an enzyme (e.g., laccase or other redox enzymes) can be further immobilized in the composite scaffold (Figure 58a). Such an enzyme can be used as a biocatalyst for the ring-opening reaction of POP. After the formation of partially degraded linear molecules, the nanoparticle photocatalyst can be further irradiated by visible light (e.g., LED light) to completely degrade such recalcitrant compounds. Here, NC can act as a support for enzyme

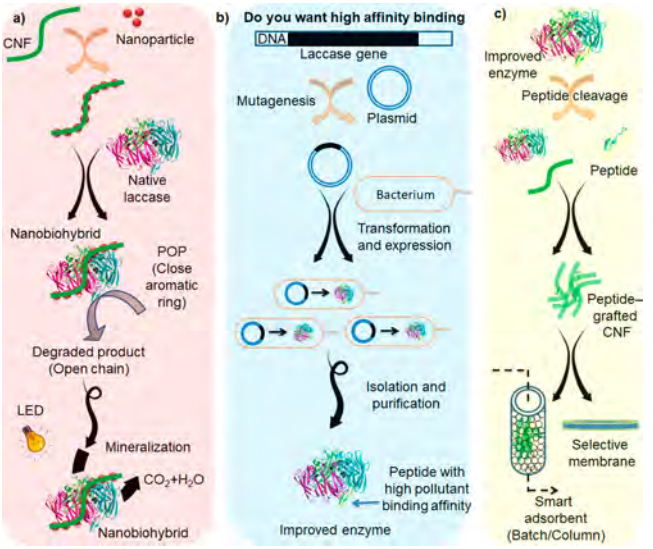

Figure 58. Simplified illustration of some enzyme-based NC technologies to tackle emerging water pollutants. (a) Demonstration of enzyme (e.g., laccase) immobilization on NC-templated nanoparticles for the mineralization of POP (e.g., dichlorodiphenyltrichloroethane, 1,4-dioxane, etc.). (b) Strategy of enzyme engineering through a genetic engineering approach called mutagenesis. (c) Peptide cleavage from an engineered enzyme, which can be grafted onto NC for its integration in batch/column-based adsorption systems and NC-based selective membrane fabrication for water purification.

attachment, which can also allow the enzyme to be recycled. More importantly, one can engineer an enzyme using the biotechnological approach to increase the affinity of interaction with specific pollutants and avoid nonselective adsorption. Furthermore, the engineered enzyme can be produced in large quantity using bacterial culture, which can keep the enzyme production cost at a reasonable level (Figure 58b). It is also possible to isolate the specific peptide sequence from this engineered enzyme, which can be used either in the column type or batch type water treatment conditions (Figure 58c).[466] A membrane can also be designed using a short-peptide sequence, which has shown very promising results for nuclear waste, cyanides and metal ions removal.[716] These areas of research are unexplored and should attract plenty of attention in the future to tackle complex water pollution problems.

Different types of NC-based membranes, such as self-standing, mixed-matrix and TFNC membranes, have been discussed earlier. Although we have highlighted their primary performance parameters, such as water permeability and solutes retention, as well as membrane's strength (wet and dry form), porosity, pore size, and stability in water; there are some notable research gaps in NC-based membranes, especially in the areas of biofouling, mineral scaling, cost-effectiveness, and recyclability. The nature of NC in the form of nanofiber will allow these membranes to carry filtration (size exclusion) and adsorption functions, as well as hosting metallic nanoparticles for photocatalytic reaction.

To deal with multiple pollutants with different physicochemical properties in the water, our current approaches are mainly based on multiple-step modifications to incorporate varying functionalities on the NC surface that can adsorb these pollutants either in a simultaneous or sequential manner. However, there is another approach to tackle the multiple pollutants challenge. It is conceivable, that a responsive NC-

https://doi.org/10.1021/acs.chemrev.1c00683
Chem. Rev. 2022, 122, 8936−9031

based system modified with stimuli molecules can be devised, where its performance (e.g., pore size, porosity, surface charge, hydrophobicity/hydrophilicity) can be controlled by electric field,[725] pH level, temperature, magnetic field, or visible light. For example, using UV/vis light, one can control the rate of wettability,[726] ion permeability,[727,728] nanopore diameter,[729] and surface charge[730] of responsive NC-based materials systems. However, none of these systems have ever been tested for NC-based water purification. This will be another interesting subject that warrants in-depth investigation. Last, but not least, after the remediation of contaminated water, the management of post/spent-NC or composite has seldom been addressed. For practical large scale water treatments, the following strategies should be considered and integrated:

(a) The preparation of NC-based materials should be achieved by simple and low-cost approaches (e.g., coating, doping, casting, solvent evaporation, etc.).
(b) NC's good compatibility with inorganic and organic nanoparticles can allow us to explore performance improvement by having synergetic effects, which may be unattainable by NC or nanoparticles alone.
(c) The abundant surface functionality, such as hydroxyl, carboxyl, and many other functional groups on the extracted or modified NC surface, will permit their further modifications to generate more active sites imperative to trap multiple impurities.
(d) The pore size and porosity of NC-based membranes can be fine-tuned by selecting different building block materials with different dimensions (BNC, CNF, and CNC), concentration and surface properties, as well as processing conditions and membrane design.
(e) The mechanical strengths (dry and wet) of NC-based membranes can be controlled by the aspect ratio of the NC, cross-linking agents, surface functionality, and nanofiller addition.
(f) The fouling tendency of NC-based membranes can be reduced by enhancing the hydrophilicity and charge density of the NC surface layer.

ASSOCIATED CONTENT

Supporting Information

The Supporting Information is available free of charge at https://pubs.acs.org/doi/10.1021/acs.chemrev.1c00683.

Industrial applications of nanocellulose, structure of cellulose, relationships among aspect ratio, volume fraction, and phase formation in NC and its suspensions, aggregation mechanisms for NC coagulation and flocculation, adjusting functionalities of NC to enhance adsorption performance, band-gap energy (E_g) measurement, and other NC-based photocatalysts (PDF)

AUTHOR INFORMATION

Corresponding Authors

Tom Lindström − *Department of Chemistry, Stony Brook University, Stony Brook, New York 11794-3400, United States; KTH Royal Institute of Technology, Stockholm 100 44, Sweden*; Phone: +46-70-6570194; Email: toml@kth.se

Benjamin S. Hsiao − *Department of Chemistry, Stony Brook University, Stony Brook, New York 11794-3400, United States;* orcid.org/0000-0002-3180-1826; Phone: +1-631-632-7793; Email: benjamin.hsiao@stonybrook.edu

Authors

Rasel Das − *Department of Chemistry, Stony Brook University, Stony Brook, New York 11794-3400, United States*

Priyanka R. Sharma − *Department of Chemistry, Stony Brook University, Stony Brook, New York 11794-3400, United States*

Kai Chi − *Department of Chemistry, Stony Brook University, Stony Brook, New York 11794-3400, United States;* orcid.org/0000-0003-3396-8061

Complete contact information is available at: https://pubs.acs.org/10.1021/acs.chemrev.1c00683

Notes

The authors declare no competing financial interest.

Biographies

Dr. Rasel Das is working as a Postdoctoral Associate and Senior Scientist in the Chemistry Department, Stony Brook University, USA. He was a Visiting Researcher and JSPS Postdoctoral Fellow at the Global Innovation Center, Kyushu University, Japan, from 2018 to 2020. He was awarded the Endeavour Research Fellowship at Australian Institute for Bioengineering and Nanotechnology, The University of Queensland, Australia, in 2018. He completed DAAD Postdoctoral Fellowship at the Leibniz-Institute of Surface Engineering, Germany in 2017. His main research interests are on the development, characterization, and applications of functional nanomaterials for water purification.

Prof. Tom Lindström has broad experience in most sectors of the Forest Products Industry. The experience encompasses academic, institutional, and industrial activities. Lindström's scientific and technical interests are the physical and surface science of cellulosic fibers and wood-based materials and physicochemical swelling behavior of cellulose/lignin gels and a long focus has been on various paper chemistries. During the past years, his focus has been on manufacture and upscaling of nanocellulosic materials and various industrial applications of these materials.

Dr. Priyanka Sharma received her Ph.D. in 2014 from CSIR—National Chemical laboratory. In 2015, she joined Stony Brook University as a Postdoctoral Associate in the Department of Chemistry with Prof. Benjamin Hsiao. Currently, she is a Research Assistant Professor in Chemistry at Stony Brook University. Her research interests are in the development of novel sustainable materials for water-purification, environment, and energy related applications and structural characterization of nanocellulose by advanced microscopy and synchrotron techniques.

Dr. Kai Chi received his Ph.D. in Agricultural and Biological Engineering at Pennsylvania State University (University Park) in 2017. His doctoral work was primarily focused on sustainable biopolymers (e.g., nanocellulose, chitin/chitosan, and starch) and their applications in various composite and colloidal systems. He continues as a Postdoctoral Scholar at Penn State and Stony Brook University working on exploiting and valorizing renewable, naturally occurring materials for sustainable packaging, biomedical, and water purification applications. His current research interests include structure−processing−property relationships of biopolymer nanomaterials, natural barrier materials for plastic replacement, and low-cost biomass for water purification.

Prof. Benjamin S. Hsiao is a Distinguished Professor in Chemistry at Stony Brook University. He is the Founding Director of the Center for Integrated Electric Energy Systems with the mission of developing advanced technologies to enhance the nexus of food, energy and water. Hsiao's current research interests are focused on the development of

sustainable nanomaterials from underutilized biomass and natural resources for water purification. He is an elected fellow of AAAS, ACS, APS, MRS, and NAI.

ACKNOWLEDGMENTS

We acknowledge the financial support from the Polymer Program of the Division of Materials Research in the National Science Foundation (DMR-1808690).

REFERENCES

(1) Mekonnen, M. M.; Hoekstra, A. Y. Four Billion People Facing Severe Water Scarcity. *Sci. Adv.* **2016**, *2*, No. e1500323.
(2) News-21. *Troubled Water: News 21 Investigates Drinking Water in America*. https://troubledwater.news21.com/ (accessed 2021-03-01).
(3) Das, R.; Vecitis, C. D.; Schulze, A.; Cao, B.; Ismail, A. F.; Lu, X.; Chen, J.; Ramakrishna, S. Recent Advances in Nanomaterials for Water Protection and Monitoring. *Chem. Soc. Rev.* **2017**, *46*, 6946−7020.
(4) Das, R.; Leo, B. F.; Murphy, F. The Toxic Truth About Carbon Nanotubes in Water Purification: A Perspective View. *Nanoscale Res. Lett.* **2018**, *13*, 183.
(5) Carpenter, A. W.; de Lannoy, C.-F.; Wiesner, M. R. Cellulose Nanomaterials in Water Treatment Technologies. *Environ. Sci. Technol.* **2015**, *49*, 5277−5287.
(6) Hsiao, B. S.; Chu, B.; Sharma, P. R. U.S. Patent 10,894,838, 2021.
(7) Foster, E. J.; Moon, R. J.; Agarwal, U. P.; Bortner, M. J.; Bras, J.; Camarero-Espinosa, S.; Chan, K. J.; Clift, M. J.; Cranston, E. D.; Eichhorn, S. J.; et al. Current Characterization Methods for Cellulose Nanomaterials. *Chem. Soc. Rev.* **2018**, *47*, 2609−2679.
(8) Isogai, A. Emerging Nanocellulose Technologies: Recent Developments. *Adv. Mater.* **2021**, *33*, 2000630.
(9) Hamad, W. Y.; Hu, T. Q. Structure-process-yield Interrelations in Nanocrystalline Cellulose Extraction. *Can. J. Chem. Eng.* **2010**, *88*, 392−402.
(10) Habibi, Y.; Lucia, L. C.; Rojas, O. J. Cellulose Nanocrystal: Chemistry, Self-assembly and Applications. *Chem. Rev.* **2010**, *110*, 3479−3500.
(11) Lin, N.; Huang, J.; Dufresne, A. Preparation, Properties and Applications of Polysaccharide Nanocrystals in Advanced Functional Nanomaterials: A Review. *Nanoscale* **2012**, *4*, 3274−3294.
(12) Peng, B. L.; Dhar, N.; Liu, H. L.; Tam, K. C. Chemistry and Applications of Nanocrystalline Cellulose and Its Derivatives: A Nanotechnology Perspective. *Can. J. Chem. Eng.* **2011**, *89*, 1191−1206.
(13) Sehaqui, H.; Zhou, Q.; Ikkala, O.; Berglund, L. A. Strong and Tough Cellulose Nanopaper with High Specific Surface Area and Porosity. *Biomacromolecules* **2011**, *12*, 3638−3644.
(14) Hua, X.; Laleg, M.; Miles, K.; Amiri, R.; Ettaleb, L.; Dorris, G. U.S. Patents 9,051,684, 2015.
(15) Mahfoudhi, N.; Boufi, S. Nanocellulose as a Novel Nanostructured Adsorbent for Environmental Remediation: A Review. *Cellulose* **2017**, *24*, 1171−1197.
(16) Zhu, H.; Zhang, Y.; Yang, X.; Liu, H.; Zhang, X.; Yao, J. An Eco-friendly One-Step Synthesis of Dicarboxyl Cellulose for Potential Application in Flocculation. *Ind. Eng. Chem. Res.* **2015**, *54*, 2825−2829.
(17) Voisin, H.; Bergström, L.; Liu, P.; Mathew, A. P. Nanocellulose-based Materials for Water Purification. *Nanomaterials* **2017**, *7*, 57.
(18) Sharma, P. R.; Sharma, S. K.; Lindström, T.; Hsiao, B. S. Nanocellulose-Enabled Membranes for Water Purification: Perspectives. *Adv. Sustain. Syst* **2020**, *4*, 1900114.
(19) Ahankari, S.; George, T.; Subhedar, A.; Kar, K. K. Nanocellulose as a Sustainable Material for Water Purification. *SPE Polymers* **2020**, *1*, 69−80.
(20) Tapia-Orozco, N.; Ibarra-Cabrera, R.; Tecante, A.; Gimeno, M.; Parra, R.; Garcia-Arrazola, R. Removal Strategies for Endocrine Disrupting Chemicals using Cellulose-based Materials as Adsorbents: A Review. *J. Environ. Chem. Eng.* **2016**, *4*, 3122−3142.
(21) Mahfoudhi, N.; Boufi, S. Nanocellulose as a Millennium Material with Enhancing Adsorption Capacities. In *Biodegradable and Biobased Polymers for Environmental and Biomedical Applications*; Scrivener Publishing LLC: MA, 2016; p349.
(22) Abouzeid, R. E.; Khiari, R.; El-Wakil, N.; Dufresne, A. Current State and New Trends in the Use of Cellulose Nanomaterials for Wastewater Treatment. *Biomacromolecules* **2019**, *20*, 573−597.
(23) Köse, K.; Mavlan, M.; Youngblood, J. P. Applications and Impact of Nanocellulose based Adsorbents. *Cellulose* **2020**, *27*, 2967−2990.
(24) Mautner, A. Nanocellulose Water Treatment Membranes and Filters: A Review. *Polym. Int.* **2020**, *69*, 741−751.
(25) Tan, H.-F.; Ooi, B. S.; Leo, C. P. Future Perspectives of Nanocellulose-based Membrane for Water Treatment. *J. Water Process. Eng.* **2020**, *37*, 101502.
(26) Yuan, B.; Li, L.; Murugadoss, V.; Vupputuri, S.; Wang, J.; Alikhani, N.; Guo, Z. Nanocellulose-based Composite Materials for Wastewater Treatment and Waste-oil Remediation. *ES Food Agrofor.* **2020**, *1*, 41−52.
(27) Ibrahim, H.; Sazali, N.; Ibrahim, I.; Sharip, M. Nano-structured Cellulose as Green Adsorbents for Water Purification: A Mini Review. *J. Appl. Membrane Sci. Technol.* **2019**, *23*, 45−56.
(28) Wang, D. A Critical Review of Cellulose-based Nanomaterials for Water Purification in Industrial Processes. *Cellulose* **2019**, *26*, 687−701.
(29) Pandey, N.; Shukla, S.; Singh, N. Water Purification by Polymer Nanocomposites: An Overview. *Nanocomposites* **2017**, *3*, 47−66.
(30) Thomas, B.; Raj, M. C.; Joy, J.; Moores, A.; Drisko, G. L.; Sanchez, C.; et al. Nanocellulose, a Versatile Green Platform: from Biosources to Materials and their Applications. *Chem. Rev.* **2018**, *118* (24), 11575−11625.
(31) Ibrahim, H.; Sazali, N.; Salleh, W. N. W.; Zainal Abidin, M. N. A Short Review on Recent Utilization of Nanocellulose for Wastewater Remediation and Gas Separation. *Mater. Today: Proc.* **2021**, *42*, 45−49.
(32) Santos, E. C.; Kaldeus, T.; Senoro, D.; Malmström, E.; Hult, A. Current Cellulose Nanofibrils and Cellulose Nanocrystals as Water Purification Functional Membrane Materials. *J. Environ. Sci. Manag.* **2020**, *1*, 48−64.
(33) Kumar, D. *Nanocellulose and Its Composites for Water Treatment Application*; Taylor & Francis: Boca Raton, FL, 2021; p 230.
(34) Mathew, A. P.; Liu, P.; Karim, Z.; Lai, J. Nanocellulose-Based Membranes for Water Purification: Fundamental Concepts and Scale-Up Potentia. In *Nanocellulose and Sustainability*; CRC Press: Boca Raton, 2018; pp 129−146. DOI: 10.1201/9781351262927-7
(35) Muhamad, I.; Pa'e, N.; Yusof, A. Bacterial Nanocellulose and Its Application in Wastewater Treatment. In *Sustainable Nanocellulose and Nanohydrogels from Natural Sources*; Elsevier: Amsterdam, 2020; p 314.
(36) Wilson, R.; Joy, J.; George, G.; Anuraj, V. Nanocellulose: A Novel Support for Water Purification. In *Advanced Environmental Analysis: Applications of Nanomaterials*; Royal Society of Chemistry: London, 2016; p 534.
(37) Gopakumar, D. A.; Manna, S.; Pasquini, D.; Thomas, S.; Grohens, Y. Nanocellulose: Extraction and Application as a Sustainable Material for Wastewater Purification. In *New Polymer Nanocomposites for Environmental Remediation*; Elsevier: Amsterdam, 2018; p 486.
(38) Yusuf, M. Cellulose-Based Nanomaterials for Water Pollutant Remediation. In *Handbook of Nanomaterials and Nanocomposites for Energy and Environmental Applications*; Springer Nature: Switzerland, 2021; p 228.
(39) Malkoske, T. A.; Bérubé, P. R.; Andrews, R. C. Coagulation/Flocculation Prior to Low Pressure Membranes in Drinking Water Treatment: A Review. *Environ. Sci. Water Res. Technol.* **2020**, *6*, 2993−3023.
(40) Shewa, W. A.; Dagnew, M. Revisiting Chemically Enhanced Primary Treatment of Wastewater: A Review. *Sustainability* **2020**, *12*, 5928.
(41) Lichtenstein, K.; Lavoine, N. Toward a Deeper Understanding of the Thermal Degradation Mechanism of Nanocellulose. *Polym. Degrad. Stab.* **2017**, *146*, 53−60.
(42) Chen, L.; Zhu, J.; Baez, C.; Kitin, P.; Elder, T. Highly Thermal-stable and Functional Cellulose Nanocrystals and Nanofibrils Produced using Fully Recyclable Organic Acids. *Green Chem.* **2016**, *18*, 3835−3843.

https://doi.org/10.1021/acs.chemrev.1c00683
Chem. Rev. 2022, 122, 8936−9031

(43) Fukuzumi, H.; Saito, T.; Okita, Y.; Isogai, A. Thermal Stabilization of TEMPO-oxidized Cellulose. *Polym. Degrad. Stab.* **2010**, *95*, 1502−1508.
(44) Yildirim, N.; Shaler, S. A Study on Thermal and Nanomechanical Performance of Cellulose Nanomaterials (CNs). *Materials* **2017**, *10*, 718.
(45) Karppinen, A. *Temperature Sability of Cellulose Fibrils*, 2018. https://www.exilva.com/blog/temperature-stability-of-cellulose-fibrils (accessed 2022-01-21).
(46) Gan, P.; Sam, S.; Abdullah, M. F. b.; Omar, M. F. Thermal Properties of Nanocellulose-Reinforced Composites: A Review. *J. Appl. Polym. Sci.* **2020**, *137*, 48544.
(47) Heggset, E. B.; Chinga-Carrasco, G.; Syverud, K. Temperature Stability of Nanocellulose Dispersions. *Carbohydr. Polym.* **2017**, *157*, 114−121.
(48) Helenius, G.; Bäckdahl, H.; Bodin, A.; Nannmark, U.; Gatenholm, P.; Risberg, B. *In vivo* biocompatibility of bacterial cellulose. *J. Biomed Mater. Res. A* **2006**, *76*, 431−438.
(49) Miyamoto, T.; Takahashi, S. i.; Ito, H.; Inagaki, H.; Noishiki, Y. Tissue Biocompatibility of Cellulose and Its Derivatives. *J. Biomed. Mater. Res.* **1989**, *23*, 125−133.
(50) Andrade, F. K.; Alexandre, N.; Amorim, I.; Gartner, F.; Maurício, A. C.; Luís, A. L.; Gama, M. Studies on the Biocompatibility of Bacterial Cellulose. *J. Bioact. Compat. Polym.* **2013**, *28*, 97−112.
(51) Leitão, A. F.; Gupta, S.; Silva, J. P.; Reviakine, I.; Gama, M. Hemocompatibility Study of a Bacterial Cellulose/Polyvinyl Alcohol Nanocomposite. *Colloids Surf. B: Biointerfaces* **2013**, *111*, 493−502.
(52) Chen, H.; Huang, J.; Hao, B.; Yang, B.; Chen, S.; Yang, G.; Xu, J. Citrate-based Fluorophore-Modified Cellulose Nanocrystals as a Biocompatible Fluorescent Probe for Detecting Ferric Ions and Intracellular Imaging. *Carbohydr. Polym.* **2019**, *224*, 115198.
(53) Tummala, G. K.; Joffre, T.; Lopes, V. R.; Liszka, A.; Buznyk, O.; Ferraz, N.; Persson, C.; Griffith, M.; Mihranyan, A. Hyperelastic Nanocellulose-reinforced Hydrogel of High Water Content for Ophthalmic Applications. *ACS Biomater. Sci. Eng.* **2016**, *2*, 2072−2079.
(54) Geng, C.-z.; Hu, X.; Yang, G.-h.; Zhang, Q.; Chen, F.; Fu, Q. Mechanically Reinforced Chitosan/Cellulose Nanocrystals Composites with Good Transparency and Biocompatibility. *Chin. J. Polym. Sci.* **2015**, *33*, 61−69.
(55) He, H.; Cheng, M.; Liang, Y.; Zhu, H.; Sun, Y.; Dong, D.; Wang, S. Intelligent Cellulose Nanofibers with Excellent Biocompatibility Enable Sustained Antibacterial and Drug Release via a pH-responsive Mechanism. *J. Agric. Food. Chem.* **2020**, *68*, 3518−3527.
(56) Hua, K.; Carlsson, D. O.; Ålander, E.; Lindström, T.; Strømme, M.; Mihranyan, A.; Ferraz, N. Translational Study between Structure and Bbiological Response of Nanocellulose from Wood and Green Algae. *Rsc Adv.* **2014**, *4*, 2892−2903.
(57) Lindström, T.; Österberg, F. Evolution of Biobased and Nanotechnology Packaging-A Review. *Nord Pulp Paper Res. J.* **2020**, *35*, 491−515.
(58) Hubbe, M. A.; Ferrer, A.; Tyagi, P.; Yin, Y.; Salas, C.; Pal, L.; Rojas, O. J. Nanocellulose in Thin Films, Coatings, and Plies for Packaging Applications: A Review. *BioResources* **2016**, *12*, 2143−2233.
(59) Potivara, K.; Phisalaphong, M. Development and Characterization of Bacterial Cellulose Reinforced with Natural Rubber. *Materials* **2019**, *12*, 2323.
(60) Lin, N.; Dufresne, A. Nanocellulose in Biomedicine: Current Status and Future Prospect. *Eur. Polym. J.* **2014**, *59*, 302−325.
(61) Zinge, C.; Kandasubramanian, B. Nanocellulose Based Biodegradable Polymers. *Eur. Polym. J.* **2020**, *133*, 109758.
(62) Bagde, P.; Nadanathangam, V. Mechanical, Antibacterial and Biodegradable Properties of Starch Film Containing Bacteriocin Immobilized Crystalline Nanocellulose. *Carbohydr. Polym.* **2019**, *222*, 115021.
(63) Islam, N.; Proma, S. J.; Rahman, A.; Chakraborty, A. K. Preparation and Biodegradation of Nanocellulose Reinforced Polyvinyl Alcohol Blend Films in Bioenvironmental Media. *Chem. Sci. Int. J.* **2017**, *19*, 1−8.
(64) Babaee, M.; Jonoobi, M.; Hamzeh, Y.; Ashori, A. Biodegradability and Mechanical Properties of Reinforced Starch Nanocomposites using Cellulose Nanofibers. *Carbohydr. Polym.* **2015**, *132*, 1−8.
(65) Lai, Y.-Z.; Ontto, D. E. Kinetics of Base-catalyzed Degradation of Phenyl D-gluco-pyranosides. *Carbohydr. Res.* **1979**, *75*, 51−59.
(66) Wan, Y.; Luo, H.; He, F.; Liang, H.; Huang, Y.; Li, X. Mechanical, Moisture Absorption, and Biodegradation Behaviours of Bacterial Cellulose Fibre-reinforced Starch Biocomposites. *Compos. Sci. Technol.* **2009**, *69*, 1212−1217.
(67) Hua, K.; Rocha, I.; Zhang, P.; Gustafsson, S.; Ning, Y.; Strømme, M.; Mihranyan, A.; Ferraz, N. Transition from Bioinert to Bioactive Material by Tailoring the Biological Cell Response to Carboxylated Nanocellulose. *Biomacromolecules* **2016**, *17*, 1224−1233.
(68) Chinga-Carrasco, G. Potential and Limitations of Nanocelluloses as Components in Biocomposite Inks for Three-dimensional Bioprinting and for Biomedical Devices. *Biomacromolecules* **2018**, *19*, 701−711.
(69) Moohan, J.; Stewart, S. A.; Espinosa, E.; Rosal, A.; Rodríguez, A.; Larrañeta, E.; Donnelly, R. F.; Domínguez-Robles, J. Cellulose Nanofibers and Other Biopolymers for Biomedical Applications. A Review. *Appl. Sci.* **2020**, *10*, 65.
(70) Klemm, D.; Kramer, F.; Moritz, S.; Lindström, T.; Ankerfors, M.; Gray, D.; Dorris, A. Nanocelluloses: A New Family of Nature-based Materials. *Angew. Chem., Int. Ed.* **2011**, *50*, 5438−5466.
(71) Klemm, D.; Cranston, E. D.; Fischer, D.; Gama, M.; Kedzior, S. A.; Kralisch, D.; Kramer, F.; Kondo, T.; Lindström, T.; Nietzsche, S.; et al. Nanocellulose as a Natural Source for Groundbreaking Applications in Materials Science: Today's State. *Mater. Today* **2018**, *21*, 720−748.
(72) Zhou, S.; Nyholm, L.; Strømme, M.; Wang, Z. Cladophora Cellulose: Unique Biopolymer Nanofibrils for Emerging Energy, Environmental, and Life Science Applications. *Acc. Acc. Chem. Res.* **2019**, *52*, 2232−2243.
(73) Jonoobi, M.; Oladi, R.; Davoudpour, Y.; Oksman, K.; Dufresne, A.; Hamzeh, Y.; Davoodi, R. Different Preparation Methods and Properties of Nanostructured Cellulose from Various Natural Resources and Residues: A Review. *Cellulose* **2015**, *22*, 935−969.
(74) Pires, J. R.; Souza, V. G.; Fernando, A. L. Valorization of Energy Crops as a Source for Nanocellulose Production-current Knowledge and Future Prospects. *Ind. Crops. Prod.* **2019**, *140*, 111642.
(75) Rajinipriya, M.; Nagalakshmaiah, M.; Robert, M.; Elkoun, S. Importance of Agricultural and Industrial Waste in the Field of Nanocellulose and Recent Industrial Developments of Wood based Nanocellulose: A Review. *ACS Sustain. Chem. Eng.* **2018**, *6*, 2807−2828.
(76) Schorning, P. Studies of Sulphite Pulping Without Base. *Faserforsch. Textiltech.* **1957**, *8*, 487−494.
(77) Westmoreland, R. A.; Jefcoat, L. A. Sulfor Dioxide-Ethanol-Water Pulping of Hardwoods. *Chem. Eng. Commun.* **1991**, *104*, 101−115.
(78) Iakovlev, M.; Survase, S.; Hill, L.; Sideri, S.; Rouzinou, S.; Kroff, P.; Pylkkanen, V.; Rutherford, S.; Retsina, T. Pilot Scale Sulfur Dioxide-Ethanol-Water Fractionation of Recycled Wood to Sugars, Bioethanol, Lignin and Lignosulfonates: Carbohydrate Balance. *Bioresour. Technol.* **2020**, *307*, 123240.
(79) Iakovlev, M.; Survase, S.; Segers, P.; Sideri, S.; Rouzinou, S.; Pylkkanen, V.; Retsina, T. Sulfur Dioxide-Ethanol-Water Fractionation Platform for Conversion of Recycled Wood to Sugars, Lignin and Lignosulfonates. *Bioresour. Technol.* **2020**, *300*, 122652.
(80) Iakovlev, M.; van Heiningen, A. Kinetics of Fractionation by SO_2-Ethanol-Water (SEW) Treatment: Understanding the Deconstruction of Spruce Wood Chips. *RSC Adv.* **2012**, *2*, 3057−3068.
(81) Iakovlev, M.; van Heiningen, A. Efficient Fractionation of Spruce by SO_2-Ethanol-Water Treatment: Closed Mass Balances for Carbohydrates and Sulfur. *ChemSusChem* **2012**, *5*, 1625−1637.
(82) Nelson, K.; Retsina, T.; Iakovlev, M.; van Heiningen, A.; Deng, Y.; Shatkin, J. A.; Mulyadi, A. American Process: Production of Low Cost Nanocellulose for Renewable, Advanced Materials Applications.

https://doi.org/10.1021/acs.chemrev.1c00683
Chem. Rev. 2022, 122, 8936−9031

In *Materials Research for Manufacturing*; Springer International Publishing: Switzerland, 2016. pp 267−302.
(83) Turbak, A. F.; Snyder, F. W.; Sandberg, K. R. Microfibrillated Cellulose, A New Cellulose Product: Properties, Uses and Commercial Potential. *J. Appl. Polym. Sci, Appl. Polym. Symp.* **1983**, *37*, 815−827.
(84) Herrick, F. W.; Casebier, R. L.; Hamilton, J. K.; Sandberg, K. R. Microfibrillated Cellulose: Morphology and Accessibility. *J. Appl. Polym. Sci, Appl. Polym. Symp.* **1983**, *37*, 797−813.
(85) Oliaei, E.; Lindén, P. A.; Wu, Q.; Berthold, F.; Berglund, L.; Lindström, T. Microfibrillated Lignocellulose (MFLC) and Nanopaper Films from Unbleached Kraft Softwood Pulp. *Cellulose* **2020**, *27*, 2325−2341.
(86) Trovagunta, R.; Zou, T.; Österberg, M.; Kelley, S. S.; Lavoine, N. Design Strategies, Properties and Applications of Cellulose Nanomaterials-enhanced Products with Residual, Technical or Nanoscale Lignin-A Review. *Carbohydr. Polym.* **2021**, *254*, 117480.
(87) Fernandes Diniz, J. M. B.; Gil, M. H.; Castro, J. A. A. M. Hornification-Its Origin and Interpretation in Wood Pulps. *Wood Sci. Technol.* **2004**, *37*, 489−494.
(88) Nordenström, M. Colloidal Interactions and Arrested Dynamics of Cellulose Nanofibrils: Fibre and Polymer Science, PhD Thesis. KTH Royal Institute of Technology, 2020; p 61. https://www.divaportal.org/smash/record.jsf?pid=diva2%3A1479861&dswid=-1634.
(89) Page, D. H. *Trans. IXth Fund. Res. Symp. Cambridge* **1989**, 1.
(90) Abe, K.; Iwamoto, S.; Yano, H. Obtaining Cellulose Nanofibres with a Uniform Width of 15 nm from Wood. *Biomacromolecules* **2007**, *8*, 3276−3278.
(91) Pääkkö, M.; Ankerfors, M.; Kosonen, H.; Nykänen, A.; Ahola, S.; Österberg, M.; Ruokolainen, J.; Laine, J.; Larsson, P. T.; Ikkala, O.; et al. Enzymatic Hydrolysis Combined with Mechanical Shearing and High-pressure Homogenization for Nanoscale Cellulose Fibrils and Strong Gels. *Biomacromolecules* **2007**, *8*, 1934−1941.
(92) Baati, R.; Magnin, A.; Boufi, S. High Solid Content Production of Nanofibrillar Cellulose via Continuous Extrusion. *ACS Sustain. Chem. Eng.* **2017**, *5*, 2350−2359.
(93) Abdul Khalil, H. P. S.; Bhat, A. H.; Ireana Yusra, A. F. Green Composites from Sustainable Cellulose Nanofibrils: A Review. *Carbohydr. Polym.* **2012**, *87*, 963−979.
(94) Teramoto, Y.; Tanaka, N.; Lee, S.-H.; Endo, T. Pretreatment of Eucalyptus Wood Chips for Enzymatic Saccharification Using Combined Sulfuric Acid-Free Ethanol Cooking and Ball Milling. *Biotechnol. Bioeng.* **2008**, *99*, 75−85.
(95) Zhao, H.-P.; Feng, X.-Q.; Gao, H. Ultrasonic Technique for Extracting Nanofibres from Nature Materials. *Appl. Phys. Lett.* **2007**, *90*, 073112.
(96) Hamid, S. B. A.; Zain, S. K.; Das, R.; Centi, G. Synergic Effect of Tungstophosphoric Acid and Sonication for Rapid Synthesis of Crystalline Nanocellulose. *Carbohydr. Polym.* **2016**, *138*, 349−355.
(97) Kondo, T.; Kose, R.; Naito, H.; Kasai, W. Aqueous Counter Collision using Paired Water Jets as Novel Means of Preparing Bio-nanofibers. *Carbohydr. Polym.* **2014**, *112*, 284−290.
(98) Wang, B.; Sain, M. Isolation of Nanofibers from Soybean Source and their Reinforcing Capability on Synthetic Polymers. *Compos. Sci. Technol.* **2007**, *67*, 2521−2527.
(99) Zheng, H. Production of Fibrillated Cellulose Materials-Effects of Pretreatments and Refining Strategy on Pulp Properties. Master's Thesis, Aalto University, 2014, https://aaltodoc.aalto.fi/handle/123456789/13018.
(100) Uetani, K.; Yano, H. Nanofibrillation of Wood Pulp using a High-speed Blender. *Biomacromolecules* **2011**, *12*, 348−353.
(101) Turbak, A. F.; Snyder, F. W.; Sandberg, K. R. U.S. Patent 4,341,807, 1982.
(102) Isogai, A.; Saito, T.; Fukuzumi, H. TEMPO-oxidized Cellulose Nanofibers. *Nanoscale* **2011**, *3*, 71−85.
(103) Liimatainen, H.; Visanko, M.; Sirviö, J.; Hormi, O. E. O.; Niinimaki, J. Enhancement of the Nanofibrillation of Wood Cellulose Through Sequential Periodate-chlorite Oxidation. *Biomacromolecules* **2012**, *13*, 1592−1597.
(104) Tejado, A.; Alam, M. N.; Antal, M.; Yang, H.; van de Ven, T. G. M. Energy Requirements for the Disintegration of Cellulose Fibers into Cellulose Nanofibers. *Cellulose* **2012**, *19*, 831−842.
(105) Naderi, A.; Koschella, A.; Heinze, T.; Shih, K.-C.; Nieh, M.-P.; Pfeifer, A.; Chang, C.-C.; Erlandsson, J. Sulfoethylated Nanofibrillated Cellulose: Production and Properties. *Carbohydr. Polym.* **2017**, *169*, 515−523.
(106) Wågberg, L.; Decher, G.; Norgren, M.; Lindström, T.; Ankerfors, M.; Axnäs, K. The Build-up of Polyelectrolyte Multilayers of Microfibrillated Cellulose and Cationic Polyelectrolytes. *Langmuir* **2008**, *24*, 784−795.
(107) Olszewska, A.; Eronen, P.; Johansson, L.-S.; Malho, J.-M.; Ankerfors, M.; Lindström, T.; Ruokolainen, J.; Laine, J.; Österberg, M. The Behaviour of Cationic Nanofibrillar Cellulose in Aqueous Media. *Cellulose* **2011**, *18*, 1213−1226.
(108) Sharma, P. R.; Zheng, B.; Sharma, S. K.; Zhan, C.; Wang, R.; Bhatia, S. R.; Hsiao, B. S. High Aspect Ratio Carboxycellulose Nanofibers Prepared by Nitro-oxidation Method and their Nanopaper Properties. *ACS Appl. Nano Mater.* **2018**, *1*, 3969−3980.
(109) Sharma, P. R.; Joshi, R.; Sharma, S. K.; Hsiao, B. S. A Simple Approach to Prepare Carboxycellulose Nanofibers from Untreated Biomass. *Biomacromolecules* **2017**, *18*, 2333−2342.
(110) Geng, L.; Mittal, N.; Zhan, C.; Ansari, F.; Sharma, P. R.; Peng, X.; Hsiao, B. S.; Söderberg, L. D. Understanding the Mechanistic Behavior of Highly Charged Cellulose Nanofibers in Aqueous Systems. *Macromolecules* **2018**, *51*, 1498−1506.
(111) Ghanadpour, M.; Carosio, F.; Larsson, P. T.; Wågberg, L. Phosphorylated Cellulose Nanofibrils: A Renewable Nanomaterial for the Preparation of Intrinsically Flame-retardant Materials. *Biomacromolecules* **2015**, *16*, 3399−3410.
(112) Lindström, T. Aspects on Nanofibrillated Cellulose (NFC) Processing, Rheology and NFC-film Properties. *Curr. Opin. Colloid Interface Sci.* **2017**, *29*, 68−75.
(113) Nickerson, R. F.; Habrle, J. A. Cellulose Intercrystalline Structure. *Ind, Eng. Chem.* **1947**, *39*, 1507−1512.
(114) Ranby, B. *Aqueous Colloidal Solutions of Cellulose Micelles*; Munksgaard Int. Publ. Ltd.: Copenhagen, 1949; Vol. *35*, p 649.
(115) Mukherjee, S.M.; Woods, H.J. X-ray and Electron Microscopy Studies of the Degradation of Cellulose by Sulphuric Acid. *Biochim. Biophys. Acta* **1953**, *10*, 499−511.
(116) Battista, O. A.; Coppick, S.; Howsmon, J. A.; Morehead, F. F.; Sisson, W. A. Level-off Degree of Polymerization. Relation to Polyphase Structure of Cellulose Fibers. *Ind. Eng. Chem.* **1956**, *48*, 333−335.
(117) Battista, O. A. *Microcrystalline Polymer Science*; McGraw-Hill: New York, 1975.
(118) Marchessault, R. H.; Morehead, F. F.; Walter, N. M. Liquid Crystal Systems from Fibrillar Polysaccharides. *Nature* **1959**, *184*, 632−633.
(119) Dong, X. M.; Kimura, T.; Revol, J.-F.; Gray, D. G. Effects of Ionic Strength on the Isotropic-Chiral Nematic Phase Transition of Suspensions of Cellulose Crystallites. *Langmuir* **1996**, *12*, 2076−2082.
(120) Dong, X. M.; Gray, D. G. Effect of Counterions on Ordered Phase Formation in Suspensions of Charged Rodlike Cellulose Crystallites. *Langmuir* **1997**, *13*, 2404−2409.
(121) Vanderfleet, O. M.; Cranston, E. D. Production Routes to Tailor the Performance of Cellulose Nanocrystals. *Nat. Rev. Mater.* **2021**, *6*, 124−144.
(122) Dong, X. M.; Revol, J.-F.; Gray, D. G. Effect of Microcrystallite Prparation Conditions on the Formation of Colloid Crystals of Cellulose. *Cellulose* **1998**, *5*, 19−32.
(123) Bouchard, J.; Méthot, M.; Fraschini, C.; Beck, S. Effect of Oligosaccharide Deposition on the Surface of Cellulose Nanocrystals as a Function of Acid Hydrolysis Temperature. *Cellulose* **2016**, *23*, 3555−3567.
(124) Wang, Q.; Zhao, X.; Zhu, J. Y. Kinetics of Strong Acid Hydrolysis of a Bleached Kraft Pulp for Producing Cellulose Nanocrystals (CNCs). *Ind. Eng. Chem. Res.* **2014**, *53*, 11007−11014.

https://doi.org/10.1021/acs.chemrev.1c00683
Chem. Rev. 2022, 122, 8936−9031

(125) Dong, S.; Bortner, M. J.; Roman, M. Analysis of the Sulfuric Acid Hydrolysis of Wood Pulp for Cellulose Nanocrystal Production: A Central Composite Design Study. *Ind. Crops. Prod.* **2016**, *93*, 76−87.
(126) Sèbe, G.; Ham-Pichavant, F. d. r.; Ibarboure, E.; Koffi, A. L. C.; Tingaut, P. Supramolecular Structure Characterization of Cellulose II Nanowhiskers Produced by Acid Hydrolysis of Cellulose I Substrates. *Biomacromolecules* **2012**, *13*, 570−578.
(127) Xing, L.; Gu, J.; Zhang, W.; Tu, D.; Hu, C. Cellulose I and II Nanocrystals Produced by Sulfuric Acid Hydrolysis of Tetra Pak Cellulose I. *Carbohydr. Polym.* **2018**, *192*, 184−192.
(128) Camarero Espinosa, S.; Kuhnt, T.; Foster, E. J.; Weder, C. Isolation of Thermally Stable Cellulose Nanocrystals by Phosphoric Acid Hydrolysis. *Biomacromolecules* **2013**, *14*, 1223−1230.
(129) Sadeghifar, H.; Filpponen, I.; Clarke, S. P.; Brougham, D. F.; Argyropoulos, D. S. Production of Cellulose Nanocrystals using Hydrobromic Acid and Click Reactions on Their Surface. *J. Mater. Sci.* **2011**, *46*, 7344−7355.
(130) Yu, H.-Y.; Zhang, D.-Z.; Lu, F.-F.; Yao, J. New Approach for Single-step Extraction of Carboxylated Cellulose Nanocrystals for their Use as Adsorbents and Flocculants. *ACS Sustain. Chem. Eng.* **2016**, *4*, 2632−2643.
(131) Leung, A. C.; Hrapovic, S.; Lam, E.; Liu, Y.; Male, K. B.; Mahmoud, K. A.; Luong, J. H. Characteristics and Properties of Carboxylated Cellulose Nanocrystals Prepared from a Novel One-step Procedure. *Small* **2011**, *7*, 302−305.
(132) Henschen, J.; Li, D.; Ek, M. Preparation of Cellulose Nanomaterials via Cellulose Oxalates. *Carbohydr. Polym.* **2019**, *213*, 208−216.
(133) Miao, J.; Yu, Y.; Jiang, Z.; Zhang, L. One-pot Preparation of Hydrophobic Cellulose Nanocrystals in an Ionic Liquid. *Cellulose* **2016**, *23*, 1209−1219.
(134) de Oliveira Barud, H. G.; da Silva, R. R.; da Silva Barud, H.; Tercjak, A.; Gutierrez, J.; Lustri, W. R.; de Oliveira, O. B., Jr.; Ribeiro, S. J. A Multipurpose Natural and Renewable Polymer in Medical Applications: Bacterial Cellulose. *Carbohydr. Polym.* **2016**, *153*, 406−420.
(135) Gallegos, A. M. A.; Herrera Carrera, S.; Parra, R.; Keshavarz, T.; Iqbal, H. M. N. Bacterial Cellulose: A Sustainable Source to Develop Value-added Products-A Review. *BioResources* **2016**, *11*, 5641−5655.
(136) Jozala, A. F.; de Lencastre-Novaes, L. C.; Lopes, A. M.; de Carvalho Santos-Ebinuma, V.; Mazzola, P. G.; Pessoa-Jr, A.; Grotto, D.; Gerenutti, M.; Chaud, M. V. Bacterial Nanocellulose Production and Application: a 10-year Overview. *Appl. Microbiol. Biotechnol.* **2016**, *100*, 2063−2072.
(137) Sharma, P. R.; Chattopadhyay, A.; Sharma, S. K.; Geng, L.; Amiralian, N.; Martin, D.; Hsiao, B. S. Nanocellulose from Spinifex as an Effective Adsorbent to Remove Cadmium (II) from Water. *ACS Sustain. Chem. Eng.* **2018**, *6*, 3279−3290.
(138) Sharma, P. R.; Chattopadhyay, A.; Zhan, C.; Sharma, S. K.; Geng, L.; Hsiao, B. S. Lead Removal from Water using Carboxycellulose Nanofibers Prepared by Nitro-oxidation Method. *Cellulose* **2018**, *25*, 1961−1973.
(139) Sharma, P. R.; Chattopadhyay, A.; Sharma, S. K.; Hsiao, B. S. Efficient Removal of UO_2^{2+} from Water using Carboxycellulose Nanofibers Prepared by the Nitro-oxidation Method. *Ind. Eng. Chem. Res.* **2017**, *56*, 13885−13893.
(140) Rydholm, S. A. *Pulping Processes*; Interscience Publishers: New York, 1965; p 1269.
(141) Bolker, H. I. Delignification by Nitrogen Compounds. Action of Nitrous Acid on Unbleached Sulfate Pulp. *Ind. Eng. Chem. Prod. Res. Dev.* **1965**, *4*, 74−79.
(142) Cox, L.; Worster, H. Assessment of Some Sulfur-free Chemical Pulping Processes. *Tappi Tech Ass Pulp Pap Indus* **1971**, *54*, 18901892.
(143) Samuelson, O.; Sjoeberg, L. Pretreatment of Kraft Pulp with Nitrogen Dioxide/Oxygen before Oxygen Bleaching. *Svensk Papperstidning* **1983**, *86*, r95−r99.
(144) Brink, D. I. Processing Conditions and Properties of Pulps Prepared in Soda Pulping using Nitric oxide-oxygen Pretreatment. *Pulping Conf. Proc. of the Techn. Assoc. of the Pulp and Paper Industry (TAPPI)*; 1980. https://imisrise.tappi.org/TAPPI/Products/.
(145) Brink, D. L. Aspects of an Integrated Nitric Acid Pulping Process. *TAPPI* **1961**, *44*, 256−262.
(146) Galland, S.; Berthold, F.; Prakobna, K.; Berglund, L. A. Holocellulose Nanofibers of High Molar Mass and Small Diameter for High-strength Nanopaper. *Biomacromolecules* **2015**, *16*, 2427−2435.
(147) Yang, X.; Berthold, F.; Berglund, L. A. Preserving Cellulose Structure: Delignified Wood Fibers for Paper Structures of High Strength and Transparency. *Biomacromolecules* **2018**, *19*, 3020−3029.
(148) Yang, X.; Reid, M. S.; Olsén, P.; Berglund, L. A. Eco-friendly Cellulose Nanofibrils Designed by Nature: Effects from Preserving Native State. *ACS Nano* **2020**, *14*, 724−735.
(149) Rapson, W. H. The Role of pH in Bleaching Pulp. *Tappi J.* **1956**, *39*, 284−290.
(150) Suchy, M.; Argyropoulos, D. S. Catalysis and Activation of Oxygen and Peroxide Delignification of Chemical Pulps: A Review. *Tappi J.* **2002**, *1*, 1−18.
(151) Sharma, N.; Bhardwaj, N. K.; Singh, R. B. P. Environmental Issues of Pulp Bleaching and Prospects of Peracetic Acid Pulp Bleaching: A Review. *J. Clean. Prod.* **2020**, *256*, 120338.
(152) Amiralian, N.; Annamalai, P. K.; Memmott, P.; Taran, E.; Schmidt, S.; Martin, D. J. Easily Deconstructed, High Aspect Ratio Cellulose Nanofibres from *Triodia Pungens*; An Abundant Grass of Australia's Arid Zone. *Rsc Adv.* **2015**, *5*, 32124−32132.
(153) Kleppe, P. J. Kraft Pulping. *Tappi* **1970**, *53*, 35−47.
(154) López, F.; Dıaz, M.; Eugenio, M.; Ariza, J.; Rodrıguez, A.; Jiménez, L. Optimization of Hydrogen Peroxide in Totally Chlorine Free Bleaching of Cellulose Pulp from Olive Tree Residues. *Bioresour. Technol.* **2003**, *87*, 255−261.
(155) Marth, D. E. Studies on the Lignin Fraction of Aspenwood Pulps Produced by Sulfite-bisulfite Cooking Liquor Systems. PhD Thesis, Georgia Institute of Technology, 1958. https://smartech.gatech.edu/bitstream/handle/1853/5672/marth_de.pdf.
(156) Matsuki, S.; Kayano, H.; Takada, J.; Kono, H.; Fujisawa, S.; Saito, T.; Isogai, A. Nanocellulose Production via One-Pot Formation of C_2 and C_3 Carboxylate Groups Using Highly Concentrated NaClO Aqueous Solution. *ACS Sustain. Chem. Eng.* **2020**, *8*, 17800−17806.
(157) Li, Q.; McGinnis, S.; Sydnor, C.; Wong, A.; Renneckar, S. Nanocellulose Life Cycle Assessment. *ACS Sustain. Chem. Eng.* **2013**, *1*, 919−928.
(158) Hervy, M.; Evangelisti, S.; Lettieri, P.; Lee, K.-Y. Life Cycle Assessment of Nanocellulose-Reinforced Advanced Fibre Composites. *Compos. Sci. Technol.* **2015**, *118*, 154−162.
(159) Foroughi, F.; Rezvani Ghomi, E.; Morshedi Dehaghi, F.; Borayek, R.; Ramakrishna, S. A Review on the Life Cycle Assessment of Cellulose: From Properties to the Potential of Making It a Low Carbon Material. *Materials* **2021**, *14*, 714.
(160) Piccinno, F.; Hischier, R.; Seeger, S.; Som, C. Predicting the Environmental Impact of a Future Nanocellulose Production at Industrial Scale: Application of the Life Cycle Assessment Scale-up Framework. *J. Clean. Prod.* **2018**, *174*, 283−295.
(161) Balea, A.; Blanco, A.; Delgado-Aguilar, M.; Monte, M. C.; Tarres, Q.; Fuente, E.; Mutje, P.; Negro, C. Nanocellulose Characterization Challenges. *BioResources* **2021**, *16*, 4382−4410.
(162) Desmaisons, J.; Boutonnet, E.; Rueff, M.; Dufresne, A.; Bras, J. A New Quality Index for Benchmarking of Different Cellulose Nanofibrils. *Carbohydr. Polym.* **2017**, *174*, 318−329.
(163) Kangas, H.; Lahtinen, P.; Sneck, A.; Saariaho, A.-M.; Laitinen, O.; Hellén, E. Characterization of Fibrillated Celluloses. A Short Review and Evaluation of Characteristics with a Combination of Methods. *Nord Pulp Paper Res. J.* **2014**, *29*, 129−143.
(164) Kovacs, T.; Naish, V.; O'Connor, B.; Blaise, C.; Gagné, F.; Hall, L.; Trudeau, V.; Martel, P. An Ecotoxicological Characterization of Nanocrystalline Cellulose (NCC). *Nanotoxicology* **2010**, *4*, 255−270.
(165) Endes, C.; Camarero-Espinosa, S.; Mueller, S.; Foster, E.; Petri-Fink, A.; Rothen-Rutishauser, B.; Weder, C.; Clift, M. A Critical Review of the Current Knowledge Regarding the Biological Impact of Nanocellulose. *J. Nanobiotechnology* **2016**, *14*, 78.

https://doi.org/10.1021/acs.chemrev.1c00683
Chem. Rev. 2022, 122, 8936−9031

(166) Sinquefield, S.; Ciesielski, P. N.; Li, K.; Gardner, D. J.; Ozcan, S. Nanocellulose Dewatering and Drying: Current State and Future Perspectives. *ACS Sustain. Chem. Eng.* **2020**, *8*, 9601−9615.
(167) De France, K.; Zeng, Z.; Wu, T.; Nyström, G. Functional Materials from Nanocellulose: Utilizing Structure-property Relationships in Bottom-up Fabrication. *Adv. Mater.* **2021**, *33*, 2000657.
(168) Kádár, R.; Spirk, S.; Nypelö, T. Cellulose Nanocrystal Liquid Crystal Phases: Progress and Challenges in Characterization Using Rheology Coupled to Optics, Scattering, and Spectroscopy. *ACS Nano* **2021**, *15*, 7931−7945.
(169) Li, K.; Clarkson, C. M.; Wang, L.; Liu, Y.; Lamm, M.; Pang, Z.; Zhou, Y.; Qian, J.; Tajvidi, M.; Gardner, D. J.; et al. Alignment of Cellulose Nanofibers: Harnessing Nanoscale Properties to Macroscale Benefits. *ACS Nano* **2021**, *15*, 3646−3673.
(170) Prathapan, R.; Tabor, R. F.; Garnier, G.; Hu, J. Recent Progress in Cellulose Nanocrystal Alignment and Its Applications. *ACS Appl. Bio Mater.* **2020**, *3*, 1828−1844.
(171) Glasser, W. G.; Atalla, R. H.; Blackwell, J.; Malcolm Brown, R.; Burchard, W.; French, A. D.; Klemm, D. O.; Nishiyama, Y. About the Structure of Cellulose: Debating the Lindman Hypothesis. *Cellulose* **2012**, *19*, 589−598.
(172) Rosén, T.; He, H.; Wang, R.; Zhan, C.; Chodankar, S.; Fall, A.; Aulin, C.; Larsson, P. T.; Lindstrom, T.; Hsiao, B. S. Cross-sections of Nanocellulose from Wood Analyzed by Quantized Polydispersity of Elementary Microfibrils. *ACS Nano* **2020**, *14*, 16743−16754.
(173) Fahlén, J.; Salmén, L. Pore and Matrix Distribution in the Fiber Wall Revealed by Atomic Force Microscopy and Image Analysis. *Biomacromolecus* **2005**, *6*, 433−438.
(174) Bardage, S.; Donaldson, L.; Tokoh, C.; Daniel, G. Ultrastructure of the Cell Wall of Unbeaten Norway Spruce Pulp Fibre Surfaces. *Nordic Pulp & Paper Res, J.* **2004**, *19*, 448−452.
(175) Donaldson, L. Cellulose Microfibril Aggregates and their Size Variation with Cell Wall Type. *Wood Sci. Technol.* **2007**, *41*, 443−460.
(176) Thomas, L. H.; Forsyth, V. T.; Martel, A.; Grillo, I.; Altaner, C. M.; Jarvis, M. C. Structure and Spacing of Cellulose Microfibrils in Woody Cell Walls of Dicots. *Cellulose* **2014**, *21*, 3887−3895.
(177) Chi, K.; Catchmark, J. M. The Influences of Added Polysaccharides on the Properties of Bacterial Crystalline Nanocellulose. *Nanoscale* **2017**, *9*, 15144−15158.
(178) Sarkar, P.; Bosneaga, E.; Auer, M. Plant Cell Walls Throughout Evolution: Towards a Molecular Understanding of their Design Principles. *J. Exp. Bot.* **2009**, *60*, 3615−3635.
(179) Park, S.; Baker, J. O.; Himmel, M. E.; Parilla, P. A.; Johnson, D. K. Cellulose Crystallinity Index: Measurement Techniques and Their Impact on Interpreting Cellulase Performance. *Biotechnol. Biofuels* **2010**, *3*, 10.
(180) Kim, S. H.; Lee, C. M.; Kafle, K. Characterization of Crystalline Cellulose in Biomass: Basic Principles, Applications, and Limitations of XRD, NMR, IR, Raman, and SFG. *Korean J. Chem. Eng.* **2013**, *30*, 2127−2141.
(181) Scallan, A. A Quantitative Picture of the Fringed Micellar Model of Cellulose. *Text. Res. J.* **1971**, *41*, 647−653.
(182) Atalla, R. H.; Isogai, A. *Cellulose in Comprehensive Natural Products II*; Elsevier Science: USA, 2010.
(183) Heise, K.; Kontturi, E.; Allahverdiyeva, Y.; Tammelin, T.; Linder, M. B.; Ikkala, O.; et al. Nanocellulose: Recent Fundamental Advances and Emerging Biological and Biomimicking Applications. *Adv. Mater.* **2021**, *33*, 2004349.
(184) Nishiyama, Y.; Kim, U.-J.; Kim, D.-Y.; Katsumata, K. S.; May, R. P.; Langan, P. Periodic Disorder along Ramie Cellulose Microfibrils. *Biomacromolecules* **2003**, *4*, 1013−1017.
(185) Fernandes, A. N.; Thomas, L. H.; Altaner, C. M.; Callow, P.; Forsyth, V. T.; Apperley, D. C.; Kennedy, C. J.; Jarvis, M. C. Nanostructure of Cellulose Microfibrils in Spruce Wood. *Proc. Natl. Acad. Sci. U S A* **2011**, *108*, E1195−E1203.
(186) Jarvis, M. C. Structure of Native Cellulose Microfibrils, the Starting Point for Nanocellulose Manufacture. *Philos. Trans. A Math. Phys. Eng. Sci.* **2018**, *376*, 20170045.
(187) Usov, I.; Nystrom, G.; Adamcik, J.; Handschin, S.; Schutz, C.; Fall, A.; Bergstrom, L.; Mezzenga, R. Understanding Nanocellulose Chirality and Structure-properties Relationship at the Single Fibril Level. *Nat. Commun.* **2015**, *6*, 7564.
(188) Nishiyama, Y. Structure and Properties of the Cellulose Microfibril. *J. Wood Sci.* **2009**, *55*, 241−249.
(189) Iotti, M.; Gregersen, Ø. W.; Moe, S.; Lenes, M. Rheological Studies of Microfibrillar Cellulose Water Dispersions. *J. Polym. Environ.* **2011**, *19*, 137−145.
(190) Naderi, A. Nanofibrillated Cellulose: Properties Reinvestigated. *Cellulose* **2017**, *24*, 1933−1945.
(191) Nechyporchuk, O.; Belgacem, M. N.; Pignon, F. Current Progress in Rheology of Cellulose Nanofibril Suspensions. *Biomacromolecules* **2016**, *17*, 2311−2320.
(192) Gong, G. Rheological Properties of Nanocellulose Materials. In *Handbook of Green Materials*; World Scientific: Singapore, 2014; p157.
(193) Saarinen, T.; Haavisto, S.; Sorvari, A.; Salmela, J.; Seppälä, J. The Effect of Wall Depletion on the Rheology of Microfibrillated Cellulose Water Suspensions by Optical Coherence Tomography. *Cellulose* **2014**, *21*, 1261−1275.
(194) Saarinen, T.; Lille, M.; Seppälä, J. Technical Aspects on Rheological Characterization of Microfibrillar Cellulose Water Suspensions. *Ann. Trans. of the Rheological Society* **2009**, *17*, 121−128.
(195) Naderi, A.; Lindström, T. Rheological Measurements on Nanofibrillated Cellulose Systems: A Science in Progress. In *Cellulose and Cellulose Derivatives*; Nova Science Publishers: New York, 2015; p 565.
(196) Nechyporchuk, O.; Belgacem, M. N.; Pignon, F. Rheological Properties of Micro-/Nanofibrillated Cellulose Suspensions: Wall-slip and Shear Banding Phenomena. *Carbohydr. Polym.* **2014**, *112*, 432−439.
(197) Karppinen, A.; Saarinen, T.; Salmela, J.; Laukkanen, A.; Nuopponen, M.; Seppälä, J. Flocculation of Microfibrillated Cellulose in Shear Flow. *Cellulose* **2012**, *19*, 1807−1819.
(198) Martoia, F.; Perge, C.; Dumont, P. J. J.; Orgéas, L.; Fardin, M. A.; Manneville, S.; Belgacem, M. N. Heterogenous Flow Kinematics of Cellulose Nanofibril Suspensions Under Shear. *Soft Matter* **2015**, *11*, 4742−4755.
(199) Fall, A. B.; Lindstrom, S. B.; Sundman, O.; Odberg, L.; Wagberg, L. Colloidal Stability of Aqueous Nanofibrillated Cellulose Dispersions. *Langmuir* **2011**, *27*, 11332−11338.
(200) Naderi, A.; Lindström, T.; Sundström, J. Carboxymethylated Nanofibrillated Cellulose: Rheological Studies. *Cellulose* **2014**, *21*, 1561−1571.
(201) Tatsumi, D.; Ishioka, S.; Matsumoto, T. Effect of Fibre Concenbtration and Axial Ratio on the Rheological Properties of Cellulose Fibre Suspensions. *J. of Soc. Rheol., Japan* **2002**, *30*, 27−32.
(202) Lasseuguette, E.; Roux, D.; Nishiyama, Y. Rheological Properties of Microfibrillar Suspension of TEMPO-oxidized Pulp. *Cellulose* **2008**, *15*, 425−433.
(203) de Gennes, P.-G. *Scaling Concepts in Polymer Physics*; Cornell University Press: Ithaca, NY, 1979.
(204) MacKintosh, F. C.; Kas, J.; Janmey, P. A. Elasticity of Semiflexible Biopolymer Networks. *Phys. Rev. Lett.* **1995**, *75*, 4425−4429.
(205) Naderi, A.; Lindström, T.; Pettersson, T. The State of Carboxymethylated Nanofibrils After Homogenization-aided Dilution from Concentrated Suspensions: A Rheological Perspective. *Cellulose* **2014**, *21*, 2357−2368.
(206) Hill, R. J. Elastic Modulus of Microfibrillar Cellulose Gels. *Biomacromolecules* **2008**, *9*, 2963−2966.
(207) Jowkarderis, L.; van de Ven, T. G. Rheology of Semi-dilute Suspensions of Carboxylated Cellulose Nanofibrils. *Carbohydr. Polym.* **2015**, *123*, 416−423.
(208) Tanaka, R.; Saito, T.; Ishii, D.; Isogai, A. Determination of Nanocellulose Fibril Length by Shear Viscosity Measurement. *Cellulose* **2014**, *21*, 1581−1589.

https://doi.org/10.1021/acs.chemrev.1c00683
Chem. Rev. 2022, 122, 8936−9031

(209) Jowkarderis, L.; van de Ven, T. G. M. Intrinsic Viscosity of Aqueous Suspensions of Cellulose Nanofibrils. *Cellulose* **2014**, *21*, 2511−2517.
(210) Iwamoto, S.; Lee, S.-H.; Endo, T. Relationship between Aspect Ratio and Suspension Viscosity of Wood Cellulose Nanofibers. *Polymer J.* **2014**, *46*, 73−76.
(211) Rosen, T.; Mittal, N.; Roth, S. V.; Zhang, P.; Lundell, F.; Soderberg, L. D. Flow Fields Control Nanostructural Organization in Semiflexible Networks. *Soft Matter* **2020**, *16*, 5439−5449.
(212) Peng, B.; Tang, J.; Wang, P.; Luo, J.; Xiao, P.; Lin, Y.; Tam, K. C. Rheological Properties of Cellulose Nanocrystal-polymeric Systems. *Cellulose* **2018**, *25*, 3229−3240.
(213) Boluk, Y.; Lahiji, R.; Zhao, L.; McDermott, M. T. Suspension Viscosities and Shape Parameter of Cellulose Nanocrystals (CNC). *Colloids Surf. A: Physicochem. Eng. Asp.* **2011**, *377*, 297−303.
(214) Oguzlu, H.; Danumah, C.; Boluk, Y. Colloidal Behavior of Aqueous Cellulose Nanocrystal Suspensions. *Curr. Opin. Colloid Interface Sci.* **2017**, *29*, 46−56.
(215) Phan-Xuan, T.; Thuresson, A.; Skepö, M.; Labrador, A.; Bordes, R.; Matic, A. Aggregation Behavior of Aqueous Cellulose Nanocrystals: The Effect of Inorganic Salts. *Cellulose* **2016**, *23*, 3653−3663.
(216) Onsager, L. The Effects of Shape on the Interaction of Colloidal Particles. *Ann. N.Y. Acad. Sci.* **1949**, *51*, 627−659.
(217) Flory, P. J. Phase Equilibria in Solutions of Rod-like Particles. *Proc. R. Soc. London, A Math. Phys. Sci.* **1956**, *234*, 73−89.
(218) Stroobants, A.; Lekkerkerker, H. N. W.; Odijk, T. Effect of Electrostatic Interaction on the Liquid Crystal Phase Transition in Solutions of Rodlike Polyelectrolytes. *Macromolecules* **1986**, *19*, 2232−2238.
(219) Odijk, T. Theory of Lyotropic Polymer Liquid Crystals. *Macromolecules* **1986**, *19*, 2313−2329.
(220) Hu, Z.; Cranston, E. D.; Ng, R.; Pelton, R. Tuning Cellulose Nanocrystal Gelation with Polysaccharides and Surfactants. *Langmuir* **2014**, *30*, 2684−2692.
(221) Shafeiei-Sabet, S.; Hamad, W. Y.; Hatzikiriakos, S. G. Influence of Degree of Sulfation on the Rheology of Cellulose Nanocrystal Suspensions. *Rheol. Acta* **2013**, *52*, 741−751.
(222) Shafiei-Sabet, S.; Hamad, W. Y.; Hatzikiriakos, S. G. Rheology of Nanocrystalline Cellulose Aqueous Suspensions. *Langmuir* **2012**, *28*, 17124−17133.
(223) Shafiei-Sabet, S.; Hamad, W. Y.; Hatzikiriakos, S. G. Ionic Strength Effects on the Microstructure and Shear Rheology of Cellulose Nanocrystal Suspensions. *Cellulose* **2014**, *21*, 3347−3359.
(224) Ureña-Benavides, E. E.; Ao, G.; Davis, V. A.; Kitchens, C. L. Rheology and Phase Behavior of Lyotropic Cellulose Nanocrystal Suspensions. *Macromolecules* **2011**, *44*, 8990−8998.
(225) Tjipto-Margo, B.; Evans, G. T. The Onsager Theory of the Isotropic-nematic Liquid Crystal Transition: Incorporation of the Higher Virial Coefficients. *J. Chem. Phys.* **1990**, *93*, 4254−4265.
(226) Saito, T.; Uematsu, T.; Kimura, S.; Enomae, T.; Isogai, A. Self-aligned Integration of Native Cellulose Nanofibrils Towards Producing Diverse Bulk Materials. *Soft Matter* **2011**, *7*, 8804−8809.
(227) Zhao, M.; Ansari, F.; Takeuchi, M.; Shimizu, M.; Saito, T.; Berglund, L. A.; Isogai, A. Nematic Structuring of Transparent and Multifunctional Nanocellulose Papers. *Nanoscale Horiz.* **2018**, *3*, 28−34.
(228) Nordenstrom, M.; Fall, A.; Nystrom, G.; Wagberg, L. Formation of Colloidal Nanocellulose Glasses and Gels. *Langmuir* **2017**, *33*, 9772−9780.
(229) Tanaka, H.; Meunier, J.; Bonn, D. Nonergodic States of Charged Colloidal Suspensions: Repulsive and Attractive Glasses and Gels. *Phys. Rev. E Stat. Nonlin. Soft. Matter. Phys.* **2004**, *69*, 031404.
(230) Appel, J.; Folker, B.; Sprakel, J. Mechanics at the Glass-to-gel Transition of Thermoresponsive Microgel Suspensions. *Soft Matter* **2016**, *12*, 2515−2522.
(231) Sluiter, A.; Hames, B.; Ruiz, R.; Scarlata, C.; Sluiter, J.; Templeton, D.; Crocker, D. *Determination of Structural Carbohydrates and Lignin in Biomass*, Laboratory Analytical Procedure; NREL, 2008; pp 1−16
(232) Sluiter, A.; Ruiz, R.; Scarlata, C.; Sluiter, J.; Templeton, D. *Determination of Extractives in Biomass*, Laboratory Analytical Procedure; National Renewable Energy Laboratory; Golden, CO, USA, 2008. https://www.nrel.gov/docs/gen/fy08/42619.pdf.
(233) Sluiter, A.; Sluiter, J.; Wolfrum, E. J. Methods for biomass compositional analysis. *Procedings of Catalysis for the Conversion of Biomass and Its Derivatives*, 2013. https://www.mprlseries.mpg.de/proceedings/2/9/.
(234) Daicho, K.; Saito, T.; Fujisawa, S.; Isogai, A. The Crystallinity of Nanocellulose: Dispersion-induced Disordering of the Grain Boundary in Biologically Structured Cellulose. *ACS Appl. Nano Mater.* **2018**, *1*, 5774−5785.
(235) Nakamura, Y.; Ono, Y.; Saito, T.; Isogai, A. Characterization of Cellulose Microfibrils, Cellulose Molecules, and Hemicelluloses in Buckwheat and Rice Husks. *Cellulose* **2019**, *26*, 6529−6541.
(236) Reid, M. S.; Villalobos, M.; Cranston, E. D. Benchmarking Cellulose Nanocrystals: from the Laboratory to Industrial Production. *Langmuir* **2017**, *33*, 1583−1598.
(237) Vanderfleet, O. M.; Reid, M. S.; Bras, J.; Heux, L.; Godoy-Vargas, J.; Panga, M. K.; Cranston, E. D. Insight into Thermal Stability of Cellulose Nanocrystals from New Hydrolysis Methods with Acid Blends. *Cellulose* **2019**, *26*, 507−528.
(238) Schenker, M.; Schoelkopf, J.; Gane, P.; Mangin, P. Rheology of Microfibrillated Cellulose (MFC) Suspensions: Influence of the Degree of Fibrillation and Residual Fibre Content on Flow and Viscoelastic Properties. *Cellulose* **2019**, *26*, 845−860.
(239) Lin, N.; Dufresne, A. Surface Chemistry, Morphological Analysis and Properties of Cellulose Nanocrystals with Gradiented Sulfation Degrees. *Nanoscale* **2014**, *6*, 5384−5393.
(240) Delepierre, G.; Heise, K.; Malinen, K.; Koso, T.; Pitkänen, L.; Cranston, E. D.; Kilpeläinen, I.; Kostiainen, M. A.; Kontturi, E.; Weder, C.; et al. Challenges in Synthesis and Analysis of Asymmetrically Grafted Cellulose Nanocrystals via Atom Transfer Radical Polymerization. *Biomacromolecules* **2021**, *22*, 2702−2717.
(241) Heise, K.; Delepierre, G.; King, A. W.; Kostiainen, M. A.; Zoppe, J.; Weder, C.; Kontturi, E. Chemical Modification of Reducing End-groups in Cellulose Nanocrystals. *Angew. Chem., Int. Ed.* **2021**, *60*, 66−87.
(242) Tao, H.; Lavoine, N.; Jiang, F.; Tang, J.; Lin, N. Reducing End Modification on Cellulose Nanocrystals: Strategy, Characterization, Applications and Challenges. *Nanoscale Horiz.* **2020**, *5*, 607−627.
(243) Villares, A.; Moreau, C.; Cathala, B. Star-like Supramolecular Complexes of Reducing-end-Functionalized Cellulose Nanocrystals. *ACS Omega* **2018**, *3*, 16203−16211.
(244) Lin, F.; Putaux, J.-L.; Jean, B. Optimized Reducing-end Labeling of Cellulose Nanocrystals: Implication for the Structure of Microfibril Bundles in Plant Cell Walls. *Carbohydr. Polym.* **2021**, *257*, 117618.
(245) Imlimthan, S.; Otaru, S.; Keinänen, O.; Correia, A.; Lintinen, K.; Santos, H. l. A.; Airaksinen, A. J.; Kostiainen, M. A.; Sarparanta, M. Radiolabeled Molecular Imaging Probes for the *In vivo* Evaluation of Cellulose Nanocrystals for Biomedical Applications. *Biomacromolecules* **2019**, *20*, 674−683.
(246) Peng, Y.; Gardner, D. J.; Han, Y.; Kiziltas, A.; Cai, Z.; Tshabalala, M. A. Influence of Drying Method on the Material Properties of Nanocellulose I: Thermostability and Crystallinity. *Cellulose* **2013**, *20*, 2379−2392.
(247) Zhu, J.; Agarwal, U. P.; Ciesielski, P. N.; Himmel, M. E.; Gao, R.; Deng, Y.; Morits, M.; Österberg, M. Towards Sustainable Production and Utilization of Plant-biomass-based Nanomaterials: A Review and Analysis of Recent Developments. *Biotechnol. Biofuels.* **2021**, *14*, 114.
(248) Bushell, M.; Meija, J.; Chen, M.; Batchelor, W.; Browne, C.; Cho, J.-Y.; Clifford, C. A.; Al-Rekabi, Z.; Vanderfleet, O. M.; Cranston, E. D.; et al. Particle Size Distributions for Cellulose Nanocrystals Measured by Atomic Force Microscopy: An Interlaboratory Comparison. *Cellulose* **2021**, *28*, 1387−1403.
(249) Meija, J.; Bushell, M.; Couillard, M.; Beck, S.; Bonevich, J.; Cui, K.; Foster, J.; Will, J.; Fox, D.; Cho, W.; et al. Particle Size Distributions for Cellulose Nanocrystals Measured by Transmission Electron

https://doi.org/10.1021/acs.chemrev.1c00683
Chem. Rev. 2022, 122, 8936−9031

Microscopy: An Interlaboratory Comparison. *Anal. Chem.* **2020**, *92*, 13434−13442.
(250) Yucel, S.; Moon, R. J.; Johnston, L. J.; Yucel, B.; Kalidindi, S. R. Semi-automatic Image Analysis of Particle Morphology of Cellulose Nanocrystals. *Cellulose* **2021**, *28*, 2183−2201.
(251) Chen, M.; Parot, J.; Hackley, V. A.; Zou, S.; Johnston, L. J. AFM Characterization of Cellulose Nanocrystal Height and Width using Internal Calibration Standards. *Cellulose* **2021**, *28*, 1933−1946.
(252) Ang, S.; Narayanan, J. R.; Kargupta, W.; Haritos, V.; Batchelor, W. Cellulose Nanofiber Diameter Distributions from Microscopy Image Analysis: Effect of Measurement Statistics and Operator. *Cellulose* **2020**, *27*, 4189−4208.
(253) Campano, C.; Balea, A.; Blanco, Á.; Negro, C. A Reproducible Method to Characterize the Bulk Morphology of Cellulose Nanocrystals and Nanofibers by Transmission Electron Microscopy. *Cellulose* **2020**, *27*, 4871−4887.
(254) Liao, J.; Pham, K. A.; Breedveld, V. Rheological Characterization and Modeling of Cellulose Nanocrystal and TEMPO-oxidized Cellulose Nanofibril Suspensions. *Cellulose* **2020**, *27*, 3741−3757.
(255) Liao, J.; Pham, K. A.; Breedveld, V. TEMPO-CNF Suspensions in the Viscoelastic Regime: Capturing the Effect of Morphology and Surface Charge with a Rheological Parameter. *Cellulose* **2021**, *28*, 813−827.
(256) del Cerro, D. R.; Koso, T. V.; Kakko, T.; King, A. W.; Kilpeläinen, I. Crystallinity Reduction and Enhancement in the Chemical Reactivity of Cellulose by Non-dissolving Pre-treatment with Tetrabutylphosphonium Acetate. *Cellulose* **2020**, *27*, 5545−5562.
(257) Yao, W.; Weng, Y.; Catchmark, J. M. Improved Cellulose X-ray Diffraction Analysis using Fourier Series Modeling. *Cellulose* **2020**, *27*, 5563−5579.
(258) French, A. D. Increment in evolution of cellulose crystallinity analysis. *Cellulose* **2020**, *27*, 5445−5448.
(259) Wang, H.; Tsuchikawa, S.; Inagaki, T. Terahertz Time-domain Spectroscopy as a Novel Tool for Crystallographic Analysis in Cellulose: the Potentiality of Being a New Standard for Evaluating Crystallinity. *Cellulose* **2021**, *28*, 5293−5304.
(260) Zhu, Q.; Yao, Q.; Sun, J.; Chen, H.; Xu, W.; Liu, J.; Wang, Q. Stimuli Induced Cellulose Nanomaterials Alignment and Its Emerging Applications: A Review. *Carbohydr. Polym.* **2020**, *230*, 115609.
(261) Chowdhury, R. A.; Peng, S. X.; Youngblood, J. Improved Order Parameter (alignment) Determination in Cellulose Nanocrystal (CNC) Films by a Simple Optical Birefringence Method. *Cellulose* **2017**, *24*, 1957−1970.
(262) Chae, I.; Bokhari, S. M.; Chen, X.; Zu, R.; Liu, K.; Borhan, A.; Gopalan, V.; Catchmark, J. M.; Kim, S. H. Shear-induced Unidirectional Deposition of Bacterial Cellulose Microfibrils using Rising Bubble Stream Cultivation. *Carbohydr. Polym.* **2021**, *255*, 117328.
(263) Delepierre, G.; Eyley, S.; Thielemans, W.; Weder, C.; Cranston, E. D.; Zoppe, J. O. Patience is a Virtue: Self-assembly and Physicochemical Properties of Cellulose Nanocrystal Allomorphs. *Nanoscale* **2020**, *12*, 17480−17493.
(264) Xiong, R.; Singh, A.; Yu, S.; Zhang, S.; Lee, H.; Yingling, Y. G.; Nepal, D.; Bunning, T. J.; Tsukruk, V. V. Co-assembling Polysaccharide Nanocrystals and Nanofibers for Robust Chiral Iridescent Films. *ACS Appl. Mater. Interfaces.* **2020**, *12*, 35345−35353.
(265) Xiong, R.; Luan, J.; Kang, S.; Ye, C.; Singamaneni, S.; Tsukruk, V. V. Biopolymeric Photonic Structures: Design, Fabrication, and Emerging Applications. *Chem. Soc. Rev.* **2020**, *49*, 983−1031.
(266) Cheng, G.; Zhang, X.; Simmons, B.; Singh, S. Theory, Practice and Prospects of X-ray and Neutron Scattering for Lignocellulosic Biomass Characterization: Towards Understanding Biomass Pretreatment. *Energy Environ. Sci.* **2015**, *8*, 436−455.
(267) Chu, B.; Hsiao, B. S. Small-angle X-ray Scattering of Polymers. *Chem. Rev.* **2001**, *101*, 1727−1762.
(268) De France, K. J.; Yager, K. G.; Hoare, T.; Cranston, E. D. Cooperative Ordering and Kinetics of Cellulose Nanocrystal Alignment in a Magnetic Field. *Langmuir* **2016**, *32*, 7564−7571.
(269) Håkansson, K. M. Online Determination of Anisotropy During Cellulose Nanofibril Assembly in a Flow Focusing Device. *Rsc Adv.* **2015**, *5*, 18601−18608.
(270) Mao, Y.; Liu, K.; Zhan, C.; Geng, L.; Chu, B.; Hsiao, B. S. Characterization of Nanocellulose using Small-angle Neutron, X-ray, and Dynamic Light Scattering Techniques. *J. Phys. Chem. B* **2017**, *121*, 1340−1351.
(271) Su, Y.; Burger, C.; Hsiao, B. S.; Chu, B. Characterization of TEMPO-oxidized Cellulose Nanofibers in Aqueous Suspension by Small-angle X-ray Scattering. *J. Appl. Crystallogr.* **2014**, *47*, 788−798.
(272) Schütz, C.; Agthe, M.; Fall, A. B.; Gordeyeva, K.; Guccini, V.; Salajkova, M.; Plivelic, T. S.; Lagerwall, J. P.; Salazar-Alvarez, G.; Bergström, L. Rod Packing in Chiral Nematic Cellulose Nanocrystal Dispersions Studied by Small-angle X-ray Scattering and Laser Diffraction. *Langmuir* **2015**, *31*, 6507−6513.
(273) Šturcová, A.; Davies, G. R.; Eichhorn, S. J. Elastic Modulus and Stress-transfer Properties of Tunicate Cellulose Whiskers. *Biomacromolecules* **2005**, *6*, 1055−1061.
(274) Sakurada, I.; Nukushina, Y.; Ito, T. Experimental Determination of the Elastic Modulus of Crystalline Regions in Oriented Polymere. *J. Plym. Sci.* **1962**, *57*, 651−660.
(275) Iwamoto, S.; Kai, W.; Isogai, A.; Iwata, T. Elastic Modulus of Single Cellulose Microfibrils from Tunicate Measured by Atomic Force Microscopy. *Biomacromolecules* **2009**, *10*, 2571−2576.
(276) Saito, T.; Kuramae, R.; Wohlert, J.; Berglund, L. A.; Isogai, A. An Ultrastrong Nanofibrillar Biomaterial: The Strength of Single Cellulose Nanofibrils Revealed via Sonication-induced Fragmentation. *Biomacromolecules* **2013**, *14*, 248−253.
(277) Benítez, A. J.; Walther, A. Cellulose Nanofibril Nanopapers and Bioinspired Nanocomposites: A Review to Understand the Mechanical Property Space. *J. Mater. Chem. A* **2017**, *5*, 16003−16024.
(278) Henriksson, M.; Berglund, L. A.; Isaksson, P.; Lindström, T.; Nishino, T. Cellulose Nanopaper Structures of High Toughness. *Biomacromolecules* **2008**, *9*, 1579−1585.
(279) Shinoda, R.; Saito, T.; Okita, Y.; Isogai, A. Relationship between Length and Degree of Polymerization of TEMPO-oxidized Cellulose Nanofibrils. *Biomacromolecules* **2012**, *13*, 842−849.
(280) Fukuzumi, H.; Saito, T.; Isogai, A. Influence of TEMPO-oxidized Cellulose Nanofibril Length on Film Properties. *Carbohydr. Polym.* **2013**, *93*, 172−177.
(281) Lindstrom, T.; Fellers, C.; Ankerfors, M.; Nordmark, G. G. On the Nature of Joint Strength of Paper-Effect of Dry Strength Agents-Revisiting the Page Equation. *Nordic Pulp & Paper Res, J.* **2016**, *31*, 459−468.
(282) Lindström, T. A Proposition for the Estimation of the Maximum Tensile Strength of Variously Charged Nanocellulosic Film Materials Provided by Vacuum Filtration. *Nanomaterials* **2021**, *11*, 543.
(283) Arcari, M.; Axelrod, R.; Adamcik, J.; Handschin, S.; Sánchez-Ferrer, A.; Mezzenga, R.; Nyström, G. Structure-property Relationships of Cellulose Nanofibril Hydro-and Aerogels and their Building Blocks. *Nanoscale* **2020**, *12*, 11638−11646.
(284) Benitez, A. J.; Torres-Rendon, J.; Poutanen, M.; Walther, A. Humidity and Multiscale Structure Govern Mechanical Properties and Deformation Modes in Films of Native Cellulose Nanofibrils. *Biomacromolecules* **2013**, *14*, 4497−4506.
(285) Shimizu, M.; Saito, T.; Isogai, A. Water-resistant and High Oxygen-barrier Nanocellulose Films with Interfibrillar Cross-linkages Formed through Multivalent Metal Ions. *J. Membr. Sci.* **2016**, *500*, 1−7.
(286) Shimizu, M.; Saito, T.; Fukuzumi, H.; Isogai, A. Hydrophobic, Ductile, and Transparent Nanocellulose Films with Quaternary Alkylammonium Carboxylates on Nanofibril Surfaces. *Biomacromolecules* **2014**, *15*, 4320−4325.
(287) Shimizu, M.; Saito, T.; Isogai, A. Bulky Quaternary Alkylammonium Counterions Enhance the Nanodispersibility of 2,2,6,6-tetramethylpiperidine-1-oxyl-oxidized Cellulose in Diverse Solvents. *Biomacromolecules* **2014**, *15*, 1904−1909.

https://doi.org/10.1021/acs.chemrev.1c00683
Chem. Rev. 2022, 122, 8936−9031

(288) Benitez, A. J.; Walther, A. Counterion Size and Nature Control Structural and Mechanical Response in Cellulose Nanofibril Nanopapers. *Biomacromolecules* **2017**, *18*, 1642−1653.
(289) Benselfelt, T.; Nordenström, M.; Lindström, S. B.; Wågberg, L. Explaining the Exceptional Wet Integrity of Transparent Cellulose Nanofibril Films in the Presence of Multivalent Ions—Suitable Substrates for Biointerfaces. *Adv. Mater. Interfaces* **2019**, *6*, 1900333.
(290) Benselfelt, T.; Nordenström, M.; Hamedi, M. M.; Wågberg, L. Ion-induced Assemblies of Highly Anisotropic Nanoparticles are Governed by Ion-Ion Correlation and Specific Ion Effects. *Nanoscale* **2019**, *11*, 3514−3520.
(291) Kroy, K.; Frey, E. Dynamic Scattering from Solutions of Semiflexible Polymers. *Phys. Rev. E* **1997**, *55*, 3092−3101.
(292) Arcari, M.; Zuccarella, E.; Axelrod, R.; Adamcik, J.; Sánchez-Ferrer, A.; Mezzenga, R.; Nyström, G. Nanostructural Properties and Twist Periodicity of Cellulose Nanofibrils with Variable Charge Density. *Biomacromolecules* **2019**, *20*, 1288−1296.
(293) Hou, Y.; Guan, Q.-F.; Xia, J.; Ling, Z.-C.; He, Z.; Han, Z.-M.; Yang, H.-B.; Gu, P.; Zhu, Y.; Yu, S.-H.; Wu, H. Strengthening and Toughening Hierarchical Nanocellulose via Humidity-Mediated Interface. *ACS Nano* **2021**, *15*, 1310−1320.
(294) Adstedt, K.; Popenov, E. A.; Pierce, K. J.; Xiong, R.; Geryak, R.; Cherpak, V.; Nepal, D.; Bunning, T. J.; Tsukruk, V. V. Chiral Cellulose Nanocrystals with Intercalated Amorphous Polysaccharides for Controlled Iridescence and Enhanced Mechanics. *Adv. Funct. Mater.* **2020**, *30*, 2003597.
(295) Zhang, X.; Xiong, R.; Kang, S.; Yang, Y.; Tsukruk, V. V. Alternating Stacking of Nanocrystals and Nanofibers into Ultrastrong Chiral Biocomposite Laminates. *ACS Nano* **2020**, *14*, 14675−14685.
(296) Favier, V.; Chanzy, H.; Cavaille, J. Y. Polymer Nanocomposites Reinforced by Cellulose Whiskers. *Macromolecules* **1995**, *28*, 6365−6367.
(297) Kargarzadeh, H.; Mariano, M.; Huang, J.; Lin, N.; Ahmad, I.; Dufresne, A.; Thomas, S. Recent Developments on Nanocellulose Reinforced Polymer Nanocomposites: A Review. *Polymer* **2017**, *132*, 368−393.
(298) Kargarzadeh, H.; Huang, J.; Lin, N.; Ahmad, I.; Mariano, M.; Dufresne, A.; Thomas, S.; Gałęski, A. Recent Developments in Nanocellulose-based Biodegradable Polymers, Thermoplastic Polymers, and Porous Nanocomposites. *Prog. Polym. Sci.* **2018**, *87*, 197−227.
(299) Dufresne, A. Cellulose Nanomaterials as Green Nanoreinforcements for Polymer Nanocomposites. *Philos. Trans. A Math. Phys. Eng. Sci.* **2018**, *376*, 20170040.
(300) Shen, R.; Xue, S.; Xu, Y.; Liu, Q.; Feng, Z.; Ren, H.; Zhai, H.; Kong, F. Research Progress and Development Demand of Nanocellulose Reinforced Polymer Composites. *Polymers* **2020**, *12*, 2113.
(301) Ganguly, K.; Lim, K.-T. Nanocellulose-based Polymer Nanohybrids and Nanocomposite Applications. In *Multifunctional Hybrid Nanomaterials for Sustainable Agri-Food and Ecosystems*; Elsevier: Amsterdam, 2020; p 504.
(302) Moon, R. J.; Martini, A.; Nairn, J.; Simonsen, J.; Youngblood, J. Cellulose Nanomaterials Review: Structure, Properties and Nanocomposites. *Chem. Soc. Rev.* **2011**, *40*, 3941−3994.
(303) Mousa, M. H.; Dong, Y.; Davies, I. J. Recent Advances in Bionanocomposites: Preparation, Properties, and Applications. *Int. J. Polym. Mater. Polym. Biomater.* **2016**, *65*, 225−254.
(304) Ritchie, R. O. The Conflicts between Strength and Toughness. *Nat. Mater.* **2011**, *10*, 817−822.
(305) Barthelat, F.; Yin, Z.; Buehler, M. J. Structure and Mechanics of Interfaces in Biological Materials. *Nat. Rev. Mater.* **2016**, *1*, 16007.
(306) Benitez, A. J.; Lossada, F.; Zhu, B.; Rudolph, T.; Walther, A. Understanding Toughness in Bioinspired Cellulose Nanofibril/Polymer Nanocomposites. *Biomacromolecules* **2016**, *17*, 2417−2426.
(307) Mittal, N.; Jansson, R.; Widhe, M.; Benselfelt, T.; Hakansson, K. M. O.; Lundell, F.; Hedhammar, M.; Soderberg, L. D. Ultrastrong and Bioactive Nanostructured Bio-based Composites. *ACS Nano* **2017**, *11*, 5148−5159.
(308) Cai, Y.; Geng, L.; Chen, S.; Shi, S.; Hsiao, B. S.; Peng, X. Hierarchical Assembly of Nanocellulose into Filaments by Flow-assisted Alignment and Interfacial Complexation: Conquering the Conflicts between Strength and Toughness. *ACS Appl. Mater. Interfaces* **2020**, *12*, 32090−32098.
(309) Chen, F.; Xiang, W.; Sawada, D.; Bai, L.; Hummel, M.; Sixta, H.; Budtova, T. Exploring Large Ductility in Cellulose Nanopaper Combining High Toughness and Strength. *ACS Nano* **2020**, *14*, 11150−11159.
(310) Revol, J.-F.; Bradford, H.; Giasson, J.; Marchessault, R. H.; Gray, D. G. Helicoidal Self-ordering of Cellulose Microfibrils in Aqueous Suspension. *Int. J. Biol. Macromol.* **1992**, *14*, 170−172.
(311) Chen, Q.; Liu, P.; Nan, F.; Zhou, L.; Zhang, J. Tuning the Iridescence of Chiral Nematic Cellulose Nanocrystal Films with a Vacuum-assisted Self-assembly Technique. *Biomacromolecules* **2014**, *15*, 4343−4350.
(312) Natarajan, B.; Krishnamurthy, A.; Qin, X.; Emiroglu, C. D.; Forster, A.; Foster, E. J.; Weder, C.; Fox, D. M.; Keten, S.; Obrzut, J.; Gilman, J. W. Binary Cellulose Nanocrystal Blends for Bioinspired Damage Tolerant Photonic Films. *Adv. Funct. Mater.* **2018**, *28*, 1800032.
(313) Kelly, J. A.; Giese, M.; Shopsowitz, K. E.; Hamad, W. Y.; MacLachlan, M. J. The Development of Chiral Nematic Mesoporous Materials. *Acc. Chem. Res.* **2014**, *47*, 1088−1096.
(314) Giese, M.; Blusch, L. K.; Khan, M. K.; Hamad, W. Y.; MacLachlan, M. J. Responsive Mesoporous Photonic Cellulose Films by Supramolecular Cotemplating. *Angew. Chem.* **2014**, *126*, 9026−9030.
(315) Tran, A.; Hamad, W. Y.; MacLachlan, M. J. Tactoid Annealing Improves Order in Self-Assembled Cellulose Nanocrystal Films with Chiral Nematic Structures. *Langmuir* **2018**, *34*, 646−652.
(316) Giese, M.; Blusch, L. K.; Khan, M. K.; MacLachlan, M. J. Functional Materials from Cellulose-Derived Liquid-crystal Templates. *Angew. Chem., Int. Ed.* **2015**, *54*, 2888−2910.
(317) Peng, N.; Huang, D.; Gong, C.; Wang, Y.; Zhou, J.; Chang, C. Controlled Arrangement of Nanocellulose in Polymeric Matrix: From Reinforcement to Functionality. *ACS Nano* **2020**, *14*, 16169−16179.
(318) Rosén, T.; Hsiao, B. S.; Söderberg, L. D. Elucidating the Opportunities and Challenges for Nanocellulose Spinning. *Adv. Mater.* **2021**, *33*, 2001238.
(319) Hooshmand, S.; Aitomaki, Y.; Norberg, N.; Mathew, A. P.; Oksman, K. Dry-spun Single-filament Fibers Comprising Solely Cellulose Nanofibers from Bioresidue. *ACS Appl. Mater. Interfaces* **2015**, *7*, 13022−13028.
(320) Shen, Y.; Orelma, H.; Sneck, A.; Kataja, K.; Salmela, J.; Qvintus, P.; Suurnäkki, A.; Harlin, A. High Velocity Dry Spinning of Nanofibrillated Cellulose (CNF) Filaments on an Adhesion Controlled Surface with Low Friction. *Cellulose* **2016**, *23*, 3393−3398.
(321) Ghasemi, S.; Tajvidi, M.; Bousfield, D. W.; Gardner, D. J.; Gramlich, W. M. Dry-spun Neat Cellulose Nanofibril Filaments: Influence of Drying Temperature and Nanofibril Structure on Filament Properties. *Polymers* **2017**, *9*, 392.
(322) Iwamoto, S.; Isogai, A.; Iwata, T. Structure and Mechanical Properties of Wet-spun Fibers Made from Natural Cellulose Nanofibers. *Biomacromolecules* **2011**, *12*, 831−836.
(323) Walther, A.; Timonen, J. V.; Diez, I.; Laukkanen, A.; Ikkala, O. Multifunctional High-performance Biofibers based on Wet-extrusion of Renewable Native Cellulose Nanofibrils. *Adv. Mater.* **2011**, *23*, 2924−2928.
(324) Lundahl, M. J.; Cunha, A. G.; Rojo, E.; Papageorgiou, A. C.; Rautkari, L.; Arboleda, J. C.; Rojas, O. J. Strength and Water Interactions of Cellulose I Filaments Wet-spun from Cellulose Nanofibril Hydrogels. *Sci. Rep.* **2016**, *6*, 30695.
(325) Mittal, N.; Ansari, F.; Gowda V, K.; Brouzet, C.; Chen, P.; Larsson, P. T.; Roth, S. V.; Lundell, F.; Wågberg, L.; Kotov, N. A.; Söderberg, L. D.; et al. Multiscale Control of Nanocellulose Assembly: Transferring Remarkable Nanoscale Fibril Mechanics to Macroscale Fibers. *ACS Nano* **2018**, *12*, 6378−6388.

https://doi.org/10.1021/acs.chemrev.1c00683
Chem. Rev. 2022, 122, 8936−9031

(326) Håkansson, K. M.; Fall, A. B.; Lundell, F.; Yu, S.; Krywka, C.; Roth, S. V.; Santoro, G.; Kvick, M.; Prahl Wittberg, L.; Wagberg, L.; et al. Hydrodynamic Alignment and Assembly of Nanofibrils Resulting in Strong Cellulose Filaments. *Nat. Commun.* **2014**, *5*, 4018.
(327) Martin-Martinez, F. J.; Jin, K.; Lopez Barreiro, D.; Buehler, M. J. The Rise of Hierarchical Nanostructured Materials from Renewable Sources: Learning from Nature. *ACS Nano* **2018**, *12*, 7425−7433.
(328) Ling, S.; Kaplan, D. L.; Buehler, M. J. Nanofibrils in Nature and Materials Engineering. *Nat. Rev. Mater.* **2018**, *3*, 18016.
(329) Rosen, T.; Wang, R.; Zhan, C.; He, H.; Chodankar, S.; Hsiao, B. S. Cellulose Nanofibrils and Nanocrystals in Confined Flow: Single-particle Dynamics to Collective Alignment Revealed through Scanning Small-angle X-ray Scattering and Numerical Simulations. *Phys. Rev. E* **2020**, *101*, 032610.
(330) Rosén, T.; Brouzet, C.; Roth, S. V.; Lundell, F.; Söderberg, L. D. Three-Dimensional Orientation of Nanofibrils in Axially Symmetric Systems Using Small-Angle X-ray Scattering. *J. Phys. Chem. C* **2018**, *122*, 6889−6899.
(331) La Mer, V. K. Filtration of Colloidal Dispersions Flocculated by Anionic and Cationic Polyelectrolytes. *Disc. Faraday Soc.* **1966**, *42*, 248−254.
(332) La Mer, V. K. Coagulation Symposium Introduction. *J. Coll. Sci.* **1964**, *19*, 291−293.
(333) Othmani, B.; Rasteiro, M. G.; Khadhraoui, M. Toward Green Technology: A Review on Some Efficient Model Plant-based Coagulants/Flocculants for Freshwater and Wastewater Remediation. *Clean Technol. Environ. Policy* **2020**, *22*, 1025−1040.
(334) Saleem, M.; Bachmann, R. T. A Contemporary Review on Plant-based Coagulants for Applications in Water Treatment. *J. Ind. Eng. Chem.* **2019**, *72*, 281−297.
(335) Gautam, S.; Saini, G. The Use of Natural Coagulants for Industrial Wastewater Treatment. *Global J. Environ. Sci. Manage.* **2020**, *6*, 553−578.
(336) Mohd-Salleh, S. N. A.; Mohd-Zin, N. S.; Othman, N. A Review of Wastewater Treatment using Natural Material and Its Potential as Aid and Composite Coagulant. *Sains Malays.* **2019**, *48*, 155−164.
(337) Mohammed, N.; Grishkewich, N.; Tam, K. C. Cellulose Nanomaterials: Promising Sustainable Nanomaterials for Application in Water/Wastewater Treatment Processes. *Environ. Sci. Nano* **2018**, *5*, 623−658.
(338) Grishkewich, N.; Mohammed, N.; Tang, J.; Tam, K. C. Recent Advances in the Application of Cellulose Nanocrystals. *Curr. Opin. Colloid Interface Sci.* **2017**, *29*, 32−45.
(339) Vold, R. D.; Vold, M. J *Colloid and Interface Chemistry*; Addison-Wesley: Boston, 1983; p 694.
(340) Hunter, R. J. *Foundation of Colloid Science*; Oxford University Press: Oxford, UK, 2001; p 816.
(341) Hiemenz, P. C. *Principles of Colloid and Surface Chemistry*; Marcel and Dekker. Inc.: New York, USA, 1986.
(342) Gregory, J.; O'Melia, C. R. Fundamentalks of flocculation. *Crit. Rev. Environ, Control* **1989**, *19*, 185−230.
(343) Gregory, J. Rates of Flocculation of Latex Particles by Cationic Polymers. *J. Colloid Interface Sci.* **1973**, *42*, 448−456.
(344) Kasper, D. R. Theoretical and Experimental Investigations of the Flocculation of Charged Particles in Aqueous Solutions by Polyelectrolytes of Opposite Charge. PhD Dissertation, California Institute of Technology, 1971. DOI: 10.7907/K31R-A990.
(345) Sandell, L. S.; Luner, P. Flocculation of Microcrystalline Cellulose with Cationic Ionene Polymers. *J. Appl. Polym. Sci.* **1974**, *18*, 2075−2083.
(346) Hogg, R.; Healy, T. W.; Furstenau, D. W. Mutual Coagulation of Colloidal Dispersions. *Trans. Faraday Soc.* **1966**, *62*, 1638−1651.
(347) Ohshima, H.; Chan, D. Y. C.; Healy, T. W.; White, L. R. Improvement on the Hogg-Healy-Fuerstenau Formulas for the Interaction of Dissimilar Double Layers. *J. Colloid Interface Sci.* **1983**, *92*, 232−242.
(348) Fleer, G. J. Polymer Adsorption and Its Effect on Colloidal Stability. Ph.D Thesis, The Netherlands Agricultural University, Wageningen, 1971. https://edepot.wur.nl/194575.
(349) La Mer, V. K.; Healy, T. W. Adsorption−Flocculation Reactions of Macrolecules at the Solid−Liquid Interface. *Rev. Pure Appl. Chem.* **1963**, *13*, 112−133.
(350) Bolto, B.; Gregory, J. Organic Polyelectrolytes in Water Treatment. *Water Res.* **2007**, *41*, 2301−2324.
(351) Fleer, G. J.; Koopal, L. K.; Lyklema, J. Polymer Adsorption and Its Effect on the Stability of Hydrophobic Colloids. *Kolloid Zeitschrift & Zeitschrift fuer Polymere* **1972**, *250*, 689−702.
(352) Vincent, B. The Effect of Adsorped Polymers on Dispersion Stabliity. *Adv. Colloid Interface Sci.* **1974**, *4*, 193−277.
(353) Lindström, T. *Fundamentals of Papermaking*, Transactions of the Ninth Fundamental Research Symposium, Cambridge, UK; 1989; p 311.
(354) Wågberg, L.; Lindström, T. Some Fundamental Aspects on Dual Component Retention Aid Systems. *Nord Pulp Paper Res. J.* **1987**, *2*, 49−55.
(355) Ghernaout, D.; Ghernaout, B. Sweep Flocculation as a Second form of Charge Neutralisation. *Des. and Water Treat.* **2012**, *44*, 15−28.
(356) Lindström, T.; Glad-Nordmark, G. Network Flocculation and Fractionation of Latex Particles by Means of a Polyethyleneoxide-phenolformaldehyde Resin Complex. *J. Colloid Interface Sci.* **1984**, *97*, 62−67.
(357) Revol, J.-F.; Godbout, L.; Dong, X.-M.; Gray, D. G.; Chanzy, H.; Maret, G. Chiral Nematic Suspensions of Cellulose Crystallites; Phase Separation and Magnetic Field Orientation. *Liq. Cryst.* **1994**, *16*, 127−134.
(358) Peyre, J.; Pääkkönen, T.; Reza, M.; Kontturi, E. Simultaneous Preparation of Cellulose Nanocrystals and Micron-sized Porous Colloidal Particles of Cellulose by TEMPO-mediated Oxidation. *Green Chem.* **2015**, *17*, 808−811.
(359) Nevell, T. P. In *Cellulose Chemistry and Its Applications*; Ellis Horwood Limited: New York, 1985.
(360) Sirviö, J.; Hyvakko, U.; Liimatainen, H.; Niinimaki, J.; Hormi, O. Periodate Oxidation of Cellulose at Elevated Temperatures using Metal Salts as Cellulose Activators. *Carbohydr. Polym.* **2011**, *83*, 1293−1297.
(361) Yu, H.; Abdalkarim, S. Y. H.; Zhang, H.; Wang, C.; Tam, K. C. Simple Process to Produce High-yield Cellulose Nanocrystals using Recyclable Citric/Hydrochloric Acids. *ACS Sustain. Chem. Eng.* **2019**, *7*, 4912−4923.
(362) Yang, H.; van de Ven, T. G. M. Preparation of Hairy Cationic Nanocrystalline Cellulose. *Cellulose* **2016**, *23*, 1791−1801.
(363) Sheikhi, A.; van de Ven, T. G. M. Colloidal Aspects of Janus-like Hairy Cellulose Nanocrystalloids. *Curr. Opin. Colloid Interface Sci.* **2017**, *29*, 21−31.
(364) Kim, U.-J.; Wada, M.; Kuga, S. Solubilization of Dialdehyde Cellulose by Hot Water. *Carbohydr. Polym.* **2004**, *56*, 7−10.
(365) Yang, H.; Chen, D.; van de Ven, T. G. M. Preparation and Characterization of Sterically Stabilized Nanocrystalline Cellulose Obtained by Periodate Oxidation of Cellulose Fibers. *Cellulose* **2015**, *22*, 1743−1752.
(366) van de Ven, T. G.; Sheikhi, A. Hairy Cellulose Nanocrystalloids: A Novel Class of Nanocellulose. *Nanoscale* **2016**, *8*, 15101−15114.
(367) Hasani, M.; Cranston, E. D.; Westman, G.; Gray, D. G. Cationic Surface Functionalization of Cellulose Nanocrystals. *Soft Matter* **2008**, *4*, 2238−2244.
(368) Suopajärvi, T.; Sirviö, J. A.; Liimatainen, H. Cationic Nanocelluloses in Dewatering of Municipal Activated Sludge. *J. Environ. Chem. Eng.* **2017**, *5*, 86−92.
(369) Eyley, S.; Thielemans, W. Imidazolium Grafted Cellulose Nanocrystals for Ion Exchange Applications. *Commun. Chem.* **2011**, *47*, 4177−4179.
(370) Jasmani, L.; Eyley, S.; Wallbridge, R.; Thielemans, W. A Facile One-pot Route to Cationic Cellulose Nanocrystals. *Nanoscale* **2013**, *5*, 10207−10211.
(371) Wang, H.-D.; Jessop, P. G.; Bouchard, J.; Champagne, P.; Cunningham, M. F. Cellulose Nanocrystals with CO_2-Switchable Aggregation and Redispersion Properties. *Cellulose* **2015**, *22*, 3105−3116.

(372) Kan, K. H.; Li, J.; Wijesekera, K.; Cranston, E. D. Polymer-grafted Cellulose Nanocrystals as pH-Responsive Reversible Flocculants. *Biomacromolecules* **2013**, *14*, 3130−3139.
(373) Decher, G.; Schlenhoff, J. B. *Multilayer Thin Films: Sequential Assembly of Nanocomposite Materials*; Wiley-VCH: Weinheim, Germany, 2003; p 1112.
(374) Eronen, P.; Laine, J.; Ruokolainen, J.; Osterberg, M. Comparison of Multilayer Formation between Different Cellulose Nanofibrils and Cationic Polymers. *J. Colloid Interface Sci.* **2012**, *373*, 84−93.
(375) Saito, T.; Kimura, T.; Nishiyama, Y.; Isogai, A. Cellulose Nanofibers Prepared by TEMPO-mediated Oxidation of Native Cellulose. *Biomacromolecules* **2007**, *8*, 2485−2491.
(376) Liimatainen, H.; Visanko, M.; Sirviö, J.; Hormi, O.; Niinimäki, J. Sulfonated Cellulose Nanofibrils Obtained from Wood Pulp through Regioselective Oxidative Bisulfite Pre-treatment. *Cellulose* **2013**, *20*, 741−749.
(377) Pei, A.; Butchosa, N.; Berglund, L. A.; Zhou, Q. Surface Quaternized Cellulose Nanofibrils with High Water Absorbency and Adsorption Capacity for Anionic Dyes. *Soft Matter* **2013**, *9*, 2047−2055.
(378) Ho, T. T. T.; Zimmermann, T.; Hauert, R.; Caseri, W. Preparation and Characterization of Cationic Nanofibrillated Cellulose from Etherification and High-shear Disintegration Processes. *Cellulose* **2011**, *18*, 1391−1406.
(379) Sirviö, J.; Honka, A.; Liimatainen, H.; Niinimäki, J.; Hormi, O. Synthesis of Highly Cationic Water-soluble Cellulose Derivative and Its Potential as Novel Biopolymeric Flocculation Agent. *Carbohydr. Polym.* **2011**, *86*, 266−270.
(380) Liimatainen, H.; Suopajarvi, T.; Sirvio, J.; Hormi, O.; Niinimaki, J. Fabrication of Cationic Cellulosic Nanofibrils through Aqueous Quaternization Pretreatment and their Use in Colloid Aggregation. *Carbohydr. Polym.* **2014**, *103*, 187−192.
(381) Liimatainen, H.; Sirviö, J.; Haapala, A.; Hormi, O.; Niinimäki, J. Characterization of Highly Acessible Cellulose Microfibers Generated by Wet Stirred Media Milling. *Carbohydr. Polym.* **2011**, *83*, 2005−2010.
(382) Aimin, T.; Hongwei, Z.; Gang, C.; Guohui, X.; Wenzhi, L. Influence of Ultrasound Treatment on Accessibility and Regioselective Oxidation Reactivity of Cellulose. *Ultrason. Sonochem.* **2005**, *12*, 467−472.
(383) Pahimanolis, N.; Hippi, U.; Johansson, L.-S.; Saarinen, T.; Houbenov, N.; Ruokolainen, J.; Seppälä, J. Surface Functionalization of Nanofibrillated Cellulose using Click-chemistry Approach in Aqueous Media. *Cellulose* **2011**, *18*, 1201−1212.
(384) Suopajärvi, T.; Liimatainen, H.; Hormi, O.; Niinimäki, J. Coagulation-Flocculation Treatment of Municipal Wastewater based on Anionized Nanocelluloses. *Chem. Eng. Sci.* **2013**, *231*, 59−67.
(385) Tang, F.; Yu, H.; Yassin Hussain Abdalkarim, S.; Sun, J.; Fan, X.; Li, Y.; Zhou, Y.; Chiu Tam, K. Green Acid-free Hydrolysis of Wasted Pomelo Peel to Produce Carboxylated Cellulose Nanofibers with Super Absorption/Flocculation Ability for Environmental Remediation Materials. *Chem. Eng. Sci.* **2020**, *395*, 125070.
(386) Suopajärvi, T.; Koivuranta, E.; Liimatainen, H.; Niinimäki, J. Flocculation of Municipal Wastewaters with Anionic Nanocelluloses: Influence of Nanocellulose Characteristics on Floc Morphology and Strength. *J. Environ. Chem. Eng.* **2014**, *2*, 2005−2012.
(387) Jiang, X.; Lou, C.; Hua, F.; Deng, H.; Tian, X. Cellulose Nanocrystals-based Flocculants for High-speed and High-efficiency Decolorization of Colored Effluents. *J. Clean. Prod.* **2020**, *251*, 119749.
(388) Nkalane, A.; Oyewo, O. A.; Leswifi, T.; Onyango, M. S. Application of Coagulant Obtained through Charge Reversal of Sawdust-derived Cellulose Nanocrystals in the Enhancement of Water Turbidity Removal. *Mater. Res. Express* **2019**, *6*, 105060.
(389) Chen, D.; van de Ven, T. G. M. Flocculation Kinetics of Precipitated Calcium Carbonate Induced by Electrosterically Stabilized Nanocrystalline Cellulose. *Colloids Surf, A Physicochem. Eng. Asp.* **2016**, *504*, 11−17.
(390) Chen, D.; van de Ven, T. G. M. Flocculation Kinetics of Precipitated Calcium Carbonate (PCC) with Sterically Stabilized Nanocrystalline Cellulose (SNCC). *Colloids Surf, A Physicochem. Eng. Asp.* **2016**, *506*, 789−793.
(391) Campano, C.; Lopez-Exposito, P.; Blanco, A.; Negro, C.; van de Ven, T. G. M. Hairy Cationic Nanocrystalline Cellulose as Retention Additive in Recycled Paper. *Cellulose* **2019**, *26*, 6275−6289.
(392) Vandamme, D.; Eyley, S.; Van den Mooter, G.; Muylaert, K.; Thielemans, W. Highly Charged Cellulose-based Nanocrystals as Flocculants for Harvesting *Chlorella vulgaris*. *Bioresour. Technol.* **2015**, *194*, 270−275.
(393) Ge, S.; Champagne, P.; Wang, H.; Jessop, P. G.; Cunningham, M. F. Microalgae Recovery from Water for Biofuel Production using CO_2-switchable Crystalline Nanocellulose. *Environ. Sci. Technol.* **2016**, *50*, 7896−7903.
(394) Manfredi, L.; Hill, R. J.; van de Ven, T. G. Bridging Flocculation of PEI-functionalized Latex Particles using Nanocrystalline Cellulose. *J. Colloid Interface Sci.* **2011**, *360*, 117−123.
(395) Xu, Q.; Gao, Y.; Qin, M.; Wu, K.; Fu, Y.; Zhao, J. Nanocrystalline Cellulose from Aspen Kraft Pulp and Its Application in Deinked Pulp. *Int. J. Biol. Macromol.* **2013**, *60*, 241−247.
(396) Xu, Q. H.; Li, W. G.; Cheng, Z. L.; Yang, G.; Qin, M. H. TEMPO/NaBr/NaCLO-mediated Surface Oxidation of Nanocrystalline Cellulose and Its Microparticulate Retention with Cationic Polyacrylamide. *Bioresources* **2014**, *9*, 994−1006.
(397) Korhonen, M.; Laine, J. Flocculation and Retention of Fillers with Nanocelluloses. *Nordic Pulp & Paper J.* **2014**, *29*, 119−128.
(398) Ämmälä, A.; Liimatainen, H.; Burmeister, C.; Niinimäki, J. Effect of Tempo and Periodate-Chlorite Oxidized Nanofibrils on Ground Calcium Carbonate Flocculation and Retention in Sheet Forming and on the Physical Properties of Sheets. *Cellulose* **2013**, *20*, 2451−2460.
(399) Quinlan, P. J.; Tanvir, A.; Tam, K. C. Application of the Central Composite Design to Study the Flocculation of an Anionic Azo Dye using Quaternized Cellulose Nanofibrils. *Carbohydr. Polym.* **2015**, *133*, 80−89.
(400) Taipale, T.; Österberg, M.; Nykänen, A.; Ruokolainen, J.; Laine, J. Effect of Microfibrillated Cellulose and Fines on the Drainage of Kraft Pulp Suspension and Paper Strength. *Cellulose* **2010**, *17*, 1005−1020.
(401) Merayo, N.; Balea, A.; de la Fuente, E.; Blanco, Á.; Negro, C. Synergies between Cellulose Nanofibers and Retention Additives to Improve Recycled Paper Properties and the Drainage Process. *Cellulose* **2017**, *24*, 2987−3000.
(402) He, M.; Cho, B.-U.; Lee, Y. K.; Won, J. M. Utilizing Cellulose Nanofibril as an Eco-friendly Floccculant for Filler Flocculation in Papermaking. *Bioresoures* **2016**, *11*, 10296−10313.
(403) Jin, L.; Wei, Y.; Xu, Q.; Yao, W.; Cheng, Z. Cellulose Nanofibers Prepared from TEMPO-oxidation of Kraft Pulp and Its Flocculation Effect on Kaolin Clay. *J. Appl. Polym. Sci.* **2014**, *131*, 40450.
(404) Singh, N. B.; Nagpal, G.; Agrawal, S.; Rachna. Water Purification by Using Adsorbents: A Review. *Environ. Technol. Innov.* **2018**, *11*, 187−240.
(405) Yang, J.; Ma, C.; Tao, J.; Li, J.; Du, K.; Wei, Z.; Chen, C.; Wang, Z.; Zhao, C.; Ma, M. Optimization of Polyvinylamine-modified Nanocellulose for Chlorpyrifos Adsorption by Central Composite Design. *Carbohydr. Polym.* **2020**, *245*, 116542.
(406) Liu, P.; Sehaqui, H.; Tingaut, P.; Wichser, A.; Oksman, K.; Mathew, A. P. Cellulose and Chitin Nanomaterials for Capturing Silver Ions (Ag^+) from Water via Surface Adsorption. *Cellulose* **2014**, *21*, 449−461.
(407) Tavakolian, M.; Jafari, S. M.; van de Ven, T. G. A Review on Surface-Functionalized Cellulosic Nanostructures as Biocompatible Antibacterial Materials. *Nano-Micro Lett.* **2020**, *12*, 73.
(408) Tavakolian, M.; Wiebe, H.; Sadeghi, M. A.; van de Ven, T. G. Dye Removal using Hairy Nanocellulose: Experimental and Theoretical Investigations. *ACS Appl. Mater. Interfaces* **2020**, *12*, 5040−5049.
(409) Dwivedi, A. D.; Sanandiya, N. D.; Singh, J. P.; Husnain, S. M.; Chae, K. H.; Hwang, D. S.; Chang, Y.-S. Tuning and Characterizing Nanocellulose Interface for Enhanced Removal of Dual-Sorbate As(V) and Cr(VI) from water matrices. *ACS Sustain. Chem. Eng.* **2017**, *5*, 518−528.

https://doi.org/10.1021/acs.chemrev.1c00683
Chem. Rev. 2022, 122, 8936−9031

(410) Shahnaz, T.; Narayanasamy, S.; et al. Surface Modification of Nanocellulose using Polypyrrole for the Adsorptive Removal of Congo Red Dye and Chromium in Binary Mixture. *Int. J. Biol. Macromol.* **2020**, *151*, 322−332.
(411) Yue, Y.; Wang, X.; Han, J.; Yu, L.; Chen, J.; Wu, Q.; Jiang, J. Effects of Nanocellulose on Sodium Alginate/Polyacrylamide Hydrogel: Mechanical Properties and Adsorption-Desorption Capacities. *Carbohydr. Polym.* **2019**, *206*, 289−301.
(412) Wei, J.; Gui, S.-H.; Wu, J.-H.; Xu, D.-D.; Sun, Y.; Dong, X.-Y.; Dai, Y.-Y.; Li, Y.-F. Nanocellulose-Graphene Oxide Hybrid Aerogel to Water Purification. *Appl. Environ. Biotechnol.* **2019**, *4*, 11−17.
(413) Tasrin, S.; Mohamed Madhar Fazil, S.; Senthilmurugan, S.; Selvaraju, N. Facile Preparation of Nanocellulose Embedded Polypyrrole for Dye Removal: Unary and Binary Process Optimization and Seed Toxicity. *Int. J. Environ. Sci.Technol.* **2021**, *18*, 365−378.
(414) Sharma, V.; Shahnaz, T.; Subbiah, S.; Narayanasamy, S. New Insights into the Remediation of Water Pollutants using Nanobentonite Incorporated Nanocellulose Chitosan Based Aerogel. *J. Polym. Environ.* **2020**, *28*, 2008−2019.
(415) Gu, H.; Zhou, X.; Lyu, S.; Pan, D.; Dong, M.; Wu, S.; Ding, T.; Wei, X.; Seok, I.; Wei, S.; Guo, Z. Magnetic Nanocellulose-magnetite Aerogel for Easy Oil Adsorption. *J. Colloid Interface Sci.* **2020**, *560*, 849−856.
(416) Adejumo, A. L.; Azeez, L.; Oyedeji, A. O.; Adetoro, R. O.; Aderibigbe, F. A. Nanostructured and Surface Functionalized Corncob as Unique Adsorbents for Anionic Dye Remediation. *SN Appl. Sci.* **2020**, *2*, 301.
(417) Zhang, H.; Lyu, S.; Zhou, X.; Gu, H.; Ma, C.; Wang, C.; Ding, T.; Shao, Q.; Liu, H.; Guo, Z. Super Light 3D Hierarchical Nanocellulose Aerogel Foam with Superior Oil Adsorption. *J. Colloid Interface Sci.* **2019**, *536*, 245−251.
(418) Zaghoud, L.; Gouamid, M.; Benmenine, A.; Khanblouche, A. Kinetic and Thermodynamic of Gentian Violet Removal by 2, 3-Dialdehyde Nanocellulose. *J. Biochem. Technol.* **2019**, *10*, 38−42.
(419) Emam, A. A.; Abo Faraha, S. A.; Kamal, F. H.; Gamal, A. M.; Basseem, M. Modification and Characterization of Nano Cellulose Crystalline from *Eichhornia Crassipes* using Citric Acid: An Adsorption Study. *Carbohydr. Polym.* **2020**, *240*, 116202.
(420) Ashour, R. M.; Abdel-Magied, A. F.; Wu, Q.; Olsson, R. T.; Forsberg, K. Green Synthesis of Metal-Organic Framework Bacterial Cellulose Nanocomposites for Separation Applications. *Polymers* **2020**, *12*, 1104.
(421) Jin, L.; Sun, Q.; Xu, Q.; Xu, Y. Adsorptive Removal of Anionic Dyes from Aqueous Solutions using Microgel based on Nanocellulose and Polyvinylamine. *Bioresour. Technol.* **2015**, *197*, 348−355.
(422) Yu, Z.; Hu, C.; Dichiara, A. B.; Jiang, W.; Gu, J. Cellulose Nanofibril/Carbon Nanomaterial Hybrid Aerogels for Adsorption Removal of Cationic and Anionic Organic Dyes. *Nanomaterials* **2020**, *10*, 169.
(423) Zheng, X.; Zhang, Y.; Bian, T.; Zhang, Y.; Li, Z.; Pan, J. Oxidized Carbon Materials Cooperative Construct Ionic Imprinted Cellulose Nanocrystals Films for Efficient Adsorption of Dy(III). *Chem. Eng. Sci.* **2020**, *381*, 122669.
(424) Li, D.; Tian, X.; Wang, Z.; Guan, Z.; Li, X.; Qiao, H.; Ke, H.; Luo, L.; Wei, Q. Multifunctional Adsorbent based on Metal-organic Framework Modified Bacterial Cellulose/Chitosan Composite Aerogel for High Efficient Removal of Heavy Metal Ion and Organic Pollutant. *Chem. Eng. Sci.* **2020**, *383*, 123127.
(425) Vadakkekara, G. J.; Thomas, S.; Nair, C. R. Sodium Itaconate Grafted Nanocellulose for Facile Elimination of Lead Ion from Water. *Cellulose* **2020**, *27*, 3233−3248.
(426) Li, J.; Tan, S.; Xu, Z. Anisotropic Nanocellulose Aerogel Loaded with Modified UiO-66 as Efficient Adsorbent for Heavy Metal Ions Removal. *Nanomaterials* **2020**, *10*, 1114.
(427) Hong, H.-J.; Yu, H.; Hong, S.; Hwang, J. Y.; Kim, S. M.; Park, M. S.; Jeong, H. S. Modified Tunicate Nanocellulose Liquid Crystalline Fiber as Closed Loop for Recycling Platinum-group Metals. *Carbohydr. Polym.* **2020**, *228*, 115424.
(428) Rodrigues, F. H.; de C. Magalhães, C. E.; Medina, A. L.; Fajardo, A. R. Hydrogel Composites Containing Nanocellulose as Adsorbents for Aqueous Removal of Heavy Metals: Design, Optimization, and Application. *Cellulose* **2019**, *26*, 9119−9133.
(429) Yang, X.; Biswas, S. K.; Han, J.; Tanpichai, S.; Li, M. C.; Chen, C.; Zhu, S.; Das, A. K.; Yano, H. Surface and Interface Engineering for Nanocellulosic Advanced Materials. *Adv. Mater.* **2021**, *33*, 2002264.
(430) Habibi, Y. Key Advances in the Chemical Modification of Nanocelluloses. *Chem. Soc. Rev.* **2014**, *43*, 1519−1542.
(431) Yu, X.; Tong, S.; Ge, M.; Wu, L.; Zuo, J.; Cao, C.; Song, W. Adsorption of Heavy Metal Ions from Aqueous Solution by Carboxylated Cellulose Nanocrystals. *J. Environ. Sci.* **2013**, *25*, 933−943.
(432) Suopajärvi, T.; Liimatainen, H.; Karjalainen, M.; Upola, H.; Niinimäki, J. Lead Adsorption with Sulfonated Wheat Pulp Nanocelluloses. *J. Water Process. Eng.* **2015**, *5*, 136−142.
(433) Qiao, H.; Zhou, Y.; Yu, F.; Wang, E.; Min, Y.; Huang, Q.; Pang, L.; Ma, T. Effective Removal of Cationic Dyes using Carboxylate-Functionalized Cellulose Nanocrystals. *Chemosphere* **2015**, *141*, 297−303.
(434) Batmaz, R.; Mohammed, N.; Zaman, M.; Minhas, G.; Berry, R. M.; Tam, K. C. Cellulose Nanocrystals as Promising Adsorbents for the Removal of Cationic Dyes. *Cellulose* **2014**, *21*, 1655−1665.
(435) Ma, H.; Hsiao, B. S.; Chu, B. Ultrafine Cellulose Nanofibers as Efficient Adsorbents for Removal of UO_2^{2+} in water. *ACS Macro Lett.* **2012**, *1*, 213−216.
(436) Sehaqui, H.; de Larraya, U. P.; Liu, P.; Pfenninger, N.; Mathew, A. P.; Zimmermann, T.; Tingaut, P. Enhancing Adsorption of Heavy Metal Ions onto Biobased Nanofibers from Waste Pulp Residues for Application in Wastewater Treatment. *Cellulose* **2014**, *21*, 2831−2844.
(437) Singh, K.; Arora, J. K.; Sinha, T. J. M.; Srivastava, S. Functionalization of Nanocrystalline Cellulose for Decontamination of Cr (III) and Cr (VI) from Aqueous System: Computational Modeling Approach. *Clean Technol. Environ. Policy* **2014**, *16*, 1179−1191.
(438) Sheikhi, A.; Safari, S.; Yang, H.; Van De Ven, T. G. Copper Removal using Electrosterically Stabilized Nanocrystalline Cellulose. *ACS Appl. Mater. Interfaces.* **2015**, *7*, 11301−11308.
(439) He, X.; Male, K. B.; Nesterenko, P. N.; Brabazon, D.; Paull, B.; Luong, J. H. Adsorption and Desorption of Methylene Blue on Porous Carbon Monoliths and Nanocrystalline Cellulose. *ACS Appl. Mater. Interfaces.* **2013**, *5*, 8796−8804.
(440) Jin, L.; Li, W.; Xu, Q.; Sun, Q. Amino-functionalized Nanocrystalline Cellulose as an Adsorbent for Anionic Dyes. *Cellulose* **2015**, *22*, 2443−2456.
(441) Hamid, H. A.; Jenidi, Y.; Thielemans, W.; Somerfield, C.; Gomes, R. L. Predicting the Capability of Carboxylated Cellulose Nanowhiskers for the Remediation of Copper from Water using Response Surface Methodology (RSM) and Artificial Neural Network (ANN) models. *Ind. Crops. Prod.* **2016**, *93*, 108−120.
(442) Singh, K.; Sinha, T. J. M.; Srivastava, S. Functionalized Nanocrystalline Cellulose: Smart Biosorbent for Decontamination of Arsenic. *Int. J. Miner. Process.* **2015**, *139*, 51−63.
(443) Hokkanen, S.; Repo, E.; Sillanpää, M. Removal of Heavy Metals from Aqueous Solutions by Succinic Anhydride Modified Mercerized Nanocellulose. *Chem. Eng. Sci.* **2013**, *223*, 40−47.
(444) Liu, P.; Oksman, K.; Mathew, A. P. Surface Adsorption and Self-assembly of Cu(II) ions on TEMPO-oxidized Cellulose Nanofibers in Aqueous Media. *J. Colloid Interface Sci.* **2016**, *464*, 175−182.
(445) Liu, P.; Borrell, P. F.; Božič, M.; Kokol, V.; Oksman, K.; Mathew, A. P. Nanocelluloses and their Phosphorylated Derivatives for Selective Adsorption of Ag^+, Cu^{2+} and Fe^{3+} from Industrial Effluents. *J. Hazard. Mater.* **2015**, *294*, 177−185.
(446) Brandes, R.; Belosinschi, D.; Brouillette, F.; Chabot, B. A New Electrospun Chitosan/Phosphorylated Nanocellulose Biosorbent for the Removal of Cadmium Ions from Aqueous Solutions. *J. Environ. Chem. Eng.* **2019**, *7*, 103477.

https://doi.org/10.1021/acs.chemrev.1c00683
Chem. Rev. 2022, 122, 8936−9031

(447) Zhang, Q.; Zhang, L.; Wu, W.; Xiao, H. Methods and Applications of Nanocellulose Loaded with Inorganic Nanomaterials: A Review. *Carbohydr. Polym.* **2020**, *229*, 115454.
(448) Tshikovhi, A.; Mishra, S. B.; Mishra, A. K. Nanocellulose-based Composites for the Rmoval of Contaminants from Wastewater. *Int. J. Biol. Macromol.* **2020**, *152*, 616−632.
(449) Alipour, A.; Zarinabadi, S.; Azimi, A.; Mirzaei, M. Adsorptive Removal of Pb(II) Ions from Aqueous Solutions by Thiourea-functionalized Magnetic ZnO/Nanocellulose Composite: Optimization by Response Surface Methodology (RSM). *Int. J. Biol. Macromol.* **2020**, *151*, 124−135.
(450) Anirudhan, T.; Deepa, J.; et al. Synthesis and Characterization of Multi-carboxyl-functionalized Nanocellulose/Nanobentonite Composite for the Adsorption of Uranium (VI) from Aqueous Solutions: Kinetic and Equilibrium Profiles. *Chem. Eng. Sci.* **2015**, *273*, 390−400.
(451) Sajab, M. S.; Chia, C. H.; Chan, C. H.; Zakaria, S.; Kaco, H.; Chook, S. W.; Chin, S. X.; et al. Bifunctional Graphene Oxide-Cellulose Nanofibril Aerogel Loaded with Fe (III) for the Removal of Cationic Dye via Simultaneous Adsorption and Fenton Oxidation. *Rsc Adv.* **2016**, *6*, 19819−19825.
(452) Ma, C.; Yi, L.; Yang, J.; Tao, J.; Li, J. Nanocellulose-organic Montmorillonite Nanocomposite Adsorbent for Diuron Removal from Aqueous Solution: Optimization using Response Surface Methodology. *Rsc Adv.* **2020**, *10*, 30734−30745.
(453) Herrera-Morales, J.; Morales, K.; Ramos, D.; Ortiz-Quiles, E. O.; Lopez-Encarnacion, J. M.; Nicolau, E. Examining the Use of Nanocellulose Composites for the Sorption of Contaminants of Emerging Concern: An Experimental and Computational Study. *ACS omega* **2017**, *2*, 7714−7722.
(454) Wang, N.; Wang, Y.-F.; Omer, A. M.; Ouyang, X.-k. Fabrication of Novel Surface-Imprinted Magnetic Graphene Oxide-grafted Cellulose Nanocrystals for Selective Extraction and Fast Adsorption of Fluoroquinolones from Water. *Anal. Bioanal. Chem.* **2017**, *409*, 6643−6653.
(455) Nath, B.; Chaliha, C.; Kalita, E.; Kalita, M. Synthesis and Characterization of ZnO: CeO_2: Nanocellulose: PANI Bionanocomposite. A Bimodal Agent for Arsenic Adsorption and Antibacterial Action. *Carbohydr. Polym.* **2016**, *148*, 397−405.
(456) Yu, H.; Zhang, S.; Wang, Y.; Yin, D.; Huang, J. Covalent Modification of Nanocellulose (NCC) by Functionalized Graphene oxide (GO) and the Study of Adsorption Mechanism. *Compos. Interfaces* **2021**, *28*, 145−158.
(457) Ma, J.; Sun, Y.; Zhang, M.; Yang, M.; Gong, X.; Yu, F.; Zheng, J. Comparative Study of Graphene Hydrogels and Aerogels Reveals the Important Role of Buried Water in Pollutant Adsorption. *Environ. Sci. Technol.* **2017**, *51*, 12283−12292.
(458) Lavoine, N.; Bergström, L. Nanocellulose-based Foams and Aerogels: Processing, Properties, and Applications. *J. Mater. Chem. A* **2017**, *5*, 16105−16117.
(459) De France, K. J.; Hoare, T.; Cranston, E. D. Review of Hydrogels and Aerogels Containing Nanocellulose. *Chem. Mater.* **2017**, *29*, 4609−4631.
(460) Zhu, L.; Zong, L.; Wu, X.; Li, M.; Wang, H.; You, J.; Li, C. Shapeable Fibrous Aerogels of Metal-organic-frameworks Templated with Nanocellulose for Rapid and Large-capacity Adsorption. *ACS Nano* **2018**, *12*, 4462−4468.
(461) Tang, J.; Song, Y.; Zhao, F.; Spinney, S.; da Silva Bernardes, J.; Tam, K. C. Compressible Cellulose Nanofibril (CNF) based Aerogels Produced via a Bio-inspired Strategy for Heavy Metal Ion and Dye Removal. *Carbohydr. Polym.* **2019**, *208*, 404−412.
(462) Nia, M. H.; Tavakolian, M.; Kiasat, A. R.; van de Ven, T. G. Hybrid Aerogel Nanocomposite of Dendritic Colloidal Silica and Hairy Nanocellulose: an Effective Dye Adsorbent. *Langmuir* **2020**, *36*, 11963−11974.
(463) Zhang, X.; Elsayed, I.; Navarathna, C.; Schueneman, G. T.; Hassan, E. B. Biohybrid Hydrogel and Aerogel from Self-assembled Nanocellulose and Nanochitin as a High-efficiency Adsorbent for Water Purification. *ACS Appl. Mater. Interfaces.* **2019**, *11*, 46714−46725.
(464) Zhu, G.; Xu, H.; Dufresne, A.; Lin, N. High-adsorption, Self-extinguishing, Thermal, and Acoustic-resistance Aerogels Based on Organic and Inorganic Waste Valorization from Cellulose Nanocrystals and Red Mud. *ACS Sustain. Chem. Eng.* **2018**, *6*, 7168−7180.
(465) Yang, X.; Cranston, E. D. Chemically Cross-linked Cellulose Nanocrystal Aerogels with Shape Recovery and Superabsorbent Properties. *Chem. Mater.* **2014**, *26*, 6016−6025.
(466) Hubbe, M.; Hadi Hasan, S.; Ducoste, J. Cellulosic Substrates for Removal of Pollutants from Aqueous Systems: A Review. 1. Metals. *BioResources* **2011**, *6*, 2161−2287.
(467) Chen, X. Modeling of Experimental Adsorption Isotherm Data. *Information* **2015**, *6*, 14−22.
(468) Tan, K.; Hameed, B. Insight into the Adsorption Kinetics Models for the Removal of Contaminants from Aqueous Solutions. *J. Taiwan Inst. Chem. Eng.* **2017**, *74*, 25−48.
(469) Mukherjee, S.; Ramireddy, H.; Baidya, A.; Amala, A.; Sudhakar, C.; Mondal, B.; Philip, L.; Pradeep, T. Nanocellulose-Reinforced Organo-Inorganic Nanocomposite for Synergistic and Affordable Defluoridation of Water and an Evaluation of Its Sustainability Metrics. *ACS Sustain. Chem. Eng.* **2020**, *8*, 139−147.
(470) Bratko, D.; Jönsson, B.; Wennerström, H. Electrical Double Layer Interactions with Image Charges. *Chem. Phys. Lett.* **1986**, *128*, 449−454.
(471) Williams, R. J. P. The Stability of the Complexes of the Group II_A Metal Ions. *J. Chem. Soc.* **1952**, 3770−3778.
(472) Huang, X.; Dognani, G.; Hadi, P.; Yang, M.; Job, A. E.; Hsiao, B. S. Cationic Dialdehyde Nanocellulose from Sugarcane Bagasse for Efficient Chromium(VI) Removal. *ACS Sustain. Chem. Eng.* **2020**, *8*, 4734−4744.
(473) Lawrance, G. A. *Introduction to Coordination Chemistry*; John Wiley & Sons: Great Britain, 2013; p 304.
(474) Li, W.; Ju, B.; Zhang, S. A Green L-cysteine Modified Cellulose Nanocrystals Biosorbent for Adsorption of Mercury Ions from Aqueous Solutions. *Rsc Adv.* **2019**, *9*, 6986−6994.
(475) Avery, S. V.; Tobin, J. M. Mechanism of Adsorption of Hard and Soft Metal Ions to *Saccharomyces cerevisiae* and Influence of Hard and Soft Anions. *Appl. Environ. Microbiol.* **1993**, *59*, 2851−2856.
(476) Herrera-Morales, J.; Turley, T. A.; Betancourt-Ponce, M.; Nicolau, E. Nanocellulose-Block Copolymer Films for the Removal of Emerging Organic Contaminants from Aqueous Solutions. *Materials* **2019**, *12*, 230.
(477) Moradeeya, P. G.; Kumar, M. A.; Thorat, R. B.; Rathod, M.; Khambhaty, Y.; Basha, S. Nanocellulose for Biosorption of Chlorpyrifos from Water: Chemometric Optimization, Kinetics and Equilibrium. *Cellulose* **2017**, *24*, 1319−1332.
(478) Li, J.; Zuo, K.; Wu, W.; Xu, Z.; Yi, Y.; Jing, Y.; Dai, H.; Fang, G. Shape Memory Aerogels from Nanocellulose and Polyethyleneimine as a Novel Adsorbent for Removal of Cu (II) and Pb (II). *Carbohydr. Polym.* **2018**, *196*, 376−384.
(479) Wei, J.; Yang, Z.; Sun, Y.; Wang, C.; Fan, J.; Kang, G.; Zhang, R.; Dong, X.; Li, Y. Nanocellulose-based Magnetic Hybrid Aerogel for Adsorption of Heavy Metal Ions from Water. *J. Mater. Sci.* **2019**, *54*, 6709−6718.
(480) Mohammed, N.; Grishkewich, N.; Waeijen, H. A.; Berry, R. M.; Tam, K. C. Continuous Flow Adsorption of Methylene Blue by Cellulose Nanocrystal-alginate Hydrogel Beads in Fixed Bed Columns. *Carbohydr. Polym.* **2016**, *136*, 1194−1202.
(481) Hokkanen, S.; Bhatnagar, A.; Sillanpää, M. A Review on Modification Methods to Cellulose-based Adsorbents to Improve Adsorption Capacity. *Water Res.* **2016**, *91*, 156−173.
(482) Ling, S.; Qin, Z.; Huang, W.; Cao, S.; Kaplan, D. L.; Buehler, M. J. Design and Function of Biomimetic Multilayer Water Purification Membranes. *Sci. Adv.* **2017**, *3*, No. e1601939.
(483) Mukherjee, S.; Kumar, A. A.; Sudhakar, C.; Kumar, R.; Ahuja, T.; Mondal, B.; Srikrishnarka, P.; Philip, L.; Pradeep, T. Sustainable and Affordable Composites Built using Microstructures Performing Better than Nanostructures for Arsenic Removal. *ACS Sustain. Chem. Eng.* **2019**, *7*, 3222−3233.

https://doi.org/10.1021/acs.chemrev.1c00683
Chem. Rev. 2022, 122, 8936−9031

(484) Raja, S.; Mattoso, L. H. Functionalized Polymer-Based Composite Photocatalysts. In *Green Photocatalysts*; Springer: Cham, 2020; p 188.
(485) Fujishima, A.; Honda, K. TiO_2 Photoelectrochemistry and Photocatalysis. *Nature* **1972**, *238*, 37−38.
(486) Abdalkarim, S. Y. H.; Yu, H.-Y.; Wang, C.; Huang, L.-X.; Yao, J. Green Synthesis of Sheet-like Cellulose Nanocrystal-Zinc Oxide Nanohybrids with Multifunctional Performance through One-step Hydrothermal Method. *Cellulose* **2018**, *25*, 6433−6446.
(487) Rathod, M.; Moradeeya, P. G.; Haldar, S.; Basha, S. Nanocellulose/TiO_2 Composites: Preparation, Characterization and Application in the Photocatalytic Degradation of a Potential Endocrine Disruptor, Mefenamic Acid, in Aqueous Media. *Photochem. Photobiol. Sci.* **2018**, *17*, 1301−1309.
(488) Gupta, K.; Kaushik, A.; Tikoo, K.; Kumar, V.; Singhal, S. Enhanced Catalytic Activity of Composites of $NiFe_2O_4$ and Nano Cellulose Derived from Waste Biomass for the Mitigation of Organic Pollutants. *Arab. J. Chem.* **2020**, *13*, 783−798.
(489) Rahman, K. U.; Ferreira-Neto, E. P.; Rahman, G. U.; Parveen, R.; Monteiro, A. S.; Rahman, G.; Van Le, Q.; Domeneguetti, R. R.; Ribeiro, S. J.; Ullah, S. Flexible Bacterial Cellulose-based BC-SiO_2-TiO_2-Ag Membranes with Self-cleaning, Photocatalytic, Antibacterial and UV-shielding Properties as a Potential Multifunctional Material for Combating Infections and Environmental Applications. *J. Environ. Chem. Eng.* **2021**, *9*, 104708.
(490) Xiao, H.; Zhang, W.; Wei, Y.; Yu, L.; Chen, L. Fabrication of Fe/ZnO Composite Nanosheets by Nanofibrillated Cellulose as Soft Template and Photocatalytic Degradation for Tetracycline. *J. Inorg. Organomet. Polym. Mater.* **2018**, *28*, 1299−1304.
(491) Su, X.; Chen, W.; Han, Y.; Wang, D.; Yao, J. *In situ* Synthesis of Cu_2O on Cotton Fibers with Antibacterial Properties and Reusable Photocatalytic Degradation of Dyes. *Appl. Surf. Sci.* **2021**, *536*, 147945.
(492) Evdokimova, O.; Fedulova, A.; Evdokimova, A.; Kusova, T.; Agafonov, A. Preparation of Hybrid Nanocomposites Based on Nanoscale Cellulose and Magnetic Nanoparticles with Photocatalytic Properties. *Inorg. Mater. Appl. Res.* **2020**, *11*, 371−376.
(493) Zhang, Y.; Zhou, Z.; Yuan, K.; Wen, F.; Tan, J.; Hu, C.; Wang, H. Fabrication of a Modified Straw Cellulose and Cerium Oxide Nanocomposite and Its Visible-light Photocatalytic Reduction Activity. *J. Environ. Chem. Eng.* **2017**, *5*, 3734−3740.
(494) Tian, C.; Luo, S.; She, J.; Qing, Y.; Yan, N.; Wu, Y.; Liu, Z. Cellulose Nanofibrils Enable Flower-like BiOCl for High-performance Photocatalysis under Visible-light Irradiation. *Appl. Surf. Sci.* **2019**, *464*, 606−615.
(495) Lin, Z.; Lu, Y.; Huang, J. A Hierarchical Ag_2O-Nanoparticle/TiO_2-Nanotube Composite Derived from Natural Cellulose Substance with Enhanced Photocatalytic Performance. *Cellulose* **2019**, *26*, 6683−6700.
(496) Tian, C.; Tao, X.; Luo, S.; Qing, Y.; Lu, X.; She, J.; Wu, Y. Cellulose Nanofibrils Anchored Ag on Graphitic Carbon Nitride for Efficient Photocatalysis under Visible Light. *Environ. Sci. Nano* **2018**, *5*, 2129−2143.
(497) Yang, J.; Yu, J.; Fan, J.; Sun, D.; Tang, W.; Yang, X. Biotemplated Preparation of CdS Nanoparticles/Bacterial Cellulose Hybrid Nanofibers for Photocatalysis Application. *J. Hazard. Mater.* **2011**, *189*, 377−383.
(498) Shak, K. P. Y.; Pang, Y. L.; Mah, S. K. Nanocellulose: Recent Advances and Its Prospects in Environmental Remediation. *Beilstein J. Nanotechnol.* **2018**, *9*, 2479−2498.
(499) Wei, H.; Rodriguez, K.; Renneckar, S.; Vikesland, P. J. Environmental Science and Engineering Applications of Nanocellulose-based Nanocomposites. *Environ. Sci. Nano* **2014**, *1*, 302−316.
(500) Kaushik, M.; Moores, A. Nanocelluloses as Versatile Supports for Metal Nanoparticles and their Applications in Catalysis. *Green Chem.* **2016**, *18*, 622−637.
(501) Oun, A. A.; Shankar, S.; Rhim, J.-W. Multifunctional Nanocellulose/Metal and Metal Oxide Nanoparticle Hybrid Nanomaterials. *Crit. Rev. Food Sci. Nutr.* **2020**, *60*, 435−460.
(502) Liu, J.; Liu, X.; Li, D.; Yue, G.; Li, H.; Li, S.; Gao, S.; Wang, N.; Cui, Z.; Bai, J.; Zhao, Y. Multi-Structure Hollow Nanofibers: Controlled Synthesis and Photocatalytic Applications. *ChemNanoMat* **2020**, *6*, 1149−1163.
(503) Li, H.; Zhang, L.; Lu, H.; Ma, J.; Zhou, X.; Wang, Z.; Yi, C. Macro-/Nanoporous Al-doped ZnO/Cellulose Composites based on Tunable Cellulose Fiber Sizes for Enhancing Photocatalytic Properties. *Carbohydr. Polym.* **2020**, *250*, 116873.
(504) Wei, G.; Zuo, H.-F.; Guo, Y.-R.; Pan, Q.-J. Synthesis of ZnO with Enhanced Photocatalytic Activity: A Novel Approach using Nanocellulose. *BioResources* **2016**, *11*, 6244−6253.
(505) Lefatshe, K.; Muiva, C. M.; Kebaabetswe, L. P. Extraction of Nanocellulose and *In situ* Casting of ZnO/Cellulose Nanocomposite with Enhanced Photocatalytic and Antibacterial Activity. *Carbohydr. Polym.* **2017**, *164*, 301−308.
(506) Korhonen, J. T.; Hiekkataipale, P.; Malm, J.; Karppinen, M.; Ikkala, O.; Ras, R. H. Inorganic Hollow Nanotube Aerogels by Atomic Layer Deposition onto Native Nanocellulose Templates. *ACS Nano* **2011**, *5*, 1967−1974.
(507) Zhang, D.; Qi, L. Synthesis of Mesoporous Titania Networks Consisting of Anatase Nanowires by Templating of Bacterial Cellulose Membranes. *Commun. Chem.* **2005**, *21*, 2735−2737.
(508) Shi, F.; Yu, T.; Hu, S.-C.; Liu, J.-X.; Yu, L.; Liu, S.-H. Synthesis of Highly Porous SiO_2-(WO_3) x· TiO_2 Composite Aerogels using Bacterial Cellulose as Template with Solvothermal Assisted Crystallization. *Chem. Eng. Sci.* **2016**, *292*, 105−112.
(509) Zheng, W.-l.; Hu, W.-l.; Chen, S.-y.; Zheng, Y.; Zhou, B.-h.; Wang, H.-p. High Photocatalytic Properties of Zinc Oxide Nanoparticles with Amidoximated Bacterial Cellulose Nanofibers as Templates. *Chin. J. Polym. Sci.* **2014**, *32*, 169−176.
(510) Wahid, F.; Duan, Y.-X.; Hu, X.-H.; Chu, L.-Q.; Jia, S.-R.; Cui, J.-D.; Zhong, C. A Facile Construction of Bacterial Cellulose/ZnO Nanocomposite Films and their Photocatalytic and Antibacterial Properties. *Int. J. Biol. Macromol.* **2019**, *132*, 692−700.
(511) Xiao, H.; Shan, Y.; Zhang, W.; Huang, L.; Chen, L.; Ni, Y.; Boury, B.; Wu, H. C-nanocoated ZnO by TEMPO-oxidized Cellulose Templating for Improved Photocatalytic Performance. *Carbohydr. Polym.* **2020**, *235*, 115958.
(512) Zhang, H.; Banfield, J. F. Thermodynamic Analysis of Phase Stability of Nanocrystalline Titania. *J. Mater. Chem. A* **1998**, *8*, 2073−2076.
(513) Zou, R.; Zhang, Z.; Yu, L.; Tian, Q.; Chen, Z.; Hu, J. A General Approach for the Growth of Metal Oxide Nanorod Arrays on Graphene Sheets and their Applications. *Chem. - Eur. J.* **2011**, *17*, 13912−13917.
(514) Reyes-Coronado, D.; Rodríguez-Gattorno, G.; Espinosa-Pesqueira, M.; Cab, C.; de Coss, R. d.; Oskam, G. Phase-pure TiO_2 Nanoparticles: Anatase, Brookite and Rutile. *Nanotechnology* **2008**, *19*, 145605.
(515) Kandiel, T. A.; Feldhoff, A.; Robben, L.; Dillert, R.; Bahnemann, D. W. Tailored Titanium Dioxide Nanomaterials: Anatase Nanoparticles and Brookite Nanorods as Highly Active Photocatalysts. *Chem. Mater.* **2010**, *22*, 2050−2060.
(516) Nunes, D.; Pimentel, A.; Araujo, A.; Calmeiro, T.; Panigrahi, S.; Pinto, J.; Barquinha, P.; Gama, M.; Fortunato, E.; Martins, R. Enhanced UV Flexible Photodetectors and Photocatalysts based on TiO_2 Nanoplatforms. *Top. Catal.* **2018**, *61*, 1591−1606.
(517) Ivanova, A.; Fattakhova-Rohlfing, D.; Kayaalp, B. E.; Rathouský, J.; Bein, T. Tailoring the Morphology of Mesoporous Titania Thin Films through Biotemplating with Nanocrystalline Cellulose. *J. Am. Chem. Soc.* **2014**, *136*, 5930−5937.
(518) Ivanova, A.; Fravventura, M. C.; Fattakhova-Rohlfing, D.; Rathouský, J.; Movsesyan, L.; Ganter, P.; Savenije, T. J.; Bein, T. Nanocellulose-templated Porous Titania Scaffolds Incorporating Presynthesized Titania Nanocrystals. *Chem. Mater.* **2015**, *27*, 6205−6212.
(519) Li, Y.; Zhang, J.; Zhan, C.; Kong, F.; Li, W.; Yang, C.; Hsiao, B. S. Facile Synthesis of TiO_2/CNC Nanocomposites for Enhanced Cr (VI) Photoreduction: Synergistic Roles of Cellulose Nanocrystals. *Carbohydr. Polym.* **2020**, *233*, 115838.

https://doi.org/10.1021/acs.chemrev.1c00683
Chem. Rev. 2022, 122, 8936−9031

(520) Li, Y.; Cao, L.; Li, L.; Yang, C. *In situ* Growing Directional Spindle TiO_2 Nanocrystals on Cellulose Fibers for Enhanced Pb^{2+} Adsorption from Water. *J. Hazard. Mater.* **2015**, *289*, 140−148.
(521) Xiao, H.; Li, J.; He, B. Anatase-titania Templated by Nanofibrillated Cellulose and Photocatalytic Dgradation for Methyl Orange. *J. Inorg. Organomet. Polym. Mater.* **2017**, *27*, 1022−1027.
(522) Henry, A. l.; Plumejeau, S.; Heux, L.; Louvain, N.; Monconduit, L.; Stievano, L.; Boury, B. Conversion of Nanocellulose Aerogel into TiO_2 and TiO_2@C Nano-thorns by Direct Anhydrous Mineralization with $TiCl_4$. Evaluation of Electrochemical Properties in Li Batteries. *ACS Appl. Mater. Interfaces.* **2015**, *7*, 14584−14592.
(523) Rauwel, E.; Clavel, G.; Willinger, M. G.; Rauwel, P.; Pinna, N. Non-aqueous Routes to Metal Oxide Thin Films by Atomic Layer Deposition. *Angew. Chem.* **2008**, *120*, 3648−3651.
(524) Zhan, C.; Li, Y.; Sharma, P. R.; He, H.; Sharma, S. K.; Wang, R.; Hsiao, B. S. A Study of TiO_2 Nanocrystal Growth and Environmental Remediation Capability of TiO_2/CNC Nanocomposites. *Rsc Adv.* **2019**, *9*, 40565−40576.
(525) Lazar, M. A.; Varghese, S.; Nair, S. S. Photocatalytic Water Treatment by Titanium Dioxide: Recent Updates. *Catalysts* **2012**, *2*, 572−601.
(526) Yu, J. C.; Zhang, L.; Yu, J. Rapid Synthesis of Mesoporous TiO_2 with High Photocatalytic Activity by Ultrasound-induced Agglomeration. *New J. Chem.* **2002**, *26*, 416−420.
(527) Wang, W.; Wang, J.; Shi, X.; Yu, Z.; Song, Z.; Dong, L.; Jiang, G.; Han, S. Synthesis of Mesoporous TiO_2 Induced by Nanocellulose and Its Photocatalytic Properties. *BioResources* **2016**, *11*, 3084−3093.
(528) Yang, D.; Qi, L.; Ma, J. Eggshell Membrane Templating of Hierarchically Ordered Macroporous Networks Composed of TiO_2 Tubes. *Adv. Mater.* **2002**, *14*, 1543−1546.
(529) Chen, Y.; Liu, H.; Geng, B.; Ru, J.; Cheng, C.; Zhao, Y.; Wang, L. A Reusable Surface-Quaternized Nanocellulose-based Hybrid Cryogel Loaded with N-doped TiO_2 for Self-integrated Adsorption/Photo-degradation of Methyl Orange Dye. *Rsc Adv.* **2017**, *7*, 17279−17288.
(530) Sampaio, M. J.; Bacsa, R.; Benyounes, A.; Axet, R.; Serp, P.; Silva, C. G.; Silva, A. M.; Faria, J. L. Synergistic Effect between Carbon Nanomaterials and ZnO for Photocatalytic Water Decontamination. *J. Catal.* **2015**, *331*, 172−180.
(531) Ning, R.; Takeuchi, M.; Lin, J.-M.; Saito, T.; Isogai, A. Influence of the Morphology of Zinc Oxide Nanoparticles on the Properties of Zinc Oxide/Nanocellulose Composite Films. *React. Funct. Polym.* **2018**, *131*, 293−298.
(532) Nahi, J.; Radhakrishnan, A.; Beena, B. Green Synthesis of Zinc Oxide Incorporated Nanocellulose with Visible Light Photocatalytic Activity and Application for the Removal of Antibiotic Enrofloxacin from Aqueousmedia. *Mater. Today: Proc.* **2021**, *41*, 583−589.
(533) Nahi, J.; Beena, B.; Radhakrishnan, A. Nano Zinc Oxide Incorporated Nanocellulose Composite for the Photodegradation of Antibiotic Aueromycine Hydrochloride from Aqueous Solutions Under Visible Light Irradiation. *Sci. Technol. Dev.* **2020**, *IX* (II), 65−70.
(534) Modi, S.; Fulekar, M. Synthesis and Characterization of Zinc Oxide Nanoparticles and Zinc Oxide/Cellulose Nanocrystals Nanocomposite for Photocatalytic Degradation of Methylene Blue Dye Under Solar Light Irradiation. *Nanotechnol. Environ. Eng.* **2020**, *5*, 18.
(535) Zhao, S.-W.; Zuo, H.-F.; Guo, Y.-R.; Pan, Q.-J. Carbon-doped ZnO Aided by Carboxymethyl Cellulose: Fabrication, Photoluminescence and Photocatalytic Applications. *J. Alloys Compd.* **2017**, *695*, 1029−1037.
(536) Yang, R.-T.; Yu, H.-Y.; Song, M.-L.; Zhou, Y.-W.; Yao, J.-M. Flower-like Zinc Oxide Nanorod Clusters Grown on Spherical Cellulose Nanocrystals via Simple Chemical Precipitation Method. *Cellulose* **2016**, *23*, 1871−1884.
(537) Jamal, N.; Radhakrishnan, A.; Raghavan, R.; Bhaskaran, B. Efficient Photocatalytic Degradation of Organic Dye from Aqueous Solutions Over Zinc Oxide Incorporated Nanocellulose Under Visible Light Irradiation. *Main Group Met. Chem.* **2020**, *43*, 84−91.
(538) Anirudhan, T.; Deepa, J. Nano-zinc Oxide Incorporated Graphene Oxide/Nanocellulose Composite for the Adsorption and Photocatalytic Degradation of Ciprofloxacin Hydrochloride from Aqueous Solutions. *J. Colloid Interface Sci.* **2017**, *490*, 343−356.
(539) Nair, S. S.; Chen, J.; Slabon, A.; Mathew, A. P. Converting Cellulose Nanocrystals into Photocatalysts by Functionalisation with Titanium Dioxide Nanorods and Gold Nanocrystals. *Rsc Adv.* **2020**, *10*, 37374−37381.
(540) Liu, B.; Pan, Y.; Sun, G.; Huang, J. The Preparation and Characterization of the Ni−NiO/TiO_2 Hollow Composite Materials on Micro-nano Cellulose Fibers. *Vacuum* **2018**, *155*, 553−558.
(541) Hou, D.; Goei, R.; Wang, X.; Wang, P.; Lim, T.-T. Preparation of Carbon-sensitized and Fe-Er Codoped TiO_2 with Response Surface Methodology for Bisphenol A Photocatalytic Degradation Under Visible-light Irradiation. *Appl. Catal. B: Environ.* **2012**, *126*, 121−133.
(542) Rauf, M. A.; Meetani, M. A.; Hisaindee, S. An Overview on the Photocatalytic Degradation of Azo Dyes in the Presence of TiO_2 Doped with Selective Transition Metals. *Desalination* **2011**, *276*, 13−27.
(543) Gan, L.; Geng, A.; Song, C.; Xu, L.; Wang, L.; Fang, X.; Han, S.; Cui, J.; Mei, C. Simultaneous Removal of Rhodamine B and Cr(VI) from Water using Cellulose Carbon Nanofiber Incorporated with Bismuth Oxybromide: The Effect of Cellulose Pyrolysis Temperature on Photocatalytic Performance. *Environ. Res.* **2020**, *185*, 109414.
(544) Melone, L.; Altomare, L.; Alfieri, I.; Lorenzi, A.; De Nardo, L.; Punta, C. Ceramic Aerogels from TEMPO-oxidized Cellulose Nanofibre Templates: Synthesis, Characterization, and Photocatalytic Properties. *J. Photochem. Photobiol. A: Chem.* **2013**, *261*, 53−60.
(545) Ferreira-Neto, E. P.; Ullah, S.; da Silva, T. C.; Domeneguetti, R. R.; Perissinotto, A. P.; de Vicente, F. S.; Rodrigues-Filho, U. P.; Ribeiro, S. J. Bacterial Nanocellulose/MoS_2 Hybrid Aerogels as Bifunctional Adsorbent/Photocatalyst Membranes for In-flow Water Decontamination. *ACS Appl. Mater. Interfaces.* **2020**, *12*, 41627−41643.
(546) Lebogang, L.; Bosigo, R.; Lefatshe, K.; Muiva, C. Ag_3PO_4/Nanocellulose Composite for Effective Sunlight Driven Photodegradation of Organic Dyes in Wastewater. *Mater. Chem. Phys.* **2019**, *236*, 121756.
(547) Kayaci, F.; Vempati, S.; Donmez, I.; Biyikli, N.; Uyar, T. Role of Zinc Interstitials and Oxygen Vacancies of ZnO in Photocatalysis: A Bottom-up Approach to Control Defect Density. *Nanoscale* **2014**, *6*, 10224−10234.
(548) Wang, J.; Wang, Z.; Huang, B.; Ma, Y.; Liu, Y.; Qin, X.; Zhang, X.; Dai, Y. Oxygen Vacancy Induced Band-gap Narrowing and Enhanced Visible Light Photocatalytic Activity of ZnO. *ACS Appl. Mater. Interfaces.* **2012**, *4*, 4024−4030.
(549) Chen, R.; Wang, J.; Fang, F.; Zhang, X. Influence of Buried Modified Layer on Crack Propagation and Diamond Turning of Silicon. *Precis. Eng.* **2019**, *55*, 426−432.
(550) Ansari, S. A.; Ansari, S.; Foaud, H.; Cho, M. H. Facile and Sustainable Synthesis of Carbon-Doped ZnO Nanostructures Towards the Superior Visible Light Photocatalytic Performance. *New J. Chem.* **2017**, *41*, 9314−9320.
(551) Pan, L.; Muhammad, T.; Ma, L.; Huang, Z.-F.; Wang, S.; Wang, L.; Zou, J.-J.; Zhang, X. MOF-derived C-doped ZnO Prepared via a Two-step Calcination for Efficient Photocatalysis. *Appl. Catal. B: Environ.* **2016**, *189*, 181−191.
(552) Miller, D. J.; Dreyer, D. R.; Bielawski, C. W.; Paul, D. R.; Freeman, B. D. Surface Modification of Water Purification Membranes. *Angew. Chem., Int. Ed. Engl.* **2017**, *56*, 4662−4711.
(553) Werber, J. R.; Osuji, C. O.; Elimelech, M. Materials for Next-generation Desalination and Water Purification Membranes. *Nat. Rev. Mater.* **2016**, *1*, 16018.
(554) Park, H. B.; Kamcev, J.; Robeson, L. M.; Elimelech, M.; Freeman, B. D. Maximizing the Right Stuff: The Trade-off Between Membrane Permeability and Selectivity. *Science* **2017**, *356*, No. eaab0530.
(555) Favier, V.; Cavaille, J. Y.; Canova, G. R.; Shrivastava, S. C. Mechanical Percolation in Cellulose Whisker Nanocomposites. *Polym. Eng. Sci.* **1997**, *37*, 1732−1739.
(556) Favier, S.; Dendievel, R.; Canova, G.; Cavaille, J. Y.; Gilormini, P. Simulation and Modelling of Three-dimensional Percolating

https://doi.org/10.1021/acs.chemrev.1c00683
Chem. Rev. 2022, 122, 8936−9031

Structures: Case of a Latex Reinforced by a Network of Cellulose Fibres. *Acta Mater.* **1997**, *45*, 1557−1565.
(557) Ansari, F.; Berglund, L. A. *Multifunctional Polymeric Nanocomposites Based on Cellulose Reinforcements*; William Andrew Publishing: Oxford, UK, 2016.
(558) Page, D. H. A Theory for the Tensile Strength of Paper. *Tappi* **1969**, *52*, 674−681.
(559) Hagiopol, C.; Johnston, J. W. *Chemistry of Modern Papermaking*; CRC Press, Taylor & Francis Group: Boca Raton, FL, USA, 2012; p 431.
(560) Espy, H. H. The Mechanism of Wet-Strength Development in Paper—A Review. *Tappi J.* **1995**, *78*, 90−99.
(561) Yang, W.; Bian, H.; Jiao, L.; Wu, W.; Deng, Y.; Dai, H. High Wet-strength, Thermally Stable and Transparent TEMPO-oxidized Cellulose Nanofibril Film via Cross-linking with Poly-amide Epichlorohydrin Resin. *RSC Adv.* **2017**, *7*, 31567−31573.
(562) Quellmalz, A.; Mihranyan, A. Citric Acid Cross-linked Nanocellulose-based Paper for Size-Exclusion Nanofiltration. *ACS Biomater. Sci. Eng.* **2015**, *1*, 271−276.
(563) Mautner, A.; Lee, K.-Y.; Tammelin, T.; Mathew, A. P.; Nedoma, A. J.; Li, K.; Bismarck, A. Cellulose Nanopapers as Tight Aqueous Ultrafiltration Membranes. *React. Funct Polym.* **2015**, *86*, 209−214.
(564) Lee, K. Y.; Buldum, G.; Mantalaris, A.; Bismarck, A. More than Meets the Eye in Bacterial Cellulose: Biosynthesis, Bioprocessing, and Applications in Advanced Fiber Composites. *Macromol. Biosci.* **2014**, *14*, 10−32.
(565) Ma, H.; Burger, C.; Hsiao, B. S.; Chu, B. Ultra-fine Cellulose Nanofibers: New Nano-scale Materials for Water Purification. *J. Mater. Chem.* **2011**, *21*, 7507−7510.
(566) Zhang, W. Experimental and Computational Analysis of Random Cylinder Packing and Applications. Agricultural and Mechanical College, Louisiana State University, LSU Doctoral Dissertations, 2006. https://digitalcommons.lsu.edu/gradschool_dissertations/163.
(567) Fisher, L. R.; Israelachvili, J. N. Experimental Studies on the Applicability of the Kelvin Equation to Highly Curved Concave Menisci. *J. Colloid Interface Sci.* **1981**, *80*, 528−541.
(568) Minelli, M.; Baschetti, M. G.; Doghieri, F.; Ankerfors, M.; Lindström, T.; Siró, I.; Plackett, D. Investigation of Mass Transport Properties of Microfibrillated Cellulose (MFC) films. *J. Membr. Sci.* **2010**, *358*, 67−75.
(569) Aulin, C.; Gällstedt, M.; Lindström, T. Oxygen and Oil Barrier Properties of Microfibrillated Cellulose Films and Coatings. *Cellulose* **2010**, *17*, 559−574.
(570) Wang, Z.; Zhang, W.; Yu, J.; Zhang, L.; Liu, L.; Zhou, X.; Huang, C.; Fan, Y. Preparation of Nanocellulose/Filter Paper (NC/FP) Composite Membranes for High-performance Filtration. *Cellulose* **2019**, *26*, 1183−1194.
(571) Gustafsson, S.; Mihranyan, A. Strategies for Tailoring the Pore-size Distribution of Virus Retention Filter Papers. *ACS Appl. Mater. Interfaces* **2016**, *8*, 13759−13767.
(572) Orsolini, P.; Marchesi D'Alvise, T.; Boi, C.; Geiger, T.; Caseri, W. R.; Zimmermann, T. Nanofibrillated Cellulose Templated Membranes with High Permeance. *ACS Appl. Mater. Interfaces* **2016**, *8*, 33943−33954.
(573) Mautner, A.; Lee, K. Y.; Lahtinen, P.; Hakalahti, M.; Tammelin, T.; Li, K.; Bismarck, A. Nanopapers for Organic Solvent Nanofiltration. *Chem. Commun.* **2014**, *50*, 5778−5781.
(574) Karim, Z.; Claudpierre, S.; Grahn, M.; Oksman, K.; Mathew, A. P. Nanocellulose based Functional Membranes for Water Cleaning: Tailoring of Mechanical Properties, Porosity and Metal Ion Capture. *J. Membr. Sci.* **2016**, *514*, 418−428.
(575) Sehaqui, H.; Zhou, Q.; Berglund, L. A. High-porosity Aerogels of High Specific Surface Area Prepared from Nanofibrillated Cellulose (NFC). *Compos. Sci. Technol.* **2011**, *71*, 1593−1599.
(576) Visanko, M.; Liimatainen, H.; Sirvio, J. A.; Haapala, A.; Sliz, R.; Niinimaki, J.; Hormi, O. Porous Thin Film Barrier Layers from 2,3-dicarboxylic Acid Cellulose Nanofibrils for Membrane Structures. *Carbohydr. Polym.* **2014**, *102*, 584−589.
(577) Ma, H.; Burger, C.; Hsiao, B. S.; Chu, B. Nanofibrous Microfiltration Membrane Based on Cellulose Nanowhiskers. *Biomacromolecules* **2012**, *13*, 180−186.
(578) Hu, M.-X.; Niu, H.-M.; Chen, X.-L.; Zhan, H.-B. Natural Cellulose Microfiltration Membranes for Oil/Water Nanoemulsions Separation. *Colloids Surf. A: Physicochem. Eng. Asp.* **2019**, *564*, 142−151.
(579) Aguilar-Sanchez, A.; Jalvo, B.; Mautner, A.; Rissanen, V.; Kontturi, K. S.; Abdelhamid, H. N.; Tammelin, T.; Mathew, A. P. Charged Ultrafiltration Membranes based on TEMPO-oxidized Cellulose Nanofibrils/Poly(vinyl alcohol) Antifouling Coating. *Rsc Adv.* **2021**, *11*, 6859−6868.
(580) Bai, L.; Liu, Y.; Bossa, N.; Ding, A.; Ren, N.; Li, G.; Liang, H.; Wiesner, M. R. Incorporation of Cellulose Nanocrystals (CNCs) into the Polyamide Layer of Thin-film Composite (TFC) Nanofiltration Membranes for Enhanced Separation Performance and Antifouling Properties. *Environ. Sci. Technol.* **2018**, *52*, 11178−11187.
(581) Kadhom, M.; Albayati, N.; Salih, S.; Al-Furaiji, M.; Bayati, M.; Deng, B. Role of Cellulose Micro and Nano Crystals in Thin Film and Support Layer of Nanocomposite Membranes for Brackish Water Desalination. *Membranes* **2019**, *9*, 101.
(582) Asempour, F.; Emadzadeh, D.; Matsuura, T.; Kruczek, B. Synthesis and Characterization of Novel Cellulose Nanocrystals-based Thin Film Nanocomposite Membranes for Reverse Osmosis Applications. *Desalination* **2018**, *439*, 179−187.
(583) Cruz-Tato, P.; Ortiz-Quiles, E. O.; Vega-Figueroa, K.; Santiago-Martoral, L.; Flynn, M.; Díaz-Vázquez, L. M.; Nicolau, E. Metalized Nanocellulose Composites as a Feasible Material for Membrane Supports: Design and Applications for Water Treatment. *Environ. Sci. Technol.* **2017**, *51*, 4585−4595.
(584) Wu, X.; Cao, S.; Ghim, D.; Jiang, Q.; Singamaneni, S.; Jun, Y.-S. A Thermally Engineered Polydopamine and Bacterial Nanocellulose Bilayer Membrane for Photothermal Membrane Distillation with Bactericidal Capability. *Nano Energy* **2021**, *79*, 105353.
(585) Ferraz, N.; Carlsson, D. O.; Hong, J.; Larsson, R.; Fellström, B.; Nyholm, L.; Strømme, M.; Mihranyan, A. Haemocompatibility and Ion Exchange Capability of Nanocellulose Ppolypyrrole Membranes Intended for Blood Purification. *J. Royal Soc., Interface* **2012**, *9*, 1943−1955.
(586) Ferraz, N.; Leschinskaya, A.; Toomadj, F.; Fellström, B.; Strømme, M.; Mihranyan, A. Membrane Characterization and Solute Diffusion in Porous Composite Nanocellulose Membranes for Hemodialysis. *Cellulose* **2013**, *20*, 2959−2970.
(587) Zimmermann, T.; Pöhler, E.; Geiger, T. Cellulose Fibrils for Polymer Reinforcement. *Adv. Eng. Mater.* **2004**, *6*, 754−761.
(588) Fukuzumi, H.; Saito, T.; Iwamoto, S.; Kumamoto, Y.; Ohdaira, T.; Suzuki, R.; Isogai, A. Pore Size Distribution of TEMPO-oxidized Cellulose Nanofibril Films by Positron Anihilation Lifetime Spectroscopy. *Biomacromolecules* **2011**, *12*, 4057−4062.
(589) Sehaqui, H.; Liu, A.; Zhou, Q.; Berglund, L. A. Fast Preparation Procedure for Large, Flat Cellulose and Cellulose/Inorganic Nanopaper Structures. *Biomacromolecules* **2010**, *11*, 2195−2198.
(590) Syverud, K.; Stenius, P. Strength and Barrier Properties of MFC Films. *Cellulose* **2009**, *16*, 75−85.
(591) Nogi, M.; Iwamoto, S.; Nakagaito, A. N.; Yano, H. Optically Transparent Nanofiber Paper. *Adv. Mater.* **2009**, *21*, 1595−1598.
(592) Aulin, C.; Lindström, T. Biopolymer Coatings for Paper and Paperboard. In *Biopolymers-New Materials for Sustainable Films and Coatings*; John Wiley & Sons: Chichester, Sussex, UK, 2011; p 255.
(593) Ma, H.; Yoon, K.; Rong, L.; Mao, Y.; Mo, Z.; Fang, D.; Hollander, Z.; Gaiteri, J.; Hsiao, B. S.; Chu, B. High-flux Thin-film Nanofibrous Composite Ultrafiltration Membranes Containing Cellulose Barrier Layer. *J. Mater. Chem.* **2010**, *20*, 4692−4704.
(594) Ma, H.; Burger, C.; Hsiao, B. S.; Chu, B. Fabrication and Characterization of Cellulose Nanofiber based Thin-film Nanofibrous Composite Membranes. *J. Membr. Sci.* **2014**, *454*, 272−282.
(595) Mbakop, S.; Nthunya, L. N.; Onyango, M. S. Recent Advances in the Synthesis of Nanocellulose Functionalized-Hybrid Membranes and Application in Water Quality Improvement. *Processes* **2021**, *9*, 611.

https://doi.org/10.1021/acs.chemrev.1c00683
Chem. Rev. 2022, 122, 8936−9031

(596) Palacios Hinestroza, H.; Urena-Saborio, H.; Zurita, F.; Guerrero de León, A. A.; Sundaram, G.; Sulbarán-Rangel, B. Nanocellulose and Polycaprolactone Nanospun Composite Membranes and Their Potential for the Removal of Pollutants from Water. *Molecules* **2020**, *25*, 683.
(597) Liao, Y.; Loh, C.-H.; Tian, M.; Wang, R.; Fane, A. G. Progress in Electrospun Polymeric Nanofibrous Membranes for Water Treatment: Fabrication, Mmodification and Applications. *Prog. Polym. Sci.* **2018**, *77*, 69−94.
(598) Ma, H.; Burger, C.; Hsiao, B. S.; Chu, B. Highly Permeable Polymer Membranes Containing Directed Channels for Water Purification. *ACS Macro Lett.* **2012**, *1*, 723−726.
(599) Chu, B.; Hsiao, B. S. The Role of Polymers in Breakthrough Technologies for Water Purification. *J. Polym. Sci. B Polym. Phys.* **2009**, *47*, 2431−2435.
(600) Jimenez-Solomon, M. F.; Song, Q.; Jelfs, K. E.; Munoz-Ibanez, M.; Livingston, A. G. Polymer Nanofilms with Enhanced Microporosity by Interfacial Polymerization. *Nat. Mater.* **2016**, *15*, 760−767.
(601) Wang, X.; Fang, D.; Hsiao, B. S.; Chu, B. Nanofiltration Membranes based on Thin-film Nanofibrous Composites. *J. Membr. Sci.* **2014**, *469*, 188−197.
(602) Valencia, L.; Kumar, S.; Jalvo, B.; Mautner, A.; Salazar-Alvarez, G.; Mathew, A. P. Fully Bio-based Zwitterionic Membranes with Superior Antifouling and Antibacterial Properties Prepared via Surface-initiated Free-radical Polymerization of Poly(cysteine methacrylate). *J. Mater. Chem. A* **2018**, *6*, 16361−16370.
(603) Wang, R.; Guan, S.; Sato, A.; Wang, X.; Wang, Z.; Yang, R.; Hsiao, B.; Chu, B. Nanofibrous Microfiltration Membranes Capable of Removing Bacteria, Viruses and Heavy Metal Ions. *J. Membr. Sci.* **2013**, *446*, 376−382.
(604) Hassan, M. L.; Fadel, S. M.; Abouzeid, R. E.; Abou Elseoud, W. S.; Hassan, E. A.; Berglund, L.; Oksman, K. Water Purification Ultrafiltration Membranes using Nanofibers from Unbleached and Bleached Rice Straw. *Sci. Rep.* **2020**, *10*, 11278.
(605) Liu, P.; Zhu, C.; Mathew, A. P. Mechanically Robust High Flux Graphene Oxide - Nanocellulose Membranes for Dye Removal from Water. *J. Hazard. Mater.* **2019**, *371*, 484−493.
(606) Valencia, L.; Monti, S.; Kumar, S.; Zhu, C.; Liu, P.; Yu, S.; Mathew, A. P. Nanocellulose/Graphene Oxide Layered Membranes: Elucidating their Behaviour During Filtration of Water and Metal Ions in Real Time. *Nanoscale* **2019**, *11*, 22413−22422.
(607) Roy, S.; Zhai, L.; Van Hai, L.; Kim, J. W.; Park, J. H.; Kim, H. C.; Kim, J. One-step Nanocellulose Coating Converts Tissue Paper into an Efficient Separation Membrane. *Cellulose* **2018**, *25*, 4871−4886.
(608) Zhang, W.; Wang, X.; Zhang, Y.; van Bochove, B.; Mäkilä, E.; Seppälä, J.; Xu, W.; Willför, S.; Xu, C. Robust Shape-retaining Nanocellulose-based Aerogels Decorated with Silver Nanoparticles for Fast Continuous Catalytic Discoloration of Organic Dyes. *Sep. Purif. Technol.* **2020**, *242*, 116523.
(609) Song, Y.; Seo, J. Y.; Kim, H.; Beak, K.-Y. Structural Control of Cellulose Nanofibrous Composite Membrane with Metal Organic Framework (ZIF-8) for Highly Selective Removal of Cationic Dye. *Carbohydr. Polym.* **2019**, *222*, 115018.
(610) Yang, R.; Aubrecht, K. B.; Ma, H.; Wang, R.; Grubbs, R. B.; Hsiao, B. S.; Chu, B. Thiol-modified Cellulose Nanofibrous Composite Membranes for Chromium (VI) and Lead (II) Adsorption. *Polymer* **2014**, *55*, 1167−1176.
(611) Cao, X.; Huang, M.; Ding, B.; Yu, J.; Sun, G. Robust Polyacrylonitrile Nanofibrous Membrane Reinforced with Jute Cellulose Nanowhiskers for Water Purification. *Desalination* **2013**, *316*, 120−126.
(612) Xiong, Y.; Wang, C.; Wang, H.; Jin, C.; Sun, Q.; Xu, X. Nanocellulose Hydrogel Coated Flexible Titanate-bismuth Oxide Membrane for Trinity Synergistic Treatment of Super-intricate Anion/Cation/Oily-water. *Chem. Eng. Sci.* **2018**, *337*, 143−151.
(613) Hong, S. K.; Bae, S.; Jeon, H.; Kim, M.; Cho, S. J.; Lim, G. An Underwater Superoleophobic Nanofibrous Cellulosic Membrane for Oil/Water Separation with High Separation Flux and High Chemical Stability. *Nanoscale* **2018**, *10*, 3037−3045.
(614) Zhang, Q. G.; Deng, C.; Soyekwo, F.; Liu, Q. L.; Zhu, A. M. Sub-10 nm Wide Cellulose Nanofibers for Ultrathin Nanoporous Membranes with High Organic Permeation. *Adv. Funct. Mater.* **2016**, *26*, 792−800.
(615) Soyekwo, F.; Zhang, Q.; Gao, R.; Qu, Y.; Lin, C.; Huang, X.; Zhu, A.; Liu, Q. Cellulose Nanofiber Intermediary to Fabricate Highly-permeable Ultrathin Nanofiltration Membranes for Fast Water Purification. *J. Membr. Sci.* **2017**, *524*, 174−185.
(616) Karim, Z.; Mathew, A. P.; Grahn, M.; Mouzon, J.; Oksman, K. Nanoporous Membranes with Cellulose Nanocrystals as Functional Entity in Chitosan: Removal of Dyes from Water. *Carbohydr. Polym.* **2014**, *112*, 668−676.
(617) Rafieian, F.; Jonoobi, M.; Yu, Q. A Novel Nanocomposite Membrane Containing Modified Cellulose Nanocrystals for Copper Ion Removal and Dye Adsorption from Water. *Cellulose* **2019**, *26*, 3359−3373.
(618) Jonoobi, M.; Ashori, A.; Siracusa, V. Characterization and Properties of Polyethersulfone/ Modified Cellulose Nanocrystals Nanocomposite Membranes. *Polym. Test.* **2019**, *76*, 333−339.
(619) Karim, Z.; Mathew, A. P.; Kokol, V.; Wei, J.; Grahn, M. High-flux Affinity Membranes based on Cellulose Nanocomposites for Removal of Heavy Metal Ions from Industrial Effluents. *Rsc Adv.* **2016**, *6*, 20644−20653.
(620) Zhan, H.; Peng, N.; Lei, X.; Huang, Y.; Li, D.; Tao, R.; Chang, C. UV-induced Self-cleanable TiO_2/Nanocellulose Membrane for Selective Separation of Oil/Water Emulsion. *Carbohydr. Polym.* **2018**, *201*, 464−470.
(621) Cheng, Q.; Ye, D.; Chang, C.; Zhang, L. Facile Fabrication of Superhydrophilic Membranes Consisted of Fibrous Tunicate Cellulose Nanocrystals for Highly Efficient Oil/Water Separation. *J. Membr. Sci.* **2017**, *525*, 1−8.
(622) Zhu, Q.; Wang, Y.; Li, M.; Liu, K.; Hu, C.; Yan, K.; Sun, G.; Wang, D. Activable Carboxylic Acid Functionalized Crystalline Nanocellulose/PVA-co-PE Composite Nanofibrous Membrane with Enhanced Adsorption for Heavy Metal Ions. *Sep. Purif. Technol.* **2017**, *186*, 70−77.
(623) Vilela, C.; Moreirinha, C.; Almeida, A.; Silvestre, A. J. D.; Freire, C. S. R. Zwitterionic Nanocellulose-Based Membranes for Organic Dye Removal. *Materials* **2019**, *12*, 1404.
(624) Yang, Y.; Chen, Z.; Wu, X.; Zhang, X.; Yuan, G. Nanoporous Cellulose Membrane Doped with Silver for Continuous Catalytic Decolorization of Organic Dyes. *Cellulose* **2018**, *25*, 2547−2558.
(625) Xu, T.; Jiang, Q.; Ghim, D.; Liu, K.-K.; Sun, H.; Derami, H. G.; Wang, Z.; Tadepalli, S.; Jun, Y.-S.; Zhang, Q.; et al. Catalytically Active Bacterial Nanocellulose-Based Ultrafiltration Membrane. *Small* **2018**, *14*, 1704006.
(626) Gholami Derami, H.; Gupta, P.; Gupta, R.; Rathi, P.; Morrissey, J. J.; Singamaneni, S. Palladium Nanoparticle-Decorated Mesoporous Polydopamine/Bacterial Nanocellulose as a Catalytically Active Universal Dye Removal Ultrafiltration Membrane. *ACS Appl. Nano Mater.* **2020**, *3*, 5437−5448.
(627) Gholami Derami, H.; Jiang, Q.; Ghim, D.; Cao, S.; Chandar, Y. J.; Morrissey, J. J.; Jun, Y.-S.; Singamaneni, S. A Robust and Scalable Polydopamine/Bacterial Nanocellulose Hybrid Membrane for Efficient Wastewater Treatment. *ACS Appl. Nano Mater.* **2019**, *2*, 1092−1101.
(628) Yang, L.; Chen, C.; Hu, Y.; Wei, F.; Cui, J.; Zhao, Y.; Xu, X.; Chen, X.; Sun, D. Three-dimensional Bacterial Cellulose/Polydopamine/TiO_2 Nanocomposite Membrane with Enhanced Adsorption and Photocatalytic Degradation for Dyes under Ultraviolet-visible Irradiation. *J. Colloid Interface Sci.* **2020**, *562*, 21−28.
(629) Hou, Y.; Duan, C.; Zhu, G.; Luo, H.; Liang, S.; Jin, Y.; Zhao, N.; Xu, J. Functional Bacterial Cellulose Membranes with 3D Porous Architectures: Conventional Drying, Tunable Wettability and Water/Oil Separation. *J. Membr. Sci.* **2019**, *591*, 117312.
(630) Wang, Z.; Ma, H.; Chu, B.; Hsiao, B. S. Fabrication of Cellulose Nanofiber-based Ultrafiltration Membranes by Spray Coating Approach. *J. Appl. Polym. Sci.* **2017**, *134*, 44583.
(631) Soon, C. Y.; Rahman, N. A.; Tee, Y. B.; Talib, R. A.; Tan, C. H.; Abdan, K.; Chan, E. W. C. Electrospun Biocomposite: Nanocellulose

https://doi.org/10.1021/acs.chemrev.1c00683
Chem. Rev. 2022, 122, 8936−9031

and Chitosan Entrapped Within a Poly(hydroxyalkanoate) Matrix for Congo Red Removal. *J. Mater. Res. Technol.* **2019**, *8*, 5091−5102.
(632) Mihranyan, A. Cellulose from Cladophorales Green Algae: From Environmental Problem to High-tech Composite Materials. *J. Appl. Polym. Sci.* **2011**, *119*, 2449−2460.
(633) Metreveli, G.; Wagberg, L.; Emmoth, E.; Belak, S.; Stromme, M.; Mihranyan, A. A Size-Exclusion Nanocellulose Filter Paper for Virus Removal. *Adv. Healthc. Mater.* **2014**, *3*, 1546−1550.
(634) Asper, M.; Hanrieder, T.; Quellmalz, A.; Mihranyan, A. Removal of Xenotropic Murine Leukemia Virus by Nanocellulose based Filter Paper. *Biologicals* **2015**, *43*, 452−456.
(635) Gustafsson, S.; Lordat, P.; Hanrieder, T.; Asper, M.; Schaefer, O.; Mihranyan, A. Mille-feuille Paper: A Novel Type of Filter Architecture for Advanced Virus Separation Applications. *Mater. Horiz.* **2016**, *3*, 320−327.
(636) Goswami, R.; Mishra, A.; Bhatt, N.; Mishra, A.; Naithani, P. Potential of Chitosan/Nanocellulose based Composite Membrane for the Removal of Heavy Metal (Chromium Ion). *Mater. Today: Proc.* **2021**, *46*, 10954−10959.
(637) Karim, Z.; Hakalahti, M.; Tammelin, T.; Mathew, A. P. *In situ* TEMPO Surface Functionalization of Nanocellulose Membranes for Enhanced Adsorption of Metal Ions from Aqueous Medium. *Rsc Adv.* **2017**, *7*, 5232−5241.
(638) Goetz, L. A.; Naseri, N.; Nair, S. S.; Karim, Z.; Mathew, A. P. All Cellulose Electrospun Water Purification Membranes Nanotextured using Cellulose Nanocrystals. *Cellulose* **2018**, *25*, 3011−3023.
(639) Goetz, L. A.; Jalvo, B.; Rosal, R.; Mathew, A. P. Superhydrophilic Anti-fouling Electrospun Cellulose Acetate Membranes Coated with Chitin Nanocrystals for Water Filtration. *J. Membr. Sci.* **2016**, *510*, 238−248.
(640) Bai, L.; Liu, Y.; Ding, A.; Ren, N.; Li, G.; Liang, H. Surface Coating of UF Membranes to Improve Antifouling Properties: A Comparison Study Between Cellulose Nanocrystals (CNCs) and Cellulose Nanofibrils (CNFs). *Chemosphere* **2019**, *217*, 76−84.
(641) Wang, R.; Sakai, N.; Fujishima, A.; Watanabe, T.; Hashimoto, K. Studies of Surface Wettability Conversion on TiO_2 Single-crystal Surfaces. *J. Phys. Chem. B* **1999**, *103*, 2188−2194.
(642) Lv, J.; Zhang, G.; Zhang, H.; Yang, F. Exploration of Permeability and Antifouling Performance on Modified Cellulose Acetate Ultrafiltration Membrane with Cellulose Nanocrystals. *Carbohydr. Polym.* **2017**, *174*, 190−199.
(643) Bai, H.; Wang, X.; Zhou, Y.; Zhang, L. Preparation and Characterization of Poly(vinylidene fluoride) Composite Membranes Blended with Nano-crystalline Cellulose. *Prog. Nat. Sci.: Mater. Int.*. **2012**, *22*, 250−257.
(644) Klemm, D.; Schumann, D.; Udhardt, U.; Marsch, S. Bacterial Synthesized Cellulose-Artificial Blood Vessels for Microsurgery. *Prog. Polym. Sci.* **2001**, *26*, 1561−1603.
(645) Fang, Q.; Zhou, X.; Deng, W.; Zheng, Z.; Liu, Z. Freestanding Bacterial Cellulose-Graphene Oxide Composite Membranes with High Mechanical Strength for Selective Ion Permeation. *Sci. Rep.* **2016**, *6*, 33185.
(646) Hu, Y.; Yue, M.; Yuan, F.; Yang, L.; Chen, C.; Sun, D. Bio-inspired Fabrication of Highly Permeable and Anti-fouling Ultrafiltration Membranes based on Bacterial Cellulose for Efficient Removal of Soluble Dyes and Insoluble Oils. *J. Membr. Sci.* **2021**, *621*, 118982.
(647) Hassan, E.; Hassan, M.; Abou-Zeid, R.; Berglund, L.; Oksman, K. Use of Bacterial Cellulose and Crosslinked Cellulose Nanofibers Membranes for Removal of Oil from Oil-in-Water Emulsions. *Polymers* **2017**, *9*, 388.
(648) Mautner, A.; Bismarck, A. Bacterial Nanocellulose Papers with High Porosity for Optimized Permeance and Rejection of nm-sized Pollutants. *Carbohydr. Polym.* **2021**, *251*, 117130.
(649) Takai, M.; Nonomura, F.; Inukai, T.; Fujiwara, M.; Hayashi, J. Filtration and Permeation Characteristsics of Bacterial Cellulose Cellulose Composite. *Sen-I- Gakkaishi* **1991**, *47*, 119−129.
(650) Shibazaki, H.; Kuga, S.; Onabe, F.; Usuda, M. Bacterial Cellulose Membrane as Separation Medium. *J. Appl. Polym. Sci.* **1993**, *50*, 965−969.
(651) Ferguson, A.; Khan, U.; Walsh, M.; Lee, K. Y.; Bismarck, A.; Shaffer, M. S.; Coleman, J. N.; Bergin, S. D. Understanding the Dispersion and Assembly of Bacterial Cellulose in Organic Solvents. *Biomacromolecules* **2016**, *17*, 1845−1853.
(652) Jiang, Q.; Ghim, D.; Cao, S.; Tadepalli, S.; Liu, K.-K.; Kwon, H.; Luan, J.; Min, Y.; Jun, Y.-S.; Singamaneni, S. Photothermally Active Reduced Graphene Oxide/Bacterial Nanocellulose Composites as Biofouling-resistant Ultrafiltration Membranes. *Environ. Sci. Technol.* **2019**, *53*, 412−421.
(653) Chen, S.; Li, L.; Zhao, C.; Zheng, J. Surface Hydration: Principles and Applications Toward Low-fouling/Nonfouling Biomaterials. *Polymer* **2010**, *51*, 5283−5293.
(654) Mansouri, J.; Harrisson, S.; Chen, V. Strategies for Controlling Biofouling in Membrane Filtration Systems: Challenges and Opportunities. *J. Mater. Chem.* **2010**, *20*, 4567−4586.
(655) Zhang, R.; Liu, Y.; He, M.; Su, Y.; Zhao, X.; Elimelech, M.; Jiang, Z. Antifouling Membranes for Sustainable Water Purification: Strategies and Mechanisms. *Chem. Soc. Rev.* **2016**, *45*, 5888−5924.
(656) Kang, G. D.; Cao, Y. M. Development of Antifouling Reverse Osmosis Membranes for Water Treatment: A Review. *Water Res.* **2012**, *46*, 584−600.
(657) Koo, C. H.; Mohammad, A. W.; Suja', F.; Meor Talib, M. Z. Review of the Effect of Selected Physicochemical Factors on Membrane Fouling Propensity based on Fouling Indices. *Desalination* **2012**, *287*, 167−177.
(658) Rana, D.; Matsuura, T. Surface Modifications for Antifouling Membranes. *Chem. Rev.* **2010**, *110*, 2448−2471.
(659) Liang, Y.; Ma, H.; Taha, A. A.; Hsiao, B. S. High-flux Antifouling Nanofibrous Composite Ultrafiltration Membranes Containing Negatively Charged Water Channels. *J. Membr. Sci.* **2020**, *612*, 118382.
(660) Yang, M.; Hadi, P.; Yin, X.; Yu, J.; Huang, X.; Ma, H.; Walker, H.; Hsiao, B. S. Antifouling Nanocellulose Membranes: How Subtle Adjustment of Surface Charge Lead to Self-cleaning Property. *J. Membr. Sci.* **2021**, *618*, 118739.
(661) Hadi, P.; Yang, M.; Ma, H.; Huang, X.; Walker, H.; Hsiao, B. S. Biofouling-resistant Nanocellulose Layer in Hierarchical Polymeric Membranes: Synthesis, Characterization and Performance. *J. Membr. Sci.* **2019**, *579*, 162−171.
(662) Harris, J. M. *Poly(ethylene glycol) Chemistry: Biotechnical and Biomedical Application*; Plenum Press: New York, 1992; p 385.
(663) Steen, M. I.; Jordan, A. C.; Fisher, E. R. Hydrophilic Modification of Polymeric Membranes by Low Temperature H_2O Plasma Treatment. *J. Membr. Sci.* **2002**, *204*, 341−357.
(664) Liang, S.; Gao, P.; Gao, X.; Xiao, K.; Huang, X. Improved Blending Strategy for Membrane Modification by Virtue of Surface Segregation using Surface-tailored Amphiphilic Nanoparticles. *Front. Environ. Sci. Eng.* **2016**, *10*, 9.
(665) Li, X.; Cai, T.; Chen, C.; Chung, T. S. Negatively Charged Hyperbranched Polyglycerol Grafted Membranes for Osmotic Power Generation from Municipal Wastewater. *Water Res.* **2016**, *89*, 50−58.
(666) Wandera, D.; Wickramasinghe, S. R.; Husson, S. M. Modification and Characterization of Ultrafiltration Membranes for Treatment of Produced Water. *J. Membr. Sci.* **2011**, *373*, 178−188.
(667) Bengani-Lutz, P.; Converse, E.; Cebe, P.; Asatekin, A. Self-assembling Zwitterionic Copolymers as Membrane Selective Layers with Excellent Fouling Resistance: Effect of Zwitterion Chemistry. *ACS Appl. Mater. Interfaces* **2017**, *9*, 20859−20872.
(668) Sundaram, H. S.; Han, X.; Nowinski, A. K.; Ella-Menye, J. R.; Wimbish, C.; Marek, P.; Senecal, K.; Jiang, S. One-step Dip Coating of Zwitterionic Sulfobetaine Polymers on Hydrophobic and Hydrophilic Surfaces. *ACS Appl. Mater. Interfaces* **2014**, *6*, 6664−6671.
(669) Shen, X.; Gao, Y.; He, Y.; Zhao, Y.; Chen, L. Preparation and Anti-fouling Property of Carboxybetaine-based Zwitterionic PVDF Membrane. *Sep. Sci. Technol.* **2016**, *51*, 1189−1198.
(670) Rostami, J.; Mathew, A. P.; Edlund, U. Zwitterionic Acetylated Cellulose Nanofibrils. *Molecules* **2019**, *24*, 3147.

https://doi.org/10.1021/acs.chemrev.1c00683
Chem. Rev. 2022, 122, 8936−9031

(671) Kolewe, K. W.; Dobosz, K. M.; Rieger, K. A.; Chang, C. C.; Emrick, T.; Schiffman, J. D. Antifouling Electrospun Nanofiber Mats Functionalized with Polymer Zwitterions. *ACS Appl. Mater. Interfaces* **2016**, *8*, 27585−27593.
(672) Georgouvelas, D.; Jalvo, B.; Valencia, L.; Papawassiliou, W.; Pell, A. J.; Edlund, U.; Mathew, A. P. Residual Lignin and Zwitterionic Polymer Grafts on Cellulose Nanocrystals for Antifouling and Antibacterial Applications. *ACS Appl. Polym. Mater.* **2020**, *2*, 3060−3071.
(673) Lv, J.; Zhang, G.; Zhang, H.; Zhao, C.; Yang, F. Improvement of Antifouling Performances for Modified PVDF Ultrafiltration Membrane with Hydrophilic Cellulose Nanocrystal. *Appl. Surf. Sci.* **2018**, *440*, 1091−1100.
(674) Huang, W.; Huang, J.; Xu, C.; Gu, S.; Xu, W. Surface Functionalization of Cellulose Membrane via Heterogeneous "Click" Grafting of Zwitterionic Sulfobetaine. *Polym. Bull.* **2014**, *71*, 2559−2569.
(675) Holmlin, R. E.; Chen, X.; Chapman, R. G.; Takayama, S.; Whitesides, G. M. Zwitterionic SAMs that Resist Nonspecific Adsorption of Protein from Aqueous Buffer. *Langmuir* **2001**, *17*, 2841−2850.
(676) Kane, R. S.; Deschatelets, P.; Whitesides, G. M. Kosmotropes Form the Basis of Protein-resistant Surfaces. *Langmuir* **2003**, *19*, 2388−2391.
(677) Hower, J. S.; Bernards, M. T.; Chen, S.; Tsao, H.-K.; Sheng, Y.-J.; Jiang, S. Hydration of "Nonfouling" Functional Groups. *J. Phys. Chem. B* **2009**, *113*, 197−201.
(678) Prime, K. L.; Whitesides, G. M. Self-assembled Organic Monolayers: Model Systems for Studying Adsorption of Proteins at Surfaces. *Science* **1991**, *252*, 1164−1167.
(679) Senevirathne, S. W. M. A. I.; Hasan, J.; Mathew, A.; Woodruff, M.; Yarlagadda, P. K. D. V. Bactericidal Efficiency of Micro- and Nanostructured Surfaces: A Critical Perspective. *Rsc Adv.* **2021**, *11*, 1883−1900.
(680) Nasser, M. S.; James, A. E. The Effect of Polyacrylamide Charge Density and Molecular Weight on the Flocculation and Sedimentation Behaviour of Kaolinite Suspensions. *Sep. Purif. Technol.* **2006**, *52*, 241−252.
(681) Nasser, M. S.; James, A. E. Effect of Polyacrylamide Polymers on Floc Size and Rheological Behaviour of Kaolinite Suspensions. *Colloids Surf. A: Physicochem. Eng. Asp.* **2007**, *301*, 311−322.
(682) Li, Q.; Raj, P.; Husain, F. A.; Varanasi, S.; Rainey, T.; Garnier, G.; Batchelor, W. Engineering Cellulose Nanofibre Suspensions to Control Filtration Resistance and Sheet Permeability. *Cellulose* **2016**, *23*, 391−402.
(683) Pillai, K. V.; Renneckar, S. Cation−π Interactions as a Mechanism in Technical Lignin Adsorption to Cationic Surfaces. *Biomacromolecules* **2009**, *10*, 798−804.
(684) Sirviö, J. A.; Visanko, M. Lignin-rich Sulfated Wood Nanofibers as High-performing Adsorbents for the Removal of Lead and Copper from Water. *J. Hazard. Mater.* **2020**, *383*, 121174.
(685) Ugochukwu, U. C. Characteristics of Clay Minerals Relevant to Bioremediation of Environmental Contaminated Systems. In *Modified Clay and Zeolite Nanocomposite Materials*; Elsevier: Amsterdam, 2019; p 219.
(686) Das, R.; Kuehnert, M.; Sadat Kazemi, A.; Abdi, Y.; Schulze, A. Water Softening using a Light-Responsive, Spiropyran-Modified Nanofiltration Membrane. *Polymers* **2019**, *11*, 344.
(687) Anirudhan, T.; Deepa, J.; Shainy, F. Thorium (IV) Recovery from Water and Sea Water using Surface Modified Nanocellulose/Nanobentonite Composite: Process Design. *J. Polym. Environ.* **2017**, *25*, 1147−1162.
(688) Yang, H.; Sheikhi, A.; Van De Ven, T. G. Reusable Green Aerogels from Cross-linked Hairy Nanocrystalline Cellulose and Modified Chitosan for Dye Removal. *Langmuir* **2016**, *32*, 11771−11779.
(689) Hong, H.-J.; Yu, H.; Park, M.; Jeong, H. S. Recovery of Platinum from Waste Effluent Using Polyethyleneimine-Modified Nanocelluloses: Effects of the Cellulose Source and Type. *Carbohydr. Polym.* **2019**, *210*, 167−174.
(690) Lucchini, M. A.; Lizundia, E.; Moser, S.; Niederberger, M.; Nyström, G. Titania-cellulose Hybrid Monolith for In-flow Purification of Water Under Solar Illumination. *ACS Appl. Mater. Interfaces.* **2018**, *10*, 29599−29607.
(691) Chen, X.; Liu, L.; Yu, P. Y.; Mao, S. S. Increasing Solar Absorption for Photocatalysis with Black Hydrogenated Titanium Dioxide Nanocrystals. *Science* **2011**, *331*, 746−750.
(692) Gusakova, J.; Wang, X.; Shiau, L. L.; Krivosheeva, A.; Shaposhnikov, V.; Borisenko, V.; Gusakov, V.; Tay, B. K. Electronic Properties of Bulk and Monolayer TMDs: Theoretical Study Within DFT Framework (GVJ-2e Method). *Phys. Status Solidi (A)* **2017**, *214*, 1700218.
(693) Das, R.; Solís-Fernández, P.; Breite, D.; Prager, A.; Lotnyk, A.; Schulze, A.; Ago, H. High Flux and Adsorption based Non-functionalized Hexagonal Boron Nitride Lamellar Membrane for Ultrafast Water Purification. *Chem. Eng. Sci.* **2021**, *420*, 127721.
(694) Serpone, N.; Lawless, D.; Khairutdinov, R. Size Effects on the Photophysical Properties of Colloidal Anatase TiO_2 Particles: Size Quantization Versus Direct Transitions in this Indirect Semiconductor? *J. Phys. Chem.* **1995**, *99*, 16646−16654.
(695) Ma, H.; Yoon, K.; Rong, L.; Shokralla, M.; Kopot, A.; Wang, X.; Fang, D.; Hsiao, B. S.; Chu, B. Thin-film Nanofibrous Composite Ultrafiltration Membranes based on Polyvinyl Alcohol Barrier Layer Containing Directional Water Channels. *Ind. Eng. Chem.* **2010**, *49*, 11978−11984.
(696) Liu, P.; Milletto, C.; Monti, S.; Zhu, C.; Mathew, A. P. Design of Ultrathin Hybrid Membranes with Improved Retention Efficiency of Molecular Dyes. *Rsc. Adv.* **2019**, *9*, 28657−28669.
(697) Dovjuu, O.; Kim, S.; Lee, A.; Baek, S.; Kim, J.; Noh, J.; Huh, S.; Choi, B.; Sung, Y.; Jeong, H. Structural Characterization of the Crystalline Nanocellulose and Nanocellulose-reinforced Carbon Buckypaper. *Diam. Relat. Mater.* **2020**, *106*, 107821.
(698) Sijabat, E. K; Nuruddin, A.; Aditiawati, P.; Sunendar Purwasasmita, B. Flat Sheet Membrane Composite for Desalinisation Applications based on Bacterial Nanocellulose (BNC) from Banana Peel Waste, Cellulose, and Silica. *Mater. Res. Express* **2020**, *7*, 105004.
(699) Sampaio, L. M.; Padrão, J.; Faria, J.; Silva, J. P.; Silva, C. J.; Dourado, F.; Zille, A. Laccase Immobilization on Bacterial Nanocellulose Membranes: Antimicrobial, Kinetic and Stability Properties. *Carbohydr. Polym.* **2016**, *145*, 1−12.
(700) Hlongwane, G. N.; Sekoai, P. T.; Meyyappan, M.; Moothi, K. Simultaneous Removal of Pollutants from Water using Nanoparticles: A Shift from Single Pollutant Control to Multiple Pollutant Control. *Sci. Total Environ.* **2019**, *656*, 808−833.
(701) Bradley, P. M.; Journey, C. A.; Romanok, K. M.; Barber, L. B.; Buxton, H. T.; Foreman, W. T.; Furlong, E. T.; Glassmeyer, S. T.; Hladik, M. L.; Iwanowicz, L. R.; et al. Expanded Target-chemical Analysis Reveals Extensive Mixed-organic-contaminant Exposure in US Streams. *Environ. Sci. Technol.* **2017**, *51*, 4792−4802.
(702) Saito, T.; Isogai, A. Ion-exchange Behavior of Carboxylate Groups in Fibrous Cellulose Oxidized by the TEMPO-mediated System. *Carbohydr. Polym.* **2005**, *61*, 183−190.
(703) Hribar, B.; Southall, N. T.; Vlachy, V.; Dill, K. A. How Ions Affect the Structure of Water. *J. Am. Chem. Soc.* **2002**, *124*, 12302−12311.
(704) Fennell, C. J.; Dill, K. A. Physical Modeling of Aqueous Solvation. *J. Stat. Phys.* **2011**, *145*, 209−226.
(705) Deng, Y.; Tang, L.; Zeng, G.; Zhu, Z.; Yan, M.; Zhou, Y.; Wang, J.; Liu, Y.; Wang, J. Insight into Highly Efficient Simultaneous Photocatalytic Removal of Cr(VI) and 2,4-diclorophenol Under Visible Light Irradiation by Phosphorus Doped Porous Ultrathin g-C_3N_4 Nanosheets from Aqueous Media: Performance and Reaction Mechanism. *Appl. Catal. B: Environ.* **2017**, *203*, 343−354.
(706) Yang, L.; Mukhopadhyay, A.; Jiao, Y.; Yong, Q.; Chen, L.; Xing, Y.; Hamel, J.; Zhu, H. Ultralight, Highly Thermally Insulating and Fire Resistant Aerogel by Encapsulating Cellulose Nanofibers with Two-dimensional MoS_2. *Nanoscale* **2017**, *9*, 11452−11462.

https://doi.org/10.1021/acs.chemrev.1c00683
Chem. Rev. 2022, 122, 8936−9031

(707) Kinniburgh, D. G.; Milne, C. J.; Benedetti, M. F.; Pinheiro, J. P.; Filius, J.; Koopal, L. K.; Van Riemsdijk, W. H. Metal Ion Binding by Humic Acid: Application of the NICA-Donnan Model. *Environ. Sci. Technol.* **1996**, *30*, 1687−1698.
(708) Harikishore Kumar Reddy, D.; Vijayaraghavan, K.; Kim, J. A.; Yun, Y.-S. Valorisation of Post-sorption Materials: Opportunities, Strategies, and Challenges. *Adv. Colloid Interface Sci.* **2017**, *242*, 35−58.
(709) European Commission. *Final Implementation Report for Directive 1999/31/EC on the Landfill of Waste: 2013−2015*. https://ec.europa.eu/environment/archives/waste/reporting/pdf/Final_Implementation_Report_2013_2015_Landfill_Directive.pdf (accessed 2021-03-01).
(710) Messa, L. L.; Faez, R. Spray-dried Chitosan/Nanocellulose Microparticles: Synergistic Effects for the Sustained Release of NPK Fertilizer. *Cellulose* **2020**, *27*, 10077−10093.
(711) Auffan, M.; Rose, J.; Bottero, J.-Y.; Lowry, G. V.; Jolivet, J.-P.; Wiesner, M. R. Towards a Definition of Inorganic Nanoparticles from an Environmental, Health and Safety Perspective. *Nat. Nanotechnol.* **2009**, *4*, 634−641.
(712) Dutta, T.; Kwon, E.; Bhattacharya, S. S.; Jeon, B. H.; Deep, A.; Uchimiya, M.; Kim, K. H. Polycyclic Aromatic Hydrocarbons and Volatile Organic Compounds in Biochar and Biochar-Amended Soil: A Review. *Gcb Bioenergy* **2017**, *9*, 990−1004.
(713) Gómez H, C.; Serpa, A.; Velásquez-Cock, J.; Gañán, P.; Castro, C.; Vélez, L.; Zuluaga, R. Vegetable Nanocellulose in Food Science: A Review. *Food Hydrocoll.* **2016**, *57*, 178−186.
(714) Gamarra, D.; Munuera, G.; Hungría, A.; Fernández-García, M.; Conesa, J.; Midgley, P.; Wang, X.; Hanson, J.; Rodríguez, J.; Martínez-Arias, A. Structure-activity Relationship in Nanostructured Copper-ceria-based Preferential CO Oxidation Catalysts. *J. Phys. Chem. C* **2007**, *111*, 11026−11038.
(715) Guillot, S.; Chemelli, A.; Bhattacharyya, S.; Warmont, F.; Glatter, O. Ordered Structures in Carboxymethylcellulose-Cationic Surfactants-Copper Ions Precipitated Phases: *In situ* Formation of Copper Nanoparticles. *J. Phys. Chem. B* **2009**, *113*, 15−23.
(716) Bolisetty, S.; Mezzenga, R. Amyloid-carbon Hybrid Membranes for Universal Water Purification. *Nat. Nanotechnol.* **2016**, *11*, 365−371.
(717) Cywinska, M. A.; Bystrzejewski, M.; Poplawska, M.; Kosmider, A.; Zdanowski, R.; Lewicki, S.; Fijalek, Z.; Ostrowska, A.; Bamburowicz, M.; Cieszanowski, A.; et al. Internalization and Cytotoxicity Effects of Carbon-encapsulated Iron Nanoparticles in Murine Endothelial Cells: Studies on Internal Dosages due to Loaded Mass Agglomerates. *Toxicol. In Vitro* **2016**, *34*, 229−236.
(718) Sunny, V.; Sakthi Kumar, D.; Yoshida, Y.; Makarewicz, M.; Tabiś, W.; Anantharaman, M. R. Synthesis and Properties of Highly Stable Nickel/Carbon Core/Shell Nanostructures. *Carbon* **2010**, *48*, 1643−1651.
(719) Zhang, Y.; Duan, D.; Lei, H.; Wang, C.; Qian, M.; Villota, E.; Mateo, W. From Douglas Fir to Renewable H_2-enriched Syngas via *Ex situ* Catalytic Pyrolysis Over Metal Nanoparticles-Nanocellulose Derived Carbon Catalysts. *Sustain. Energy Fuels* **2020**, *4*, 1084−1087.
(720) Yan, H.; Zhang, W.; Kan, X.; Dong, L.; Jiang, Z.; Li, H.; Yang, H.; Cheng, R. Sorption of Methylene Blue by Carboxymethyl Cellulose and Reuse Process in a Secondary Sorption. *Colloids Surf. A: Physicochem. Eng. Asp.* **2011**, *380*, 143−151.
(721) Chouchene, A.; Jeguirim, M.; Trouvé, G. Biosorption Performance, Combustion Behavior, and Leaching Characteristics of Olive Solid Waste During the Removal of Copper and Nickel from Aqueous Solutions. *Clean Technol. Environ. Policy.* **2014**, *16*, 979−986.
(722) Liu, W.-J.; Zeng, F.-X.; Jiang, H.; Zhang, X.-S.; Yu, H.-Q. Techno-economic Evaluation of the Integrated Biosorption-pyrolysis Technology for Lead (Pb) Recovery from Aqueous Solution. *Bioresour. Technol.* **2011**, *102*, 6260−6265.
(723) Pooi, C. K.; Ng, H. Y. Review of Low-cost Point-of-use Water Treatment Systems for Developing Communities. *npj Clean Water* **2018**, *1*, 11.
(724) Tietz, T.; Lenzner, A.; Kolbaum, A. E.; Zellmer, S.; Riebeling, C.; Gurtler, R.; Jung, C.; Kappenstein, O.; Tentschert, J.; Giulbudagian, M.; et al. Aggregated Aluminium Exposure: Risk Assessment for the General Population. *Arch. Toxicol.* **2019**, *93*, 3503−3521.
(725) Jiao, D.; Lossada, F.; Guo, J.; Skarsetz, O.; Hoenders, D.; Liu, J.; Walther, A. Electrical Switching of High-performance Bioinspired Nanocellulose Nanocomposites. *Nat. Commun.* **2021**, *12*, 1312.
(726) Koçer, A.; Walko, M.; Meijberg, W.; Feringa, B. L. A Light-actuated Nanovalve Derived from a Channel Protein. *Science* **2005**, *309*, 755−758.
(727) Vlassiouk, I.; Park, C.-D.; Vail, S. A.; Gust, D.; Smirnov, S. Control of Nanopore Wetting by a Photochromic Spiropyran: a Light-controlled Valve and Electrical Switch. *Nano Lett.* **2006**, *6*, 1013−1017.
(728) Fujiwara, M. Water Desalination Using Visible Light by Disperse Red 1 Modified PTFE Membrane. *Desalination* **2017**, *404*, 79−86.
(729) Liu, N.; Dunphy, D. R.; Atanassov, P.; Bunge, S. D.; Chen, Z.; López, G. P.; Boyle, T. J.; Brinker, C. J. Photoregulation of Mass Transport Through a Photoresponsive Azobenzene-Modified Nanoporous Membrane. *Nano Lett.* **2004**, *4*, 551−554.
(730) Plecis, A.; Schoch, R. B.; Renaud, P. Ionic Transport Phenomena in Nanofluidics: Experimental and Theoretical Study of the Exclusion-enrichment Effect on a Chip. *Nano Lett.* **2005**, *5*, 1147−1155.

https://doi.org/10.1021/acs.chemrev.1c00683
Chem. Rev. 2022, 122, 8936−9031

Supporting Information

Nanocellulose for Sustainable Water Purification

Rasel Das, [†] Tom Lindström,[*,†,‡] Priyanka R. Sharma,[†] Kai Chi,[†] and Benjamin S. Hsiao[*,†]

[†] Department of Chemistry

Stony Brook University

Stony Brook, NY11794-3400, USA

[‡] KTH Royal Institute of Technology

Stockholm 100 44, Sweden

Contents

* Corresponding authors

E-mail: toml@kth.se; Tel: +46-70-6570194

E-mail: benjamin.hsiao@stonybrook.edu; Tel: +1-631-6327793

Table S1. Compositions of cellulose, hemicellulose and lignin from various biomass feedstocks (values extracted from Ref.[1]).

Biomass Feedstocks	Cellulose %	Hemicellulose %	Lignin %
Softwood	45-50	18-35	23-35
Hardwood	40-50	24-40	18-25
Wheat straw	35-39	22-30	12-16
Rice straw	29.2-34.7	23-25.9	17-19
Corn stover	35.1-39.5	20.7-24.6	11.0-19.1
Corn cob	32.3-45.6	39.8	6.7-13.9
Cotton stalk	31	11	30
Barley straw	36-43	24-33	6.3-9.8
Sorghum straw	32-35	24-27	15-21
Nut-shell	25-30	22-28	30-40
Rice husk	28.7-35.6	11.9-29.3	15.4-20
Bagasse	25-45	28-32	15-25
Agave leave	64-70	22-28	5-7
Switchgrass	30-35	20-25	15-20

1. Industrial Applications of Nanocellulose

As our society is transitioning to a sustainable and circular economy, developments of advanced materials from renewable resources and their applications have become a fast-growing field. In specific, nanocellulose (NC) that can be extracted from the most abundant natural polymer i.e. cellulose, is emerging as a versatile nanoscale platform for a wide range of applications. Extensive reviews are available for varying NC applications,[2-5] enabled by commercial processing of large scale NC materials and advancement of nanotechnology. Herein, we highlight recent progress on the applications of NC materials in four major categories, namely nanocomposites, biomedical engineering (*e.g.*, drug delivery, tissue engineering, wound healing *etc*.), energy storage, and sustainable packaging. In addition, some other applications, such as drilling mud, coating, cement, cosmetics are briefly covered in the last part of this section.

1.1. Nanocomposites

NC materials are well known for their high stiffness, strength, high crystalline structure, versatile functionalization, low thermal expansion, high surface area, light weight (density ~1.6

g/cm^3), renewability, and biodegradability. These characteristics have entitled NC materials to be used as reinforcing nanofillers for a variety of polymer matrices (thermoplastic, thermoset, natural polysaccharides and proteins, cement, latex, *etc*.) with a broad range of material formats (*e.g*., films, filaments, fibers, foams, aerogels, hydrogels, *etc*.). Due to the inherent hydrophilicity and gelation tendency (especially when the concentration is high) of NC materials, interface compatibility and industrial feasible and scalable continuous processing are major challenges to expand their further applications. Moon et al.[6] reported that the performance of NC-polymer nanocomposites could be affected by several factors including NC particle morphology, surface chemistry, alignment, dispersion state, percolation level, and polymer matrix. As different production routes can yield NC materials with differentiated surface chemistry, particle size, aspect ratio, crystallinity, and network structure,[7] it is thus critical for end users to select specified NC materials that meet either processing or performance criteria. For instance, melt compounding of NC-polymer nanocomposites typically requires high thermal stability of NC materials, whereby surface chemistry (*i.e*., low charge density and non-sulfated surface) is a key parameter to consider. When formulated with latices, coatings or paints, the colloidal stability and percolated network structure of NC materials can play a vital role in the stability and quality of final products. To solve interface compatibility with nonpolar matrices and further exploit the full reinforcing potential of NC materials, various surface functionalization routes have been demonstrated.[8] However, the environmental impact (especially concern from organic solvents), cost, and industrial feasibility of these modification strategies can be major hurdles for scale up applications. To overcome these challenges, recently demonstrated research include water-based modification approaches, liquid feeding of NC materials into melt polymers, and blending with compatible additives that enable compounding and extrusion, to name a few.[9] Furthermore, motivated by achieving better macroscale performance (*i.e*., anisotropic properties, better stiffness and strength, and improved reinforcing efficiency), alignment of NC materials in polymer composites is emerging as a viable strategy to further enhance the mechanical performance. Although challenged by large-scale manufacturing process to align NC materials in polymer composites, efforts are being undertaken to develop industrial scalable processing strategies, such as combination of pre-aligned NC materials with melt compounding and additive manufacturing.[10]

1.2. Biomedical Engineering

The inherent biodegradability, biocompatibility, and low cytotoxicity have rendered NC materials to be promising candidates for biomedical applications, such as drug delivery, tissue engineering, and wound healing. Bacterial nanocellulose (BNC) and cellulose nanofiber (CNF) are two major materials that can be easily functionalized for biomedical applications, due to their highly interconnected network structure, moldability, tailored nanostructure (*e.g.*, porosity and pore size), and templating ability. Nascent NC materials have abundant hydroxyl groups but their applications in biomedical fields are relatively limited. With proper surface functionalization and compounding strategies, these materials become suitable for varying applications. For example, various additives, such as polysaccharides, proteins, synthetic polymers, graphene oxides, phenolic acids, and metal oxides,[11-13] have been incorporated into the NC scaffold to fabricate novel materials with new functionalities (*e.g.*, antimicrobial, excellent cell attachment, pH responsive, good thermal stability and chemical resistance, high water holding capacity, good compressive properties, hierarchical pore structure, *etc*.) that become suitable for wound dressing, soft tissue engineering, drug delivery, and tumor cell culture. For drug delivery, NC possesses excellent loading capacity, high surface area, and biocompatibility, and has been explored for oral and controlled release, topical and transdermal delivery, and proven to be capable of improving the overall release of drugs in a sustained manner.[13] NC-based hydrogel systems are effective bioactive scaffolds that have high potential in achieving cell adhesion, tissue proliferation, and functioning as carriers of biologically active molecules, which are key properties to become effective three dimensional (3D) extracellular matrices for tissue engineering. Furthermore, the excellent water holding and adsorption capacity, large surface area, and mechanical stability have enabled BNC to promising candidates for wound healing applications. For instance, antimicrobial treated BNCs are effective dressings for chronic wounds, burns, or skin repair treatment.

1.3. Energy Storage

The applications of NC in electrochemical energy storage have recently been extensively demonstrated, such as in supercapacitors, robust and multifunctional electrodes, electrolytes, separators, and batteries (*e.g.*, lithium-ion, lithium-sulfur, and sodium-ion batteries). Due to their

high aspect ratio, high surface area, robust mechanical strength, and templating feature enabled by interconnected network structure, NC materials can be incorporated with electrical active materials, pyrolyzed into carbon materials, composited with conductive polymers (*e.g.*, polypyrrole, polyaniline, *etc.*), nanocarbons and metal nanoparticles, and developed into various flexible substrate or scaffolds for advanced electrochemical applications.[14] One example is the emergence of wearable electronics (*e.g.*, smart watch, healthy monitoring and tracking, and smart fabrics) which require flexible, functional, and reliable energy storage systems, where NC-based composites have become very promising candidates to deliver desired properties such as stretchability, self-healing, compressible, bendable or foldable. Different synthesizing strategies for flexible NC-based composites have been reported, including 1D (*e.g.*, wet or microfluidic spinning), 2D (*e.g.*, electrospinning or vacuum filtration), and 3D (*e.g.*, 3D printing or lyophilization) nanostructured functional composite materials. In addition, *in-situ*, *ex-situ* and interfacial engineering approaches have been adopted to functionalize NC to endow superior conductivity, hierarchical nanostructure, and anisotropic properties.[15] Some critical issues that need to be addressed to fully exploit the potential of NC for energy storage applications are: (a) large-scale and continuous manufacturing of NC-based composites, (b) cost-effective and industrially feasible surface functionalization of NC materials and their integration with other electrochemically active materials, (c) further improvement of mechanical robustness and flexibility of NC-based compounds for practical applications, and (d) precise control of materials interface, constituent, pore size/porosity, and nanostructure engineering to reimburse lack of conductivity of NC materials.[14,15]

1.4. Sustainable Packaging

The climate crisis has significantly raised environmental concerns of global communities. Along with changing our typical ways of plastics usage and recycling, we have been progressively propelled to explore bio-based resources and renewable energy towards achieving carbon neutrality and true sustainability. For example, petroleum-derived synthetic plastics have been widely used as the primary packaging materials, while cellulose fiber-based materials (paper and paperboard) are only considered for secondary and tertiary packaging applications. This is because synthetic plastics offer many advantages over cellulosic materials such as easy processability, low cost, and most importantly, very high barrier performances that prevent

deterioration from gas, liquid, oil/grease penetration and thus extend shelf-life of packaged food products.[16-18] However, most synthetic materials are not degradable and not environmentally friendly. Furthermore, our recycling systems have been poorly managed, leading to the accumulation of a large volume of plastic waste in landfills and marine environments. As a result, single-use plastics are banned in some countries (*e.g.*, European Union) and more regulations and policies have been released to control the consumption of plastics (even include bioplastics, such as poly(lactic acid) and polyhydroxyalkanoates). To combat this problem, bio-based packaging solutions have attracted a great deal of attention and are under extensive research investigation.

The inherent renewability, biodegradability, robust mechanical properties, and highly stable crystalline structure of NC materials have allowed them to be formulated with various aqueous barrier coatings, or as reinforcing nanofillers in polymeric nanocomposites that can be laminated, to enhance cellulose fiber-based packaging materials. However, NC materials, whether in forms of microfibrillated cellulose (MFC), cellulose nanocrystals (CNC), and CNF, have abundant hydroxyl groups on their surface, and thus possess poor moisture barrier performance, especially at high relative humidity (RH). Nevertheless, their oxygen and oil/grease barrier properties are excellent at reasonable RH range (< 65%).[19] When applied as a barrier layer coating, the internal extensive hydrogen bonding, high crystallinity, and densely packed structure provide a torturous pathway that prevents the permeation of oxygen gas, while the surface tension and outstanding film formation properties can resist the oil or grease penetration. Many recent studies have demonstrated the applications of NC materials in polysaccharide matrix, bioplastic, latex, or other aqueous coating systems, yielding improved barrier performance with good potential to replace plastics in food packaging applications.[16,19,20] Nonetheless, some challenges still need to be overcome before industrial-scale implementation of NC materials for sustainable packaging. For instance, NC materials in suspension are usually present in low solid content, but they can easily form gels at elevated concentration, leading to high viscosity, long drying time, increased cost in transportation, and poor processability. In addition, the low solid content of NC materials would require specific coating apparatuses, such as curtain coating or slot die, which would impose additional capital cost. Furthermore, when used in multilayer coatings, NC materials are not heat sealable and thus can only be sandwiched between heat sealable polymeric layers, where the adhesion between the NC layer and polymer

needs to be addressed. Future research foci should be in the following areas: fundamental understanding of processing-structure-barrier property relationships of NC materials derived from numerous production routes; balanced moisture/oxygen barrier properties; development of NC-based high barrier materials via green chemistry and formulation with other emerging sustainable materials; active and intelligent NC-based packaging materials.

1.5. Other Applications

There are several other notable applications of NC. Firstly, NC has been useful in drilling applications, where CNF-based drilling fluid can be used to control the fluid loss, offer wellbore stabilization and hole cleaning. A recent study further justified that CNC can also be effective as a water-based mud additive, especially for controlling the rheology of the drilling mud.[21] (Readers interested in exploring the suitability of NC and its derivatives for use in drilling fluid are encouraged to read a recent review published by Rana et al.[22]). Secondly, the barrier properties of NC can be useful in the applications of barrier layer coating to enhance the performance of paperboard, conductive paper, and food packaging, as reviewed by Hubbe et al.[23] Thirdly, the strength of cement, *i.e*. mechanical performance as well as the degree of hydration, can be increased by addition of cellulose filaments. The intrinsic hydrophilicity, viscosity modifying ability, and hygroscopicity in NC materials might be responsible for the enhanced flexural strength and energy absorption in cement.[24] Fourthly, NC has recently been recognized in green cosmetics. Many personal care products have begun to incorporate NC to improve texture, especially for lotions, creams, facials, *etc*. In addition, the incorporation of NC in these cosmetics can eliminate the use of synthetic chemicals, which are not environmentally friendly. The applicability of NC for cosmetics design has been reviewed by Almeida et al.[25] Lastly, NC has many other emerging applications, such as sensing (including biosensing), electronic packaging, and fire retardation, as reviewed by Thomas et al.[26]

2. Structure of Cellulose

The crystalline cellulose I structure is commonly found in various plant species such as trees, non-woody plants, algae, *etc*. The naturally produced cellulose I has two polymorphic structures: triclinic structure (I_α) and monoclinic structure (I_β).[27] Algae, bacteria, and lower

plants produce mostly the I_α allomorph, whereas higher plants mostly produce the I_β allomorph. Nishiyama et al. comprehensively characterized the lattice structures for these two polymorphs using synchrotron X-ray and neutron fiber diffraction techniques.[28] The main difference between the two polymorphs is the displacement of the celluloses sheets across the 110_t plane *(t* stands for triclinic) and the 200_m plane *(m* stands for monoclinic, the hydrogen-bonded plane). The characteristics of hydrogen bonding are difficult to determine completely, but there is some consensus of the hydrogen bonding configuration.[28] Currently, the most accepted configuration is that the hydroxyl groups (equatorial to the cellulose's ring plane) and the intra- and interchain hydrogen bonding are widespread within the 110_t and 200_m crystallographic planes. Two different hydrogen bonding configurations are shown in Figure S1.[29] In this figure, it has been suggested that the network A is the I_β allomorph, whereas the network B has less occupancy than that in the I_α allomorph. Thus, it has been further suggested that the hydrogen bonding is weaker in the I_α configuration than that in the I_β configuration, and the I_α allomorph is metastable and can be hydrothermally (*e.g.*, in alkaline solutions) converted to the more stable I_β allomorph, as discussed by Moon et al.[30]

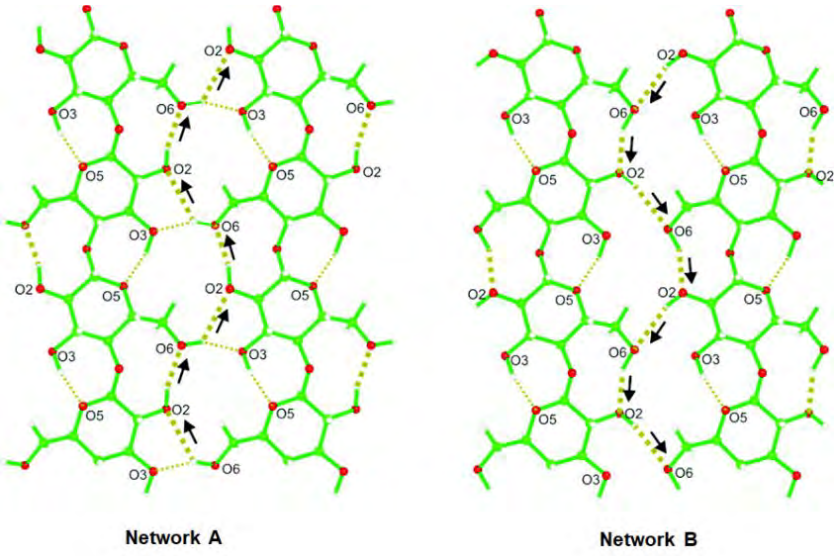

Figure S1. Illustration of cellulose chains showing hydrogen (H)-bonding's cooperative networks (indicated by thick dotted line). The donor−acceptor−donor command is shown by arrows (A and B networks). The H-bonding between O3−H···O5 and the O6−H···O3 linkage are indicated by thin dotted lines. This figure is reproduced with permission from ref.[29] Copyright 2008 American Chemical Society.

3. Relationships among Aspect Ratio, Volume Fraction and Phase Formation in Nanocellulose and Its Suspensions

Another interesting subject of the cellulose structure is the twisting of its microfibrils and macrofibrils, which has been observed and discussed quite extensively.[31,32] Currently, there is a strong consensus from the experimental data that a right-hand twist is present in these nanoscale fibrils. Molecular dynamics modeling in water solvent has recently been performed to investigate the dynamics of cellulose chains with I_β configuration, where the results point to a right-hand twist and the twist angle decreases with the number of glucan chains in the fibrils (Figure S2). However, the length of the glucan chains does not affect the twist angle.[33] The relationships among the aspect ratio, volume fraction and phase formation of NC in the dispersion state (as suspensions, gels and glasses) are illustrated in Figure S3. The classification of the gels *vs*. glass order is, however, not straight forward, but Tanaka et al.[34] discussed the two different classes. Both classes have a solid-like character and are not flowing in inverted cuvettes. The glass state is based on repulsive particle-particle interactions also referred to as caging, as explained by Appel et al.[35] and Nordenström et al.[36]

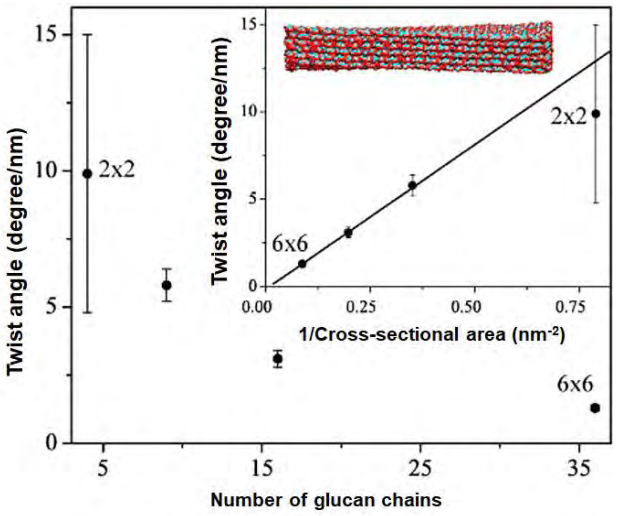

Figure S2. Twist angle variations with the β-(1–4)-linked D-glucan chains of the cellulose microfibril (CMF). The inverse cross-sectional area of microfibril is shown in the Inset. Reprinted with permission from ref.[33] Copyright 2013 American Chemical Society.

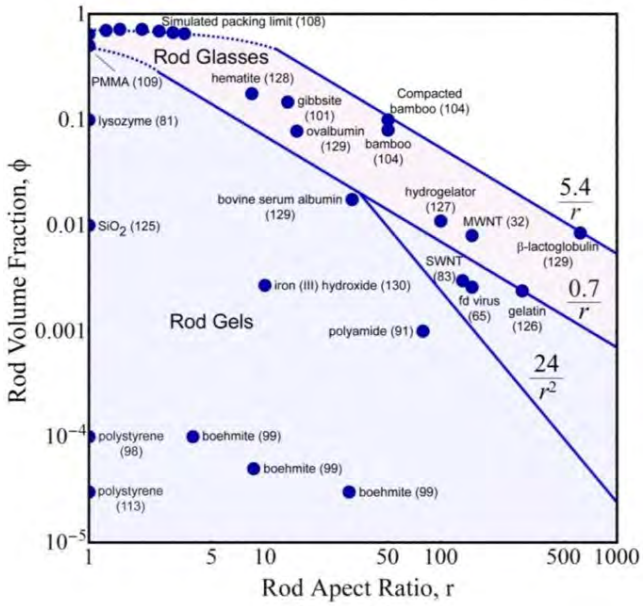

Figure S3. Mapping of the aspect ratio and volume fraction relationship in determining the boundary of different phases, such as NC suspensions, gels and glasses. Reprinted with permission from ref.[37] Copyright 2010 Royal Society of Chemistry. The inserted solid line shows the relationships fitted to the experimental data on medium charge (MC)-CNF, low charge (LC)-CNF, and high charge (HC)-CNF: CNFs with different aspect ratios of, BNC, and MC-CNC, S-CNC: CNCs with different aspect ratios.[36]

4. Aggregation Mechanisms for Nanocellulose Coagulation and Flocculation

Different types of aggregation mechanisms are illustrated in Table 3 (See main body of the manuscript), where in-depth discussion of the complex adsorption phenomena can be found in corresponding references.[38-42] In Table 3, charge neutralization and charge reversal phenomena are the simplest class. In this class, coagulation can take place by simple electrolyte or multivalent ion interactions, which can lead to charge reversal (particularly the hydrolyzed Al/Fe complexes)[43] or oppositely charged polyelectrolytes. In principle, coagulation is due to van der Waal´s forces taking over electrostatic repulsion forces, leading to coagulation. It may be difficult to distinguish between charge neutralization, patch flocculation and bridging flocculation (bridging is more common for high molecular weight polymers). Generally, the flocculation is shifted from the isoelectric point to a lower value with the increasing molecular weight of the polyelectrolyte. In the relationship between charge neutralization, charge reversal phenomena and the DLVO-theory, there are extensive publications and textbook chapters dealing with this subject (Table 3).

In contrast, the patch flocculation mechanism is different from the classical charge neutralization or bridging mechanism. The difference between these mechanisms is that patches of charged poly-ions are formed on the oppositely charged surface. Hence, particles are not smoothed out when a polymer is adsorbed, and patches of oppositely charged surfaces found on the particles can attract oppositely charged patches on another particle.

In another class, heterocoagulation is akin to the patch model as the term is assigned to particle-particle interactions, where the particles and their surface have opposite charges[44] and can attract each other. The theoretical treatment of heterocoagulation is essentially an extension of the DLVO-theory.[45,46]

Bridging flocculation has been postulated for many years,[47-49] where the direct evidence was first obtained by electron microscopy.[50] The literature on this subject is quite extensive, but the complexity of bridging flocculation is difficult to grasp in detail. This is because the kinetics of adsorption and the surface morphology of polyelectrolytes and the collision frequency is governed by both Brownian motion of the particles (*e.g.,* the perikinetic aggregation) and collisions induced by the shear-field (*e.g*., the orthokinetic aggregation). For small particles, the collision frequency is dominated by the Brownian motion, whereas the collision of larger particles is dominated by the shear field. Bridging occurs through interparticle connections at the ends, which was proposed by La Mer et al. and Fleer.[51,52] It is believed that the polymer is first adsorbed in an extended conformation onto one particle surface. In the second step, the polymer can also be adsorbed onto a bare surface on a different particle. The probability of bridging is thus proportional to the fraction of the surface covered by the polymer (Θ), and to the fraction of the uncovered surface on the particle ($1-\Theta$). Consequently, it is easy to show that the optimum polymer dosage should be a half surface coverage ($\Theta = 0.5$), which was first reported by La Mer et al.[51] In general, adsorption flocculation can be promoted by a high molecular weight oppositely charged polymer. It has been found that there is an optimum charge density for flocculation because the high charge density can result in a flattened conformation on the surface, whereas low charge density can decrease the adsorption behavior. Bridging flocculation in dispersions by nonionic polymers can also occur by non-electrostatic interactions and this phenomenon has also been investigated.[53,54] As the nonionic polymers are not as stretched out in solution as polyelectrolytes, it is often necessary to decrease the electrostatic double-layer by the

addition of electrolytes. In this scenario, polyvalent counter-ions are more efficient in sensitizing the flocculation process than monovalent ions.

Finally, complex flocculation systems often involve the usage of two interactive components: a cationic component and an anionic component, or multiple interactive components. In the last case, the system is a multi-component system, which is complex in nature but effective in industrial operations. The multi-component systems are rarely investigated by academic scientists because of the complexity, but they have been studied extensively by industrial researchers. These systems are generally superior to mono-component systems in practical applications as they exhibit synergistic effects between the additives, *e.g*., the multicomponent systems generally create stronger flocs-structure. A classic example of such systems is the use of dual additives, *e.g*., a cationic component (polyelectrolyte or hydrolyzed Al/Fe-species) followed by an anionic polymer. The rate of flocculation in this system is generally extremely fast and the residence time can be very short. However, the mixing is complex, depending on the type of dispersion that can be flocculated. Microparticulate flocculation systems were first demonstrated by Lindström et al.[55] This is very relevant to this review, as its behavior is closely related to the NC materials. Such systems are based primarily on cationic polymers in conjunction with colloidal silica or bentonite materials, which are essential to the reversibility of flocculation after high-shear treatment and can be very useful for decreasing the water content (*e.g*. dewatering of sludge from wastewater treatment). In the water treatment community, the term sweep-flocculation is often used to describe the large mass of $Al(OH)_3$/$Fe(OH)_3$ created when Al/Fe salt is added in water forming cationic aggregates that can incept anionic dispersions. However, this mechanism is not fully understood.[56] In the above systems, the important physical-chemical interactions are taking place at the particle surface. However, there is also a multitude of systems, where the second additive can cause gelation, coacervation, or precipitation, thus creating an intermolecular complex resulting in the interception of particles. Thus, interactions can take place in solution rather than on the particle surface. However, in many practical cases, the combined events are often found. In such systems, the flocculation is induced by the phase separation of formed complex.[57,58]

Table S2. Advantages and disadvantages of different forms of NC-based adsorption materials and their preparation methods.

Adsorbent	Processing/ modification	Advantage	Disadvantage	Target Pollutants	Ref.*
CNC-polypyrrole	Composite prepared by stirring	Polypyrrole is stable, low cost and eco-friendly; stirring is simple and easy to apply	Cooling and lyophilization are necessary; separability is difficult	Cr(VI) Congo Red	59
Sludge microfibers+CNF_{SL} (Support layer) /Active layer (CNC_{BE} +gelatin)	Layered membranes fabricated by vacuum filtration	Layers of specific materials are feasible to apply, easy to operate, lab availability and low-cost method, quickly draws a filtrate, continuous operation, easy to control operating parameters, high surface charge in TEMPO oxidized NC, available – COOH group for adsorption	High power consumption by the vacuum pump, time consuming and support material is necessary	Cu(II) Fe(II) Fe(III)	60
Chitosan and phosphorylated NC	Electrospun mat fabricated by electrospinning	Ease surface functionalization, good water permeability due to high porosities, interconnected network structures, and minimal pressure drops, tailor able to adsorb specific contaminants, good affinity of Cd (II) interaction with amine and phosphate groups	Expensive electrospinning setups, additional polymers requirement, difficult to achieve nanofiber with sub-nm diameter, necessary for parameters optimization *etc*.	Cd(II)	61
Sodium alginate and polyacrylamide-NC	Hydrogels fabricated by stirring	Crosslinked 3D network, transparent, high water-holding	Water swollen, ions requirement for cross-	Methylene blue	62

(BC/CNC/TEMPO oxidized NC)		capacity, light-weight, excellent flexibility, superior homogeneity, easy access for dye adsorption	linking (*e.g.* $CaCl_2$), lack of mechanical strength, covalently crosslinking is necessary		
CNC-alginate-hydrogel	Beads prepared by mixing and gelation	Feasible for fixed bed columns and large scale implementation, effective for cyclic sorption/desorption, fast gelation method	Cross-linker needed ($CaCl_2$), Acute toxicity of alginic acid	Methylene blue	63
NC-graphene oxide	Aerogels fabricated by stirring and ultrasonication	Porous ultralight material, crosslinked 3D network, increased strength and stiffness, lightweight, excellent flexibility, easy access for solutes due to high porosity (>90%)	Necessary for freezing/subcritical drying	Methylene Blue Congo Red Waste oil	64 65
NC-aerogel-oleic acid -Fe_3O_4	Magnetic aerogel prepared by blending > mixing > stirring	Hydrophobic adsorbents, ease of separability after adsorption, preparation methods are easy to implement	Freeze-drying is needed but energy and time-consuming process	Cyclohexane Ethyl acetate Vacuum Pump oil	66

* The cited references are only for adsorbent, processing/modification and target pollutants columns, excluding advantage and disadvantage columns.

5. Adjusting Functionalities of Nanocellulose to Enhance Adsorption Performance

The functionalities of NC can be adjusted or modified by different chemical pathways to enhance the adsorption performance. Some example pathways are discussed as follows. In the first pathway, TEMPO mediated oxidation is effective to yield carboxylated NC (Figure 24(I) in the main body of the manuscript). The adsorption capacity of the resultant adsorbent is shown in Figure 25 in the main body of the manuscript. However, this method has some drawbacks; including toxic reagents, long reaction time and selective oxidation (only the C_6 primary OH group is oxidized). Alternatively, periodate-chlorite oxidized NC, or dialdehyde nanocellulose (DAC), could be converted to dicarboxylated-NC using chlorite.[67] Periodate is also a toxic reagent with environmental issues. In addition, this oxidation method can cleave the glycosidic bond/rings and result in smaller NC with lower degree of polymerization (DP) and less rigidity.[68] To overcome this problem, Yu et al. used citric/hydrochloric acid hydrolysis to produce carboxylated CNC without sacrificing its DP.[69] They reported that H_3O^+ from HCl or RCOOH dissociation not only can hydrolyze the amorphous regions of microcrystalline cellulose but also can catalyze the esterification of the OH groups on the exposed cellulose chains with the COOH groups of citric acid (Figure S4). However, the average DP of the produced CNC was found to decrease with increasing the reaction time from 2 to 6 h. CNC-COOH (4 h) and exhibited better MB removal capacity than the TEMPO-oxidized NC at a similar adsorbent dosage (18 mg/L) and dye concentration (200 mg/L). This removal capacity was significantly higher than sulfuric acid, formic and hydrochloric acid-functionalized CNC.

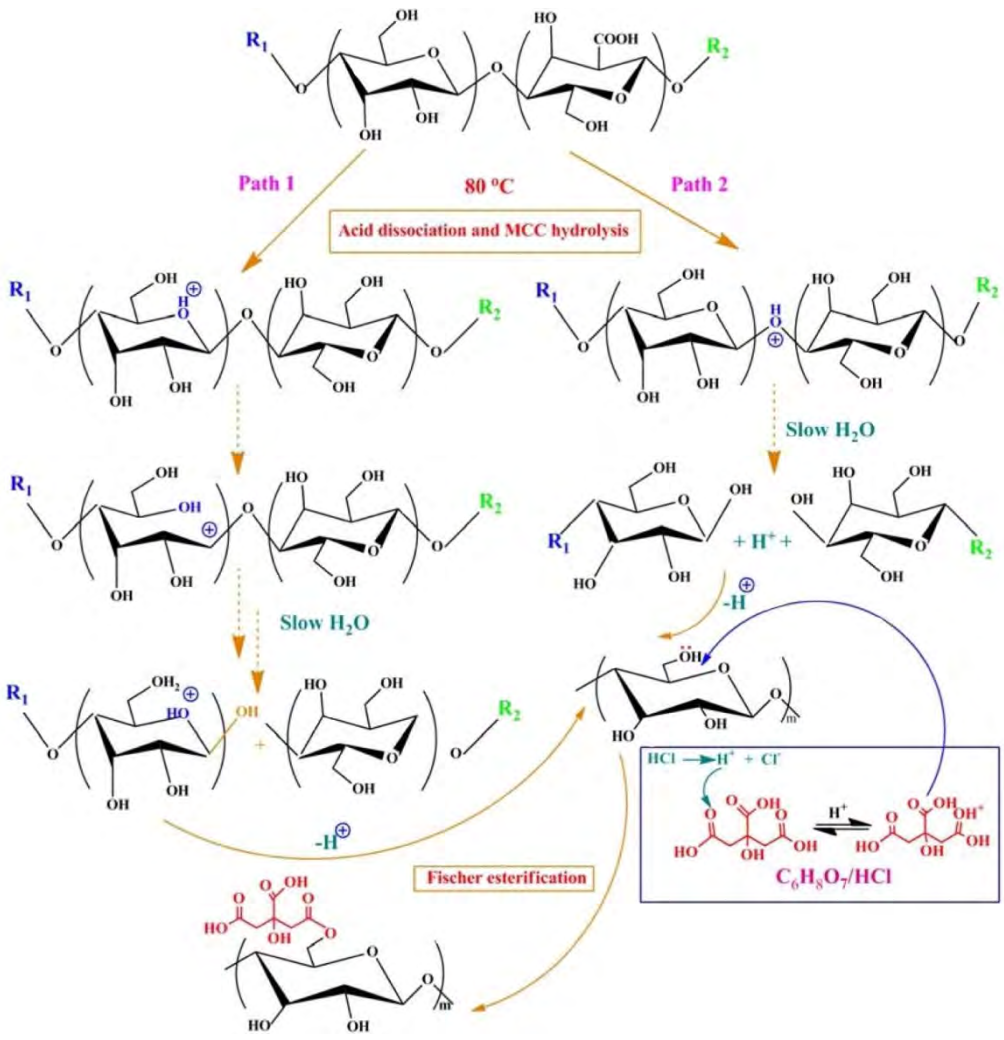

Figure S4. Two possible routes (acid dissociation and hydrolysis) to fabricating carboxylated CNC from microcrystalline cellulose. Reprinted with permission from ref.[69] Copyright 2016 American Chemical Society.

In the second pathway, periodate oxidant has been extensively used to prepare DAC (Figure 24(II)).[70] This oxidation treatment can open the pyranose ring, where the CHO group on DAC typically attracts less water as compared to the primary OH group on pristine NC. The less hydrophilic derivative can be useful for adsorption of organic solvents. However, opening the pyranose group will also destroy some crystalline regions of NC and increase the amorphous fraction,[70] which is more susceptible to pollutants adsorption. As seen in Figure 24(IIa), the reducing group CHO (oxidation potential, ε = +0.58V) can reduce the adsorbed metals ions, such as Cd(II), Ag(I), Hg(I), Ni(II), Pb(II), Pt(II), Cu(II), and Au(III), to their zerovalent nanoparticle

forms. The CHO group in DAC can be further used to graft amino acids (Figure 24(IIb)) or crosslink with chitosan (Figure 24(IIc)). Based on this pathway, several unique DAC derivatives can be obtained. For example, L-cysteine amino acid-functionalized DAC can be prepared by a reductive amination reaction. The –SH group of L- cysteine exhibited the maximum adsorption capacity against Hg(II) to be 923 mg/g (the value based on the Langmuir modeling was 1034 mg/g) with a removal efficiency of 93% at pH = 5.[71] The removal efficiency was not significantly decreased (87.4%) in the presence of coexisting metal ions, such as Cu(II), Pb(II), Cd(II) and Zn(II). Also, the -SH group functionalization has been carried out using 3-mercaptopropionic on spherical NC, which exhibited maximum adsorption capacity of around 190 mg/g against Hg(II). In addition, its selectivity toward Hg(II) is quite good in varying types of water, *e.g*., the selectivity was 99%, 78% and 88% in distilled water, water with competing ions and tap water, respectively.[72] This type of adsorbent would be beneficial in the situation where raw cellulose is ineffective due to low specific surface area, few metal chelating groups, and poor selectivity towards Hg(II) ions. In another scenario, the grafting of DAC with ethylenediamine can be carried out to produce amino-functionalized NC through a reductive amination treatment (Figure 24(IIe)).[73] This system exhibited maximum adsorption capacity (by the Langmuir modeling) of 555.6 mg/g against acid red GR, and could remove Congo Red 4BS and Reactive light yellow K-4G with efficiency of 100 and 98%, respectively. The removal mechanism is mainly due to electrostatic and hydrogen bonding interactions between anionic dyes with the amino (NH_2) and hydroxyl (OH) groups on grafted NC, respectively. Finally, cationic (cDAC) can be produced from sugarcane bagasse for removal of Cr(VI).[74] The objective of this study was to control the degree of oxidation (DAC-0.5, DAC-1 and DAC-2) followed by cationization using the Girard's reagent T. It was found that c-DAC-2 exhibited the highest charge density with the Langmuir maximum adsorption capacity of 80.5 mg/g. The mechanism of Cr(VI) adsorption on cDAC appeared to be due to the electrostatic interactions between Cr(VI) ions and quaternary ammonium cations. Relatively high adsorption capacity of cDAC was observed under a wide pH range (2-10).

In the third pathway, *β*-cyclodextrin (CD), an inexpensive and efficient class of bioadsorbent capable of removing a range of micropollutants[75] can be grafted onto NC and/or amine-functionalized NC (Figure 24(IIIa)). The resulting material exhibited enhanced maximum adsorption capacity against multiple wastewater pollutants. Although CD functionalized

cellulose has been extensively reported for pollutants removal,[76] its functionalization on NC is sparsely reported. We note that both positively and negatively charged CDs are available commercially; it is conceivable that NC materials modified with these positively charged CD can be used to adsorb both anionic and cationic pollutants simultaneously.

In the fourth pathway, one can use quaternary ammonium moieties-bearing molecules (QAM) to prepare multifunctional cationic NC as illustrated in Figure 24(IV). In this pathway, the chosen QAM consists of pentavalent nitrogen, which is attached to four alkyl/heterocyclic radicals and a small ion (*e.g.*, iodide, chloride and bromide). Therefore, besides electrostatic interactions between cationic nitrogen in QAM with anionic pollutants, ion exchange of QAM with target pollutants is also possible. Depending on the chain length of the alkyl group ($C_{(n)}$) in QAM, one can tune its lipophilicity to assist the oil/organic solvents adsorption. Tavakolian et al. recently reviewed that QAMs have strong antimicrobial activity.[77] However, the multifunctionality of QAM modified NC has yet to be fully explored by the community.

In the fifth pathway, metal-binding bio-compatible peptides, which are effective to enhance the heavy metal ion adsorption, can be grafted onto NC. In this scenario, the *N*-terminus amino, *C*-terminus carboxylate group as well as side chains of the peptide moiety are ideal locations for attachment onto NC (Figure 24(Va)). In addition to metal ion removal, organic pollutants can also be removed with high adsorption capacity by such materials.[78] We note that peptide-functionalized NC has mainly been demonstrated for biomedical applications,[79] and there is a lack of knowledge on its selective adsorption of heavy metal ions and organic pollutants.

In the final pathway, sulfuric acid-treated CNC can be reacted with azetidinium ions, as demonstrated by Börjesson et al [80] (Figure 24(VI)). The goal of their study was to increase the thermal stability of NC, where modified NC showed an increase of 100 ^{o}C in thermal stability compared with pristine CNC. We believe such modification can also increase the hydrophobicity of NC, which will be useful for adsorption of some organic pollutants, such as polycyclic aromatic hydrocarbons. Since azetidinium is available in many forms, this functionalization pathway can be used to create new properties of NC and warrants further exploration.

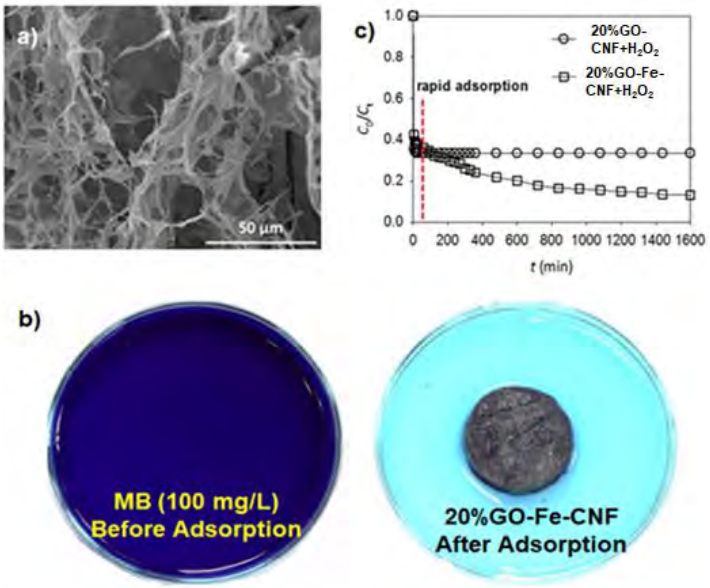

Figure S5. (a) SEM image of 20% GO-Fe-CNF. (b) Photograph of MB solution adsorption (100 mg/L) before and after 30 min into 20% GO-Fe-CNF. (c) Fenton oxidation of MB on adsorption of GO-Fe-CNF nanocomposite. This figure is reproduced with permission from ref.[81] Copyright 2016 Royal Society of Chemistry.

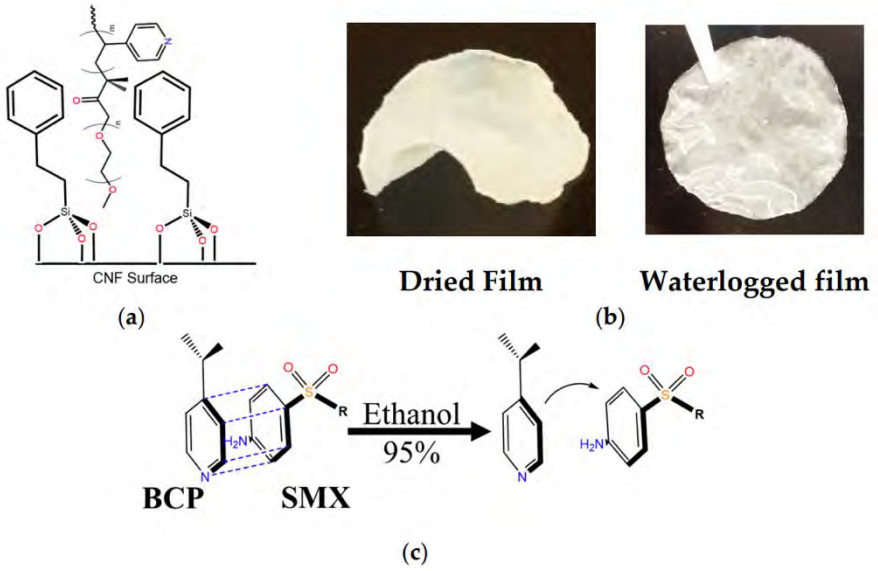

Figure S6. (a) Covalent functionalization of TMPES onto CNF, then modified with BCP (P4VP-PEO). (b) Photographs of the dried and waterlogged CNF films modified with TMPES and BCP. (c) Mechanism of SMX adsorption based on the electron-donor-acceptor interaction. Adapted from ref.[82] Copyright 2019 Multidisciplinary Digital Publishing Institute.

6. Band-Gap Energy Measurement

Tauc's plot is commonly used to calculate the band-gap energy (E_g) from the optical absorption spectra as depicted in equation S1.[83] This formula was modified by Davis and Mot in 1970.[84]

$$(\alpha.h\nu)^{1/\gamma} = B\,(h\nu - E_g) \qquad (S1)$$

where α is the energy-dependent absorption coefficient, h is Planck's constant, ν represents the light/photon's frequency, factor γ can be 1/2 or 2 for the direct and indirect transition band-gaps, respectively, and B is a constant. Based on the theory proposed by Kubelka and Munk in 1931,[85] it is possible to measure a reflectance spectrum that can be transformed to the corresponding absorption spectra by using the Kubelka-Munk (K-M) function, $F(R\alpha)$, as shown in equation S2.

$$\frac{K}{S} = \frac{(1-R\alpha)^2}{2R\alpha} = F(R\alpha) \qquad (S2)$$

where K is the absorption coefficient, S is the scattering coefficient, $R\alpha = \frac{R_{sample}}{R_{standard}}$, *i.e.*, the reflectance of an infinitely thick sample. Placing $F(R\alpha)$ in lieu of α in equation S1 will give rise the following equation (equation S3).

$$(F(R\alpha).h\nu)^{1/\gamma} = B(h\nu - E_g) \qquad (S3)$$

The above equations are widely used in the literature to determine the E_g value of different photocatalysts. However, an error-free measurement of E_g is essential to evaluate the photo-physicochemical properties of semiconductors. Tailoring E_g from equation S1 is very straightforward and is suitable for single-component catalysts without defects and/or modifications, where no sub-band-gap energy exists. However, following our discussions (See section 5.3 in the main body of the manuscript), it is apparent that scientists often modify the surface, create defects, and dope different materials into the catalysts to engineer E_g, which would introduce intra-band-gap states. The presence of intra-band-gap states can influence Tauc's plot and give an inaccurate E_g estimation. Such errors are often noticed in some publications, where an incorrect interpretation of Tauc's plot has been made, leading to a reduced E_g value. Many had attempted to avoid such mistakes, where an improved method to estimate the E_g value has been demonstrated as in the work of Makuła et al.[86]

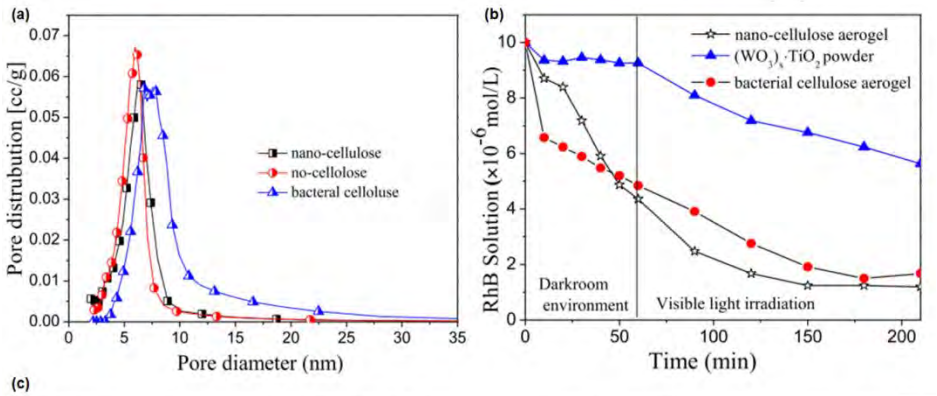

(c)

Template	Specific surface area (m^2/g)	Pore volume (cc/g)	Pore diameter (nm)
No BC template	417	0.86	8.22
Nano-cellulose	393	0.84	8.58
Bacterial cellulose	399	1.33	13.34
No BC/SiO_2 gel*	106	0.31	11.62

* The $(WO_3)_x$·TiO_2 powder sample synthesized without using BC/SiO_2 gel as template.

Figure S7. (a) Distribution profiles of pore size with and without NC/BC-templated SiO_2–$(WO_3)xTiO_2$. (b) Adsorption/photocatalytic degradation of RhB using BC/NC-templated SiO_2–$(WO_3)xTiO_2$ and $(WO_3)xTiO_2$ powder. (c) The BET analysis results with and without templated photocatalysts. The figure is reproduced with permission from ref.[87] Copyright 2016 Elsevier.

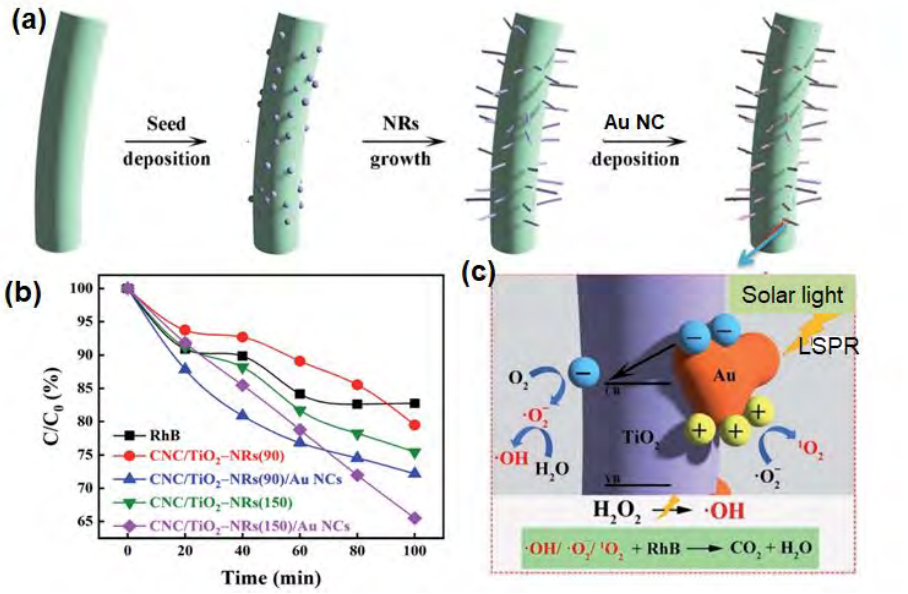

Figure S8. (a) An illustration of the seed-mediated TiO_2-NR synthesis onto CNC, where titanium butoxide is used as the seed and $TiCl_4$ is used for TiO_2-NR growth. CNC-TiO_2-NR is further used as a template for Au NCs deposition. (b) Photo-degradation of RhB under simulated sunlight irradiation in the presence of H_2O_2. (c) An illustration of the putative photocatalytic mechanism for RhB degradation on a bi-metallic photocatalyst in the presence of H_2O_2. Adapted from ref.[88] Copyright 2020 Royal Society of Chemistry.

7. Other Nanocellulose-Based Photocatalysts

Silver phosphate (Ag_3PO_4) shows great potential for photo-degradation of some pollutants under visible light irradiation because of its low band-gap: 2.45 eV [89] and low toxicity. Its conduction band (CB) states are Ag 5s and 5p, while O_{2p} and Ag 4d dominate its valence band (VB).[89] However, this compound is unstable and can result in photocorrosion that often requires electron scavengers to ensure good photocatalytic activity.[90] Compared to TiO_2 and ZnO nanoparticles, Ag_3PO_4 nanoparticles also exhibit tendency to agglomerate. These drawbacks can be overcome by using NC as a template. For example, Lebogang et al. demonstrated a simple ion-exchange *in-situ* casting method to prepare (Ag_3PO_4)-NC composite photocatalyst which has been used for the degradation of MB and MO under direct sunlight irradiation (solar flux at 1000 W/m^2).[91] The band-gap of the (Ag_3PO_4)-NC composite was 2.1 eV. This suggests the suitability of using this catalyst to use solar radiation to initiate the photodegradation process (the photon energy at the maximum solar irradiance at 550 nm is 2.23 eV). The (Ag_3PO_4)-NC composite showed complete photo-degradation of MB after 45 min at a rate of 0.042 min^{-1}. On the other hand, MO showed relatively slower photo-degradation at a rate of 0.008 min^{-1}. This may be due to the azo bond (-N=N) of MO, which can resist photo-degradation. In addition, we think the anionic MO would have less adsorption efficiency onto negatively charged NC, which can further decrease its degradation efficiency. To explore the performance of this photocatalyst in real wastewater, Lebogang et al. adopted pond water for MO photo-degradation.[91] The corresponding reaction rate constant was found to be 0.0099 min^{-1}, lower than MO photo-degradation in pure deionized water (0.0177 min^{-1}).

While many researchers removed NC using calcination/pyrolysis after nanoparticles growth/deposition, Gan et al. conducted an interesting study where they first converted CNF to graphite-like carbon scaffolds using different pyrolysis treatments.[92] In the second step, they used the graphitic carbon substrate to prepare a composite with bismuth oxybromide (BiOBr) hydrothermally. The composite was named BiOBr/CCNF (CCNF stands for cellulose-derived carbon nanofibers). In general, BiOBr has a band-gap of 2.7 eV, good chemical stability and low toxicity, which becomes a suitable candidate for pollutant removal by photo-degradation. The doping of CCNF narrowed the band-gap to 2.4 eV. Graphitic CCNF increased the light absorption and stabilized the photon energy. Compared to pristine CNF, two new diffraction

peaks at 26° and 44° in wide-angle X-ray diffraction (WAXD) were observed on CCNF, where these peaks are characteristic of graphitic materials.[93] With increasing pyrolysis temperature, the diffraction intensity at 44° increased notably, suggesting a higher degree of graphitization in CCNF. In addition, Raman spectra showed two major peaks at nearly 1360 and 1580 cm^{-1}, corresponding to D (defective sp^3 carbon) and G (graphitic sp^2 carbon) bands, respectively. The degree of graphitization can be calculated by the intensity ratio between ID and IG. It was found that the ID/IG ratio from the Raman spectra was increased by increasing temperature, indicating the increase of defects in graphitized carbon.[94,95] Furthermore, the BiOBr/CCNF composite made at the highest temperature pyrolysis showed the weakest photoluminescence emission. Therefore, these composites can offer a lower rate of electron–hole recombination (compared to BiOBr), allowing greater lifespan of photo-generated electrons and holes, hence increasing the redox reactions through reactive oxygen species generation. Based on the above observation, BiOBr/CCNF pyrolyzed at 1000 ^oC should show the highest pollutant degradation efficiency, which was not seen. Instead, BiOBr/CCNF pyrolyzed at 800/900 ^oC exhibited higher photo-degradation efficiency, which took only 60 min to mineralize 10 and 5 mg/L of RhB and Cr(VI), respectively, under visible-light (LED lamp, 200 W) irradiation at ambient temperature. The rate of reaction for RhB and Cr(VI) degradation was 8.15 x 10^{-2} and 0.21 mmol/g/h using the BiOBr/CCNF-900 composite, respectively. Its quantum yields of 1.56×10^{-6} (RhB) and 3.83 x 10^{-6} (Cr(VI)) molecules per photon were higher than that of the pristine BiOBr (0.51 x 10^{-6} (RhB) molecules per photon). It should be noted that higher calcination temperature removed most of the oxy-functional groups from the CNF scaffold, but it did not destroy the overall fibrous network morphology.

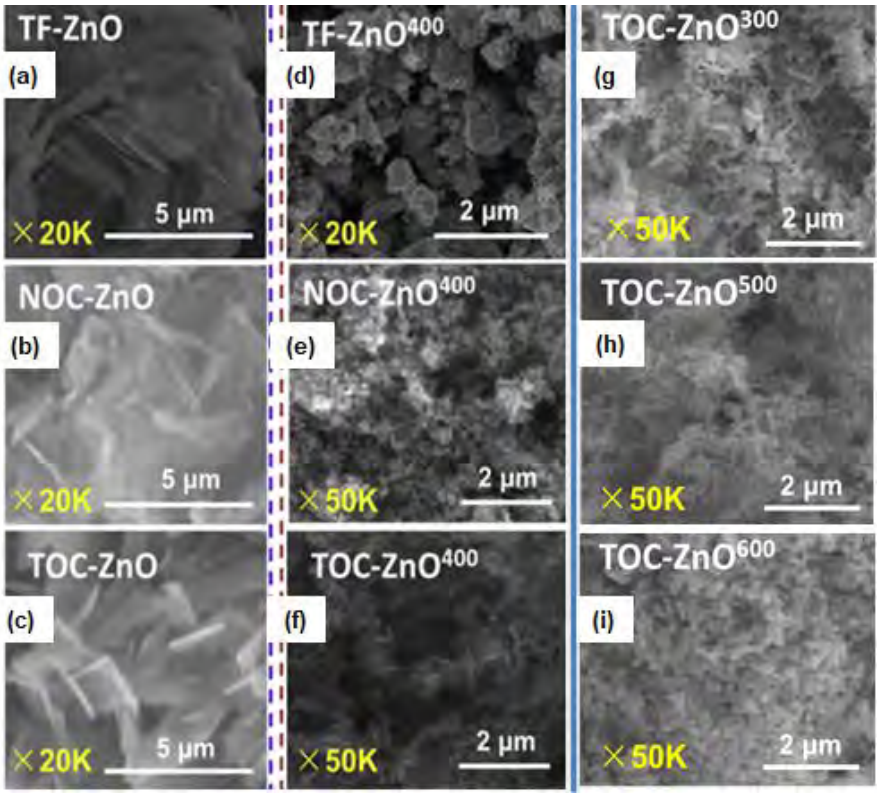

Figure S9. SEM images of different NC-based ZnOx-photocatalysts (a-c) Before and (d-i) After calcination. The figure is reproduced with permission from ref.[96] Copyright 2020 Elsevier.

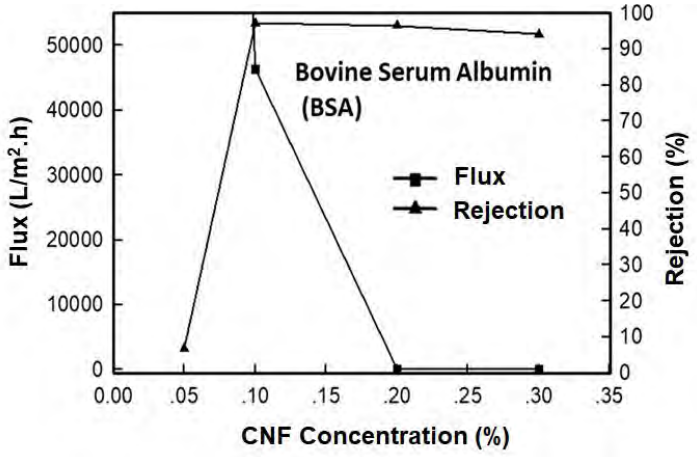

Figure S10. The flux and rejection of bovine serum albumin (BSA) for TEMPO-CNF films (by vacuum-filtration) prepared at different CNF concentrations. The selection of concentration is critical to creating the optimal thickness to yield good flux and high rejection properties against BSA, simultaneously. Reprinted with permission from ref.[97] Copyright 2019 Springer-Nature.

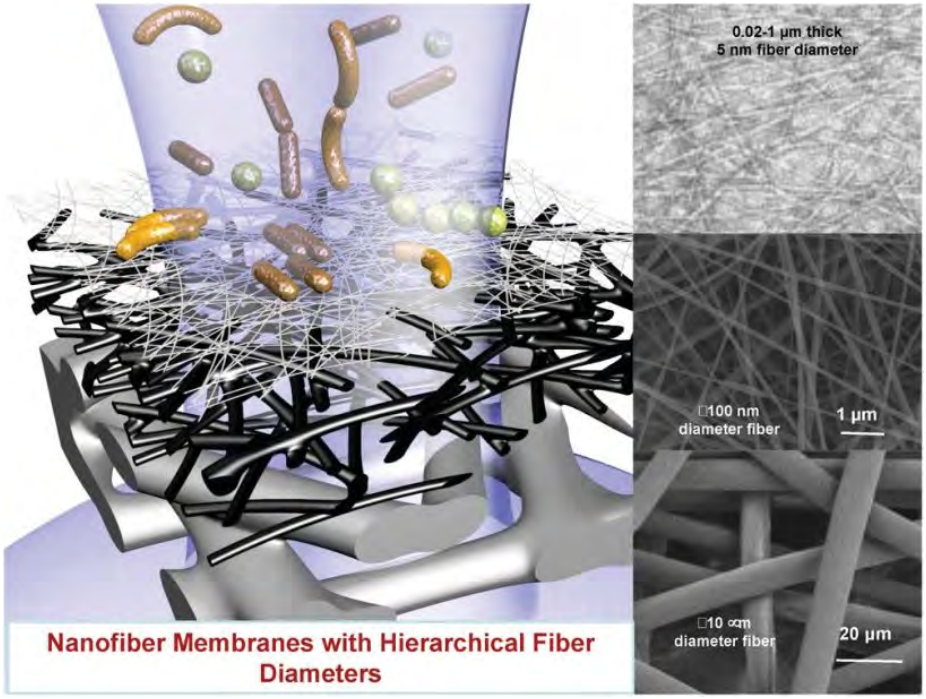

Figure S11. Schematic illustration of CNF-based TFNC membrane consisting of three unique layers of non-woven fibers with different sizes for UF applications (membrane pore size: 2-100 nm). Reprinted with permission from ref.[1] Copyright 2020 WILEY-VCH Verlag GmbH & Co.

Table S3. Some representative publications discussed by the TFNC platform technology.

Filter type	NC type	Filtration medium	Highlights	Ref.
RO	T-CNF (wood pulp)	NaCl	Interfacial polymerization by UF-membrane	98
NF	T-CNF (wood pulp)	$MgSO_4$, $MgCl_2$, NaCl	Interfacial polymerization on polyamide by UF-membrane	99
NF	T-CNF (wood pulp)	$MgSO_4$	Interfacial polymerization by UF-membrane	100
UF	T-CNF (wood pulp)	BSA	Mixing between polyethylene glycol and T-CNF	101
UF	T-CNF (wood pulp)	Emulsified oil/water, microspheres	Morphology issues and charge density of T-CNF	102
UF	CNF (rice straw)	BSA, lime nanoparticles	Non-bleached fiber shows higher water flux than bleached fibers	103
UF	T-CNF (wood pulp)	BSA	Antifouling issues	104
UF	T-CNF (bamboo pulp)	Dextrane, BSA, polypeptides	Antifouling issues and water channels	105
UF	T-CNF (jute pulp)	BSA	Antifouling issues and charge density of T-CNF	106

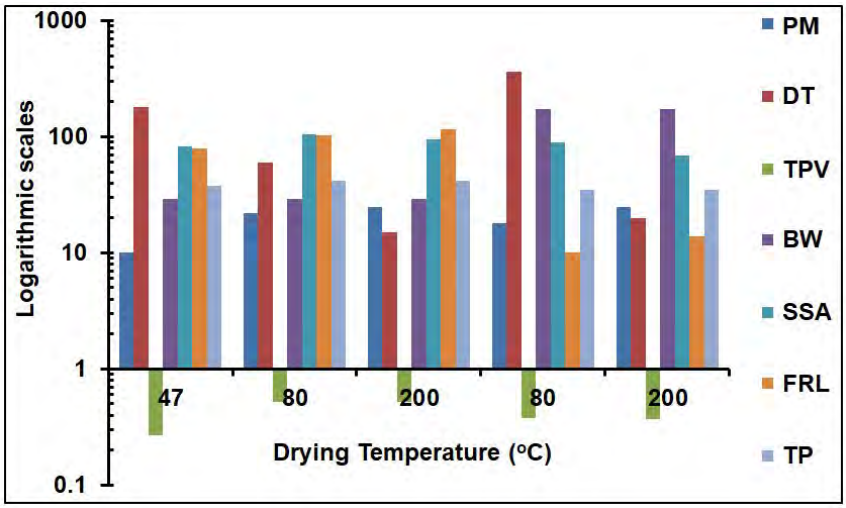

Figure S12. Effect of drying temperatures on the properties of Cladophora-based membranes (PM: pore mode (nm), DT: drying time (min), TPV: total pore volume (cm^3/g), BW: basis weight (g/m^2), SSA: specific surface area (m^2/g), FRL: flow rate (L/m^2 .h. bar) and TP: total porosity (%)). Reported values are collected from ref.[107]

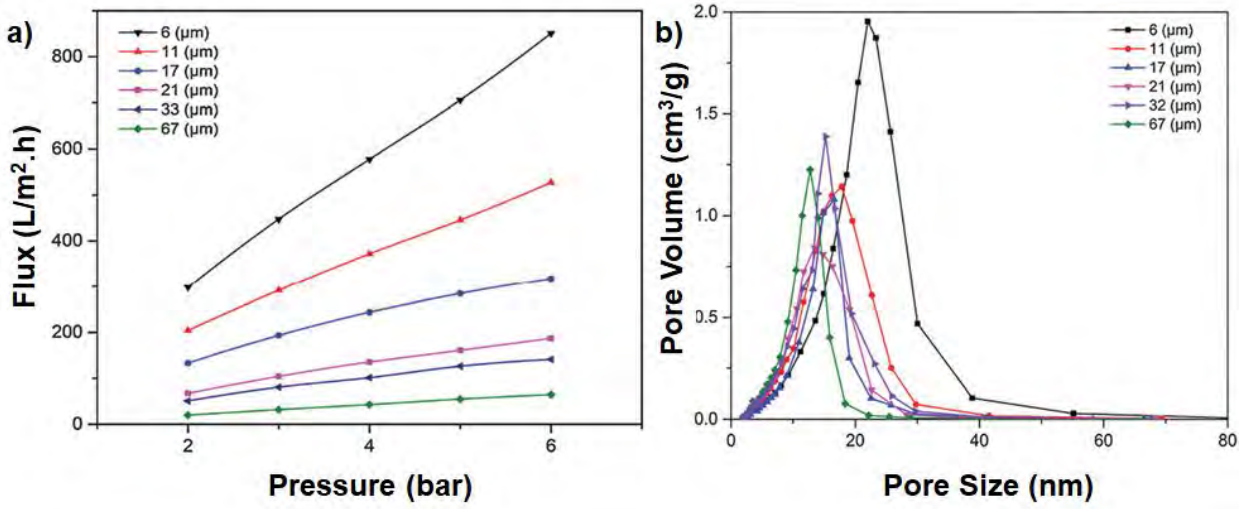

Figure S13. (a) Flux from the Barret-Joyner-Halenda method with different membrane thicknesses. (b) Size distributions of membranes with different thicknesses. The figure is reproduced from ref.[108] with permission. Copyright 2016 Royal Society of Chemistry.

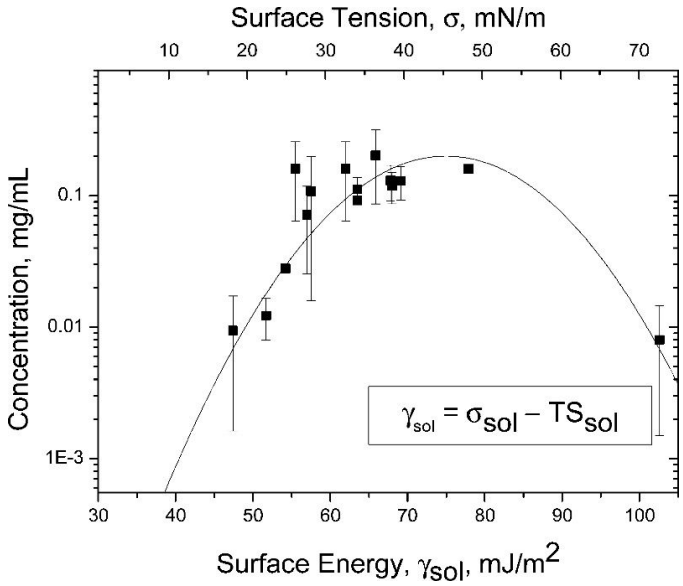

Figure S14. Correlation between the BC concentration dispersed in different organic solvent and surface energy (γ) and liquid surface tension (σ). Reprinted with permission from ref.[109] Copyright 2016 American Chemical Society.

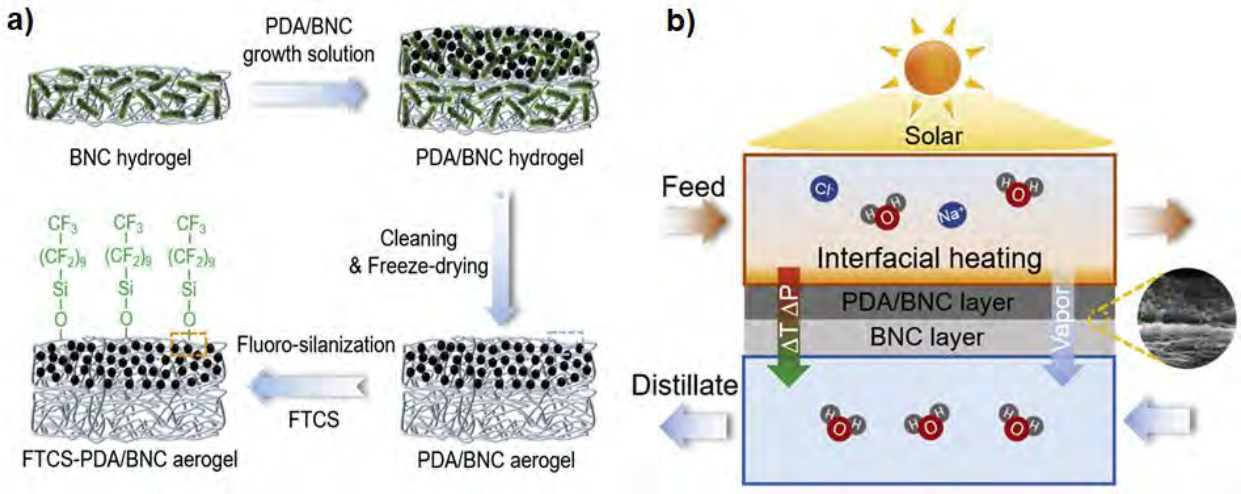

Figure S15. (a) Representation of the essential steps for fabrication of a FTCS-PDA/BC membrane. (b) Schematic illustration of the PMD system for direct contact membrane distillation operation using the FTCS-PDA/BNC membrane**.** Reprinted with permission from ref.[110] Copyright 2021 Elsevier.

References

(1) Sharma, P. R.; Sharma, S. K.; Lindström, T.; Hsiao, B. S. Nanocellulose-Enabled Membranes for Water Purification: Perspectives. *Adv. Sustain. Syst* **2020,** *4*, 1900114.

(2) Heise, K.; Kontturi, E.; Allahverdiyeva, Y.; Tammelin, T.; Linder, M. B.; Ikkala, O. Nanocellulose: Recent Fundamental Advances and Emerging Biological and Biomimicking Applications. *Adv. Mater.* **2021,** *33*, 2004349.

(3) Klemm, D.; Cranston, E. D.; Fischer, D.; Gama, M.; Kedzior, S. A.; Kralisch, D.; Kramer, F.; Kondo, T.; Lindström, T.; Nietzsche, S. Nanocellulose as a Natural Source for Groundbreaking Applications in Materials Science: Today's state. *Mater. Today* **2018,** *21*, 720-748.

(4) Prathapan, R.; Tabor, R. F.; Garnier, G.; Hu, J. Recent Progress in Cellulose Nanocrystal Alignment and Its Applications. *ACS Appl. Bio Mater.* **2020,** *3*, 1828-1844.

(5) Trovagunta, R.; Zou, T.; Österberg, M.; Kelley, S. S.; Lavoine, N. Design Strategies, Properties and Applications of Cellulose Nanomaterials-enhanced Products with Residual, Technical or Nanoscale Lignin–A Review. *Carbohydr. Polym.* **2020**, *254,* 117480.

(6) Moon, R. J.; Schueneman, G. T.; Simonsen, J. Overview of Cellulose Nanomaterials, their Capabilities and Applications. *Jom* **2016,** *68*, 2383–2394.

(7) Vanderfleet, O. M.; Cranston, E. D. Production Routes to Tailor the Performance of Cellulose Nanocrystals. *Nat. Rev. Mater.* **2021**, 6,124-144.

(8) Ghasemlou, M.; Daver, F.; Ivanova, E. P.; Habibi, Y.; Adhikari, B. Surface Modifications of Nanocellulose: From Synthesis to High-Performance Nanocomposites. *Prog. Polym. Sci.* **2021**, *119*, 101418.

(9) Clarkson, C. M.; El Awad Azrak, S. M.; Forti, E. S.; Schueneman, G. T.; Moon, R. J.; Youngblood, J. P. Recent Developments in Cellulose Nanomaterial Composites. *Adv. Mater.* **2020**, *33,* 2000718.

(10) Li, K.; Clarkson, C. M.; Wang, L.; Liu, Y.; Lamm, M.; Pang, Z.; Zhou, Y.; Qian, J.; Tajvidi, M.; Gardner, D. J. Alignment of Cellulose Nanofibers: Harnessing Nanoscale Properties to Macroscale Benefits. *ACS Nano* **2021,** *15*, 3646-3673.

(11) Tang, S.; Chi, K.; Xu, H.; Yong, Q.; Yang, J.; Catchmark, J. M. A Covalently Cross-linked Hyaluronic Acid/Bacterial Cellulose Composite Hydrogel for Potential Biological Applications. *Carbohydr. Polym.* **2021,** *252*, 117123.

(12) Tang, S.; Chi, K.; Yong, Q.; Catchmark, J. M. Synthesis of Cationic Bacterial Cellulose Using a Templated Metal Phenolic Network for Antibacterial Applications. *Cellulose* **2021**, *28*, 9283–9296.

(13) Wahid, F.; Huang, L.-H.; Zhao, X.-Q.; Li, W.-C.; Wang, Y.-Y.; Jia, S.-R.; Zhong, C. Bacterial Cellulose and Its Potential for Biomedical Applications. *Biotechnol. Adv.* **2021**, *53*, 107856.

(14) Chen, W.; Yu, H.; Lee, S.-Y.; Wei, T.; Li, J.; Fan, Z. Nanocellulose: a Promising Nanomaterial for Advanced Electrochemical Energy Storage. *Chem. Soc. Rev.* **2018,** *47*, 2837-2872.

(15) Xu, T.; Du, H.; Liu, H.; Liu, W.; Zhang, X.; Si, C.; Liu, P.; Zhang, K. Advanced Nanocellulose-Based Composites for Flexible Functional Energy Storage Devices. *Adv. Mater.* **2021**, 2101368. https://doi.org/10.1002/adma.202101368.

(16) Chi, K.; Catchmark, J. M. Improved Eco-friendly Barrier Materials Based on Crystalline Nanocellulose/Chitosan/Carboxymethyl Cellulose Polyelectrolyte Complexes. *Food Hydrocoll.* **2018,** *80*, 195-205.

(17) Chi, K.; Catchmark, J. M. Sustainable Development of Polysaccharide Polyelectrolyte Complexes as Eco-Friendly Barrier Materials for Packaging Applications. In *Green Polymer Chemistry: New Products, Processes, and Applications*; *ACS Symp. Ser.* **2018**. *1310*, 109-123.

(18) Chi, K.; Wang, H.; Catchmark, J. M. Sustainable Starch-based Barrier Coatings for Packaging Applications. *Food Hydrocoll.* **2020,** *103*, 105696.

(19) Wang, J.; Gardner, D. J.; Stark, N. M.; Bousfield, D. W.; Tajvidi, M.; Cai, Z. Moisture and Oxygen Barrier Properties of Cellulose Nanomaterial-based Films. *ACS Sustain. Chem. Eng.* **2018,** *6*, 49-70.

(20) Lindström, T.; Österberg, F. Evolution of Biobased and Nanotechnology Packaging–A Review. *Nord Pulp Paper Res J* . **2020,** *35*, 491-515.

(21) Li, M.-C.; Wu, Q.; Lei, T.; Mei, C.; Xu, X.; Lee, S.; Gwon, J. Thermothickening Drilling Fluids Containing Bentonite and Dual-Functionalized Cellulose Nanocrystals. *Energy Fuels* **2020,** *34*, 8206-8215.

(22) Rana, A.; Khan, I.; Saleh, T. A. Advances in Carbon Nanostructures and Nanocellulose as Additives for Efficient Drilling Fluids: Trends and Future Perspective—A Review. *Energy Fuels* **2021,** *35*, 7319-7339.

(23) Hubbe, M. A.; Ferrer, A.; Tyagi, P.; Yin, Y.; Salas, C.; Pal, L.; Rojas, O. J. Nanocellulose in Thin Films, Coatings, and Plies for Packaging Applications: A Review. *BioResources* **2017,** *12*, 2143-2233.

(24) Hisseine, O. A.; Wilson, W.; Sorelli, L.; Tolnai, B.; Tagnit-Hamou, A. Nanocellulose for Improved Concrete Performance: A Macro-to-micro Investigation for Disclosing the Effects of Cellulose Filaments on Strength of Cement Systems. *Constr Build Mater.* **2019,** *206*, 84-96.

(25) Almeida, T.; Silvestre, A. J.; Vilela, C.; Freire, C. S. Bacterial Nanocellulose Toward Green Cosmetics: Recent Progresses and Challenges. *Int. J. Mol. Sci.* **2021,** *22*, 2836.

(26) Thomas, B.; Raj, M. C.; Joy, J.; Moores, A.; Drisko, G. L.; Sanchez, C. Nanocellulose, a Versatile Green Platform: from Biosources to Materials and their Applications. *Chem. Rev.* **2018,** *118*, 11575-11625.

(27) Atalla, R. H.; VanderHart, D. L. Native Cellulose: A Composite of Two Distinct Crystalline Forms. *Science* **1984,** *223*, 283-285.

(28) Nishiyama, Y.; Sugiyama, J.; Chanzy, H.; Langan, P. Crystal Structure and Hydrogen Bonding System in Cellulose Iα from Synchrotron X-ray and Neutron Fiber Diffraction. *J. Am. Chem. Soc.* **2003,** *125*, 14300-14306.

(29) Nishiyama, Y.; Johnson, G. P.; French, A. D.; Forsyth, V. T.; Langan, P. Neutron Crystallography, Molecular Dynamics, and Quantum Mechanics Studies of the Nature of Hydrogen Bonding in Cellulose Iβ. *Biomacromolecules* **2008,** *9*, 3133-3140.

(30) Moon, R. J.; Martini, A.; Nairn, J.; Simonsen, J.; Youngblood, J. Cellulose Nanomaterials Review: Structure, Properties and Nanocomposites. *Chem. Soc. Rev.* **2011,** *401*, 3941-3994.

(31) Hanley, S. J.; Revol, J.-F.; Goodbout, L.; Gray, D. G. Atomic Force Microscopy and Transmission Electron Microscopy of Cellulose from Micrasterias Denticulata; Evidence for a Chiral Helical Microfbril Twist. *Cellulose* **1997,** *4*, 209-220.

(32) Usov, I.; Nystrom, G.; Adamcik, J.; Handschin, S.; Schutz, C.; Fall, A.; Bergstrom, L.; Mezzenga, R. Understanding Nanocellulose Chirality and Structure-properties Relationship at the Single Fibril Level. *Nat. Commun* **2015,** *6*, 7564.

(33) Zhao, Z.; Shklyaev, O. E.; Nili, A.; Mohamed, M. N.; Kubicki, J. D.; Crespi, V. H.; Zhong, L. Cellulose Microfibril Twist, Mechanics, and Implication for Cellulose Biosynthesis. *J. Phys. Chem. A* **2013,** *117*, 2580-2589.

(34) Tanaka, H.; Meunier, J.; Bonn, D. Nonergodic States of Charged Colloidal Suspensions: Repulsive and Attractive Glasses and Gels. *Phys. Rev. E.* **2004,** *69*, 031404.

(35) Appel, J.; Fölker, B.; Sprakel, J. Mechanics at the Glass-to-Gel Transition of Thermoresponsive Microgel Suspensions. *Soft Matter* **2016,** *12*, 2515-2522.

(36) Nordenström, M.; Fall, A.; Nyström, G.; Wågberg, L. Formation of Colloidal Nanocellulose Glasses and Gels. *Langmuir* **2017,** *33*, 9772-9780.

(37) Solomon, M. J.; Spicer, P. T. Microstructural Regimes of Colloidal Rod Suspensions, Gels, and Glasses. *Soft Matter* **2010,** *6*, 1391-1400.

(38) Vold, R. D.; Vold M. J *Colloid and Interface Chemistry*; Addison-Wesley, Boston, 1983; p 694.

(39) Hunter, R. J. *Foundation of Colloid Science*; Oxford University Press: Oxford, UK, 2001. p 816.

(40) Hiemenz, P. C. *Principles of Colloid and Surface Chemistry*; Marcel and Dekker. Inc., New York, USA, 1986.

(41) Hiemenz, P. C.; Rajagopalan, R. *Principles of Colloid and Surface Chemistry, 3rd edition*; CRC Press: Boca Raton, 1997. p 672.

(42) Lyklema, J. *Fundamentals of Interface and Colloid Science: Soft Colloids*; Elsevier Academic Press: Amsterdam, 2005. p 844.

(43) Baes, C. F.; Mesmer, R. E. *The Hydrolysis of Cations*; John Wiley and Sons: New York, 1976. p 489.

(44) Cao, H.; Zhang, L.; Wu, L.; Kong, X. Z. Characterization of Heterocoagulation with Oppositely Charged Polymer Colloid Particles Through Online Tracking of Light Transmittance. *ACS Appl. Mater. Interfaces* **2016,** *8*, 29136-29147.

(45) Hogg, R.; Healy, T. W.; Furstenau, D. W. Mutual Coagulation of Colloidal Dispersions. *Trans. Faraday Soc.* **1966,** *62*, 1638-1651.

(46) Ohshima, H.; Chan, D. Y. C.; Healy, T. W.; White, L. R. Improvement on the Hogg-Healy-Fuerstenau Formulas for the Interaction of Dissimilar Double Layers. *J. Coll. and Interface Sci.* **1982,** *92*, 232-242.

(47) Ruehwein, R. A.; Ward, W. A. Mechanism of Clay Aggregation by Polyelectrolytes. *Soil Sci.* **1952,** *73*, 485-492.

(48) Michaels, A. S. Aggregation of Suspensions by Polyelectrolytes. *J Ind. Eng. Chem.* **1954,** *46*, 1485-1490.

(49) Michaels, A. S.; Morelos, O. Polyelectrolyte Adsorption by Kaolinite. *J Ind. Eng. Chem.* **1955,** *47*, 1801-1809.

(50) Audsley, A.; Fursey, A. Examination of a Polysaccharide Flocculant and Flocculated Kaolinite by Electron Microscopy. *Nature* **1965,** *208*, 753-754.

(51) La Mer, V. K.; Healy, T. W. Adsorption-flocculation Reactions of Macrolecules at the Soolid-liquid Interface. *Rev. Pure Appl. Chem.* **1963,** *13*, 112-133.

(52) Fleer, G. J. Polymer Adsorption and Its Effect on Colloidal Stability. Ph.D Thesis, Wageningen, The Netherlands Agricultural University, 1971, https://edepot.wur.nl/194575.

(53) Vincent, B. The Effect of Adsorped Polymers on Dispersion Stabliity. *Adv. in Coll. and Interface Sci.* **1974,** *4*, 193-277.

(54) Fleer, G. J.; Koopal, L. K.; Lyklema, J. Polymer Adsorption and Its Effect on the Stability of Hydrophobic Colloids. *Kolloid Zeitschrift & Zeitschrift fuer Polymere* **1972,** *250*, 689-702.

(55) Lindström, T. "Fundamentals of Papermaking", Transactions of the Ninth Fundamental Research Symposium, Cambridge, UK, 1989; p 311.

(56) Ghernaout, D.; Ghernaout, B. Sweep Flocculation as a Second Form of Charge Neutralisation. *Des. and Water Treat.* **2012,** *44*, 15-28.

(57) Lindström, T.; Glad-Nordmark, G. Flocculation of Latex and Cellulose Dispersions by Means of Transient Polymer Networks. *Colloids Surf.* **1984,** *8*, 337-351.

(58) Lindström, T.; Glad-Nordmark, G. Network Flocculation and Fractionation of Latex Particles by Means of a Polyethyleneoxide-phenolformaldehyde Resin Complex. *J. Colloid Interface Sci.* **1984,** *97*, 62-67.

(59) Shahnaz, T.; Padmanaban, V.; Narayanasamy, S. Surface Modification of Nanocellulose using Polypyrrole for the Adsorptive Removal of Congo Red Dye and Chromium in Binary Mixture. *Int. J. Biol. Macromol.* **2020,** *151*, 322-332.

(60) Karim, Z.; Hakalahti, M.; Tammelin, T.; Mathew, A. P. *In situ* TEMPO Surface Functionalization of Nanocellulose Membranes for Enhanced Adsorption of Metal Ions from Aqueous Medium. *RSC Adv.* **2017,** *7*, 5232-5241.

(61) Brandes, R.; Belosinschi, D.; Brouillette, F.; Chabot, B. A New Electrospun Chitosan/Phosphorylated Nanocellulose Biosorbent for the Removal of Cadmium Ions from Aqueous Solutions. *J. Environ. Chem. Eng.* **2019,** *7*, 103477.

(62) Yue, Y.; Wang, X.; Han, J.; Yu, L.; Chen, J.; Wu, Q.; Jiang, J. Effects of Nanocellulose on Sodium Alginate/Polyacrylamide Hydrogel: Mechanical Properties and Adsorption-desorption Capacities. *Carbohydr. Polym.* **2019,** *206*, 289-301.

(63) Mohammed, N.; Grishkewich, N.; Waeijen, H. A.; Berry, R. M.; Tam, K. C. Continuous Flow Adsorption of Methylene Blue by Cellulose Nanocrystal-alginate Hydrogel Beads in Fixed Bed Columns. *Carbohydr. Polym.* **2016,** *136*, 1194-1202.

(64) Wei, J.; Gui, S.-H.; Wu, J.-H.; Xu, D.-D.; Sun, Y.; Dong, X.-Y.; Dai, Y.-Y.; Li, Y.-F. Nanocellulose-Graphene Oxide Hybrid Aerogel to Water Purification. *Appl. Environ. Biotechnol.* **2019,** *4* , 11-17.

(65) Lavoine, N.; Bergström, L. Nanocellulose-based Foams and Aerogels: Processing, Properties, and Applications. *J. Mater. Chem. A* **2017,** *5*, 16105-16117.

(66) Gu, H.; Zhou, X.; Lyu, S.; Pan, D.; Dong, M.; Wu, S.; Ding, T.; Wei, X.; Seok, I.; Wei, S. Magnetic Nanocellulose-magnetite Aerogel for Easy Oil Adsorption. *J. Colloid Interface Sci.* **2020,** *560*, 849-856.

(67) Suopajärvi, T.; Liimatainen, H.; Hormi, O.; Niinimäki, J. Coagulation–Flocculation Treatment of Municipal Wastewater based on Anionized Nanocelluloses. *Chem. Eng. J.* **2013,** *231*, 59-67.

(68) Sun, B.; Hou, Q.; Liu, Z.; Ni, Y. Sodium Periodate Oxidation of Cellulose Nanocrystal and Its Application as a Paper Wet Strength Additive. *Cellulose* **2015,** *22*, 1135-1146.

(69) Yu, H.-Y.; Zhang, D.-Z.; Lu, F.-F.; Yao, J. New Approach for Single-step Extraction of Carboxylated Cellulose Nanocrystals for their Use as Adsorbents and Focculants. *ACS Sustain. Chem. Eng* **2016,** *4*, 2632-2643.

(70) Yao, C.; Wang, F.; Cai, Z.; Wang, X. Aldehyde-functionalized Porous Nanocellulose for Effective Removal of Heavy Metal Ions from Aqueous Solutions. *RSC Adv.* **2016,** *6*, 92648-92654.

(71) Li, W.; Ju, B.; Zhang, S. A Green L-cysteine Modified Cellulose Nanocrystals Biosorbent for Adsorption of Mercury Ions from Aqueous Solutions. *RSC Adv.* **2019,** *9*, 6986-6994.

(72) Ram, B.; Chauhan, G. S. New Spherical Nanocellulose and Thiol-based Adsorbent for Rapid and Selective Removal of Mercuric Ions. *Chem. Eng. J.* **2018,** *331*, 587-596.

(73) Jin, L.; Li, W.; Xu, Q.; Sun, Q. Amino-functionalized Nanocrystalline Cellulose as an Adsorbent for Anionic Dyes. *Cellulose* **2015,** *22*, 2443-2456.

(74) Huang, X.; Dognani, G.; Hadi, P.; Yang, M.; Job, A. E.; Hsiao, B. S. Cationic Dialdehyde Nanocellulose from Sugarcane Bagasse for Efficient Chromium (VI) Removal. *ACS Sustain. Chem. Eng* **2020,** *8*, 4734-4744.

(75) Alsbaiee, A.; Smith, B. J.; Xiao, L.; Ling, Y.; Helbling, D. E.; Dichtel, W. R. Rapid Removal of Organic Micropollutants from Water by a Porous *β*-cyclodextrin Polymer. *Nature* **2016,** *529*, 190-194.

(76) Cova, T. F.; Murtinho, D.; Pais, A. A.; Valente, A. J. Combining Cellulose and Cyclodextrins: Fascinating Designs for Materials and Pharmaceutics. *Front. Chem.* **2018,** *6*, 271.

(77) Tavakolian, M.; Jafari, S. M.; van de Ven, T. G. A Review on Surface-Functionalized Cellulosic Nanostructures as Biocompatible Antibacterial Materials. *Nano-Micro Lett.* **2020,** *12*, 73.

(78) Brar, S. K.; Wangoo, N.; Sharma, R. K. Enhanced and Selective Adsorption of Cationic Dyes Using Novel Biocompatible Self-assembled Peptide Fibrils. *J. Environ. Manage.* **2020,** *255*, 109804.

(79) Lin, N.; Dufresne, A. Nanocellulose in Biomedicine: Current Status and Future Prospect. *Eur. Polym. J* **2014,** *59*, 302-325.

(80) Börjesson, M.; Sahlin, K.; Bernin, D.; Westman, G. Increased Thermal Stability of Nanocellulose Composites by Functionalization of the Sulfate Groups on Cellulose Nanocrystals with Azetidinium Ions. *J. Appl. Polym. Sci.* **2018,** *135*, 45963.

(81) Sajab, M. S.; Chia, C. H.; Chan, C. H.; Zakaria, S.; Kaco, H.; Chook, S. W.; Chin, S. X. Bifunctional Graphene Oxide–Cellulose Nanofibril Aerogel Loaded with Fe (III) for the Removal of Cationic Dye via Simultaneous Adsorption and Fenton oxidation. *RSC Adv.* **2016,** *6*, 19819-19825.

(82) Herrera-Morales, J.; Turley, T. A.; Betancourt-Ponce, M.; Nicolau, E. Nanocellulose-Block Copolymer Films for the Removal of Emerging Organic Contaminants from Aqueous Solutions. *Materials* **2019,** *12*, 230.

(83) Tauc, J.; Grigorovici, R.; Vancu, A. Optical Properties and Electronic Structure of Amorphous Germanium. *Phys. Status Solidi B* **1966,** *15*, 627-637.

(84) Davis, E.; Mott, N. Conduction in Non-crystalline Systems V. Conductivity, Optical Absorption and Photoconductivity in Amorphous Semiconductors. *Philos. Mag.* **1970,** *22*, 0903-0922.

(85) Kubelka, P.; Munk, F. A Contribution to the Optics of Pigments. *Z. Tech. Phys* **1931,** *12*, 593-601.

(86) Makuła, P.; Pacia, M.; Macyk, W. How to Correctly Determine the Band Gap Energy of Modified Semiconductor Photocatalysts Based on UV–Vis Spectra. *J. Phys. Chem. Lett*. 2018, 9; 6814-6817.

(87) Shi, F.; Yu, T.; Hu, S.-C.; Liu, J.-X.; Yu, L.; Liu, S.-H. Synthesis of Highly Porous SiO_2–(WO_3) x· TiO_2 Composite Aerogels Using Bacterial Cellulose as Template with Solvothermal Assisted Crystallization. *Chem. Eng. J.* **2016,** *292*, 105-112.

(88) Nair, S. S.; Chen, J.; Slabon, A.; Mathew, A. P. Converting Cellulose Nanocrystals into Photocatalysts by Functionalisation with Titanium Dioxide Nanorods and Gold Nanocrystals. *RSC Adv.* **2020,** *10*, 37374-37381.

(89) Liu, J.; Fu, X.; Chen, S.; Zhu, Y. Electronic Structure and Optical Properties of Ag_3PO_4 Photocatalyst Calculated by Hybrid Density Functional Method. *Appl. Phys. Lett.* **2011,** *99*, 191903.

(90) Xiang, Q.; Lang, D.; Shen, T.; Liu, F. Graphene-modified Nanosized Ag_3PO_4 Photocatalysts for Enhanced Visible-light Photocatalytic Activity and Stability. *Appl. Catal. B: Environ.* **2015,** *162*, 196-203.

(91) Lebogang, L.; Bosigo, R.; Lefatshe, K.; Muiva, C. Ag_3PO_4/Nanocellulose Composite for Effective Sunlight Driven Photodegradation of Organic Dyes in Wastewater. *Mater. Chem. Phys.* **2019,** *236*, 121756.

(92) Gan, L.; Geng, A.; Song, C.; Xu, L.; Wang, L.; Fang, X.; Han, S.; Cui, J.; Mei, C. Simultaneous Removal of Rhodamine B and Cr(VI) from Water using Cellulose Carbon Nanofiber Incorporated with Bismuth Oxybromide: The Effect of Cellulose Pyrolysis Temperature on Photocatalytic Performance. *Environ. Res.* **2020,** *185*, 109414.

(93) Das, R.; Ali, E.; Abd Hamid, S. B. Current Applications of X-ray Powder Diffraction-A Review. *Rev. Adv. Mater. Sci.* **2014,** *38*, 95-109.

(94) Das, R.; Hamid, S. B. A.; Ali, M.; Annuar, M.; Samsudin, E. M. B.; Bagheri, S. Covalent Functionalization Schemes for Tailoring Solubility of Multi-walled Carbon Nanotubes in Water and Acetone Solvents. *Sci. Adv. Mater.* **2015,** *7*, 2726-2737.

(95) Das, R.; Ali, M.; Bee Abd Hamid, S.; Annuar, M.; Ramakrishna, S. Common Wet Chemical Agents for Purifying Multiwalled Carbon Nanotubes. *J. Nanomater.* **2014,** *237***,** 945172. https://doi.org/10.1155/2014/945172.

(96) Xiao, H.; Shan, Y.; Zhang, W.; Huang, L.; Chen, L.; Ni, Y.; Boury, B.; Wu, H. C-nanocoated ZnO by TEMPO-oxidized Cellulose Templating for Improved Photocatalytic Performance. *Carbohydr. Polym.* **2020,** *235*, 115958.

(97) Wang, Z.; Zhang, W.; Yu, J.; Zhang, L.; Liu, L.; Zhou, X.; Huang, C.; Fan, Y. Preparation of Nanocellulose/Filter Paper (NC/FP) Composite Membranes for High-performance Filtration. *Cellulose* **2019,** *26*, 1183-1194.

(98) Wang, X.; Ma, H.; Chu, B.; Hsiao, B. S. Thin-film Nanofibrous Composite Reverse Osmosis Membranes for Desalination. *Desalination* **2017,** *420*, 91-98.

(99) Wang, X.; Yeh, T.-M.; Wang, Z.; Yang, R.; Wang, R.; Ma, H.; Hsiao, B. S.; Chu, B. Nanofiltration Membranes Prepared by Interfacial Polymerization on Thin-film Nanofibrous Composite Scaffold. *Polymer* **2014,** *55*, 1358.

(100) Wang, X.; Fang, D.; Hsiao, B. S.; Chu, B. Nanofiltration Membranes Based on Thin-film Nanofibrous Composites. *J. Membr. Sci.* **2014,** *469*, 188-197.

(101) Wang, Z.; Ma, H.; Hsiao, B. S.; Chu, B. Nanofibrous Ultrafiltration Membranes Containing Cross-linked Poly(ethylene glycol) and Cellulose Nanofiber Composite Barrier Layer. *Polymer* **2014,** *55*, 366-372.

(102) Ma, H.; Burger, C.; Hsiao, B. S.; Chu, B. Fabrication and Characterization of Cellulose Nanofiber based Thin-film Nanofibrous Composite Membranes. *J. Membr. Sci.* **2014,** *454*, 272-282.

(103) Hassan, M. L.; Fadel, S. M.; Abouzeid, R. E.; Abou Elseoud, W. S.; Hassan, E. A.; Berglund, L.; Oksman, K. Water Purification Ultrafiltration Membranes Using Nanofibers from Unbleached and Bleached Rice Straw. *Sci. Rep.* **2020,** *10*, 11278.

(104) Hadi, P.; Yang, M.; Ma, H.; Huang, X.; Walker, H.; Hsiao, B. S. Biofouling-resistant Nanocellulose Layer in Hierarchical Polymeric Membranes: Synthesis, Characterization and Performance. *J. Membr. Sci.* **2019,** *579*, 162-171.

(105) Liang, Y.; Ma, H.; Taha, A. A.; Hsiao, B. S. High-flux Anti-fouling Nanofibrous Composite Ultrafiltration Membranes Containing Negatively Charged Water Channels. *J. Membr. Sci.* **2020,** *612*, 118382.

(106) Yang, M.; Hadi, P.; Yin, X.; Yu, J.; Huang, X.; Ma, H.; Walker, H.; Hsiao, B. S. Antifouling Nanocellulose Membranes: How Subtle Adjustment of Surface Charge Lead to Self-cleaning Property. *J. Membr. Sci.* **2021,** *618*, 118739.

(107) Gustafsson, S.; Mihranyan, A. Strategies for Tailoring the Pore-size Distribution of Virus Retention Filter Papers. *ACS Appl. Mater. Interfaces* **2016,** *8*, 13759-13767.

(108) Gustafsson, S.; Lordat, P.; Hanrieder, T.; Asper, M.; Schaefer, O.; Mihranyan, A. Mille-feuille Paper: A Novel Type of Filter Architecture for Advanced Virus Separation Applications. *Mater. Horiz.* **2016,** *3*, 320-327.

(109) Ferguson, A.; Khan, U.; Walsh, M.; Lee, K. Y.; Bismarck, A.; Shaffer, M. S.; Coleman, J. N.; Bergin, S. D. Understanding the Dispersion and Assembly of Bacterial Cellulose in Organic Solvents. *Biomacromolecules* **2016,** *17*, 1845-1853.

(110) Wu, X.; Cao, S.; Ghim, D.; Jiang, Q.; Singamaneni, S.; Jun, Y.-S. A Thermally Engineered Polydopamine and Bacterial Nanocellulose Bilayer Membrane for Photothermal Membrane Distillation with Bactericidal Capability. *Nano Energy* **2021,** *79*, 105353.